
Electronic Thesis and Dissertation Repository

2-23-2018 10:00 AM

Covalently Crosslinked Organic/Inorganic Hybrid Biomaterials for Bone Tissue Engineering Applications

Dibakar Mondal

The University of Western Ontario

Supervisor

Mequanint, Kibret

The University of Western Ontario Joint Supervisor

Rizkalla, Amin S

The University of Western Ontario

Graduate Program in Chemical and Biochemical Engineering

A thesis submitted in partial fulfillment of the requirements for the degree in Doctor of Philosophy

© Dibakar Mondal 2018

Follow this and additional works at: <https://ir.lib.uwo.ca/etd>



Part of the [Biochemical and Biomolecular Engineering Commons](#), [Biology and Biomimetic Materials Commons](#), [Biomaterials Commons](#), [Ceramic Materials Commons](#), [Molecular, Cellular, and Tissue Engineering Commons](#), and the [Polymer and Organic Materials Commons](#)

Recommended Citation

Mondal, Dibakar, "Covalently Crosslinked Organic/Inorganic Hybrid Biomaterials for Bone Tissue Engineering Applications" (2018). *Electronic Thesis and Dissertation Repository*. 5229.

<https://ir.lib.uwo.ca/etd/5229>

This Dissertation/Thesis is brought to you for free and open access by Scholarship@Western. It has been accepted for inclusion in Electronic Thesis and Dissertation Repository by an authorized administrator of Scholarship@Western. For more information, please contact wlsadmin@uwo.ca.

Abstract

Scaffolds are key components for bone tissue engineering and regeneration. They guide new bone formation by mimicking bone extracellular matrix for cell recruitment and proliferation. Ideally, scaffolds for bone tissue engineering need to be osteoconductive, osteoinductive, porous, degradable and mechanically competent. As a single material can not provide all these requirements, composites of several biomaterials are viable solutions to combine various properties. However, conventional composites fail to fulfil these requirements due to their distinct phases at the microscopic level. Organic/inorganic (O/I) class II hybrid biomaterials, where the organic and inorganic phases are chemically crosslinked on a molecular scale, hence the phases are homogenously dispersed, are the ideal choices for bone tissue engineering.

In this research, polycaprolactone/borophosphosilicate glass (PCL/BPSG) and poly(vinylpyrrolidone-co-triethoxyvinylsilane)/bioactive glass (Poly(VP-co-TEVS)/BG) class II hybrid biomaterials were successfully prepared *via* a sol-gel process. PCL was functionalized with 3-glycidoxypropyl trimethoxysilane at both ends prior to hybrid syntheses. Trimethoxysilane-functionalized PCL was then polycondensed with the glass precursors *via* non-aqueous sol gel reactions to form covalently bonded O/I network with -C-Si-O-Si- bonds. The resultant amorphous and transparent hybrid materials exhibited apatite depositions when incubated with simulated body fluid. The ultimate compressive stress, modulus and toughness of these hybrids were significantly greater compared with their conventional composite counterparts, attributed to the covalent bonding between the O/I phases. In addition, these hybrids exhibited more controlled degradation and subsequent ion release without showing any abrupt features. Pre-osteoblast cells seeded on the hybrid biomaterials displayed enhanced spreading, focal adhesion formation, and cell number, indicating cytocompatibility. PCL/BPSG hybrid scaffolds were prepared by a solvent-free casting

and particulate leaching methods to obtain consistent pore size distribution, controllable porosity and pore interconnectivity. Significant number of cell infiltration and adhesion into the scaffolds were observed in cell culture conditions. Bone-associated gene expression by induced pluripotent stem cells on these scaffolds revealed that the hybrid scaffolds had an upregulating effect on gene expressions for alkaline phosphatase, osteopontin and osteocalcin.

To understand the effect of polymer functionality on the degree of covalent crosslinking, different compositions of class II hybrids biomaterials from BG and Poly(VP-co-TEVS) were prepared. Prior to the synthesis of class II hybrid biomaterials, VP and TEVS monomers were copolymerized at various molar ratios, to obtain different amounts of functional groups in polymer chains. It was possible to tailor the microstructure, bioactivity, degradation and mechanical properties of these hybrids by varying the amount of functional groups in the polymer chains and organic/inorganic ratios. Porous and interconnective scaffolds of these hybrid biomaterials were fabricated by indirect 3D printing using a sacrificial template. The work described herein provides strong evidence that class II hybrid scaffolds have great potential in bone tissue engineering due to their tailorable microstructure, bioactivity, degradation and mechanical properties.

Keywords: Class II organic/inorganic hybrid biomaterials, bioactive glass, borophosphosilicate glass, polycaprolactone, polyvinylpyrrolidone, bone tissue engineering, solvent-free casting/particulate leaching, indirect rapid prototyping, degradation, mechanical properties, osteogenic gene expression.

Co-authorship Statement

Chapters 1 and 2 entitled “Introduction” and “Literature Review”, respectively, were written by D. Mondal. Drs. A. S. Rizkalla and K. Mequanint reviewed and edited those chapters.

Chapter 3 entitled “Bioactive Borophosphosilicate-Polycaprolactone Hybrid Biomaterials *via* a Non-aqueous Sol Gel Process” is adapted from Mondal *et al.*, 2016. *RSC Advances* 6 (95), 92824-92832. The publication was written by D. Mondal, Drs. A. S. Rizkalla and K. Mequanint. All experiments were performed by D. Mondal, and were carried out in the laboratories of A. S. Rizkalla and K. Mequanint.

Chapter 4 entitled “Mechanically-competent and Cytocompatible Polycaprolactone-Borophosphosilicate Hybrid Biomaterials” is adapted from Mondal *et al.*, 2017. *Journal of the Mechanical Behavior of the Biomedical Materials*, 75, 180-189. The publication was written by D. Mondal, Drs. S. J. Dixon, K. Mequanint, and A. S. Rizkalla. Experiments were performed by D. Mondal, and were carried out in the laboratories of A. S. Rizkalla, S. J. Dixon and K. Mequanint with technical assistance from Ryan Beach from Jeff Dixon’s lab.

Chapter 5 entitled “Cell Infiltration and Differentiation on Polycaprolactone- Borophosphosilicate Glass Hybrid Scaffolds” was written by D. Mondal, Drs. A. S. Rizkalla and K. Mequanint. Experiments were performed by D. Mondal in the laboratories of A. S. Rizkalla, K. Mequanint, and S. J. Dixon. Dr. Shigang Lin helped in conducting experiments with stem cells, confocal imaging and q-PCR analysis.

Chapter 6 entitled “Effect of Copolymer Functionality and Composition on Bioactivity, Degradation and Mechanical Properties of Poly(vinyl pyrrolidone-co-triethoxy vinyl silane)/Bioactive Glass Hybrids” was written by D. Mondal, Drs. K. Mequanint, and A. S. Rizkalla. Experiments were performed by D. Mondal in the laboratories of A. S. Rizkalla, K. Mequanint, Aaron Price, and S. J. Dixon. Ben Holness prepared the sacrificial templates by 3D printing.

Chapter 7 entitled “General Discussion” was written by D. Mondal. Drs. K. Mequanint, and A. S. Rizkalla reviewed and edited the chapter.

Acknowledgements

First and foremost, I would like to express my heartfelt gratitude to my supervisors, Drs. Kibret Mequanint and Amin S Rizkalla, for giving me the opportunity to work under their guidance with continued financial support and constant encouragement to achieve my goals. My PhD experience has been wonderful, and it would not have been the same without their mentorship, valuable advice and persuasive discussions. I am always thankful to them for believing in me and constantly inspiring me towards completion of this research work.

Special thanks are also due to one of my Advisory Committee members, Dr. Jeffery S. Dixon whose intellectual support was a great source of inspiration throughout my PhD studies. My sincere admiration to his wisdom and his distinguished character. I would like to express my sincere thanks to another member of my Advisory Committee, Dr. Jose Herrera, for his valuable suggestions and constructive criticism throughout my studies.

I also thank my current and previous lab-mates for their great support and thoughtful discussions during our lab meetings and manuscript preparations. These fruitful discussions helped me widen my knowledge.

I am grateful for the financial support from Vanier Canada Graduate Scholarship during my PhD program. I am also thankful to the financial supports from Western Graduate Research Scholarships, Western Graduate Research Assistantships, and Doctoral Excellence Research Awards (The University of Western Ontario).

I also thank Dr. Paul Charpentier for allowing me access to XRD, TGA and FTIR facilities; and Dr. Aaron Price for providing the 3D printing facilities.

My utmost gratitude goes to my wife and best friend, Shampa Das, for being at my side through the highs and lows to cheer me up, for her genuine care and loving support, and for keeping me sane. I am thankful to my parents, Ashima and Arabinda Mondal, for their love and support. I finally thank my brother, Provakar, for his friendship, love and support.

Table of Contents

Abstract.....	i
Co-authorship Statement	iii
Acknowledgements	v
Table of Contents	vii
List of Tables	xiii
List of Figures.....	xiv
List of Abbreviations	xvi
Chapter 1: Introduction	1
1.1 Overview.....	1
1.2 Thesis outline	3
1.3 References.....	4
Chapter 2: Literature Review.....	7
2.1 Bone tissue engineering	7
2.1.1 Elements of bone tissue engineering.....	8
2.2 Materials for bone tissue engineering scaffolds.....	13
2.2.1 Bioceramics.....	13
2.2.2 Biocompatible and degradable polymers.....	20
2.2.3 Bioactive glass based organic/inorganic composites.....	22
2.2.4 O/I hybrid biomaterial.....	24
2.3 Challenges associated with the synthesis of class II hybrids	31
2.3.1 Synthesis route	32

2.4 O/I class II hybrid scaffolds	35
2.4.1 Electrospinning	36
2.4.2 Foaming	37
2.4.3 Freeze drying	37
2.4.4 Particulate leaching.....	38
2.4.5 3D printing.....	38
2.5 Summary	40
2.6 Hypothesis and objectives of the research	40
2.7 References.....	41
Chapter 3: Bioactive Polycaprolactone-Borophosphosilicate Hybrid Biomaterials via a Non-aqueous Sol Gel Process	53
3.1 Summary	53
3.2 Introduction.....	54
3.3 Materials and methods	56
3.3.1 Materials	56
3.3.2 Functionalization of poly (ϵ -caprolactone) diol.....	56
3.3.3 Synthesis of PCL/borophosphosilicate hybrid biomaterials	57
3.3.4. Fabrication of porous scaffold	58
3.3.5 In vitro bioactivity tests	58
3.3.6 Fourier Transform Infrared Spectroscopy (FTIR)	59
3.3.7 ^1H and ^{29}Si Nuclear Magnetic Resonance Spectroscopy (NMR)	59
3.3.8 Thermogravimetric Analysis (TGA)	60
3.3.9 X-ray Diffraction (XRD)	60
3.3.10 SEM and EDX	61

3.3.11 X-Ray Photoelectron Spectroscopy (XPS)	61
3.4 Results and discussion	62
3.4.1 Preparation of functionalized PCL-Si	62
3.4.2 Preparation of class II PCL/BPSG hybrid biomaterials	64
3.4.3 Solid state NMR, FTIR, and thermal analyses of hybrid biomaterials	65
3.4.4 Phase identification and chemical composition of hybrid materials	71
3.4.5 In vitro bioactivity of hybrid biomaterials	76
3.4.6 Porous 3D scaffolds from class II PCL/BPSG hybrid biomaterials	79
3.5 Conclusions	81
3.6 References	82
Chapter 4: Mechanically-competent and Cytocompatible Polycaprolactone- Borophosphosilicate Hybrid Biomaterials	86
4.1 Summary	86
4.2 Introduction	87
4.3 Materials and methods	90
4.3.1 Materials	90
4.3.2 Preparation of PCL/BPSG class II hybrids and composites	90
4.3.3 Evaluation of mechanical properties	91
4.3.4 Assessment of in vitro degradation	92
4.3.5 Scanning Electron Microscopy (SEM)	93
4.3.6 Cell culture and assessment of focal adhesion formation	93
4.3.7 Assessment of cytocompatibility	95
4.3.8 Statistical analyses	96
4.4 Results	96

4.4.1 Mechanical competency of hybrid materials	96
4.4.2 In vitro degradation of hybrid materials	99
4.4.3 Cytocompatibility of hybrid material.....	103
4.5 Discussion	109
4.6 Conclusions	112
4.7 References	112
Chapter 5: Cell Infiltration and Differentiation on Polycaprolactone- Borophosphosilicate Glass Hybrid Scaffolds	116
5.1 Summary	116
5.2 Introduction.....	117
5.3 Materials and methods	120
5.3.1 Materials	120
5.3.2 Fabrication of PCL/BPSG hybrid scaffolds.....	120
5.3.3 Micro-CT characterization of hybrid scaffolds.....	122
5.3.4 Evaluation of mechanical properties.....	122
5.3.5 Mechanical properties and mass loss of degraded hybrid scaffolds	123
5.3.6 MC3T3-E1 preosteoblastic cell infiltration into the scaffolds.....	123
5.3.7 Osteogenic differentiation of cells seeded on hybrid scaffolds	125
5.3.8 Statistical analyses	126
5.4 Results.....	127
5.4.1 Microstructure, pore size and porosity of hybrid scaffolds	127
5.4.2 Mechanical properties of hybrid scaffolds.....	129
5.4.3 Changes in mechanical properties of the hybrid scaffolds with degradation	131
5.4.4 Preosteoblastic MC3T3-E1 infiltration studies	134

5.3.5 Differentiation of stem cells in hybrid scaffolds.....	137
5.5 Discussion.....	139
5.6 Conclusion	142
5.7 References.....	143
Chapter 6: Effect of Copolymer Functionality and Composition on Bioactivity, Degradation and Mechanical Properties of Poly(vinyl pyrrolidone-co- triethoxy vinyl silane)/Bioactive Glass Hybrids	146
6.1 Summary.....	146
6.2 Introduction.....	147
6.3 Materials and methods	151
6.3.1 Materials	151
6.3.2 Synthesis of poly(VP-co-TEVS).....	151
6.3.3 Synthesis of poly(VP-co-TEVS)/BG class II hybrid.....	152
6.3.4 In vitro bioactivity evaluation of poly(VP-co-TEVS)/BG hybrid in SBF.....	154
6.3.5 Degradation of poly(VP-co-TEVS)/BG hybrid biomaterials in PBS	155
6.3.6 Cell culture and assessment of cellular morphology on hybrid.....	156
6.3.7 Poly(VP-co-TEVS)/BG class II hybrid scaffold fabrication	157
6.3.8 Compressive properties of poly(VP-co-TEVS)/BG hybrid scaffolds	158
6.3.9 Statistical analyses	159
6.4 Results.....	159
6.4.1 Synthesis of poly(VP-co-TEVS)/BG class II hybrid biomaterials	159
6.4.2 Apatite deposition on biomaterial surfaces.....	164
6.4.3 Degradation of poly(VP-co-TEVS)/BG hybrid in PBS.....	166
6.4.4 Hybrid biomaterials are cytocompatible.....	168

6.4.5 Microstructures and pore morphology of hybrid scaffolds.....	171
6.4.6 Compressive mechanical properties of hybrid scaffolds	175
6.5 Discussion.....	176
6.6 Conclusion	180
6.7 References.....	181
Chapter 7: General Discussion	185
7.1 Summary and conclusions	185
7.2 Contributions to the current knowledge.....	189
7.3 Limitations	191
7.4 Future directions	192
7.5 References.....	193
Appendix.....	195
Letters of copyright permission for peer-reviewed articles	195
Curriculum vitae.....	197

List of Tables

Table 2. 1: Selected examples of O/I hybrids for bone tissue engineering applications	31
Table 3. 1: Mass loss and inorganic/organic weight ratio.	69
Table 3. 2: Theoretical and experimental weight percent elemental composition.	75
Table 3. 3: Atomic compositions of Si, P and B appeared in BPSG and 50H.	75
Table 4. 1: Composition of PCL/BPSG hybrids and composites	91
Table 5. 1: Pore properties and porosity of PCL/BPSG hybrid scaffolds	129
Table 6. 1: Composition, yeild and molecular weight distribution for poly(VP-co-TEVS).....	160
Table 6. 2: Porosity and pore properties of poly(VP-co-TEVS)/BG hybrid scaffolds.....	173
Table 6. 3: Compressive mechanical properties of poly(VP-co-TEVS)/BG hybrid scaffolds ...	175

List of Figures

Figure 2. 1: Interactions between O/I phases in two classes of hybrid materials	27
Figure 2. 2: Various functionalizations of polymer.	30
Figure 3. 1: FTIR and ¹ H-NMR spectra of GPTMS, PCL diol and PCL-Si.....	63
Figure 3. 2: TGA thermograms of PCL diol and PCL-Si	64
Figure 3. 3: Solid state ²⁹ Si-NMR and FTIR spectra of hybrid materials.....	67
Figure 3. 4: FTIR spectra of the carbonyl stretching vibration.....	68
Figure 3. 5: TGA thermograms.....	70
Figure 3. 6: XRD patterns of PCL/BPSG hybrid materials.	72
Figure 3. 7: SEM image, EDX spectra and elemental mapping of BPSG and 50H.	73
Figure 3. 8: XPS analysis of BPSG and hybrid materials.	74
Figure 3. 9: SEM images of BPSG and 50H surfaces after incubated in SBF.	78
Figure 3. 10: XRD profiles of hybrid materials after incubated in SBF.....	79
Figure 3. 11: SEM images of class II PCL/BPSG hybrid scaffolds	81
Figure 4. 1: Mechanical properties of class II hybrid and composite materials	97
Figure 4. 2: Degradation behavior of hybrid 50H and composite 50C materials	100
Figure 4. 3: SEM images of surfaces after degradation in PBS.....	101
Figure 4. 4: Morphology and spreading of cells on hybrid biomaterial	103
Figure 4. 5: Morphology and spreading of cells on composite surface	104
Figure 4. 6: Quantification of cell spreading on hybrid biomaterial.....	105
Figure 4. 7: Focal adhesion formation.	106
Figure 4. 8: Biocompatibility of the hybrid material	108

Figure 5. 1: Micro-CT images of PCL/BPSG hybrid scaffolds.....	128
Figure 5. 2: Mechanical properties of 50H PCL/BPSG hybrid scaffolds.....	131
Figure 5. 3: Degradation of PCL/BPSG hybrid scaffolds.....	133
Figure 5. 4: Confocal images of infiltrated cells on scaffolds	135
Figure 5. 5: Quantification of cell infiltration in hybrid scaffolds.....	136
Figure 5. 6: ALP, OCN and OPN mRNA expression.....	138
Figure 6. 1: FTIR spectra of poly(VP-co-TEVS)	161
Figure 6. 2: ¹ H-NMR spectra of poly(VP-co-TEVS)	161
Figure 6. 3: ¹³ C-NMR spectra of poly(VP-co-TEVS)	162
Figure 6. 4: FTIR and solid state ²⁹ Si-NMR spectra of hybrid biomaterials.	164
Figure 6. 5: Apatite deposition on hybrid surfaces	165
Figure 6. 6: Thickness of deposited hydroxyapatite	166
Figure 6. 7: Degradation behavior of hybrid biomaterials.....	168
Figure 6. 8: Morphology and spreading of cells on hybrid surfaces	170
Figure 6. 9: Morphology of PCL template and hybrid scaffolds	172
Figure 6. 10: Representative stress-strain curves of hybrid scaffolds	174
List of Schematics	
Scheme 6. 1: Copolymerization of VP and TEVS.....	152
Scheme 6. 2: Synthesis of class II poly(VP-co-TEVS)/BG hybrid materials.....	153
Scheme 6. 3: Fabrication of hybrid scaffolds	158

List of Abbreviations

3D	Three dimensional
AcOH	Acetic acid
ACP	Amorphous calcium phosphate
AIBN	2,2'-Azobis(2-methylpropionitrile)
ALP	Alkaline phosphatase
ANOVA	Analysis of variance
APTES	(3-Aminopropyl)triethoxysilane
ASC	Adipose tissue-derived stem cell
BCP	Biphasic calcium phosphate
BG	Bioactive glass
BMSC	Bone marrow derived stem cells
BPSG	Borophosphosilicate glass
BSA	Bovine albumin
BSP	Bone sialoprotein
CaP	Calcium phosphates
CDA	Calcium-deficient apatite
CIHR	Canadian Institutes of Health Research
Class I	Class one
Class II	Class two
CP-MAS	Cross-polarization magic-angle spinning
DAPI	4',6-Diamidino-2-phenylindole
DCM	Dichloromethane
DNA	Deoxyribonucleic acid
ECM	Extra-cellular matrix
EDTA	Ethylenediaminetetraacetic acid
EDX	Energy Dispersive X-Ray Spectroscopy
ESC	Embryonic stem cell

FBS	Fetal bovine serum
FDA	The Food and Drug Administration
FTIR	Fourier Transform Infrared Spectroscopy
GPC	Gel permeation chromatography
GPTMS	(3-Glycidoxypropyl)trimethoxysilane
HA	Hydroxyapatite
HCA	Hydroxy carbonate apatite
hMSC	Human bone marrow-derived mesenchymal stem cell
ICP-OES	Inductively coupled plasma optical-emission spectroscopy
ICPTES	(3-Isocyanatopropyl)triethoxysilane
iPSC	Induced pluripotent stem cell
MEK	Methyl ethyl ketone
MEM	Minimal essential medium
Micro-CT	Micro computed tomography
MW	Molecular weight
NMR	Nuclear Magnetic Resonance Spectroscopy
O/I	Organic/inorganic
OCN	Osteocalcin
OCP	Octacalcium phosphate
OCT	Optimal cutting temperature
OPN	Osteopontin
PBS	Phosphate-buffered saline
PCL	Polycaprolactone
PDI	Polydispersity index
PDLLA	Poly (D,L-lactic acid)
PDMS	Polydimethoxysilane
PEG	Polyethylene glycol
PFA	Paraformaldehyde
PGA	Polyglycolic acid
PHA	Polyhydroxyalkanotes

PLA	Poly (L-lactic acid)
PLGA	Poly (lactic-coglycolide)
PMMA	Poly(methyl methacrylate)
Poly(VP-co-TEVS)	Poly(vinyl pyrrolidone-co- triethoxy vinyl silane)
PPF	Poly (propylene fumarate)
PVA	Polyvinyl alcohol
PVP	Polyvinylpyrrolidone
RNA	Ribonucleic acid
SBF	Simulated body fluid
SD	Standard deviations
SEM	Scanning Electron Microscopy
TBPC	Trabecular bone-derived progenitor cell
TEOS	Tetraethyl orthosilicate
TEP	Triethyl phosphate
TEVS	Triethoxyvinylsilane
TGA	Thermogravimetric Analysis
THF	Tetrahydrofuran
TMB	Trimethyl borate
TMSPMA	3-(Trimethoxysilyl)propyl methacrylate
UCS	Ultimate compressive stress
VP	N-Vinyl pyrrolidone
XPS	X-Ray Photoelectron Spectroscopy
XRD	X-ray Diffraction
β -TCP	Beta-tricalcium phosphate
γ -PGA	γ -Polyglutamic acid

Chapter 1

Introduction

1.1 Overview

Bone is a major structural tissue of the human body that provides support and protection of various organs, regulates blood pH, produces bone marrow cells, and stores minerals and multiple progenitor cells (haematopoietic and mesenchymal) [1-5]. Bone related disorder and subsequent bone loss is major burden in terms of quality of life, health care costs and economic impact. According to CIHR reports, injuries of musculoskeletal tissues and disorders cost the Canadian economy billions of dollars each year and exert a physical, mental and emotional toll both on those who suffer from them and on their families [6]. Bone injuries and defects can arise from a variety of causes, including bone disease such as osteoporosis [7], osteoarthritis [8], osteogenesis imperfecta [9], osteomyelitis [10] etc., traumatic injury, orthopedic surgeries (i.e., total joint arthroplasty, spine arthrodesis, implant fixation, etc.) [11] and primary tumor resection [12].

For critical-sized bone defects, a biomaterial must be used to fill the gap or non-union. The current “gold standard” treatment of critical-sized bone defects is autogenous bone grafting in which, bone graft is collected from patient’s own body (typically from the pelvis or iliac crest). However, the availability of autogenous bone graft is limited and causes severe complications such as donor site morbidity, pain, paresthesia, prolonged hospitalization and rehabilitation, increased risk of deep infection, hematoma, inflammation, etc. [13]. Bone tissue collected from other humans (typically cadavers), also known as allograft can be another option. Allografts carry risks of donor to recipient infection and disease transmission, and host immune responses [13-15]. Another source of bone tissue can be non-human which are xenografts for bone repair or replacement. However,

bone xenografts are now widely considered to be unsuitable for transplantation due to real and perceived risk of disease or virus transmission, infection, toxicity associated with sterilization, immunogenicity, and finally host rejection [16-18].

Bone tissue engineering is the viable alternative strategy to overcome the above-mentioned limitations of autograft, allograft and xenograft. The key components of bone tissue engineering are a three-dimensional (3D) scaffold biomaterial to guide the bone regeneration, bone forming cells to lay down the extracellular matrix on the scaffolds and the environment to mature the tissue construct [19-21]. This research project was focused on developing multifunctional and bioactive scaffolds for bone tissue engineering applications.

Over the last few decades, significant studies have been conducted to fabricate suitable scaffold for bone regeneration [19, 21, 22]. These scaffolds may be fabricated from metals, ceramics, natural or synthetic biopolymers, or composites to mimic the 3D matrices of native bone tissue. Metals are bio-inert and possess challenge to osseointegrate with newly native tissue [23, 24]. Several biodegradable natural and synthetic polymers and bioceramics have been studied so far as scaffold materials for bone tissue engineering. Among these biomaterials, silica, calcium and phosphate based sol-gel derived bioactive glasses (BG) attracted the most attention; however, their brittleness and difficulty to process in the form of tough 3D porous structure, restricted their application for bone regeneration [25]. Biocompatible and biodegradable polymers are easier to process, but lack mechanical properties to match with the bone tissue [25].

Ideally, scaffolds for bone tissue engineering should be osteoinductive, osteoconductive, porous and biodegradable, properties that will support the attachment and proliferation of osteoblasts,

enhance bone formation and angiogenesis, and degrade at suitable rate so that the newly formed bone can replace the biomaterials [19, 21]. The scaffold must be mechanically competent to support the bone formation. As a single material cannot provide all these requirements, bioactive composites, made of organic and inorganic bone-bioactive materials, could be good candidates for this application. However, conventional composites consist of distinct phases, resulting in non-uniform physical, chemical, mechanical and biological properties, making them unsuitable as bone biomaterials [25].

As the extracellular matrix of bone is primarily collagen and hydroxyapatite with molecular interactions between them, a logical strategy for bone tissue engineering is to develop hybrid biomaterials. These could be class I hybrids that are characterized by weak interactions, such as hydrogen bonds and/or van der Waal's forces, between components [26]. Alternatively, these could be class II hybrids that are characterized by stronger interactions, such as covalent bonding, between the organic and inorganic components [27]. As hybrid biomaterials exhibit single phases on molecular or macromolecular level, careful choice of both the organic and/or inorganic moieties and the synthesis approach affords to design novel materials with tailored properties for a biological environment.

1.2 Thesis outline

The overall objective of this research is to synthesize class II hybrid biomaterials to enhance bone formation *in vitro*. This thesis is divided into 7 Chapters. Detailed literature review is presented in Chapter 2. In Chapter 3, synthesis and characterization of a set of class II hybrid biomaterials from

polycaprolactone and borophosphosilicate glass (PCL/BPSG) through non-aqueous sol-gel synthesis is described [28]. To overcome the limitations of polymer solubility in aqueous medium, non-aqueous sol gel process was successfully utilized. Chapter 4 describes the effect of covalent cross-linking between the organic and inorganic phases on mechanical properties, degradation and biocompatibility of class II hybrid materials [29]. In Chapter 5, the detail analysis of microstructure and porosity of PCL/BPSG hybrid scaffolds, and osteogenic differentiation of stem cells seeded on these scaffolds were evaluated. Chapter 6 describes the synthesis and characterization of a different class II hybrid system from polyvinylpyrrolidone (PVP) and calcium-based bioactive glass. This chapter also discusses how functionality in polymer chain and O/I ratios affect the degree of covalent cross-linking, biodegradation and mechanical properties of hybrid biomaterials. Finally, the significance, contributions, and limitations of this research and suggestions for future work are outlined in Chapter 7.

1.3 References

- [1] Kane R, Ma PX. Mimicking the nanostructure of bone matrix to regenerate bone. *Materials Today* 2013;16:418-23.
- [2] Riddle RC, Clemens TL. Bone Cell Bioenergetics and Skeletal Energy Homeostasis. *Physiological Reviews* 2017;97:667-98.
- [3] Findlay DM. Biology of Bone and the Interaction of Bone with Other Organ Systems. In: Pivonka P, editor. *Multiscale Mechanobiology of Bone Remodeling and Adaptation*. Cham: Springer International Publishing; 2018. p. 259-87.
- [4] Morrison SJ, Scadden DT. The bone marrow niche for haematopoietic stem cells. *Nature* 2014;505:327-34.
- [5] Abdel Meguid E, Ke Y, Ji J, El-Hashash AHK. Stem cells applications in bone and tooth repair and regeneration: New insights, tools, and hopes. *Journal of Cellular Physiology* 2017;233:1825-35.
- [6] Institute of Musculoskeletal Health and Arthritis Strategic Plan 2014–2018: Enhancing Musculoskeletal, Skin and Oral Health. Canadian Institutes of Health Research 2014.

- [7] Schuit SCE, van der Klift M, Weel AEAM, de Laet CEDH, Burger H, Seeman E, et al. Fracture incidence and association with bone mineral density in elderly men and women: the Rotterdam Study. *Bone* 2004;34:195-202.
- [8] Buckwalter JA, Brown TD. Joint Injury, Repair, and Remodeling: Roles in Post-Traumatic Osteoarthritis. *Clinical Orthopaedics and Related Research* 2004;423:7-16.
- [9] Rauch F, Glorieux FH. Osteogenesis imperfecta. *The Lancet* 2004;363:1377-85.
- [10] Lew DP, Waldvogel FA. Osteomyelitis. *The Lancet* 2004;364:369-79.
- [11] Pape H-C, Giannoudis P, Krettek C. The timing of fracture treatment in polytrauma patients: relevance of damage control orthopedic surgery. *The American Journal of Surgery* 2002;183:622-9.
- [12] Phukan R, Herzog T, Boland PJ, Healey J, Rose P, Sim FH, et al. How Does the Level of Sacral Resection for Primary Malignant Bone Tumors Affect Physical and Mental Health, Pain, Mobility, Incontinence, and Sexual Function? *Clinical Orthopaedics and Related Research* 2016;474:687-96.
- [13] Giannoudis PV, Dinopoulos H, Tsiridis E. Bone substitutes: An update. *Injury* 2005;36:S20-S7.
- [14] Palmer SH, Gibbons CLMH, Athanasou NA. The pathology of bone allograft. *Journal of Bone & Joint Surgery, British Volume* 1999;81-B:333-5.
- [15] Geisinger JR, Park DK. Allograft bone: Uses in spinal surgery. *Seminars in Spine Surgery* 2016;28:190-5.
- [16] Oryan A, Alidadi S, Moshiri A, Maffulli N. Bone regenerative medicine: classic options, novel strategies, and future directions. *Journal of Orthopaedic Surgery and Research* 2014;9:18.
- [17] Kao ST, Scott DD. A Review of Bone Substitutes. *Oral and Maxillofacial Surgery Clinics of North America* 2007;19:513-21.
- [18] Tovar N, Jimbo R, Gangolli R, Perez L, Manne L, Yoo D, et al. Evaluation of bone response to various anorganic bovine bone xenografts: an experimental calvaria defect study. *International Journal of Oral and Maxillofacial Surgery* 2014;43:251-60.
- [19] Bose S, Roy M, Bandyopadhyay A. Recent advances in bone tissue engineering scaffolds. *Trends in biotechnology* 2012;30:546-54.
- [20] Porter JR, Ruckh TT, Popat KC. Bone tissue engineering: A review in bone biomimetics and drug delivery strategies. *Biotechnology Progress* 2009;25:1539-60.
- [21] Khan Y, Yaszemski MJ, Mikos AG, Laurencin CT. Tissue Engineering of Bone: Material and Matrix Considerations. *JBJS* 2008;90:36-42.
- [22] Chen F-M, Liu X. Advancing biomaterials of human origin for tissue engineering. *Progress in Polymer Science* 2016;53:86-168.

- [23] Lopez-Heredia MA, Sohier J, Gaillard C, Quillard S, Dorget M, Layrolle P. Rapid prototyped porous titanium coated with calcium phosphate as a scaffold for bone tissue engineering. *Biomaterials* 2008;29:2608-15.
- [24] Hughes TB. Bioabsorbable Implants in the Treatment of Hand Fractures: An Update. *Clinical Orthopaedics and Related Research* 2006;445:169-74.
- [25] Jones JR. Review of bioactive glass: From Hench to hybrids. *Acta Biomaterialia* 2013;9:4457-86.
- [26] Allo BA, Rizkalla AS, Mequanint K. Synthesis and Electrospinning of ϵ -Polycaprolactone-Bioactive Glass Hybrid Biomaterials via a Sol–Gel Process. *Langmuir* 2010;26:18340-8.
- [27] KICKELBICK G. Introduction to Hybrid Materials. *Hybrid Materials: Wiley-VCH Verlag GmbH & Co. KGaA*; 2006. p. 1-48.
- [28] Mondal D, Rizkalla AS, Mequanint K. Bioactive borophosphosilicate-polycaprolactone hybrid biomaterials via a non-aqueous sol gel process. *RSC Advances* 2016;6:92824-32.
- [29] Mondal D, Dixon SJ, Mequanint K, Rizkalla AS. Mechanically-competent and cytocompatible polycaprolactone-borophosphosilicate hybrid biomaterials. *Journal of the Mechanical Behavior of Biomedical Materials* 2017;75:180-9.

Chapter 2

Literature Review

Overview: This chapter provides background information on bone tissue engineering, and brief overview on developing biomaterial scaffolds for bone regeneration. Detailed literature survey on bioactive and degradable biomaterials for bone tissue engineering scaffold is presented with a focus on bioceramics, polymers, bioactive glass/polymer composites and hybrid biomaterials. In addition, different techniques for fabricating three-dimensional porous scaffold of hybrid biomaterials are discussed. An outline of hypothesis and specific objectives are described at the end.

2.1 Bone tissue engineering

For critical-sized bone defects, normal physiologic process for bone healing is not adequate to repair the damage. A bone substitute material must be used to repair this type of defects. The current gold standard is using patient's own bone, which is called 'autograft', generally collected from pelvic or iliac crest. Autografts enhance bone healing because they contain osteogenic bone cells, marrow cells, osteoinductive proteins and factors and an osteoconductive extracellular matrix (ECM) which promotes cell attachment and migration [1]. However, autografts are limited in volume and cause donor site morbidity. An alternative to autografts are allografts, in this case bone grafts are collected from other human sources (mainly from cadavers). They are also limited in their availability and pose risk of disease transmission from donor to recipient [2]. Bone grafts harvested from other animal sources (e.g. cows) are another option, but risk of disease transmission and immune-rejection are real challenges.

Tissue engineering is a multidisciplinary research field which apply knowledge of biology and engineering to develop functional substitutes same as autograft to repair damaged tissue [3]. It requires basic knowledge about the principles of new tissue formation, and applying this

knowledge to produce functional tissue grafts for clinical use [4]. By utilizing the progress in biomaterials science, knowledge of stem cells, growth and differentiation factors, and biomimetic environments, there are vast opportunities to fabricate tissues in the laboratory from combinations of engineered scaffolds, cells, and biologically active molecules.

In general, to engineer viable bone grafts by bone tissue engineering, a porous biomaterial scaffold is harvested with bone forming cells and mature the tissue constructs *in vitro* or *in vivo*. In case of both *in vitro* and *in vivo* culture conditions, it is required to carefully design the biomaterial scaffolds to encourage bone formation [5]. Responsive biomaterials which are capable of modified functionality in response to the dynamic physiological and mechanical environments found *in vivo*, will be suitable candidates for engineering bone tissue to achieve long-term repair and good clinical outcomes [6]. Bone grafts derived by mimicking natural *in vivo* conditions will eliminate the drawbacks and limitations of autografts and allografts and provide the best solution for replacing damaged bone tissue.

2.1.1 Elements of bone tissue engineering

In general, bone tissue engineering required three major components: (1) a porous three dimensional biomaterial scaffold that closely mimics natural bone extracellular matrix (ECM) and guide the new bone formation, (2) osteogenic cells to lay down bone tissue ECM and (3) a bioreactor (*in vitro* culture) to mature the tissue construct by providing all required nutrients, oxygen and bone inducing growth factors [7]. This section will highlight all these major components for bone tissue engineering.

2.1.1.1 Scaffolds

Scaffolds for bone tissue engineering are temporary templates with specific morphology, and biochemical and mechanical properties like bone ECM. Scaffolds act as a 3D support for cell adhesion, proliferation and differentiation, and guide subsequent new bone formation. Therefore, an ideal scaffold should be osteoconductive so that bone cells can adhere, function healthy, and migrate onto the surface and eventually through the scaffold and begin to proliferate before laying down new matrix [8]. To allow cell migration as well as metabolic waste removal and angiogenesis, the scaffold should have suitable pore size and interconnectivity [9]. Pore diameter of the scaffolds required to be larger than 100 μm for successful diffusion of necessary nutrients and oxygen for cell functionality [10]. Furthermore, pore sizes in the range of 200–350 μm are found to be optimum for cell infiltration and bone tissue in-growth [11]. The scaffold should also be osteoinductive so that it can induce new bone formation by recruiting progenitor cells through biomolecular signaling. Biodegradable materials need to be selected to prepare this scaffold and the degradation rate must be compatible with the rate of bone formation so that newly formed bone can replace the scaffold. If the scaffolds degrade faster than new bone formation, some parts of the scaffold will be lost before ECM formation and immature bone grafts with large gaps will be formed. In addition, rapid degradation causes mechanical instability of the scaffolds. On contrary, if the rate of degradation is slower than bone formation, newly formed ECM can cover up outer edges and necrotic core can be developed due to the limitations of cell infiltration and nutrient exchanges [12, 13].

2.1.1.2 Cell

To produce bone extracellular matrix (ECM) through the porous channels of a critical sized scaffold, an adequate number of bone forming cells are required. In normal physiologic conditions, for repairing injured tissues cell are the primary precursors for tissue development and homeostasis. In case of bone deposition, modeling, and remodeling osteoblast and osteocyte are the main stakeholders to produce bone ECM. Therefore, osteoblasts and/or their precursors are the primary cell sources to engineered bone grafts *in vitro* and *in vivo* [14].

Bone marrow derived stem cells (BMSC) can differentiate into multiple mesenchymal tissue lineages, including primary osteoblasts and form bone at normal physiologic condition [15]. It's easy accessibility and assurance of bone forming ability, made it most common choice for engineering bone grafts *in vitro* [16]. BMSCs are usually harvested from the marrow aspirate and grow on tissue culture plates, and can reach up to 50 population doublings in culture [17]. The initial number of BMSCs collected from bone marrow and their differentials potency to osteoblast lineage reportedly declines with the patient age [18]. It is necessary to apply the suitable cell phenotype for engineering bone tissues, but the exact phenotypic features are not always well defined. For engineering and regeneration of bone, the required features include good biosynthetic activity (for further development and integration into the scaffolds), expression of osteogenic markers (required for development of bone ECM), and phenotypic steadiness (to avoid non-specific tissue development) [19].

As an alternative to BMSCs, adipose tissue-derived stem cells (ASCs) are easily accessible and abundant source of autologous osteogenic cells [20, 21]. ASCs may survive in low oxygen and/or

glucose environments which are advantageous to fabricate bone constructs *in vitro* [22]. ASCs are capable of differentiating into osteogenic, adipogenic, myogenic, and neurogenic lineages [23, 24].

ASCs and BMSCs have known limitations, such as their proliferation and differentiation potentials are limited and drastically decrease after several passages, resulting in a restriction of their application in regenerative medicine [25]. Alternatively, embryonic stem cells (ESCs) have unlimited proliferation and differentiation potentials. However, ESCs cannot be established from adult cells, therefore it is impossible to make patient-derived ESCs to be used as autogenous grafts, which avoid transplantation rejection. On the other hand, induced pluripotent stem cells (iPSCs) have unlimited proliferation and differentiation potential equivalent to ESCs [26, 27]. iPSCs can be generated from both ASCs and BMSCs, as well as from adult somatic cells (e.g., human dermal fibroblasts) even after their terminal differentiation [28]. The discovery of methods to convert somatic cells into iPSCs through expression of a small combination of transcription factors has raised the possibility of producing custom-tailored cells for bone regeneration *in vitro*.

Another cell source for bone tissue engineering is trabecular bone-derived progenitor cells (TBPCs). Progenitor cells isolated from trabecular bone—or spongy bone—have osteogenic potential that can be used to engineer new bone. These TBPCs displayed higher osteogenic potential with ALP expression than BMSCs *in vivo* and more ectopic bone was formed after 5 weeks of transplantation [29]. Despite its availability and easy-processing, harvesting TBPCs also causes donor-site morbidity similar as BMSCs.

2.1.1.3 Bioreactor

Strategies for *in vivo* bone tissue engineering enclose the combined use of autologous bone-forming cells, porous 3D scaffolds as structural support for the cells, and bioreactors for studying and mimicking *in vivo* conditions as *in vitro* environment for the growth of tissue substitutes [30]. Bioreactors are designed to develop biological processes by closely monitoring and controlling the environment. In general, the bioreactor facilitates homogenous cell distribution, provides and maintains the physiological environment of the cell (e.g., nutrients, oxygen, growth factors), increases mass transport into the scaffolds, and exposes cells to mechanical stimuli [31]. Design parameters involve controlling and optimizing temperature, pH, oxygen diffusion, nutrient transport, waste removal, etc. to facilitate the *in vitro* development of new tissue by providing biochemical and physical regulatory signals to cells, enhancing differentiation and producing autologous bone graft prior to *in vivo* implantation. Cell expansion in 3D fashion is the major concern to design the bioreactor. In 3D culture condition, insufficient diffusion of nutrients to cells and removal of waste metabolites from the interior of the scaffold restrict tissue growth [32]. It requires complex and dynamic bioreactor culture systems to overcome this problem [33]. One of the advantages of dynamic culture condition is generating controlled fluid shear stress due to the mixing or perfusion of the medium because it exposes the cells to mechanical stimulation. It has shown that, mechanical stimulation increases production of prostaglandins, alkaline phosphatase, collagen type I, along with osteoblast proliferation and mineralization [34, 35]. Bioreactors are also used to improve cellular spatial distribution by controlling the media flow rate. Several types of bioreactors have been used for bone tissue engineering *in vitro*, such as Rotating Wall Vessel

Bioreactors, Spinner Flasks, Indirect and Direct Perfusion Bioreactors, Compression Bioreactors, etc. [31].

The work presented in this thesis focuses on preparing a series of novel biomaterials for bone tissue engineering scaffolds and related applications. As mentioned above in section 2.1.1.1, scaffolds should provide the microenvironment for bone forming cells, support attachment, proliferation, differentiation, and guide osteogenesis – in general, acting as a temporary synthetic ECM. Bone is a complex biological system. Therefore, developing biomaterials for bone tissue engineering scaffolds is diverse and extremely challenging [36]. The biomaterial must possess physical, mechanical and biochemical properties to fulfil the structural and multifunctional requirements while molded into porous 3D scaffolds. In view of this, the development of a suitable biomaterial based 3D scaffold is an essential component for bone tissue engineering strategy.

2.2 Materials for bone tissue engineering scaffolds

Development of suitable materials for bone tissue engineering scaffolds is manifold and extremely challenging. Several materials have been characterized and proposed as potential biomaterials for fabricating bone tissue engineering scaffolds. However, as the biodegradability is one of the major concerns, the choice of materials is limited to degradable bioceramics and biopolymers [37]. The following section will discuss some of the fundamental features of these potential biomaterials.

2.2.1 Bioceramics

Bioceramics are ceramic materials which are biocompatible and interact with living tissues. They are mainly metal oxides, phosphates, nitrides, carbides and glasses. Non-degradable bioceramics

form a non-adherent necrotic core isolated from surrounding bone. For this reason, research efforts at the end of the past century were devoted to biodegradable and bioactive bioceramics for tissue engineering applications [38]. Among several types of bioceramics, calcium phosphates (CaPs) and bioactive glasses (BGs) are of particular interest, since they can mimic natural bone's inorganic constituents, and are osteoconductive and degradable.

2.2.1.1 Calcium phosphates

Calcium phosphates (CaPs) are osteoconductive, bioresorbable and mimic the inorganic constituents of natural bone which is a calcium phosphate in the form of carbonate apatite nanocrystals [39, 40]. Synthetic CaPs have been used for bone and tooth repair since 1980s. Based on composition, current commercial calcium phosphates for bone and tooth repair are classified as (1) calcium-deficient apatite, CDA (i.e., Ca/P molar ratio less than the stoichiometric value of 1.67 for pure HA), (2) hydroxapatite (HA), $\text{Ca}_{10}(\text{PO}_4)_6(\text{OH})_2$, (3) beta-tricalcium phosphate (β -TCP), $\text{Ca}_3(\text{PO}_4)_2$, and (4) biphasic calcium phosphate (BCP), an intimate mixture of HA and β -TCP of varying HA/ β -TCP weight ratios. CaPs powder can be prepared by a variety of wet chemical methods (such as precipitation, hydrolysis, hydrothermal etc.) and solid-state reactions [40-43]. The synthesis of compact and dense CaPs powder or scaffolds for bone regeneration often requires high temperature sintering at 1000-1200 °C.

Degradation of CaPs *in vitro* or *in vivo* depends on their composition, physical shape, crystallinity, porosity, and preparation conditions [44-46]. Several *in vitro* and *in vivo* experiments have proven that the degradation or rate of dissolution proceeds in the following decreasing order: Amorphous

HA > α -TCP > β -TCP > crystalline HA. In the case of BCPs, degradation depends on the HA/ β -TCP ratio: the higher the ratio, the lower the degradation rate [47]. The rate of synthetic unsintered CaPs degradation decreases in the order ACP > OCP > CDA.

Bioactivity of CaPs bioceramics have been observed by direct attachment to native bone on HA-coated biomaterials surface or as composites, while fibrous tissue encapsulates the uncoated surface [48-51]. Biomimetic carbonated apatite formation on CaP surfaces in SBF as *in vitro* bioactivity were also evidenced by the uptake of calcium and phosphate ions from the solution [52, 53]. CaPs allow osteoblast cells to attach, proliferate, and differentiate [54]. Differentiating osteoblast cells seeded on BCPs, produce collagen (type 1), alkaline phosphatase, proteoglycans (decorin, lumican, biglycan), and matrix proteins (osteocalcin, osteopontin and bone sialoprotein) known to signify bone formation [55-57]. CaPs coatings on bioinert material for total joint arthroplasty has shown improved osseointegration at bone/implant interface resulting in superior implant stability [58]. Ectopic bone formation *in vivo* was also evidenced when CaPs coated implants were inserted in non-osseous sites [59, 60].

Despite their osteoconductive nature, the synthesis of compact and dense HA and TCP scaffolds for bone regeneration often requires high temperature sintering and are poorly degradable in their highly crystalline form, while their amorphous counterparts are mechanically too brittle to be used for fabrication of highly porous scaffolds [38, 61]. Sintered HA at high temperature exhibited high chemical stability in contact with tissue fluids, which leads to limited bioactivity and osteoconductive effect [62]. Instead, their amorphous counterparts are characterized by a high dissolution rate *in vivo*, which accelerates material desorption and incomplete tissue formation.

2.2.1.2 Bioactive glasses

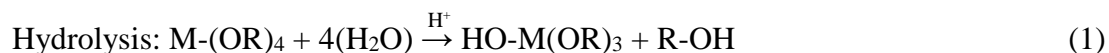
Bioactive glasses (BGs) are a class of non-crystalline silicate glasses which can stimulate bone-like mineral formation (hydroxy carbonate apatite, HCA) in presence of physiological fluids. HCA is similar to inorganic constituent of natural bone and it is believed that HCA layer interact with bone ECM to bond with the native bone [63]. BG was first invented at 1969 and consisted of 46.1 mol.% SiO₂, 24.4 mol.% Na₂O, 26.9 mol.% CaO and 2.6 mol.% P₂O₅, later named as 45S5 and Bioglass®, formed strong bond with native bone during *in vivo* studies due to the HCA layer formation at bone-implant interfaces following dissolution of glass materials [64]. Since then several types of BGs have been developed by varying the compositions of constituents such as silicate-based, phosphate-based and borate-based glasses [65, 66].

Silicate based BGs are referred to those glasses in which (SiO₄)⁴⁻ acts as the main 3D glass-forming networks. The SiO₂ concentration in silicate-based glasses varied from 45 - 71 wt%. Other components such as Na₂O, K₂O, MgO, CaO, P₂O₅ etc. used at various amounts as network modifiers [65, 67-69]. Phosphate-based glasses have [PO₄]³⁻ structural unit as main network former and CaO and Na₂O as modifiers. Many studies have shown their potential for tissue engineering applications [70, 71]. Phosphate-based glasses have a chemical affinity towards bone due to the similarity of inorganic phases of bone. These type of BGs have high dissolution rate in aqueous media due to the ease of P-O-P bond hydration [72, 73]. As their dissolution rate is strongly composition dependent and can be tailored by adding appropriate metal oxides, such as TiO₂, CuO, NiO, MnO, Fe₂O₃ etc. to the glass composition, they have been widely investigated as controlled release vehicles for antibacterial ions for tissue engineering [74, 75].

Recent investigations have shown that borate-based BGs are bioactive and due to their faster rate of dissolution they enhanced HCA mineral formation *in vitro*, when compared to some silicate-based glasses [76-79]. Boron containing BGs inhibits the formation of slightly more stable SiO₂-rich layer at early stage of dissolution in physiologic medium, which results in faster rate of dissolution and rapid HCA formation [65, 66, 76, 79, 80]. For bone tissue engineering applications, tailoring the rate of degradation of biomaterial scaffold is vital. Modification of BG composition can allow us to control their degradation rate *in vitro* and enhance the regeneration of bone. For instance, by partially replacing the SiO₂ in silicate-based BGs with B₂O₃, the degradation rate can be varied over a wide range [78, 79]. This way it is possible to match the degradation rate of borate-based BGs with the rate of *de novo* bone ECM formation.

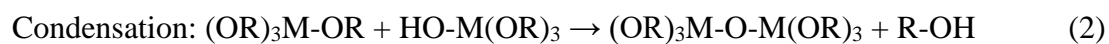
Initially BGs were synthesised through melt-quenching techniques by mixing and melting ceramic powders such as SiO₂, P₂O₅, CaO, Na₂O etc. above 1300 °C, followed by quenching in graphite mold or in cold water [64]. Since then, BGs were prepared this way until the early 1990s when sol gel synthesis of BGs was introduced [81, 82]. The sol-gel synthesis route allows chemistry-based room-temperature synthesis of BGs where colloidal suspensions (sol) of glass precursors undergo a series of hydrolysis and poly-condensation reactions to form a gel. The gel is an inorganic network of covalently bonded glass components, which can then be dried to become a glass monolith. The glass precursors are in the form of metal alkoxides and have the generic structure M-(OR)_x, where a central metallic ion (M) is bound to functional organic groups, mainly alkyl (-OR). Metal alkoxides, such as tetraethyl orthosilicate (TEOS) or tetramethyl orthosilicate (TMOS) are often used as SiO₂ precursors and triethyl phosphate (TEP) as P₂O₅ due to their abilities to readily react with water. The acid or base catalyzed hydrolysis reaction results in the replacement

of alkoxy side chains with hydroxyl groups. Hydrolysis occurs through a nucleophilic attack on the core atom (e.g. Si) by the oxygen atom in the water molecule [82].



Where, $-\text{R}$ represents an alkoxy functional group, e.g., $\text{C}_2\text{H}_5\text{O}-$.

Subsequent poly-condensation reactions result in covalently bonded inorganic glass network formation.



The nature of final inorganic glass networks depends on pH, acid or base catalysts, solvent-reactant ratios and precursor molecules [83]. Major differences between melt and sol gel derived BGs are that sol gel glasses tend to have higher purity, homogenous microstructure, and nanoporosity, whereas melt-quenched BGs have heterogenous phase distribution and dense microstructure [84]. The increased nanoporosity and surface area allow improved cellular response and bioresorbability of the BGs [85]. In addition, due to the room-temperature synthesis, there is no need to include Na_2O to decrease the melting temperature and presence of large number of silanol groups in the external surface of BG network enables the organic modification of the glass which is essential to prepare osteoinductive organic-inorganic hybrid scaffolds, by grafting the biomaterials with different active agents, such as certain peptides, proteins and growth factors.

Boron as a trace element is required for maintaining bone health [86]. Borate-based BGs support cell proliferation along with differentiation *in vitro*, whereas *in vivo* studies reported that Boron enhances tissue infiltration [87-89]. These BGs also have shown to serve as a substrate for drug release in the treatment of bone infection [90-92]. Despite their excellent bioactivity, some investigations indicated that certain compositions of borate-based BGs exhibited cytotoxicity under static *in vitro* culture conditions, whereas no considerable toxicity was detected under dynamic culture [79, 92]. A scaffold made of borate-based BG by replacing all the SiO_2 with B_2O_3 , were found to be toxic to murine MLO-A5 osteogenic cells *in vitro* [89]. However, the same scaffolds did not show any toxicity to cells *in vivo* and supported new tissue infiltration when implanted subcutaneously in rats [89, 93]. The concentration of boron in culture media entirely depends on initial composition of B_2O_3 in glass and it can be regulated by optimization. The adhesion and proliferation of bone marrow stromal cells were enhanced due to conversion of the glass to HCA, when borate ions were released into the culture media from BG containing low boron initially [66]. Osteoconductivity and bioactivity of borate-based BGs make them very promising candidates for bone tissue engineering applications.

Major disadvantages of BGs are their stiffness and requirement of high temperature to process into desired shapes rather than just powders. In addition, it is challenging to prevent cracks during the drying stage of sol gel derived BGs. Cracking occurs due to the large shrinkage during drying, and evaporation of the liquid by-products of the condensation reaction. When liquids from pore vicinity are removed from the gels, they must travel from within the gel to the surface via the interconnected pore network. This causes capillary stresses within the pore network and therefore cracking occurs [63]. For powders, coatings or fibres, the capillary stresses are nominal, as the

evaporation path is short and the stresses can be accommodated by the material. For monolithic objects such as scaffolds, the path from the centre of the monolith to the surface is long and tortuous, and the drying stresses can introduce catastrophic fracture with increasing pore size and obtaining pores with a narrow distribution. These disadvantages can be overcome by preparing composites of BGs with degradable biopolymers.

2.2.2 Biocompatible and degradable polymers

Both natural and synthetic biocompatible polymers have been widely investigated for bone tissue engineering applications [94-97]. The main sources of natural biodegradable polymers are proteins such as collagen, gelatin, albumin etc., and polysaccharides such as cellulose, hyaluronate, chitin, alginate, etc. Synthetic polymers such as polyglycolic acid (PGA), poly (L-lactic acid) (PLA), poly (lactic-co-glycolide) (PLGA), polycaprolactone (PCL), poly (propylene fumarate) (PPF), polyhydroxyalkanoates (PHA), polyamides, poly (orthoesters), polyvinylpyrrolidone (PVP), polyphosphazene, etc. are prominent candidates for bone tissue engineering applications. Although naturally derived polymers have shown better cell-material interactions, major drawbacks such as their availability in large amounts, difficulties in processing and purification had encouraged researchers to explore the use of synthetic polymers [95, 98]. Synthetic polymers are advantageous compared to natural polymers since their properties (e.g., porosity, degradation rate, and mechanical properties) can be tailored for specific applications. Synthetic polymers are often more available than naturally derived polymers, they can be produced in large uniform quantities and have a long shelf time. Many commercially available synthetic polymers exhibit physicochemical and mechanical properties comparable to those of biological tissues. They

exhibit, in general, predictable and reproducible mechanical and physical properties such as tensile strength, elastic modulus, and degradation rate. These materials can be easily manufactured into differing shapes and their physical and degradation properties can be tailored for specific application.

Although poly (α -hydroxy esters) polymers such as PGA, PLA, PCL and their co-polymers are degraded by hydrolysis and can be metabolized and excreted, their biocompatibility sometimes are challenged by the acidic degradation products [99]. Moreover, polymer biomaterials, in general have limited strength and mechanical stability when made with large volume fractions of macroporosity, which is a critical design consideration for tissue regenerative materials. These polymers undergo a bulk erosion process such that can cause scaffolds to fail prematurely [100]. In addition, they are not osteoconductive and do not adequately promote bone cells to adhere, grow and proliferate.

The scaffolds applied for bone tissue engineering should be osteoconductive and osteoinductive, having suitable porous 3D microstructure to allow cell infiltration, tissue growth and metabolic waste removal. Their rate of degradation should also be compatible with the rate of new bone formation so that the newly formed bone can replace the scaffold. One of the challenges associated with developing scaffolds for bone tissue engineering is that, no single material meets the above-mentioned properties. Composites of materials with desired properties consisting of organic and inorganic components have been proposed to be a solution to this problem.

2.2.3 Bioactive glass based organic/inorganic composites

Organic/inorganic (O/I) composites prepared from BGs and biodegradable polymers gained much attention due to the advantages of combining their properties, and possibility to obtain required bioactivity, degradation behavior and mechanical properties for bone tissue engineering scaffold. Toughness and process-ability of polymers can be added with excellent bioactivity of BGs by preparing composite materials [37]. Generally, these composites were prepared by using the polymers as matrix and BG powders as filler. Composite scaffolds prepared with BGs and polymers such as PCL, PLA, PGA, PLGA, PDLLA, etc. have shown improved mechanical properties compare with pure BGs or pure polymers [101-105]. Thin coating of PDLLA [106] or PHB [107] also have been applied to BG foam scaffolds to improve the fracture resistance. However, the efficacy of enhancing bioactivity or improving mechanical properties through introducing BG in polymer-coated scaffolds is questionable since coated polymer would cover BG surfaces until the polymer is fully degraded and when it degrades only the brittle BG scaffold will be left [63]. This is also true for conventional composites where micron or nano-sized BG particles are embedded in a polymer matrix, and bone cells come into contact with the polymer mostly. Thus the resultant bioactivity and cell-material interactions decrease for such composite biomaterials [63]. Preparing composites of BGs and bioresorbable polymers also modify the degradation behavior of polymers. Polymers degrades with acidic by-products may cause toxicity to cells, while BG degrades with releasing cations which can buffer the acidic by-products and maintain neutral pH at O/I interfaces [103, 108]. BGs are hydrophilic and incorporation of BGs in hydrophobic polymer matrices also alters the surface and bulk properties of O/I composite scaffolds by increasing the hydrophilicity and water absorption, hence modifies the degradation

kinetics [109]. However, it is difficult to match the degradation rates of the two components in O/I composites [110]. In ideal condition, both the polymer and BG phases should degrade in consort and at a suitable rate so that the scaffolds can gradually replace by the newly formed tissue, as well as can maintain their mechanical integrity to support themselves and guide bone regeneration. In conventional O/I composites, different phases degrade at different rates, which cause non-uniform dissolution and mechanical instability of the scaffolds. An alternative way to overcome these non-uniform properties is to produce O/I nanocomposites in which BG nanoparticles or nanofibers are blended with polymer matrix [111].

O/I nanocomposites prepared with nano-sized BG filler provide larger surface area compared to conventional composites (prepared with micron-sized BG particles). This increased surface area of bioactive BG positively affects the cell-material interactions. Nanoparticles of bioceramics enhanced protein adsorption and osteoblast adhesion when compared with their micron-sized counterparts [112]. To yield O/I nanocomposites with improved bioactivity, cell-material interactions and mechanical properties, the nanoparticle size is an important parameter. It was observed in a detailed study on porous 3D PLLA/BG nanocomposite scaffolds that addition of BG nanoparticles up to 20 wt% did not change their morphology, but enhanced their bioactivity [113-115]. With increasing the amount of BG from 0 to 30 wt%, the compressive modulus of the nanocomposite scaffolds increased from 5.5 to 8.0 MPa. Incorporation of BG nanoparticles with PLLA matrix also assisted the increase in the equilibrium water uptake of the nanocomposite scaffolds and affected the rate of degradation. BG nanofibers were also used to fabricate nanocomposite scaffolds. Sol gel derived electrospun BG nanofibers [116] were combined with several biodegradable polymers. these resulted in good bioactivity, HCA deposition on their

surfaces when exposed to a SBF [117-119]. In addition, these nanocomposites induced the osteoblast-like cells attachment, spreading and proliferation *in vitro*. In general, O/I nanocomposites prepared with BG nanoparticles or nanofibers demonstrated better mechanical properties and cell-material interactions compared to the conventional micro-composites due to their higher surface area to volume ratio.

However, the challenge to synchronize the degradation rates of different phases in O/I nanocomposites still exists. The mismatch between the degradation rates of the different phases may cause failure in the long term *in vitro* operations. Moreover, nanoparticles are prone to particle agglomeration and homogenous distribution of inorganic BG particles in polymer matrix is difficult to achieve if there are no physical or chemical interactions between organic and inorganic phases [63]. A viable approach to achieve homogenous dispersion can be adding the polymer in the sol during sol gel synthesis of BG. However, without having bonding sites in the polymer chain, this causes organic inorganic phase separations and micro or nano-sized phases in the final composites [120]. Therefore, in view of above discussion, it is obvious that the molecular level interactions are required among the organic-inorganic phases to fabricate suitable biomaterial scaffolds for bone tissue engineering applications.

2.2.4 O/I hybrid biomaterial

Generally, O/I hybrid biomaterials are defined as organic and inorganic biomaterials blended on a molecular scale and the phases are indistinctive in and above nanoscale [121]. Interpenetrating networks of organic and inorganic biomaterials interact below nanoscale and form O/I hybrid biomaterials. Hybrids are different from nanocomposites, in which the phases in the hybrids are

indistinguishable on a nanoscale [122]. O/I hybrid biomaterials exhibit homogeneous dispersions of organic and inorganic components as building blocks or interpenetrating networks. Due to their high degree of organization on a molecular scale, hybrid biomaterials not only display intrinsic physical properties of the constituents organic and inorganic biomaterials, but also new properties as synergistic effects [123]. As both organic and inorganic components need be mixed on a molecular level, they require low temperature synthesis route such as sol gel process to prepare these biomaterials. The intimate molecular level interactions between phases promote the O/I hybrid material to act as a single phase material with advantages of tailorable mechanical, chemical, and physical properties [124, 125]. Since the chemical nature of organic and inorganic moieties are different, without having reactive sites in both components, phase separation can occur during the synthesis. Therefore, it is required to choose appropriate polymers or functionalize the polymer prior to synthesizing hybrid biomaterials that include BG as the inorganic component. Based on the nature of interactions, hybrid materials are categorized into two classes. Class I hybrids have weak molecular interactions between the organic and inorganic phases, such as van der Waals, hydrogen bonding or weak electrostatic interactions. Class II hybrids have strong chemical interactions such as covalent bonding between the components [121]. The following sections will discuss these two class of hybrid biomaterials and their applications as scaffold materials in bone tissue engineering.

2.2.4.1 O/I class I hybrid biomaterials

BG containing class I hybrid biomaterials are prepared through sol gel synthesis of inorganic BG in presence of polymer. During the formation of BG networks (Si-O-Si) through hydrolysis and

polycondensation of organic polymers entrapped within the inorganic glass network. The efficacy of class I hybrid formation entirely depends on the polymer interaction with the silanol (Si–OH) groups in the glass network. Reaction conditions and parameters are optimised carefully so that the organic phase cannot be separated or precipitated during sol to gel and gel to dry monolith conversions, and hence optically transparent class I hybrid biomaterials can be obtained.

Incorporation of PVA in inorganic BG networks during sol gel synthesis helped obtain bioactive and crack-free O/I class I hybrid monoliths [126]. However, excess PVA content resulted in rapid disintegration while exposed to a buffer solution. Similar studies have shown that up to 30 wt% PVA could be incorporated as PVA/BG hybrid [127, 128]. The application of PVP based hybrid scaffolds in bone tissue engineering is limited due to the non-biodegradability of PVP. Another major concern of class I hybrid synthesis is the polymer needs to be soluble in the sol during the sol gel process so that it does not precipitate in liberated ethanol or water during the process.

Allo *et al.* prepared PCL/BG class I O/I hybrid monoliths and their nanofiber mesh scaffolds through the sol gel process using methyl ethyl ketone (MEK) as a solvent for PCL (80 kDa) to avoid phase separation during the synthesis [129]. Detailed analysis had shown that class I hybrids were prepared with up to 60 wt% of PCL through hydrogen bonding among carbonyl groups of polymer backbone and silanol groups in BG. This hybrid had shown numerous HCA deposition on 2D monolithic surfaces while incubated in SBF, and favoured excellent MC3T3-E1 preosteoblastic cell attachment and proliferation [130]. While prepared as 3D electrospun fibrous scaffolds, these hybrids exhibited good mechanical properties, and early expressions of transcription-level collagen type I (Col I), alkaline phosphatase (ALP), osteopontin (OPN), bone

sialoprotein (BSP) and osteocalcin (OCN) genes [131]. This hybrid biomaterial has great potential for bone regeneration *in vitro*. However, degradation study for this hybrid has not been investigated. Another drawback of this material was that the electrospun fibrous scaffolds tended to have small pore size may alter cell infiltration and scaffold remodelling.

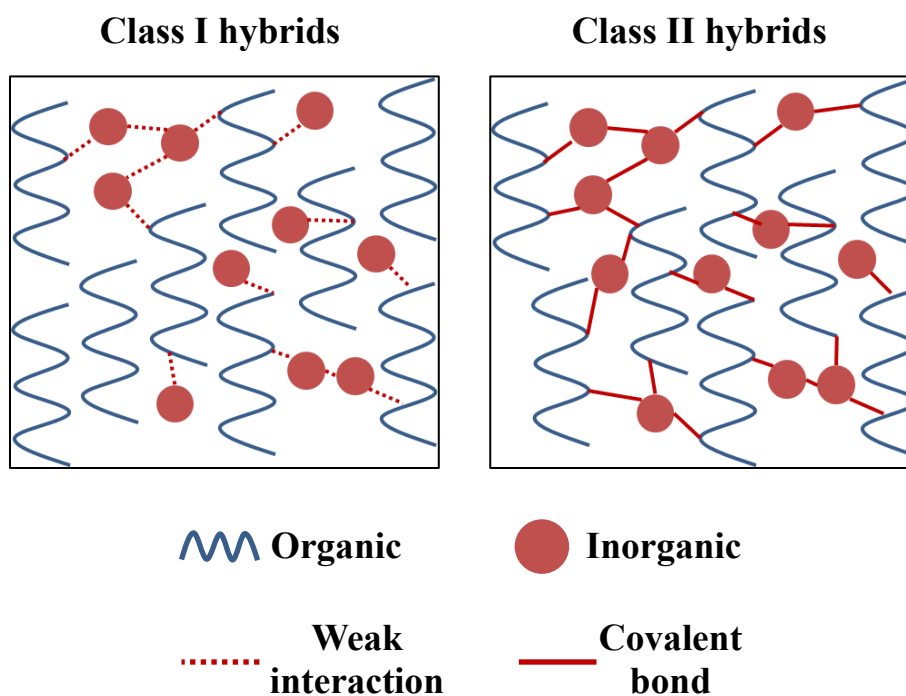


Figure 2. 1: Interactions between O/I phases in two classes of hybrid materials

2.2.4.2 O/I class II hybrid biomaterials

Although hydrogen bonding or weak interaction between the organic-inorganic moieties provides improved properties to the hybrid biomaterials compared to the conventional composites, long-term mechanical competency, predictable degradation behavior and uniform bioactivity can be achieved through strong chemical bonding between the organic and inorganic phases (class II

hybrids) [63]. Three different strategies are generally applied to synthesize class II hybrid biomaterials: i) The use of a coupling agent that can bond with both organic and inorganic phases, ii) The use of an organic polymer which is already containing trialkoxysilane ($-\text{Si}(\text{OR})_3$) functional group(s), and iii) in situ polymerization of organic and inorganic phases from their precursor monomers.

Covalent crosslinking between a degradable polymer and inorganic network can be obtained by using coupling agents. This strategy involves functionalizing the polymer with a coupling agent prior to introducing it in a sol gel process. The appropriate coupling agents should have alkoxy silane functional groups at one end and a functional group at the other end to bond with the polymer. Coupling agents such as (3-glycidoxypropyl)trimethoxysilane (GPTMS), (3-isocyanatopropyl)triethoxysilane (ICPTES), (3-aminopropyl)triethoxysilane (APTES) etc. have been used to functionalize the polymers (Table 2.1). Chitosan/ SiO_2 class II hybrids have been successfully prepared using GPTMS as coupling agent [132-134]. Epoxy groups from one end of GPTMS chemically bonded with $-\text{NH}_2$ groups of chitosan chain and trimethoxysilane groups from the other end went through hydrolysis and polycondensation reactions with TEOS to form organic-inorganic matrix. These hybrids have displayed tailorable hydrophilicity and controlled dissolution behavior as well as excellent cell-biomaterial interactions. PCL diol (a low molecular weight PCL end-capped with two $-\text{OH}$) was coupled with ICPTES prior to synthesizing class II PCL/ SiO_2 hybrid through reaction of $-\text{N}=\text{C}=\text{O}$ groups from ICPTES with $-\text{OH}$ [135, 136]. These studies have shown that coupling of PCL improved its solubility in the sol and the resultant hybrid had excellent mechanical properties. The lower molecular weight of the polymer assisted uniform HCA layer deposition due to the faster rate of dissolution of PCL and hence higher exposed surface area of

silica which might have acted as nucleation sites. The bioactivity and mechanical properties of these PCL/SiO₂ hybrids were dependant on the PCL content [135]. HCA deposition decreased with increment of PCL content, but toughness was increased.

Gelatin/SiO₂ class II hybrids were also prepared using GPTMS as coupling agent [137]. The dissolution of gelatin and silica decreased with the increase in the GPTMS amount due to the covalent cross-linking between organic-inorganic phases. The compressive properties were also increased with the increase in the covalent coupling. It has been observed that a two-fold increase in the GPTMS amount, resulted in 360% increase in the stiffness values. A major concern for using biopolymers such as gelatin is that the available functional groups are unknown and thus the amount of covalent crosslinking during the hybrid synthesis cannot be predictable. Another class II hybrid was produced using polyglutamic acid functionalized with GPTMS and SiO₂ as inorganic component [138]. This hybrid exhibited excellent bioactivity and cell-biomaterial interactions.

A disadvantage of using coupling agents for the synthesis of class II hybrids is that, these functionalized polymers provide a limited amount of functional groups related to the polymer backbone. Polymers with high molecular weight would have very poor interaction with inorganic phases and this may cause phase separation over a certain amount of organic moiety [139]. Degradable polymers with trialkoxysilane functional groups as side groups or pendant in polymer backbone can be better choice to synthesis O/I class II hybrids through sol gel process due to the predictability of degree of cross-linking regardless of molecular weight.

Polydimethoxysilane (PDMS) on the other hand is an example of a polymer that contains functional silane groups in its backbone as side groups. PDMS had has been used to prepare class

II hybrids by hydrolyzing with TEOS, and co-condensing it with Si-OH [140-142]. The *in vitro* bioactivity of these hybrids was dependant on incorporated Ca^{2+} in O/I networks evaluated after incubation in SBF [143, 144]. These studies have shown that bioactivity of these hybrids increased with higher inorganic content and therefore enhanced the mechanical properties. However, PDMS is not degradable, so its not suitable for bone regeneration.

Functionalization of the polymer with trialkoxysilane as side groups in the polymer backbone can be obtained easily by copolymerization of the monomer with an alkoxy silane monomer. Copolymer of polystyrene [145], poly(2-hydroxyethylmethacrylate) [146], acrylonitrile butadiene styrene [147], poly(methyl methacrylate) [148, 149] were prepared with several trialkoxysilyl ($-\text{Si}(\text{OR})_3$) monomers prior to introducing them into the sol gel process. However, these polymers that were used to make the hybrids were not biodegradable or water-soluble, which restricted their application for bone regeneration. Moreover, these materials contained SiO_2 as the only inorganic component and therefore they were not sufficiently bioactive to induce osteogenesis [63].

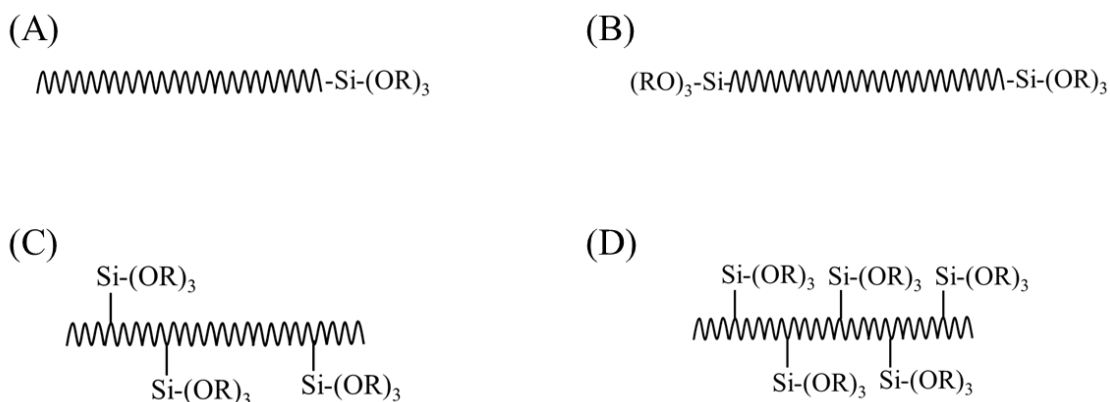


Figure 2. 2: Various functionalizations of polymer with trialkoxysilane; **A)** monofunctionalization, **B)** difunctionalization; pendant functionalization with side chains **C)** random copolymerization, **D)** block copolymerization.

Table 2. 1: Selected examples of O/I hybrids for bone tissue engineering applications

	Organic	Inorganic	Class	Coupling agents	Bonding	Scaffold fabrication	Reference
PCL/BG	PCL	SiO ₂ -P ₂ O ₅ -CaCl ₂	I	-	H-bond	Electrospinning	[129]
PVA/BG	PVA	SiO ₂ -CaCl ₂	I	-	Blend	Foaming	[128]
PLLA/Silica	PLLA	SiO ₂	I	-	Blend	Electrospinning	[150]
PDMS/BG	PDMS	SiO ₂ -Ca(NO ₃) ₂	I	-	Blend	Particle leaching	[140, 151]
Gelatin/siloxane	Gelatin	SiO ₂ -Ca(NO ₃) ₂	II	GPTMS	Covalent/Blend	Freeze-drying	[137, 152]
PCL/ Silica	PCL	SiO ₂	II	ICPTS	Covalent	-	[135]
γPGA/Silica	γPGA	SiO ₂	II	GPTMS	Covalent	Foaming	[138]
Chitosan/Silica	Chitosan	SiO ₂	II	GPTMS	Covalent	Freeze-drying	[134]
PMMA/Silica	PMMA	SiO ₂	II	TMSPMA	Covalent	-	[148]
PEG/Silica	PEG	SiO ₂	II	ICPTS	Covalent	Indirect rapid prototyping	[153]

2.3 Challenges associated with the synthesis of class II hybrids

O/I class II hybrids are most sought-after biomaterial system for assuring uniform physical, mechanical, biochemical properties at molecular level. Covalent bonding between the organic and inorganic components is the key feature to successfully prepare these novel materials. However,

the major chemical challenges are the need to prepare crack-free 3D porous microstructures with all the necessary requirements for bone regeneration *in vitro* [154]. These challenges are described below.

2.3.1 Synthesis route

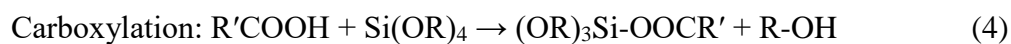
2.3.1.1 Aqueous sol gel process

Polymers having trialkoxysilane functional groups ($-\text{Si}(\text{OR})_3$) and BG precursors (TEOS, TEP etc.) are hydrolysed and polycondensed congruently in standard sol gel process to form O/I class II hybrids. Since the carbon-silicon bond is inert, hydrolysis of the functionalized polymer can easily help bond the inorganic BG network through Si-O-Si linkage through the polycondensation reaction. The room-temperature sol gel process also prevents any sort of thermal degradation of organic contents [154, 155]. As mentioned in section 2.2.4.2, in the last two decades, several O/I class II hybrid biomaterials have been prepared through the sol gel process. These hybrids were prepared by carrying out standard aqueous sol gel process, in which hydrolysis and polycondensation of trialkoxysilane (from polymer chains) and TEOS (to form inorganic network) occurred in the presence of water as reactant and solvent. This aqueous sol gel synthesis limited the choice of water-soluble and/or hydrophilic biocompatible polymers. However, many synthetic biocompatible and degradable polymers are water-insoluble, and have great potential as class II O/I hybrid biomaterial to apply for bone regeneration *in vitro*. Water-miscible organic solvents can be used as co-solvents during the sol gel synthesis to prevent the polymer from being phase-separated or precipitated. However, optimization of the volume ratio of solvents and removal of the co-solvent afterwards are further challenges. Allo *et al.* prepared PCL/BG class I hybrid and

Rhee *et al.* prepared PCL/SiO₂ class II hybrid through aqueous sol gel process using MEK and THF respectively, as co-solvents to dissolve PCL [129, 135]. Both solvents are cytotoxic and should be removed from the synthesized hybrids before seeding cells. Moreover, the process is not versatile as PCL started to phase-separated from the hybrids after some extent.

2.3.1.2 Non- aqueous sol gel process

The above limitations associated with aqueous sol gel synthesis of O/I hybrids may be resolved by non-aqueous (or non-hydrolytic) sol gel process [156-158]. In this process, the organic precursors transform into sol by reacting with carboxylic acid and the whole process takes place in an organic solvent. The carboxylic acid (e.g. formic acid, acetic acid, etc.) also may serve as the solvent. Non-aqueous sol gel process starts with carboxylation of TEOS and trialkoxysilane. The reactions occurred as follows:



Where R and R' represent alkyl groups.

Silica gel and microspheres have been prepared successfully from TEOS through non-aqueous sol gel process using formic and acetic acids as the reactants, solvents and catalysts [159, 160]. Some water is generated during the reaction as by product and it has been shown that this *in situ* water made the sol to gel transformation relatively faster than the aqueous sol gel process. The nature of carboxylic acid plays critical role in gelation time as follows [160],

Propanoic acid > Acetic acid > Formic acid

Biocompatible and degradable, yet water-insoluble polymers can be covalently crosslinked through non-aqueous sol gel process. The amount of water generated in this process is very small and should not cause any phase separation. The amount of acid needs to be optimised carefully so that the resultant O/I class II hybrids should not pose any cytotoxic effect.

2.3.2 Incorporation of necessary components

Most of O/I class II hybrids reported in literature are polymer/SiO₂ based hybrids. Synthesis of polymer/BG class II hybrids is challenging due to lack of appropriate calcium precursor for the sol gel process [63]. Calcium nitrate tetrahydrate (Ca(NO₃)₂·4H₂O) has long been used as calcium precursor to synthesize BG through sol gel process. However, it requires to be heated above 400 °C to incorporate calcium as a part of the inorganic BG network [120, 161, 162]. Which is not possible for O/I hybrids because such high temperature will destroy the polymer. Calcium chloride was also utilized as a calcium source to prepare class II hybrids [138], but calcium was not bonded with O/I network due to the low temperature of sol gel process. Organic salt of calcium, such as calcium methoxyethoxide has been tried to synthesize hybrids, but its high reactivity to water and

hence instability was a major challenge for not utilizing it during the sol gel process [150, 163]. Calcium does not necessarily need to be chemically bonded with O/I network, to make the hybrid bioactive and osteogenic. But the dissolution rate of calcium should be congruent with other bioactive components from O/I hybrid biomaterial scaffolds. This can be achieved by higher degree of crosslinking between organic and inorganic phases, so that calcium will be entrapped within the O/I network.

As mentioned in section 2.2.1.2, boron containing BG had excellent bioactivity and promoted cell attachment. Boron can be incorporated in O/I hybrid biomaterial through sol gel process [164, 165]. Organic precursors of boron, such as trimethyl borate or triethyl borate can be introduced in the sol gel process and chemically linked to O/I hybrid matrix as network modifier. Strontium doped BG had shown significant up-regulation of bone related gene expression when seeded with mouse osteoblast [166]. Strontium isopropoxide as a precursor of strontium can also be introduced into the hybrids through sol gel process.

2.4 O/I class II hybrid scaffolds

Guided bone regeneration requires a biocompatible and degradable scaffold. This scaffold should have well defined micro-porosity for cell infiltration, vascularization, and metabolic waste removal. There are several methods used for scaffold fabrication. These are gas foaming, particulate leaching, electrospinning, freeze-drying, 3D printing, etc. as well as combinations of these techniques. The method used for scaffold fabrication mostly depends on the physical and

chemical properties of the biomaterial. The following section will briefly outline some of the scaffold fabrication techniques compatible for O/I hybrid biomaterials.

2.4.1 Electrospinning

Electrospinning is one of the popular processes for bone tissue engineering scaffold fabrication since it closely mimics the nanofibrous architecture of the collagen matrix (bone ECM). In this process, a high electric field is used to create fiber jet from a polymer solution through a needle and collected into a grounded collector. At certain voltage, the generated charge overcomes the surface tension and a jet is produced. Solvent evaporates somewhere between the path from needle tip to collector. Fiber diameter depends on viscosity, conductivity, applied voltage, needle to collector distance, and humidity. Electrospinning has been widely used to fabricate polymer based tissue engineering scaffolds due to the easement of preparing polymer solution at various viscosity ranges. However, it is challenging to electrospin sol gel derived O/I hybrids since the viscosity of the sols rapidly changes towards gel formation and provides a short window of suitable viscosity. Fibrous mesh scaffold of PCL/BG class I hybrid was prepared through electrospinning with a mean fiber diameter of 320 nm, 77 – 84 vol% of porosity and mean pore size from 33 to 52 μm [129, 131]. Gelatin/BG class II hybrids were also fabricated into fibrous mesh through electrospinning with mean fiber diameter 192 nm [167]. These studies revealed that higher polymer content in hybrids reduced the gelation rate and provided longer time window for electrospinning. High molecular weight precursor polymer based hybrids should also have slow gelation time and easier to process into a fibrous mesh. The major drawback of the electrospinning process is the small and wide range of pore diameters of the fibrous scaffolds. Suitable bone tissue engineering

scaffolds should have mean pore diameter of at least 100 μm for successful diffusion of necessary nutrients and oxygen and 200–350 μm for cell infiltration and bone tissue in-growth [10].

2.4.2 Foaming

Interconnected porous structures can be fabricated through foaming during sol gel process by adding surfactants and gelling agents in the sol, followed by vigorous mixing. The resulting foam is then cast into molds and kept there until the sol is converted into a gel through condensation of Si-O-Si network. Through this method, hybrid scaffolds can be produced with spherical interconnected pores. Silica/gelatin and silica/ γ -PGA hybrid scaffolds made by the foaming process have been produced with a mean pore diameter 200 μm [137, 138]. The major drawbacks for this process are irregular pore size, pore wall thickness, lack of reproducibility from batch to batch, and additional steps to remove the surfactants, etc.

2.4.3 Freeze drying

Freeze drying is another popular method to produce polymer-based porous scaffolds for tissue engineering applications. One advantage of this process is no requirement of foaming agents. This method utilizes ice crystals as templates for pore formation that occur during freezing. The ice is dried by sublimation at very low temperature and high vacuum, leaving interconnected pores. This method has been mostly used for fabricating polymer based scaffold. A disadvantage of freeze drying is irregularity of pore sizes and pore wall thickness. Furthermore, applying this method to prepare hybrid scaffolds is limited due to the freeze-drying at sol stage will cause uncomplete hydrolysis and polycondensation of the silane.

2.4.4 Particulate leaching

Particulate leaching is a widely used scaffold fabrication technique due to its simplicity, reproducibility and predictability. Through this method, a polymer or an inorganic salt particle with specific size distribution is used as a sacrificial porogen. First the porogen/material composite is prepared by casting or hot-pressing, and then specific solvent is used to leach out the porogen. The size and vol% of the porogen determine pore size and porosity in the resultant scaffold. This method allows fabrication of the scaffold with a predefined pore size and porosity content. Particulate leaching is a versatile method to prepare polymers, ceramics and their composites scaffolds. Polymer based scaffolds are prepared by dissolving the polymers in a solvent which will not dissolve the porogen, and after casting in porogen bed the solvent is removed to solidify the polymer/porogen composites, and finally porogen particles are leached out using another solvent which will not affect the polymer. In solvent-free particulate leaching process, porogen particulates are mixed with powder of scaffold material and pressed with or without heat to prepare the composite. Sol gel derived O/I hybrid scaffolds can be prepared through casting the sol into a chamber filled with packed porogen particles and keeping until gelation and drying. When the porogen is leached out from that dried hybrid/porogen composite, a porous scaffold is obtained. Although the porosity and pore size within the scaffolds can be predefined, the pore interconnectivity using this method is poor.

2.4.5 3D printing

Rapid prototyping (3D printing) is the most popular method for fabricating scaffolds with predefined microstructure. For direct 3D printing, very specific ink-properties (properties of the

material to be printed) are required. Thus, direct 3D printing of O/I hybrids are difficult due to the rapid viscosity change during sol to gel transformation. To prepare hybrid scaffolds through direct printing, the hybrid monoliths need to be milled as fine powder and mixed with easily printable material and then print it into the desired porous scaffold. However, the produced scaffolds will result in a composite, and if the printable material is used as a sacrificial agent, the resultant scaffolds will be irregular in microstructure.

On the other hand, indirect 3D printing can solve the aforementioned issue to fabricate porous scaffolds of O/I hybrids [153]. This method is combination of 3D printing and particulate leaching techniques. In this method, first a sacrificial template scaffold is prepared by 3D printing and hybrid sol is cast into the 3D printed template. When the hybrid is converted into a gel and dried, the sacrificial template is removed by dissolving it in a specific solvent. The pore of the template will be the strut (pore wall) and the pore wall in template will be the pores of final scaffold. As the casting of O/I hybrids in 3D printed template does not require any specific properties of the hybrids, the hybrid sol can be cast anytime before gelation which make this indirect 3D printing method a versatile process. Any sol viscosities can be processed through this method. Major concern of indirect 3D printing is the shrinkage of hybrid materials during gel formation and drying of the gel. The shrinkage occurs in sol gel process due to the liberation of water and ethanol. The shrinkage of final product may cause crack formation on scaffolds surfaces and increment of pore diameter. However, the crack formation can be prevented by carefully optimizing process parameters during the synthesis of O/I class II hybrids.

2.5 Summary

This literature survey included relevant background information in the field of O/I hybrid biomaterials for bone tissue engineering scaffolds. Bone tissue engineering is a broad research field and it was not possible to cover all aspects within this short review. However, every effort is made to include important work and significant research findings, with minimal bias. Aside the various challenges and opportunities posed by bone tissue engineering strategies, this thesis will only attempt to address progress and limitations on the development of porous O/I class II hybrid biomaterial scaffolds for bone regeneration.

2.6 Hypothesis and objectives of the research

***Hypothesis:* Covalently cross-linked organic/inorganic hybrid biomaterials have tailorable bioactivity, degradation behavior and mechanical properties for bone regeneration.**

To test the above hypotheses, the following objectives were formulated:

1. Preparation and characterization of class II polycaprolactone/borophosphosilicate glass (PCL/BPSG) hybrid biomaterials.
2. Characterization of the mechanical properties, biodegradation, and biocompatibility of PCL/BPSG hybrid biomaterials.
3. Evaluation of the effect of porous PCL/BPSG hybrid scaffolds on osteogenic differentiation of mesenchymal stem cells.

4. Synthesis and characterization of class II poly(vinylpyrrolidone-co-triethoxyvinylsilane)/calcium phosphosilicate bioactive glass (PVP/BG) hybrid biomaterials.

2.7 References

- [1] Fleming JE, Jr., Cornell CN, Muschler GF. Bone Cells and Matrices in Orthopedic Tissue Engineering. *Orthopedic Clinics* 2000;31:357-74.
- [2] Centers for Disease Control. Update: allograft-associated bacterial infections- United States. *MMWR Morbidity and Mortality Weekly Report* 2002;51:207-10.
- [3] Langer R, Vacanti JP. Tissue engineering. *Science* 1993;260:920-6.
- [4] MacArthur BD, Oreffo ROC. Bridging the gap. *Nature* 2005;433:19.
- [5] Holzapfel BM, Reichert JC, Schantz J-T, Gbureck U, Rackwitz L, Nöth U, et al. How smart do biomaterials need to be? A translational science and clinical point of view. *Advanced Drug Delivery Reviews* 2013;65:581-603.
- [6] Martins AM, Alves CM, Kurtis Kasper F, Mikos AG, Reis RL. Responsive and in situ-forming chitosan scaffolds for bone tissue engineering applications: an overview of the last decade. *Journal of Materials Chemistry* 2010;20:1638-45.
- [7] Amini AR, Laurencin CT, Nukavarapu SP. Bone Tissue Engineering: Recent Advances and Challenges. *Critical reviews in biomedical engineering* 2012;40:363-408.
- [8] O'Brien FJ. Biomaterials & scaffolds for tissue engineering. *Materials Today* 2011;14:88-95.
- [9] Melchels FPW, Barradas AMC, van Blitterswijk CA, de Boer J, Feijen J, Grijpma DW. Effects of the architecture of tissue engineering scaffolds on cell seeding and culturing. *Acta Biomaterialia* 2010;6:4208-17.
- [10] Rouwkema J, Rivron NC, van Blitterswijk CA. Vascularization in tissue engineering. *Trends in Biotechnology* 2008;26:434-41.
- [11] Murphy CM, Haugh MG, O'Brien FJ. The effect of mean pore size on cell attachment, proliferation and migration in collagen–glycosaminoglycan scaffolds for bone tissue engineering. *Biomaterials* 2010;31:461-6.
- [12] Freed LE, Martin I, Vunjak-Novakovic G. *Frontiers in Tissue Engineering: In Vitro Modulation of Chondrogenesis. Clinical Orthopaedics and Related Research* 1999;367:S46-8.
- [13] Ishaug SL, Crane GM, Miller MJ, Yasko AW, Yaszemski MJ, Mikos AG. Bone formation by three-dimensional stromal osteoblast culture in biodegradable polymer scaffolds. *Journal of Biomedical Materials Research* 1997;36:17-28.

- [14] Orciani M, Fini M, Di Primio R, Mattioli-Belmonte M. Biofabrication and Bone Tissue Regeneration: Cell Source, Approaches, and Challenges. *Frontiers in Bioengineering and Biotechnology* 2017;5:17.
- [15] Pittenger MF, Mackay AM, Beck SC, Jaiswal RK, Douglas R, Mosca JD, et al. Multilineage Potential of Adult Human Mesenchymal Stem Cells. *Science* 1999;284:143-7.
- [16] Colnot C. Cell Sources for Bone Tissue Engineering: Insights from Basic Science. *Tissue Engineering Part B, Reviews* 2011;17:449-57.
- [17] Bianco P, Riminucci M, Gronthos S, Robey PG. Bone Marrow Stromal Stem Cells: Nature, Biology, and Potential Applications. *STEM CELLS* 2001;19:180-92.
- [18] Russell KC, Phinney DG, Lacey MR, Barrilleaux BL, Meyertholen KE, O'Connor KC. In Vitro High-Capacity Assay to Quantify the Clonal Heterogeneity in Trilineage Potential of Mesenchymal Stem Cells Reveals a Complex Hierarchy of Lineage Commitment. *STEM CELLS* 2010;28:788-98.
- [19] Fröhlich M, Grayson WL, Wan LQ, Marolt D, Drobnic M, Vunjak-Novakovic G. Tissue Engineered Bone Grafts: Biological Requirements, Tissue Culture and Clinical Relevance. *Current stem cell research & therapy* 2008;3:254-64.
- [20] El Tamer MK, Reis RL. Progenitor and stem cells for bone and cartilage regeneration. *Journal of Tissue Engineering and Regenerative Medicine* 2009;3:327-37.
- [21] Caroline Szpalski MB, Fabio Sagebin, and Stephen M. Warren. Bone Tissue Engineering: Current Strategies and Techniques—Part II: Cell Types. *Tissue Engineering Part B: Reviews* 2012;18:258-69.
- [22] Lafosse A, Dufey C, Beauloye C, Horman S, Dufrane D. Impact of Hyperglycemia and Low Oxygen Tension on Adipose-Derived Stem Cells Compared with Dermal Fibroblasts and Keratinocytes: Importance for Wound Healing in Type 2 Diabetes. *PLOS ONE* 2016;11:e0168058.
- [23] Rada T, Reis RL, Gomes ME. Distinct Stem Cells Subpopulations Isolated from Human Adipose Tissue Exhibit Different Chondrogenic and Osteogenic Differentiation Potential. *Stem Cell Reviews and Reports* 2011;7:64-76.
- [24] Patricia A. Zuk MZ, Hiroshi Mizuno, Jerry Huang, J. William Futrell, Adam J. Katz, Prosper Benhaim, H. Peter Lorenz, and Marc H. Hedrick. Multilineage Cells from Human Adipose Tissue: Implications for Cell-Based Therapies *Tissue Engineering Part B: Reviews* 2004;7:211-28.
- [25] Ohnishi H, Oda Y, Aoki T, Tadokoro M, Katsube Y, Ohgushi H, et al. A comparative study of induced pluripotent stem cells generated from frozen, stocked bone marrow- and adipose tissue-derived mesenchymal stem cells. *Journal of Tissue Engineering and Regenerative Medicine* 2012;6:261-71.
- [26] Takahashi K, Tanabe K, Ohnuki M, Narita M, Ichisaka T, Tomoda K, et al. Induction of Pluripotent Stem Cells from Adult Human Fibroblasts by Defined Factors. *Cell* 2007;131:861-72.

- [27] Yu J, Vodyanik MA, Smuga-Otto K, Antosiewicz-Bourget J, Frane JL, Tian S, et al. Induced Pluripotent Stem Cell Lines Derived from Human Somatic Cells. *Science* 2007;318:1917.
- [28] Wissing S, Muñoz-Lopez M, Macia A, Yang Z, Montano M, Collins W, et al. Reprogramming somatic cells into iPS cells activates LINE-1 retroelement mobility. *Human Molecular Genetics* 2012;21:208-18.
- [29] Yoshii T, Sotome S, Torigoe I, Maehara H, Sugata Y, Yamada T, et al. Isolation of osteogenic progenitor cells from trabecular bone for bone tissue engineering. *Tissue engineering Part A* 2010;16:933-42.
- [30] Rauh J, Milan F, Gunther K-P, Stiehler M. Bioreactor systems for bone tissue engineering. *Tissue Engineering Part B: Reviews* 2011; 17:263-80.
- [31] Sladkova M, de Peppo MG. Bioreactor Systems for Human Bone Tissue Engineering. *Processes* 2014;2:494-525.
- [32] Yu X, Botchwey EA, Levine EM, Pollack SR, Laurencin CT. Bioreactor-based bone tissue engineering: The influence of dynamic flow on osteoblast phenotypic expression and matrix mineralization. *Proceedings of the National Academy of Sciences of the United States of America* 2004;101:11203-8.
- [33] Zhang Z-Y, Teoh SH, Teo EY, Khoon Chong MS, Shin CW, Tien FT, et al. A comparison of bioreactors for culture of fetal mesenchymal stem cells for bone tissue engineering. *Biomaterials* 2010;31:8684-95.
- [34] Ramirez-Vick JE. Biophysical Stimulation for Bone Regeneration. *JSM biotechnology & biomedical engineering* 2013;1:1014.
- [35] Vance J, Galley S, Liu DF, Donahue SW. Mechanical stimulation of MC3T3 osteoblastic cells in a bone tissue-engineering bioreactor enhances prostaglandin E2 release. *Tissue Engineering* 2005;11:1832-9.
- [36] Khan Y, Yaszemski MJ, Mikos AG, Laurencin CT. Tissue Engineering of Bone: Material and Matrix Considerations. *JBJS* 2008;90:36-42.
- [37] Rezwan K, Chen QZ, Blaker JJ, Boccaccini AR. Biodegradable and bioactive porous polymer/inorganic composite scaffolds for bone tissue engineering. *Biomaterials* 2006;27:3413-31.
- [38] Salinas AJ, Esbrit P, Vallet-Regi M. A tissue engineering approach based on the use of bioceramics for bone repair. *Biomaterials Science* 2013;1:40-51.
- [39] LeGeros RZ. Properties of osteoconductive biomaterials: Calcium phosphates. *Clinical Orthopaedics and Related Research* 2002:81-98.
- [40] LeGeros RZ. Calcium Phosphate-Based Osteoinductive Materials. *Chemical Reviews* 2008;108:4742-53.
- [41] LeGeros RZ, LeGeros JP. Dense Hydroxyapatite. *An Introduction to Bioceramics*. World Scientific; 1993. p. 139-80.

- [42] Jevtić M, Mitrić M, Škapin S, Jančar B, Ignjatović N, Uskoković D. Crystal Structure of Hydroxyapatite Nanorods Synthesized by Sonochemical Homogeneous Precipitation. *Crystal Growth & Design* 2008;8:2217-22.
- [43] Pang YX, Bao X. Influence of temperature, ripening time and calcination on the morphology and crystallinity of hydroxyapatite nanoparticles. *Journal of the European Ceramic Society* 2003;23:1697-704.
- [44] Wang H, Lee J-K, Moursi A, Lannutti JJ. Ca/P ratio effects on the degradation of hydroxyapatite in vitro. *Journal of Biomedical Materials Research Part A* 2003;67A:599-608.
- [45] Dorozhkin SV. Calcium orthophosphates. *Journal of Materials Science* 2007;42:1061-95.
- [46] Hench LL, Best SM. Chapter I.2.4 - Ceramics, Glasses, and Glass-Ceramics: Basic Principles A2 - Ratner, Buddy D. In: Hoffman AS, Schoen FJ, Lemons JE, editors. *Biomaterials Science (Third Edition)*: Academic Press; 2013. p. 128-51.
- [47] Dorozhkin SV. Biphasic, triphasic and multiphasic calcium orthophosphates. *Acta Biomaterialia* 2012;8:963-77.
- [48] Bigi A, Fini M, Bracci B, Boanini E, Torricelli P, Giavaresi G, et al. The response of bone to nanocrystalline hydroxyapatite-coated Ti13Nb11Zr alloy in an animal model. *Biomaterials* 2008;29:1730-6.
- [49] Borsari V, Fini M, Giavaresi G, Tschon M, Chiesa R, Chiusoli L, et al. Comparative in vivo evaluation of porous and dense duplex titanium and hydroxyapatite coating with high roughnesses in different implantation environments. *Journal of Biomedical Materials Research Part A* 2009;89A:550-60.
- [50] Scaglione S, Ilengo C, Fato M, Quarto R. Hydroxyapatite-coated polycaprolacton wide mesh as a model of open structure for bone regeneration. *Tissue Engineering Part A*. 2008;15:155-63.
- [51] Lickorish D, Guan L, Davies JE. A three-phase, fully resorbable, polyester/calcium phosphate scaffold for bone tissue engineering: Evolution of scaffold design. *Biomaterials* 2007;28:1495-502.
- [52] Jongwattanapisan P, Charoenphandhu N, Krishnamra N, Thongbunchoo J, Tang IM, Hoonsawat R, et al. In vitro study of the SBF and osteoblast-like cells on hydroxyapatite/chitosan-silica nanocomposite. *Materials Science and Engineering: C* 2011;31:290-9.
- [53] Spanos N, Misirlis DY, Kanellopoulou DG, Koutsoukos PG. Seeded growth of hydroxyapatite in simulated body fluid. *Journal of Materials Science* 2006;41:1805-12.
- [54] Wilke A, Orth J, Lomb M, Fuhrmann R, Kienapfel H, Griss P, et al. Biocompatibility analysis of different biomaterials in human bone marrow cell cultures. *Journal of Biomedical Materials Research* 1998;40:301-6.
- [55] Bluteau G, Pilet P, Bourges X, Bilban M, Spaethe R, Daculsi G, et al. The modulation of gene expression in osteoblasts by thrombin coated on biphasic calcium phosphate ceramic. *Biomaterials* 2006;27:2934-43.

- [56] Sun L, Wu L, Bao C, Fu C, Wang X, Yao J, et al. Gene expressions of Collagen type I, ALP and BMP-4 in osteo-inductive BCP implants show similar pattern to that of natural healing bones. *Materials Science and Engineering: C* 2009;29:1829-34.
- [57] Rochet N, Loubat A, Laugier JP, Hofman P, Bouler JM, Daculsi G, et al. Modification of gene expression induced in human osteogenic and osteosarcoma cells by culture on a biphasic calcium phosphate bone substitute. *Bone* 2003;32:602-10.
- [58] Geesink RGT. Osteoconductive Coatings for Total Joint Arthroplasty. *Clinical Orthopaedics and Related Research* 2002;395:53-65.
- [59] Barrère F, van der Valk CM, Dalmeijer RAJ, Meijer G, van Blitterswijk CA, de Groot K, et al. Osteogenicity of octacalcium phosphate coatings applied on porous metal implants. *Journal of Biomedical Materials Research Part A* 2003;66A:779-88.
- [60] Habibovic P, van der Valk CM, van Blitterswijk CA, de Groot K, Meijer G. Influence of octacalcium phosphate coating on osteoinductive properties of biomaterials. *Journal of Materials Science: Materials in Medicine* 2004;15:373-80.
- [61] Baino F, Novajra G, Vitale-Brovarone C. Bioceramics and Scaffolds: A Winning Combination for Tissue Engineering. *Frontiers in Bioengineering and Biotechnology* 2015;3:202.
- [62] Oonishi H, Hench LL, Wilson J, Sugihara F, Tsuji E, Kushitani S, Iwaki H. Comparative bone growth behavior in granules of bioceramic materials of various sizes. *Journal of Biomedical Materials Research Part A* 1999; 44:31-43.
- [63] Jones JR. Review of bioactive glass: From Hench to hybrids. *Acta Biomaterialia* 2013;9:4457-86.
- [64] Hench LL, Splinter RJ, Allen WC, Greenlee TK. Bonding mechanisms at the interface of ceramic prosthetic materials. *Journal of Biomedical Materials Research* 1971;5:117-41.
- [65] Rahaman MN, Day DE, Bal BS, Fu Q, Jung SB, Bonewald LF, et al. Bioactive glass in tissue engineering. *Acta biomaterialia* 2011;7:2355-73.
- [66] Kaur G, Pandey OP, Singh K, Homa D, Scott B, Pickrell G. A review of bioactive glasses: Their structure, properties, fabrication and apatite formation. *Journal of Biomedical Materials Research Part A* 2014;102:254-74.
- [67] Brink M. The influence of alkali and alkaline earths on the working range for bioactive glasses. *Journal of Biomedical Materials Research* 1997;36:109-17.
- [68] Fu Q, Rahaman MN, Sonny Bal B, Brown RF, Day DE. Mechanical and in vitro performance of 13–93 bioactive glass scaffolds prepared by a polymer foam replication technique. *Acta Biomaterialia* 2008;4:1854-64.
- [69] Brovarone CV, Verné E, Appendino P. Macroporous bioactive glass-ceramic scaffolds for tissue engineering. *Journal of Materials Science: Materials in Medicine* 2006;17:1069-78.

- [70] Ahmed I, Lewis M, Olsen I, Knowles JC. Phosphate glasses for tissue engineering: Part 1. Processing and characterisation of a ternary-based P_2O_5 -CaO- Na_2O glass system. *Biomaterials* 2004;25:491-9.
- [71] Uo M, Mizuno M, Kuboki Y, Makishima A, Watari F. Properties and cytotoxicity of water soluble Na_2O -CaO- P_2O_5 glasses. *Biomaterials* 1998;19:2277-84.
- [72] Bunker BC, Arnold GW, Wilder JA. Phosphate glass dissolution in aqueous solutions. *Journal of Non-Crystalline Solids* 1984;64:291-316.
- [73] Gao H, Tan T, Wang D. Dissolution mechanism and release kinetics of phosphate controlled release glasses in aqueous medium. *Journal of Controlled Release* 2004;96:29-36.
- [74] Abou Neel EA, Mizoguchi T, Ito M, Bitar M, Salih V, Knowles JC. In vitro bioactivity and gene expression by cells cultured on titanium dioxide doped phosphate-based glasses. *Biomaterials* 2007;28:2967-77.
- [75] Valappil SP, Pickup DM, Carroll DL, Hope CK, Pratten J, Newport RJ, et al. Effect of Silver Content on the Structure and Antibacterial Activity of Silver-Doped Phosphate-Based Glasses. *Antimicrobial Agents and Chemotherapy* 2007;51:4453-61.
- [76] Fu Q, Rahaman MN, Fu H, Liu X. Silicate, borosilicate, and borate bioactive glass scaffolds with controllable degradation rate for bone tissue engineering applications. I. Preparation and in vitro degradation. *Journal of Biomedical Materials Research Part A* 2010;95A:164-71.
- [77] Han X, Day DE. Reaction of sodium calcium borate glasses to form hydroxyapatite. *Journal of Materials Science: Materials in Medicine* 2007;18:1837-47.
- [78] Huang W, Day DE, Kittiratanapiboon K, Rahaman MN. Kinetics and mechanisms of the conversion of silicate (45S5), borate, and borosilicate glasses to hydroxyapatite in dilute phosphate solutions. *Journal of Materials Science: Materials in Medicine* 2006;17:583-96.
- [79] Yao A, Wang D, Huang W, Fu Q, Rahaman MN, Day DE. In Vitro Bioactive Characteristics of Borate-Based Glasses with Controllable Degradation Behavior. *Journal of the American Ceramic Society* 2007;90:303-6.
- [80] Xu S, Yang X, Chen X, Shao H, He Y, Zhang L, et al. Effect of borosilicate glass on the mechanical and biodegradation properties of 45S5-derived bioactive glass-ceramics. *Journal of Non-Crystalline Solids* 2014;405:91-9.
- [81] Li R, Clark AE, Hench LL. An investigation of bioactive glass powders by sol-gel processing. *Journal of Applied Biomaterials* 1991;2:231-9.
- [82] Hench LL, West JK. The sol-gel process. *Chemical Reviews* 1990;90:33-72.
- [83] Brinker CJ, Scherer GW. CHAPTER 3 - Hydrolysis and Condensation II: Silicates. *Sol-Gel Science*. San Diego: Academic Press; 1990. p. 96-233.
- [84] Sepulveda P, Jones JR, Hench LL. Characterization of melt-derived 45S5 and sol-gel-derived 58S bioactive glasses. *Journal of Biomedical Materials Research* 2001;58:734-40.

- [85] Lei B, Chen X, Wang Y, Zhao N, Du C, Fang L. Surface nanoscale patterning of bioactive glass to support cellular growth and differentiation. *Journal of Biomedical Materials Research Part A* 2010;94A:1091-9.
- [86] Uysal T, Ustidal A, Sonmez MF, Ozturk F. Stimulation of Bone Formation by Dietary Boron in an Orthopedically Expanded Suture in Rabbits. *The Angle Orthodontist* 2009;79:984-90.
- [87] Marion NW, Liang W, Liang W, Reilly GC, Day DE, Rahaman MN, et al. Borate Glass Supports the In Vitro Osteogenic Differentiation of Human Mesenchymal Stem Cells. *Mechanics of Advanced Materials and Structures* 2005;12:239-46.
- [88] Vitale-Brovarone C, Miola M, Balagna C, Verné E. 3D-glass–ceramic scaffolds with antibacterial properties for bone grafting. *Chemical Engineering Journal* 2008;137:129-36.
- [89] Fu Q, Rahaman MN, Bal BS, Bonewald LF, Kuroki K, Brown RF. Silicate, borosilicate, and borate bioactive glass scaffolds with controllable degradation rate for bone tissue engineering applications. II. In vitro and in vivo biological evaluation. *Journal of Biomedical Materials Research Part A* 2010;95A:172-9.
- [90] Jia W-T, Zhang X, Luo S-H, Liu X, Huang W-H, Rahaman MN, et al. Novel borate glass/chitosan composite as a delivery vehicle for teicoplanin in the treatment of chronic osteomyelitis. *Acta Biomaterialia* 2010;6:812-9.
- [91] Liu X, Xie Z, Zhang C, Pan H, Rahaman MN, Zhang X, et al. Bioactive borate glass scaffolds: in vitro and in vivo evaluation for use as a drug delivery system in the treatment of bone infection. *Journal of Materials Science: Materials in Medicine* 2010;21:575-82.
- [92] Zhang X, Jia W, Gu Y, Xiao W, Liu X, Wang D, et al. Teicoplanin-loaded borate bioactive glass implants for treating chronic bone infection in a rabbit tibia osteomyelitis model. *Biomaterials* 2010;31:5865-74.
- [93] Jung SB, Day DE, Brown RF, Bonewald LF. Potential Toxicity of Bioactive Borate Glasses In-Vitro and In-Vivo. *Advances in Bioceramics and Porous Ceramics V: John Wiley & Sons, Inc.;* 2012. p. 65-74.
- [94] Sabir MI, Xu X, Li L. A review on biodegradable polymeric materials for bone tissue engineering applications. *Journal of Materials Science* 2009;44:5713-24.
- [95] Shrivats AR, McDermott MC, Hollinger JO. Bone tissue engineering: state of the union. *Drug Discovery Today* 2014;19:781-6.
- [96] Stratton S, Shelke NB, Hoshino K, Rudraiah S, Kumbar SG. Bioactive polymeric scaffolds for tissue engineering. *Bioactive Materials* 2016;1:93-108.
- [97] Wu S, Liu X, Yeung KWK, Liu C, Yang X. Biomimetic porous scaffolds for bone tissue engineering. *Materials Science and Engineering: R: Reports* 2014;80:1-36.
- [98] Allo BA, Costa DO, Dixon SJ, Mequanint K, Rizkalla AS. Bioactive and Biodegradable Nanocomposites and Hybrid Biomaterials for Bone Regeneration. *Journal of Functional Biomaterials* 2012;3:432-63.

- [99] Martin C, Winet H, Bao JY. Acidity near eroding polylactide-polyglycolide in vitro and in vivo in rabbit tibial bone chambers. *Biomaterials* 1996;17:2373-80.
- [100] Okamoto M, John B. Synthetic biopolymer nanocomposites for tissue engineering scaffolds. *Progress in Polymer Science* 2013;38:1487-503.
- [101] Dziadek M, Menaszek E, Zagrajczuk B, Pawlik J, Cholewa-Kowalska K. New generation poly(ϵ -caprolactone)/gel-derived bioactive glass composites for bone tissue engineering: Part I. Material properties. *Materials Science and Engineering: C* 2015;56:9-21.
- [102] Lu HH, El-Amin SF, Scott KD, Laurencin CT. Three-dimensional, bioactive, biodegradable, polymer–bioactive glass composite scaffolds with improved mechanical properties support collagen synthesis and mineralization of human osteoblast-like cells in vitro. *Journal of Biomedical Materials Research Part A* 2003;64A:465-74.
- [103] Maquet V, Boccaccini AR, Pravata L, Notingher I, Jérôme R. Porous poly(α -hydroxyacid)/Bioglass® composite scaffolds for bone tissue engineering. I: preparation and in vitro characterisation. *Biomaterials* 2004;25:4185-94.
- [104] Niemelä T, Niiranen H, Kellomäki M, Törmälä P. Self-reinforced composites of bioabsorbable polymer and bioactive glass with different bioactive glass contents. Part I: Initial mechanical properties and bioactivity. *Acta Biomaterialia* 2005;1:235-42.
- [105] Blaker JJ, Maquet V, Jérôme R, Boccaccini AR, Nazhat SN. Mechanical properties of highly porous PDLA/Bioglass® composite foams as scaffolds for bone tissue engineering. *Acta Biomaterialia* 2005;1:643-52.
- [106] Chen QZ, Boccaccini AR. Poly(D,L-lactic acid) coated 45S5 Bioglass®-based scaffolds: Processing and characterization. *Journal of Biomedical Materials Research Part A* 2006;77A:445-57.
- [107] Bretcanu O, Chen Q, Misra SK, Boccaccini AR, Roy I, Verne E, et al. Biodegradable polymer coated 45S5 Bioglass-derived glass-ceramic scaffolds for bone tissue engineering. *Glass Technology - European Journal of Glass Science and Technology Part A* 2007;48:227-34.
- [108] Li H, Chang J. pH-compensation effect of bioactive inorganic fillers on the degradation of PLGA. *Composites Science and Technology* 2005;65:2226-32.
- [109] Naseri S, Boccaccini AR, Nazhat SN. Chapter 10 Bioactive Glass Particulate-incorporated Polymer Composites. *Bioactive Glasses: Fundamentals, Technology and Applications: The Royal Society of Chemistry*; 2017. p. 236-56.
- [110] Blaker JJ, Bismarck A, Boccaccini AR, Young AM, Nazhat SN. Premature degradation of poly(α -hydroxyesters) during thermal processing of Bioglass®-containing composites. *Acta Biomaterialia* 2010;6:756-62.
- [111] Kango S, Kalia S, Celli A, Njuguna J, Habibi Y, Kumar R. Surface modification of inorganic nanoparticles for development of organic–inorganic nanocomposites—A review. *Progress in Polymer Science* 2013;38:1232-61.

- [112] Webster TJ, Ergun C, Doremus RH, Siegel RW, Bizios R. Specific proteins mediate enhanced osteoblast adhesion on nanophase ceramics. *Journal of Biomedical Materials Research* 2000;51:475-83.
- [113] Hong Z, Liu A, Chen L, Chen X, Jing X. Preparation of bioactive glass ceramic nanoparticles by combination of sol-gel and coprecipitation method. *Journal of Non-Crystalline Solids* 2009;355:368-72.
- [114] Hong Z, Reis RL, Mano JF. Preparation and in vitro characterization of scaffolds of poly(l-lactic acid) containing bioactive glass ceramic nanoparticles. *Acta Biomaterialia* 2008;4:1297-306.
- [115] Hong Z, Reis RL, Mano JF. Preparation and in vitro characterization of novel bioactive glass ceramic nanoparticles. *Journal of Biomedical Materials Research Part A* 2009;88A:304-13.
- [116] Kim HW, Kim HE, Knowles JC. Production and Potential of Bioactive Glass Nanofibers as a Next-Generation Biomaterial. *Advanced Functional Materials* 2006;16:1529-35.
- [117] Kim H-W, Lee H-H, Chun G-S. Bioactivity and osteoblast responses of novel biomedical nanocomposites of bioactive glass nanofiber filled poly(lactic acid). *Journal of Biomedical Materials Research Part A* 2008;85A:651-63.
- [118] Kim H-W, Song J-H, Kim H-E. Bioactive glass nanofiber-collagen nanocomposite as a novel bone regeneration matrix. *Journal of Biomedical Materials Research Part A* 2006;79A:698-705.
- [119] Lee H-H, Yu H-S, Jang J-H, Kim H-W. Bioactivity improvement of poly(ϵ -caprolactone) membrane with the addition of nanofibrous bioactive glass. *Acta Biomaterialia* 2008;4:622-9.
- [120] Martin RA, Yue S, Hanna JV, Lee PD, Newport RJ, Smith ME, et al. Characterizing the hierarchical structures of bioactive sol-gel silicate glass and hybrid scaffolds for bone regeneration. *Philosophical Transactions of the Royal Society A: Mathematical, Physical and Engineering Sciences* 2012;370:1422-43.
- [121] Kickelbick G. Introduction to Hybrid Materials. *Hybrid Materials: Wiley-VCH Verlag GmbH & Co. KGaA*; 2006. p. 1-48.
- [122] Novak BM. Hybrid Nanocomposite Materials—between inorganic glasses and organic polymers. *Advanced Materials* 1993;5:422-33.
- [123] Grosso D, Ribot F, Boissiere C, Sanchez C. Molecular and supramolecular dynamics of hybrid organic-inorganic interfaces for the rational construction of advanced hybrid nanomaterials. *Chemical Society Reviews* 2011;40:829-48.
- [124] Jones JR. New trends in bioactive scaffolds: The importance of nanostructure. *Journal of the European Ceramic Society* 2009;29:1275-81.
- [125] Sanchez C, Julian B, Belleville P, Popall M. Applications of hybrid organic-inorganic nanocomposites. *Journal of Materials Chemistry* 2005;15:3559-92.
- [126] Martín AI, Salinas AJ, Vallet-Regí M. Bioactive and degradable organic-inorganic hybrids. *Journal of the European Ceramic Society* 2005;25:3533-8.

- [127] Pereira MM, Jones JR, Hench LL. Bioactive glass and hybrid scaffolds prepared by sol–gel method for bone tissue engineering. *Advances in Applied Ceramics* 2005;104:35-42.
- [128] Pereira MM, Jones JR, Orefice RL, Hench LL. Preparation of bioactive glass-polyvinyl alcohol hybrid foams by the sol-gel method. *Journal of Materials Science: Materials in Medicine* 2005;16:1045-50.
- [129] Allo BA, Rizkalla AS, Mequanint K. Synthesis and Electrospinning of ϵ -Polycaprolactone-Bioactive Glass Hybrid Biomaterials via a Sol–Gel Process. *Langmuir* 2010;26:18340-8.
- [130] Allo BA, Rizkalla AS, Mequanint K. Hydroxyapatite Formation on Sol–Gel Derived Poly(ϵ -Caprolactone)/Bioactive Glass Hybrid Biomaterials. *ACS Applied Materials & Interfaces* 2012;4:3148-56.
- [131] Allo BA, Lin S, Mequanint K, Rizkalla AS. Role of Bioactive 3D Hybrid Fibrous Scaffolds on Mechanical Behavior and Spatiotemporal Osteoblast Gene Expression. *ACS Applied Materials & Interfaces* 2013;5:7574-83.
- [132] Connell LS, Romer F, Suarez M, Valliant EM, Zhang Z, Lee PD, et al. Chemical characterisation and fabrication of chitosan-silica hybrid scaffolds with 3-glycidoxypropyl trimethoxysilane. *Journal of Materials Chemistry B* 2014;2:668-80.
- [133] Liu Y-L, Su Y-H, Lai J-Y. In situ crosslinking of chitosan and formation of chitosan–silica hybrid membranes with using γ -glycidoxypropyltrimethoxysilane as a crosslinking agent. *Polymer* 2004;45:6831-7.
- [134] Shirotsaki Y, Tsuru K, Hayakawa S, Osaka A, Lopes MA, Santos JD, Costa MA et al. Physical, chemical and in vitro biological profile of chitosan hybrid membrane as a function of organosiloxane concentration. *Acta Biomaterialia* 2009;5:346-55.
- [135] Rhee S-H, Choi J-Y, Kim H-M. Preparation of a bioactive and degradable poly(ϵ -caprolactone)/silica hybrid through a sol–gel method. *Biomaterials* 2002;23:4915-21.
- [136] Tian D, Dubois P, Grandfils C, Jérôme R, Viville P, Lazzaroni R, et al. A Novel Biodegradable and Biocompatible Ceramer Prepared by the Sol–Gel Process. *Chemistry of Materials* 1997;9:871-4.
- [137] Mahony O, Tsigkou O, Ionescu C, Minelli C, Ling L, Hanly R, et al. Silica-Gelatin Hybrids with Tailorable Degradation and Mechanical Properties for Tissue Regeneration. *Advanced Functional Materials* 2010;20:3835-45.
- [138] Poologasundarampillai G, Ionescu C, Tsigkou O, Murugesan M, Hill RG, Stevens MM, et al. Synthesis of bioactive class II poly(γ -glutamic acid)/silica hybrids for bone regeneration. *Journal of Materials Chemistry* 2010;20:8952-61.
- [139] Kickelbick G. The search of a homogeneously dispersed material—the art of handling the organic polymer/metal oxide interface. *Journal of Sol-Gel Science and Technology* 2008;46:281-90.

- [140] Yabuta T, Bescher EP, Mackenzie JD, Tsuru K, Hayakawa S, Osaka A. Synthesis of PDMS-Based Porous Materials for Biomedical Applications. *Journal of Sol-Gel Science and Technology* 2003;26:1219-22.
- [141] Chen Q, Kamitakahara M, Miyata N, Kokubo T, Nakamura T. Preparation of Bioactive PDMS-Modified CaO–SiO₂–TiO₂ Hybrids by the Sol-Gel Method. *Journal of Sol-Gel Science and Technology* 2000;19:101-5.
- [142] Salinas AJ, Merino JM, Babonneau F, Gil FJ, Vallet-Regí M. Microstructure and macroscopic properties of bioactive CaO–SiO₂–PDMS hybrids. *Journal of Biomedical Materials Research Part B: Applied Biomaterials* 2007;81B:274-82.
- [143] Chen Q, Miyata N, Kokubo T, Nakamura T. Bioactivity and mechanical properties of PDMS-modified CaO–SiO₂–TiO₂ hybrids prepared by sol-gel process. *Journal of Biomedical Materials Research* 2000;51:605-11.
- [144] Chen Q, Miyata N, Kokubo T, Nakamura T. Bioactivity and Mechanical Properties of Poly(dimethylsiloxane)-Modified Calcia–Silica Hybrids with Added Titania. *Journal of the American Ceramic Society* 2003;86:806-10.
- [145] Wei Y, Yang D, Tang L, Hutchins MK. Synthesis, characterization, and properties of new polystyrene-SiO₂ hybrid sol-gel materials. *Journal of Materials Research* 2011;8:1143-52.
- [146] Costa ROR, Vasconcelos WL. Structural modification of poly(2-hydroxyethyl methacrylate)–silica hybrids utilizing 3-methacryloxypropyltrimethoxysilane. *Journal of Non-Crystalline Solids* 2002;304:84-91.
- [147] Hsu YG, Lin FJ. Organic–inorganic composite materials from acrylonitrile–butadiene–styrene copolymers (ABS) and silica through an in situ sol-gel process. *Journal of Applied Polymer Science* 2000;75:275-83.
- [148] Chung JJ, Li S, Stevens MM, Georgiou TK, Jones JR. Tailoring Mechanical Properties of Sol–Gel Hybrids for Bone Regeneration through Polymer Structure. *Chemistry of Materials* 2016;28:6127-35.
- [149] Wei Y, Jin D, Brennan DJ, Zhuang Q, DiNardo NJ, et al. Atomic Force Microscopy Study of Organic–Inorganic Hybrid Materials. *Chemistry of Materials* 1998;10:769-72.
- [150] Poologasundarampillai G, Yu B, Jones JR, Kasuga T. Electrospun silica/PLLA hybrid materials for skeletal regeneration. *Soft Matter* 2011;7:10241-51.
- [151] Tsuru K, Hayakawa S, Osaka A. Synthesis of Bioactive and Porous Organic-Inorganic Hybrids for Biomedical Applications. *Journal of Sol-Gel Science and Technology* 2004;32:201-5.
- [152] Ren L, Tsuru K, Hayakawa S, Osaka A. Novel approach to fabricate porous gelatin–siloxane hybrids for bone tissue engineering. *Biomaterials* 2002;23:4765-73.
- [153] Hendrikx S, Kascholke C, Flath T, Schumann D, Gressenbuch M, Schulze FP, et al. Indirect rapid prototyping of sol-gel hybrid glass scaffolds for bone regeneration – Effects of organic crosslinker valence, content and molecular weight on mechanical properties. *Acta Biomaterialia* 2016;35:318-29.

- [154] Valliant EM, Jones JR. Softening bioactive glass for bone regeneration: sol-gel hybrid materials. *Soft Matter* 2011;7:5083-95.
- [155] Wen J, Wilkes GL. Organic/Inorganic Hybrid Network Materials by the Sol-Gel Approach. *Chemistry of Materials* 1996;8:1667-81.
- [156] Bilecka I, Niederberger M. New developments in the nonaqueous and/or non-hydrolytic sol-gel synthesis of inorganic nanoparticles. *Electrochimica Acta* 2010;55:7717-25.
- [157] Hay JN, Raval HM. Synthesis of Organic-Inorganic Hybrids via the Non-hydrolytic Sol-Gel Process. *Chemistry of Materials* 2001;13:3396-403.
- [158] Vioux A. Nonhydrolytic Sol-Gel Routes to Oxides. *Chemistry of Materials* 1997;9:2292-9.
- [159] Karmakar B, De G, Kundu D, Ganguli D. Silica microspheres from the system tetraethyl orthosilicate-acetic acid-water. *Journal of Non-Crystalline Solids* 1991;135:29-36.
- [160] Sharp KG. A two-component, non-aqueous route to silica gel. *Journal of Sol-Gel Science and Technology* 1994;2:35-41.
- [161] Lin S, Ionescu C, Pike KJ, Smith ME, Jones JR. Nanostructure evolution and calcium distribution in sol-gel derived bioactive glass. *Journal of Materials Chemistry* 2009;19:1276-82.
- [162] Skipper LJ, Saravanapavan P, et al. The structure of a bioactive calcia-silica sol-gel glass. *Journal of Materials Chemistry* 2005;15:2369-74.
- [163] Rámila A, Balas F, Vallet-Regí M. Synthesis Routes for Bioactive Sol-Gel Glasses: Alkoxides versus Nitrates. *Chemistry of Materials* 2002;14:542-8.
- [164] Lepry WC, Nazhat SN. Highly Bioactive Sol-Gel-Derived Borate Glasses. *Chemistry of Materials* 2015;27:4821-31.
- [165] Brinker CJ, Scherer GW. CHAPTER 2 - Hydrolysis and Condensation I: Nonsilicates. *Sol-Gel Science*. San Diego: Academic Press; 1990. p. 20-95.
- [166] Isaac J, Nohra J, Lao J, Jallot E, Nedelec JM, Berdal A, Sautier JM. Effects of strontium-doped bioactive glass on the differentiation of cultured osteogenic cells. *European Cells and Materials* 2011;21:130-43.
- [167] Gao C, Gao Q, Li Y, Rahaman MN, Teramoto A, Abe K. In vitro evaluation of electrospun gelatin-bioactive glass hybrid scaffolds for bone regeneration. *Journal of Applied Polymer Science* 2013;127:2588-99.

Chapter 3

Bioactive Polycaprolactone-Borophosphosilicate Hybrid Biomaterials via a Non-aqueous Sol Gel Process*

Overview: The synthesis of Polycaprolactone (PCL) and Borophosphosilicate glass (BPSG) based novel class II hybrid biomaterials through a non-aqueous sol-gel approach is described in this chapter. The success of forming covalent bond between organic and inorganic phases was characterized by solid state Si-NMR and FTIR. Elemental analysis, conducted by XPS and EDX are also described. Biomimetic apatite deposition in SBF indicated that this hybrid material is bioactive. In addition, 3D porous hybrid scaffold, fabricated by solvent-free casting and particulate leaching technique are also reported and discussed.

3.1 Summary

In this study, non-aqueous sol-gel process was utilized to prepare novel class II hybrid biomaterials based on functionalized polycaprolactone (PCL) diol and borophosphosilicate glass (BPSG) for potential scaffold material for bone tissue engineering applications. PCL diol was first functionalized by reacting with (3-glycidoxypropyl)trimethoxysilane. The functionalized PCL (PCL-Si) was condensed with trimethyl borate, tetraethyl orthosilicate and triethyl phosphate via non-aqueous sol-gel reactions to form covalently bonded organic-inorganic networks. FTIR, TGA, XRD, and Solid state ^{29}Si CP-MAS NMR analyses revealed that the hybrid materials were successfully prepared. Furthermore, the hybrids were amorphous and transparent up to 60 wt% of PCL-Si content. Specifically, the organic-inorganic networks had a dominant T^3 network since Si-C bond from PCL-Si is covalently bonded with the inorganic glass network and resulted in a class II hybrid. EDX and XPS studies showed uniform distributions of the various elements making up the hybrid materials. When incubated with simulated body fluids (SBF), the present hybrid materials were able to stimulate the deposition of crystalline hydroxyapatite. This study

*A version of this chapter has been published: D. Mondal, A. S. Rizkalla, K. Mequanint, *RSC Adv.* **2016**, *6*, 92824-32.

demonstrated, for the first time, the chemical reactivity of calcium-free BPSG and PCL/BPSG hybrids and their ability to deposit hydroxyapatite when incubated in SBF. The present study is also the first to incorporate B_2O_3 as a glass component in class II organic-inorganic hybrid biomaterials.

3.2 Introduction

Biomaterials used for bone tissue engineering scaffolds should be osteoconductive and osteoinductive while exhibiting appropriate porosity and pore sizes to allow for cell infiltration, tissue growth and metabolic waste removal. The rate of degradation must also match the rate of tissue formation so that the newly formed bone can replace the biomaterial [1-3]. One of the challenges associated with developing biomaterials for bone tissue engineering is that no single material meets the above-mentioned properties [4]. Bioactive conventional composite materials consisting of organic and inorganic components have been proposed to be a solution to this problem [5, 6]. However, these composites have micro-scale domain sizes leading to distinct phases within these materials. This, in turn, results in non-uniform physical, chemical, mechanical and biological properties at the nano or molecular level making them unsuitable as bone biomaterials [4].

Since bone is a combination of both organic and inorganic components with molecular level interactions between them, a logical strategy in bone tissue engineering is to design hybrid biomaterials. Hybrid biomaterials made by combining organic and inorganic components may be class I hybrids (if the interactions between the components are weak hydrogen bonding and/or van

der Waal's forces) or class II hybrids (if the interactions between the organic and inorganic components occur by covalent bonding) [7, 8]. As hybrid biomaterials exhibit single phases on molecular or macromolecular level, careful choice of both the organic and/or inorganic moieties and the synthesis approach affords to design novel materials with tailored properties for a biological environment.

The sol-gel process is a unique way to synthesize organic-inorganic hybrid materials at mild temperatures to avoid the degradation of the organic component [9]. In the last fifteen years, sol-gel derived organic-inorganic hybrid materials based on silicon alkoxide and incorporating chitosan[10], gelatin [11], poly(vinyl alcohol) [12, 13], and poly glutamic acid [14] have been reported. These hybrids were synthesized through aqueous sol-gel process in which the silicon alkoxide hydrolysis and condensation reactions were carried out using water as a reactant and medium. The necessity to use water severely constrains the choice of the organic polymers to be hydrophilic and water soluble thus precluding many desirable biodegradable polymers that are not water soluble. The use of water miscible organic solvents as co-solvents alleviates this difficulty [15, 16] but the process is neither versatile nor straightforward.

The above limitations may be addressed by the use of non-aqueous sol-gel approach [17-19] which could afford a one-pot synthesis of bioactive organic-inorganic hybrid materials with different biodegradable polymers. In the current work, we propose the utility of non-aqueous sol-gel method to prepare novel bioactive class II borophosphosilicate hybrid bone biomaterials incorporating methoxysilane functionalized polycaprolactone (PCL-Si). Bioactive glasses containing boron exhibit higher bioactivity than conventional $\text{SiO}_2\text{-P}_2\text{O}_5\text{-CaO}$ glass [20-25]. Boron in bioactive

glass matrix also inhibits the formation of silica-rich layer which results in relatively faster rate of degradation and induction of cell invasion and apatite deposition on its surface [20-22, 26, 27]. Despite these benefits, organic-inorganic hybrid biomaterials containing boron have not been reported. In view of this, the objective of the present study is to synthesize and characterize a class II hybrid biomaterial consisting of PCL and $\text{SiO}_2\text{-P}_2\text{O}_5\text{-B}_2\text{O}_3$ glass in a non-aqueous sol gel route. To the best of our knowledge, this study is the first to report the synthesis of PCL-borophosphosilicate ($\text{PCL-SiO}_2\text{-P}_2\text{O}_5\text{-B}_2\text{O}_3$) organic-inorganic class II hybrid biomaterial.

3.3 Materials and methods

3.3.1 Materials

Poly (ϵ -caprolactone) diol (PCL diol; MW 3000 g/mol) was obtained from Tri-Iso Inc. (Cardiff, CA). (3-Glycidoxypropyl) trimethoxysilane (GPTMS, 97%) and trimethyl borate (TMB, 99%) were purchased from Alfa Aesar (Ward Hill, MA). Tetraethyl orthosilicate (TEOS, 98%) and triethyl phosphate (TEP, 99.8%) were purchased from Sigma-Aldrich (Milwaukee, WI). Acetic acid glacial (AcOH) and toluene were purchased from Caledon Laboratory Chemicals (Georgetown, ON). Acetone, methanol and ethanol were purchased from BDH Chemicals (Toronto, ON). All chemicals for preparing simulated body fluid (SBF) were purchased from Sigma-Aldrich (Milwaukee, WI).

3.3.2 Functionalization of poly (ϵ -caprolactone) diol

Trimethoxysilane functionalized PCL (hereinafter referred as PCL-Si) was synthesised by the reaction of PCL diol with GPTMS in the presence of trimethyl borate (TMB) as a Lewis acid

catalyst and toluene as the solvent. The molar ratio of PCL diol, GPTMS and TMB was 1:4:0.00025. The reaction was carried on a three-necked round bottom flask connected with a condenser, a thermometer and a gas inlet/outlet under dry N₂ gas flow at 70 °C. After 24 h reaction, the product was purified by repeated precipitation in cold methanol. The product was then dried under vacuum at room temperature for 24 h.

3.3.3 Synthesis of PCL/borophosphosilicate hybrid biomaterials

The borophosphosilicate glass (BPSG) composition synthesized in this study was 91 mol % SiO₂, 5 mol % B₂O₃ and 4 mol % P₂O₅. Pre-determined amount of TEOS was added to a solution of 15 vol % acetic acid in acetone. After 6 h of mixing TEP was added to the sol and stirred for 15 min. PCL-Si was separately dissolved in acetone (10% w/v) and added to the sol followed by addition of TMB. Molar ratio of (TEOS + TEP + TMB) to acetic acid was maintained at 1:4. The contents were stirred gently for 12 h at ambient temperature, then transferred into a Teflon mold and kept in a fume hood for 3 days covered by aluminum foil with pinholes. After 3 days, ethanol (10 vol % of initial acetone) was added to the sol to reduce potential cracks that may develop in the hybrid gel during solvent evaporation and drying. Pure control glass (SiO₂-P₂O₅-B₂O₃) was prepared using similar procedures as in the case of the PCL/BPSG hybrids. Following gelation of the sols, the gel was first dried for 2 days in a fume hood followed by vacuum drying (225 mm Hg) for one day at 50 °C. The resultant transparent class II PCL/BPSB hybrid materials were transferred into sealed glass vials filled with de-ionized (DI) water and shaken for 1 day at 120 rpm to wash the unreacted AcOH and solvents. The chemical composition of the synthesized PCL/BPSB hybrid biomaterials ranged between 10-70 wt% PCL-Si and 90-30 wt% BPSG. An example clarifying the

nomenclature used in this study to identify a chemical composition of a hybrid biomaterial is presented as follows: 30H represents 30 wt% PCL-Si and 70 wt% BPSG.

3.3.4. Fabrication of porous scaffold

3D porous scaffolds of PCL/BPSG hybrid were fabricated by a compression moulding and salt leaching technique. 50H hybrid biomaterial was ground in a planetary ball mill to get fine powder. NaCl crystals were sieved to yield 150-250 μm size range. Mixtures of NaCl ranging from from 40 to 70 vol% and hybrid particles were prepared by mechanical mixing. The mixtures were compression moulded for 1 h (1 MPa and 50 °C) in a stainless steel mould to produce 3 mm in height and 6 mm in diameter scaffolds. NaCl particles were leached out with excess deionised water by shaking at 100 rpm for 2 days. Fresh water was replaced every 2 h for the first 10 h, then 2–3 times a day. The scaffolds were dried in vacuum at room temperature.

3.3.5 *In vitro* bioactivity tests

The *in vitro* bioactivity tests were carried out by studying the deposition of hydroxyapatite (HA) on the surface of BPSG and PCL/BPSG hybrid disk samples (6 mm in diameter and 2 mm in thickness) following incubation in simulated body fluid (SBF). The SBF solution has a composition and concentration similar to those of the inorganic part of human blood plasma and was prepared as described in the literature [28]. The as-prepared hybrid monoliths were pulverized by a planetary ball mill (Laval Lab Inc., Germany) for 5 min; then 0.07 g of powder was weighed and heat pressed (Carver Inc., Wabash, IN) at 60 °C and 35 MPa for 15 min using a custom-made stainless steel mold to prepare cylindrical disks. Each specimen was incubated in 9 mL of SBF

contained in polypropylene bottles covered with a tight lid. The bottles were placed in an orbital shaker (MaxQ4000, Barnstead Lab-line, IL) at 120 rpm and 37 °C at different time interval ranging from 3 to 10 days. Two parallel experiments were performed; in the first one the SBF solution was refreshed daily while in second one SBF was not refreshed during the incubation times. After each incubation period, the disks were rinsed with DI water and dried under vacuum at room temperature for 24 h.

3.3.6 Fourier Transform Infrared Spectroscopy (FTIR)

Functionalized polycaprolactone (PCL-Si) was ground in a mortar and pestle under liquid nitrogen. Pure BPSG and PCL/BPSG hybrid monoliths were ground in a planetary ball mill to get fine powder. FTIR spectra were obtained using a Nicolet 6700 FT-IR Spectrometer (Thermo Scientific, USA) at a resolution of 4 cm⁻¹ with a sample scan of 32 to identify specific functional groups. All spectra were analyzed using OMNIC series software.

3.3.7 ¹H and ²⁹Si Nuclear Magnetic Resonance Spectroscopy (NMR)

One dimensional ¹H-NMR spectra were recorded at room temperature using a Varian INOVA 600 spectrometer (Agilent Technologies, USA) operating at 100.61 MHz using d-chloroform as the solvent. Solid-state cross-polarization magic-angle spinning (CPMAS) ²⁹Si NMR spectra were acquired using a Varian Infinity Plus 400 NMR spectrometer ($\nu(^1\text{H}) = 399.5$ MHz, $\nu(^{29}\text{Si}) = 79.4$ MHz) equipped with a Varian HXY triple-resonance 7.5 mm magic-angle spinning NMR probe. The samples were packed tightly into 7.5 mm outer diameter ZrO₂ rotors and rotated at 5.5 kHz. A total of 4000 scans were summed using a 6.75 μs ¹H 90-degree pulse, 2 ms contact time, 10.24

ms acquisition time, 7 s recycle delay, 50 kHz spectral width and continuous-wave ^1H decoupling during acquisition. For processing, two zero-fills and 30 Hz line broadening were applied to the FID before Fourier transformation. The NMR spectra were referenced with respect to tetramethylsilane ($\delta(^{29}\text{Si}) = 0.0$ ppm) by setting the high-frequency peak of tetrakis(trimethylsilyl)silane to -9.8 ppm.

3.3.8 Thermogravimetric Analysis (TGA)

TGA experiments were performed using a TGA analyser SDT Q600 (TA Instruments Inc., New Castle, DE) from 25-800 °C under air atmosphere at 10 °C/min heating rate. 10-15 μg samples were used per experiment. The residual masses at 800 °C were recorded to calculate the actual organic-inorganic ratio in the hybrid materials.

3.3.9 X-ray Diffraction (XRD)

XRD was performed using an X-ray diffractometer AXS D2 PHASER (Bruker Corporation, USA) operating on $\text{CuK}\alpha$ radiation with $\lambda=1.5418\text{\AA}$. The measurements were conducted in 30kV and 10 mA in 2θ range 10-60° with steps of 0.049°. PCL/BPSG hybrids and controls (PCL-Si and BPSG) were incubated in SBF and dried under vacuum at ambient temperature for 24 h. XRD experiments were carried on the surfaces exposed to SBF. XRD measurements were done on all samples before incubation; but only selected samples were used after incubation in SBF.

3.3.10 Scanning Electron Microscopy (SEM) and Energy Dispersive X-Ray Spectroscopy (EDX)

Surface morphology of BPSG and PCL/BPSG hybrid materials were visualized by using LEO 1540XB SEM (Hitachi, Japan). Elemental distribution and chemical composition of the hybrid sample were further analyzed by using an EDX detector attached to the LEO 1540XB SEM. The specimen surfaces were coated with Osmium in Osmium Plasma Coater (OPC80T, Filgen Inc. Japan) and 3 iterations per sample were used to gain the EDX spectra. Samples incubated in SBF were dried under vacuum at room temperature for 24 h before SEM imaging. Hydroxyapatite (HA) deposition on the surface of glass and hybrid materials were visualized by using LEO 1530 (Zeiss, Oberkochen, Germany) at 5 mm working distance and 3 kV of electron beam voltage. Prior to SEM imaging, the specimen surfaces were coated with 5 nm Osmium.

3.3.11 X-Ray Photoelectron Spectroscopy (XPS)

The XPS analyses were carried out on pulverized samples using a Kratos Axis Ultra spectrometer using a monochromatic Al K α source (15mA, 14kV). The instrument work function was calibrated to give a binding energy (BE) of 83.96 eV for the Au 4f $_{7/2}$ line for metallic gold and the spectrometer dispersion was adjusted to give a BE of 932.62 eV for the Cu 2p $_{3/2}$ line of metallic copper. The Kratos charge neutralizer system was used on all specimens. Survey scan analyses were carried out with an analysis area of 300 x 700 microns and a pass energy of 160 eV. High resolution analyses were carried out with an analysis area of 300 x 700 microns and a pass energy of 20 eV. Spectra have been charge corrected to the main line of the carbon 1s spectrum

(adventitious carbon) set to 284.8 eV. Spectra were analysed using CasaXPS software (version 2.3.14).

3.4 Results and discussion

3.4.1 Preparation of functionalized PCL-Si

In this study, PCL was first functionalized with trimethoxysilane by reacting with GPTMS. The epoxy ring from GPTMS opened in the presence of a Lewis acid catalyst and react with hydroxyl groups of PCL diol [29], leaving the PCL functionalized with methoxysilane groups. In non-aqueous sol gel process, these methoxysilanes underwent carboxylation and polycondensation with $\equiv\text{Si-OH}$, $=\text{B-OH}$ and $=(\text{PO})\text{-OH}$. Both FTIR and $^1\text{H-NMR}$ results showed PCL diol was successfully functionalized at both ends by reacting it with GPTMS. The FTIR spectra (Figure 3.1A) showed peaks at 1080 and 2840 cm^{-1} for both GPTMS and PCL-Si corresponding to the stretching vibrations of Si-O bond in methoxysilane (Si-OCH_3). The oxirane C-O stretching at 915 cm^{-1} was absent while Si-C bond at 1120 cm^{-1} appeared from the PCL-Si spectrum which is expected. Comparing the $^1\text{H-NMR}$ spectra (Figure 3.1B) for GPTMS, PCL diol and PCL-Si, disappearances of the signals in PCL-Si spectrum for oxirane ring adjacent protons at $\delta= 3.13, 2.6$ and 2.78 ppm denoted as 6, 7* and 7 respectively in GPTMS spectrum provided a strong agreement with the FTIR data. Signals from proton denoted as 6 in GPTMS spectrum merged with methylene proton denoted as c in PCL-Si after functionalization. Also signals from proton 3 and 4 merged with a* and 4 respectively. Signals for protons from methoxy groups in methoxysilane of GPTMS

remained the same after functionalization in PCL-Si spectrum indicating that PCL was functionalized with trimethoxysilane group from GPTMS.

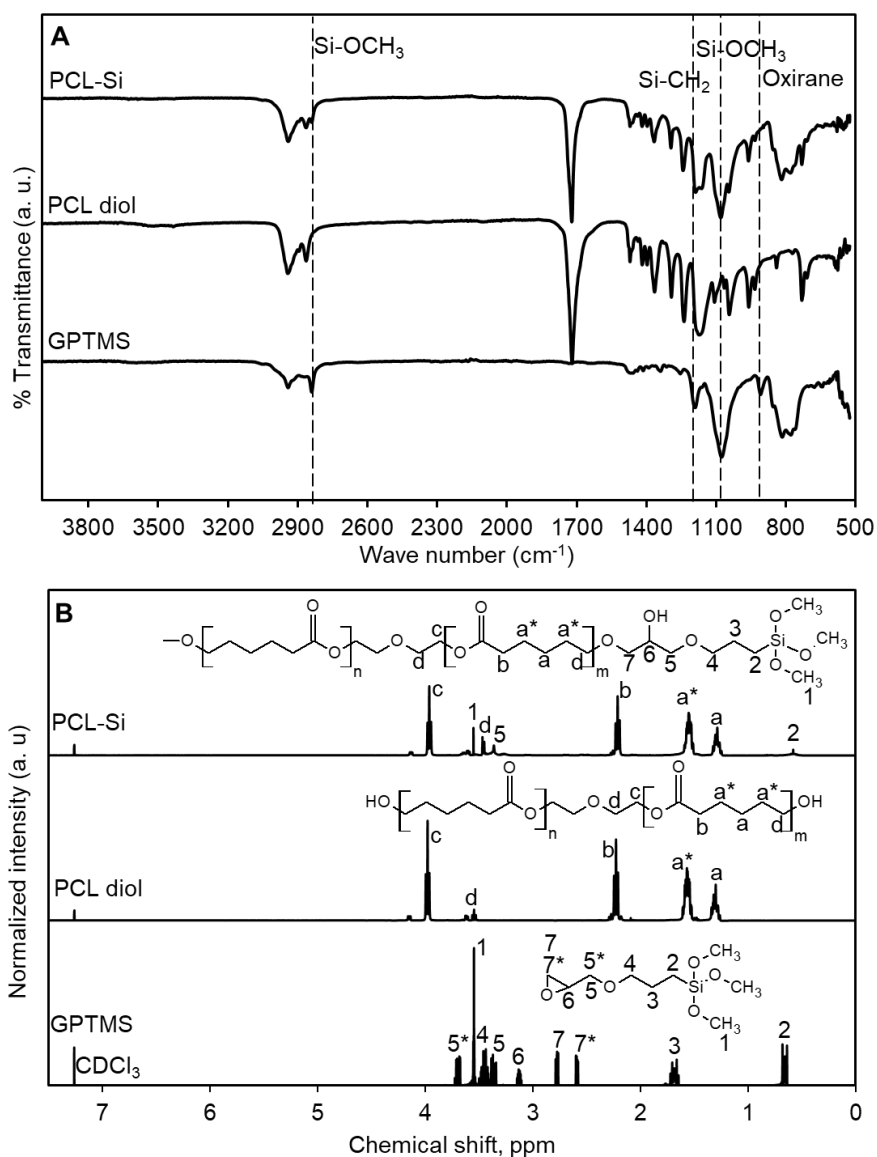


Figure 3. 1: (A) FTIR and (B) ¹H-NMR spectra (in CDCl₃) for pure GPTMS, pure PCL diol and PCL-Si.

In addition to FTIR and NMR results, TGA data showed that the PCL-Si was successfully prepared (Figure 3.2). While the PCL diol completely degraded at 535 °C, the functionalized PCL-Si had residual mass (4.0 ± 0.07 wt%) left at 800 °C, attributed to the SiO₂ from the silane group of GPTMS bonded with PCL diol and, was in agreement with that values calculated from reaction stoichiometry.

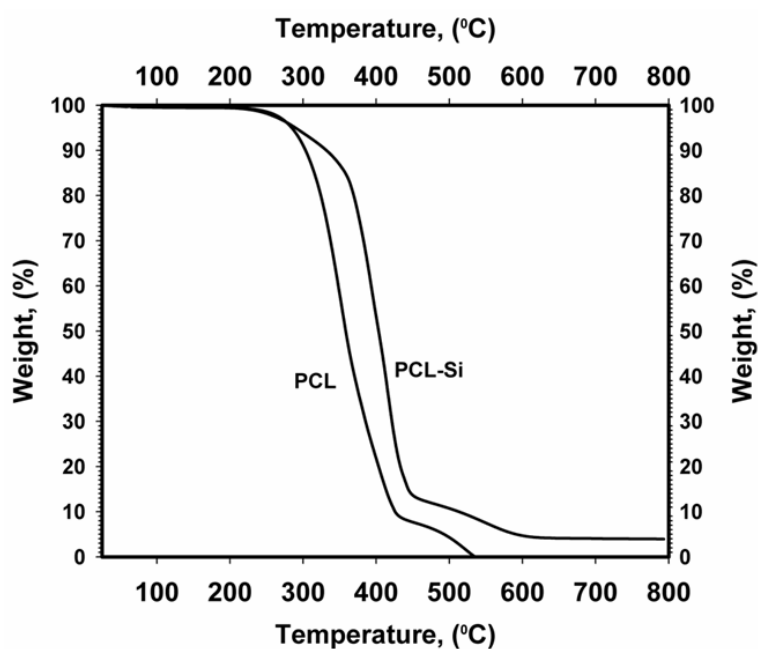


Figure 3. 2: TGA thermograms of PCL diol and PCL-Si

3.4.2 Preparation of class II PCL/BPSG hybrid biomaterials

Non-aqueous sol-gel process involves alkoxylation and polycondensation reactions of organic precursors of metal or metalloid to form metal oxides or glass systems in the absence of water. For this work, it was advantageous over conventional aqueous sol-gel since we were able to

incorporate water insoluble PCL into the hybrid matrix [18, 30-32]. Tetraethyl orthosilicate, triethyl phosphate and trimethyl borate reacted with AcOH such that the alkyl groups are replaced by the acetate on silicon, phosphorus and boron atoms, followed by the nonhydrolytic hydroxylation of acetate derivatives, as well as the esterification of AcOH, with in situ generation of water [33-35]. The reaction between TEOS and AcOH is quite slow and required a longer reaction time (ca. double) compared to other reagents such as formic acid [35]. In our system, however, formic acid was avoided since it resulted in phase-separation of trimethyl borate. This explains the prolonged gelation time taken during the synthesis of the PCL/BPSG hybrid biomaterials. As the PCL-Si content increased from 10% to 70%, the gelation time was decreased from 7 days to 5 days. Although trace amount of water is known to be generated during the non-aqueous sol-gel process [35], it did not cause phase separation of PCL from the inorganic matrix owing to the functionalization thus leading to co-condensation of the different inorganic components to form transparent and amorphous PCL- BPSG hybrid matrices.

3.4.3 Solid state ^{29}Si -MAS NMR, FTIR, and thermal analyses of class II PCL/BPSG hybrid biomaterials

To study organic-inorganic bridging, solid-state ^{29}Si -MAS NMR was conducted for BPSG and 50H hybrid materials (Figure 3.3A). In silica networks, if the silicon atom is bonded to four oxygen atoms, then the resultant structure is designated as Q network. However, if a silicon atom is bonded to three oxygen atoms and one carbon atom, then the structure is designated as T network[36]. Using ^{29}Si -NMR it is possible to detect the Q and T networks in BPSG and PCL/BPSG hybrids. Both of BPSG and 50H exhibited quaternary Si-O-Si bridging networks, which is denoted as Q⁴

network (superscript indicates the number of Si-O-Si framework connections with respect to the silicon atom). Chemical shifts at $\delta = -92$, -100 and -109 ppm were associated with Q^2 , Q^3 and Q^4 structures respectively. The dominant network was Q^3 due to the fact that the synthesized materials were not heated at high temperature and therefore resulted in Si-OH or Si-OR at one end. Chemical shifts at $\delta = -57$ and -64 ppm denoted as T^2 and T^3 were attributed to the Si-O-Si bridging networks with Si-C at one end. The control BPSG did not have any peak for T networks because it has no Si-C bonding associated with Si-O-Si bridging network. In contrast, 50H spectrum showed a T^3 network since Si-C bond from PCL-Si is covalently bonded with the inorganic glass network and resulted in a class II hybrid. In the FTIR spectra of PCL/BPSG hybrids (Figure 3.3B), characteristic peaks at 1072 cm^{-1} attributed to Si-O-Si stretching and the peaks at 920 and 670 cm^{-1} attributed to Si-O-B stretching vibration are observed. The peak at 1310 cm^{-1} is associated with P=O bond from the glass networks. The peaks observed at 1730 - 1750 cm^{-1} of PCL-Si and hybrids are due to the non-bonded carbonyl groups.

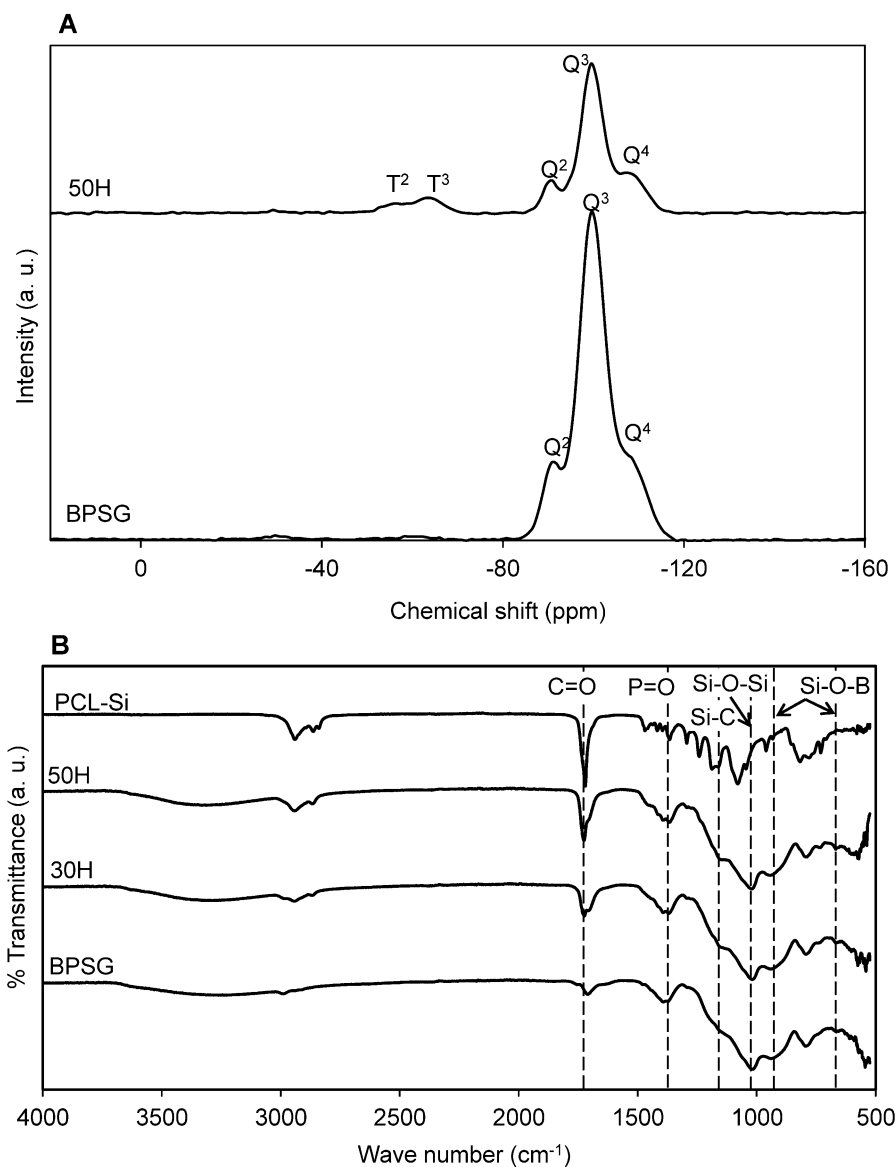


Figure 3. 3: (A) Solid state ^{29}Si -CPMAS NMR of pure glass (BPSG) and 50H hybrid material. (B) FTIR spectra of PCL/BPSG hybrid materials (30H and 50H) along with pure BPSG and PCL-Si.

A shift of the carbonyl peak from 1730 to 1750 cm^{-1} was observed with the increase in the amount of PCL-Si (Figure 3.4). If hydrogen bonding between C=O group and $\equiv\text{Si-OH}$ was the mode of

interaction (class I hybrids), the carbonyl peak shifting would have occurred at a wave number lower than 1730 cm^{-1} , which is not the case. This is a clear indication that class II hybrids were indeed formed in the present study.

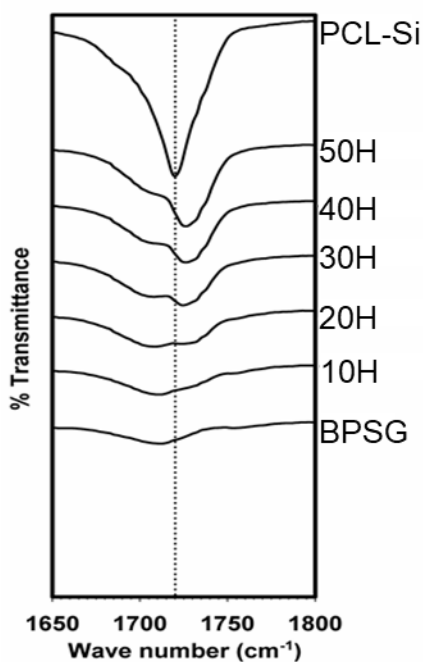


Figure 3. 4: FTIR spectra of the carbonyl stretching vibration in the range of $1650\text{--}1800\text{ cm}^{-1}$ for PCL-Si and PCL/BPSG hybrid materials.

TGA was used to evaluate the thermal stability and to estimate both the organic and inorganic contents (calculated based upon the residual weight at $800\text{ }^{\circ}\text{C}$) of the PCL/BPSG hybrid biomaterials (Table 3.1).

Table 3. 1: Mass loss during second stage (270-550 °C) thermal degradation and inorganic/organic weight ratio of PCL/BPSG hybrid materials (n=3 for each sample).

Hybrid sample	Mass loss, Wt%	Residual mass at 800 °C, Wt%	Inorganic/Organic ratio
10H	11	65	85/15
20H	17	60	78/22
30H	23	54	70/30
40H	28	49	63/37
50H	31	45	59/41

The calculated organic-inorganic ratios of the different hybrid compositions from the TGA thermograms were in good agreement with the theoretical compositions. The PCL-Si underwent degradation where complete decomposition of the polymer occurred between 310 °C and 470 °C with an inflection temperature at 419 °C (Figures 3.5). In contrast, BPSG exhibited two distinct stages of degradation and showed approximately 19 wt% weight loss below 270 °C, which could have resulted from the loss of water, solvents, and incomplete condensation of the hydrolyzed precursor compounds (specifically TEOS). The weight loss of BPSG at temperatures (270-800 °C) was insignificant. The calculated residual weight at 800 °C was 71 wt% of the initial weight.

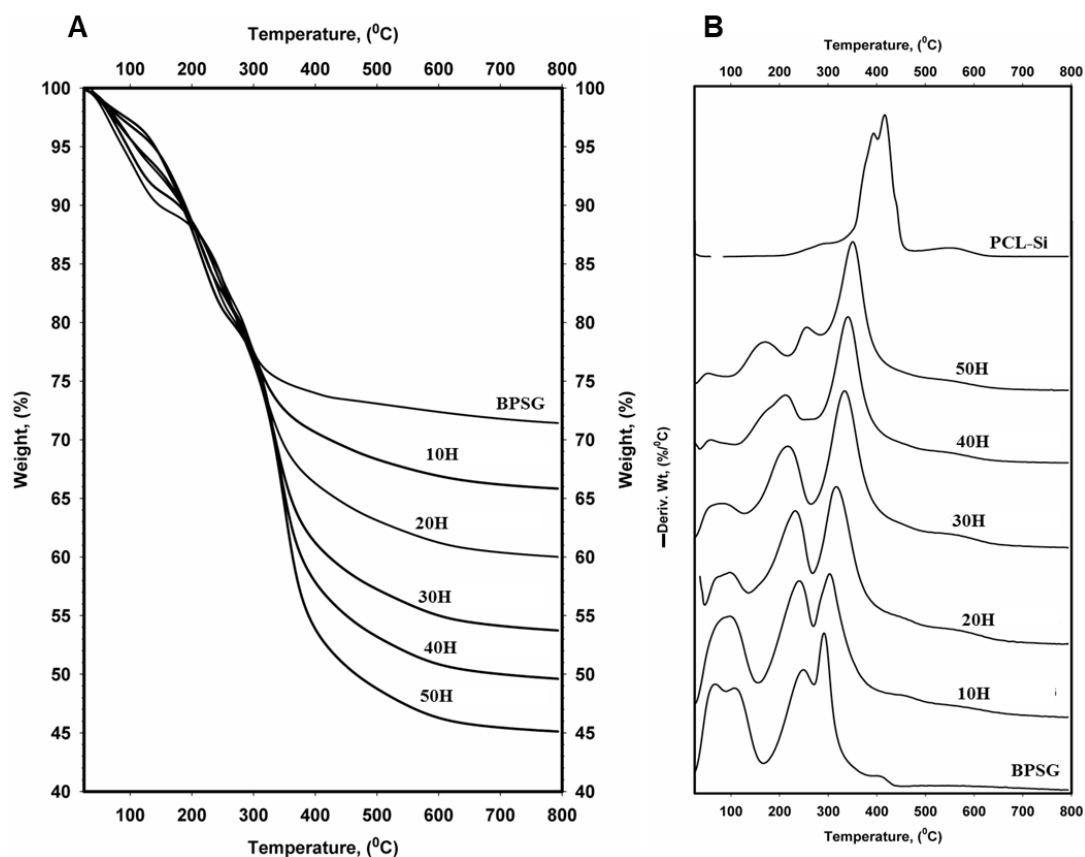


Figure 3. 5: (A) TGA thermograms and (B) first derivative of weight loss curves of BPSG, PCL-Si and PCL/BPSG hybrid materials.

The TGA thermograms of the PCL/BPSG hybrid materials displayed double stage thermal decomposition. In a similar fashion to BPSG, the first weight loss in case of the synthesized hybrids that took place below 270 °C was due to the loss of water, residual solvents and incomplete condensation of the hydrolyzed precursor compounds. The second stage weight loss (270-550 °C) was due to the decomposition of PCL. Interestingly, as the PCL content increased from 10H to 50H, the decomposition temperature range of the hybrid materials broadened. With increased PCL content, the residual weight at 800 °C decreased which was expected.

3.4.4 Phase identification and chemical composition of class II PCL/BPSG hybrid materials

Hybrid materials whose compositions ranged from 10H to 50H exhibited no diffraction peaks, indicating that the synthesized hybrid materials were completely amorphous similar to the control BPSG pure glass (Figure 3.6A). On the other hand, PCL diol and PCL-Si exhibited semi-crystalline structures having two diffraction peaks at 2θ values, 21.5° and 22.1° , which were assigned to the (110) and (111) planes [37]. Hybrid 60H, exhibited small diffraction peaks at 2θ values similar to those observed for PCL. This might have been attributed to either moderate phase separation or to the formation of PCL clusters within the hybrid matrix. Despite the fact that 10H to 50H were prepared from semi-crystalline PCL-Si, their amorphous nature strongly indicated the molecular scale interactions between BPSG and PCL phases. Furthermore, digital photos of BPSG and PCL-Si (used as controls) and 30H and 50H displayed in Figure 3.6B corroborated with XRD data providing evidence for molecular interactions between the organic and inorganic constituents of the hybrid materials. When the domain sizes of hybrid materials is reduced below the visible wavelength of light, the interaction between the different phases occur at the molecular level and reflection, diffraction or absorbance of photons will be reduced drastically resulting in a transparent material [8]. However, depending on the composition of organic and inorganic precursors a class II hybrid material could lose its transparency as the homogenous distribution of the components on a molecular level is affected.

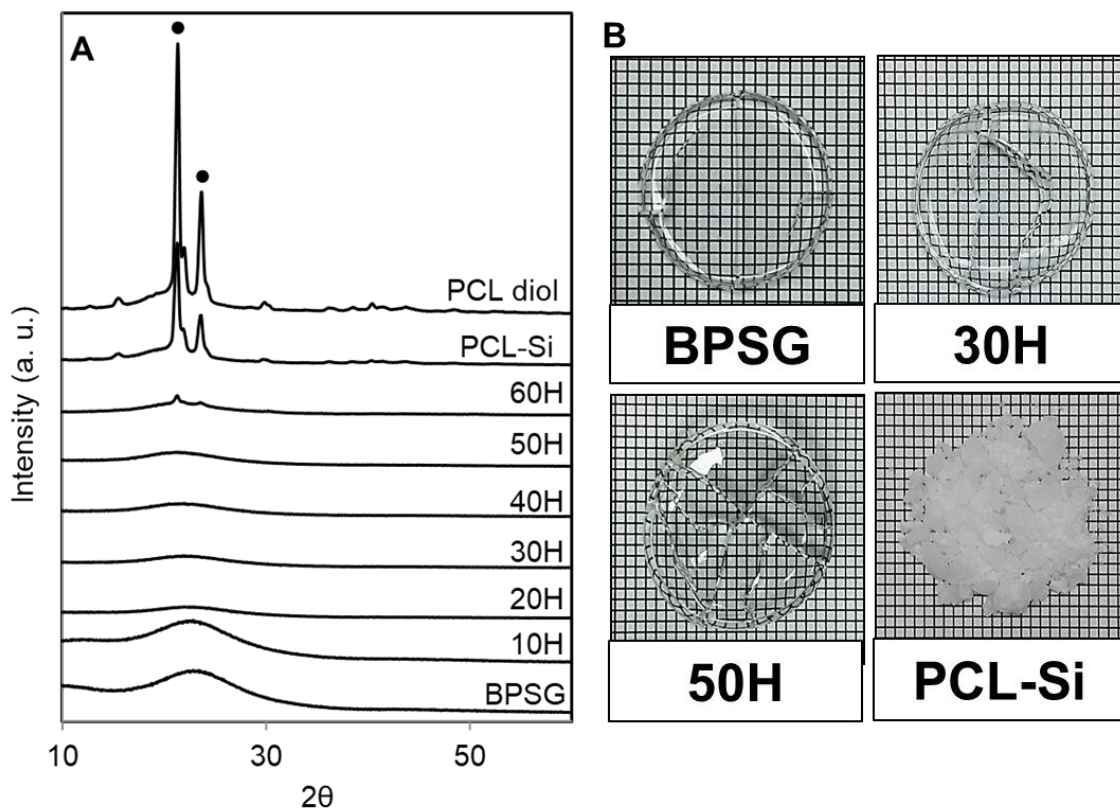


Figure 3. 6: (A) XRD patterns of PCL/BPSG hybrid materials with pure BPSG, PCL-Si and PCL diol (● denotes PCL peak), (B) digital photos of as-prepared dried glass and hybrid materials.

The surface morphology and elemental distributions for BPSG and 50H are presented in Figure 3.7. 50H exhibited rougher surface topography and larger grain size compared to the BPSG surface. Elemental analyses revealed that 50H contained higher amount of carbon due to the presence of 50 wt % PCL.

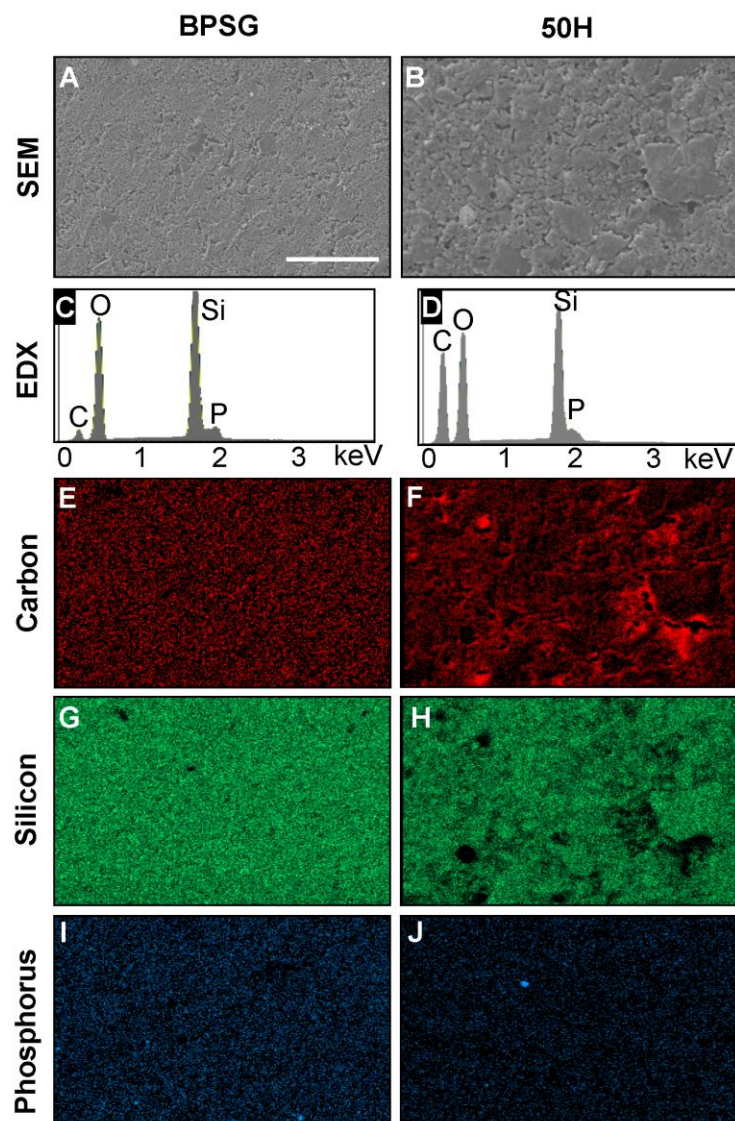


Figure 3. 7: SEM image, EDX spectra and elemental mapping of pure BPSG and 50H. (A) SEM image, (C) EDX spectrum, elemental mapping of (E) carbon, (G) silicon and (I) phosphorus for BPSG. Corresponding data for 50H is shown in Figs B, D, F, H and J.

The presence of carbon in BPSG could be due to incomplete hydrolysis of precursor compounds or solvent entrapment. Elemental mapping for carbon, silicon and phosphorus revealed that they

were all homogeneously distributed in BPSG and PCL/BPSG hybrid surfaces. Phosphorus and silicon quantification revealed good agreement between the experimental and theoretical compositions (Table 3.2). Since EDX was unable to detect boron, we examined it using XPS. In addition to demonstrating the presence of boron in both the control BPSG and 50H, chemical composition data of other elements obtained from XPS closely matched the results obtained from EDX analyses (Figure 3.8 and Table 3.3).

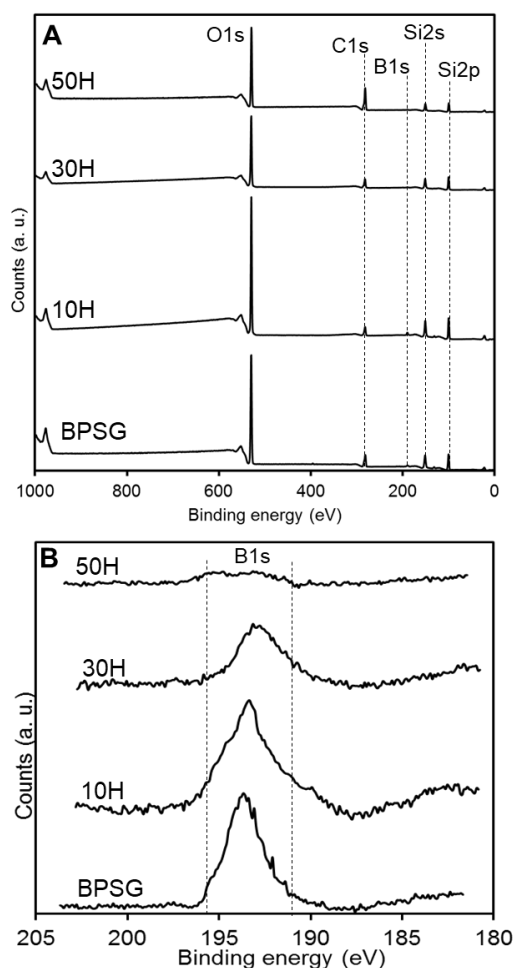


Figure 3. 8: XPS analysis of BPSG and hybrid materials. (A) Survey analysis at the surface of the specimens, (B) High resolution Boron 1s spectra.

High resolution B1s spectra (Figure B) exhibited a well-defined boron peak for BPSG, 10H and 30H, whereas in the case of 50H, broad peak was observed due to the fact that the hybrid material consisted of only 50 wt% glass, of which only 5 mol % is B₂O₃.

Table 3. 2: Theoretical and experimental weight percent elemental composition comparison for BPSB and 50H hybrid material. The experimental values were determined by EDX analysis and data are expressed as mean \pm SD for n= 15.

Elements	Pure glass (BPSG)		50H	
	Theoretical (wt%)	Experimental (wt%)	Theoretical (wt%)	Experimental (wt%)
Silicon	41.2	38.13 \pm 0.87	21.41	22.1 \pm 1.6
Phosphorus	2	3.18 \pm 0.07	1	0.66 \pm 0.15

Table 3. 3: Atomic compositions of Si, P and B appeared in BPSG and 50H measured by EDX analysis and XPS analysis.

Elements	EDX analysis		XPS analysis			
	BPSG (atomic%)	50H (atomic%)	BPSG (atomic%)	10H (atomic%)	30H (atomic%)	50H (atomic%)
Si	27.1	12.85	18.9	19.1	18.8	11.6
P	2.05	0.35	1.1	0.6	0.4	0.3
B	-	-	1.1	1.0	0.8	0.3

3.4.5 *In vitro* bioactivity of class II PCL/BPSG hybrid biomaterials

SEM images of BPSG and 50H surface before and after incubation with SBF for 7 days are shown in Figure 3.9. Before incubation in SBF, BPSG and PCL/BPSG hybrid exhibited smooth surfaces. After incubation for 7 days both BPSG and PCL/BPSG surfaces were covered by spherical hydroxyapatite particles. Interestingly, when incubation with SBF was done without refreshing the solution, BPSG surface became porous and displayed very rough morphology which may be due to bulk degradation of the pure glass after incubation in SBF (Figure 3.9E). In contrast, 50H had smooth surface even after incubation in SBF for 7 days without solution refreshment likely to be the result of the slower degrading PCL compensating the faster degradation of the glass in the hybrid material. The Ca/P ratio for the BPSG and 50H calculated from EDX spectra (Figure 3.9 C&D insets) showed 1.55 ± 0.03 and 1.71 ± 0.04 respectively suggesting that higher amount of calcium deposited as hydroxyapatite in the hybrid 50H. Since pure hydroxyapatite has a Ca/P ratio of 1.67, our data on 50H matches this stoichiometric ratio indicating the utility of boron-based hybrid biomaterials.

The XRD patterns of BPSG and 50H after incubating in SBF for 3, 7 and 10 days (Figure 3.10) showed the deposition of low crystalline hydroxyapatite within the first 3 days. After 7 and 10 days of incubation, however, strong hydroxyapatite peaks ($2\theta = 25.9, 31.77$ and 45.40) were observed indicating that both the control BPSG glass and the hybrid materials were bioactive. Consistent with our SEM images (Figure 3.9 C&D), we observed considerably dense layer of hydroxyapatite in the samples with daily SBF refreshment (Figure 3.10 A&B). Without daily SBF refreshment, the PCL peaks were detected (Figure 3.10D; $2\theta = 21.5, \text{ and } 22.10$) since the low

molecular weight PCL released during the hydroxyapatite formation remained on the surface. This study demonstrated, for the first time, the chemical reactivity of calcium free BPSG and PCL/BPSG hybrids and their ability to deposit hydroxyapatite when incubated in SBF. The present study is also the first to incorporate B_2O_3 as a glass component in class II organic-inorganic hybrids. The presence of B_2O_3 prevents the formation of silica rich layer which is known to cause discontinuous release of metal ions from glass and formation of hydroxyapatite [26, 27] [20] while accelerating bulk degradation of the glass matrix [26]. When the BPSG is bonded to a polymer to produce a class II hybrid, its subsequent degradation and formation of hydroxyapatite could be controlled by controlling the polymer content in the hybrid and the B_2O_3 in the glass. Thus, the presence of B_2O_3 into the current PCL/BPSG hybrid matrix could enhance continuous degradation and dissolution of components as well as the formation of hydroxyapatite.

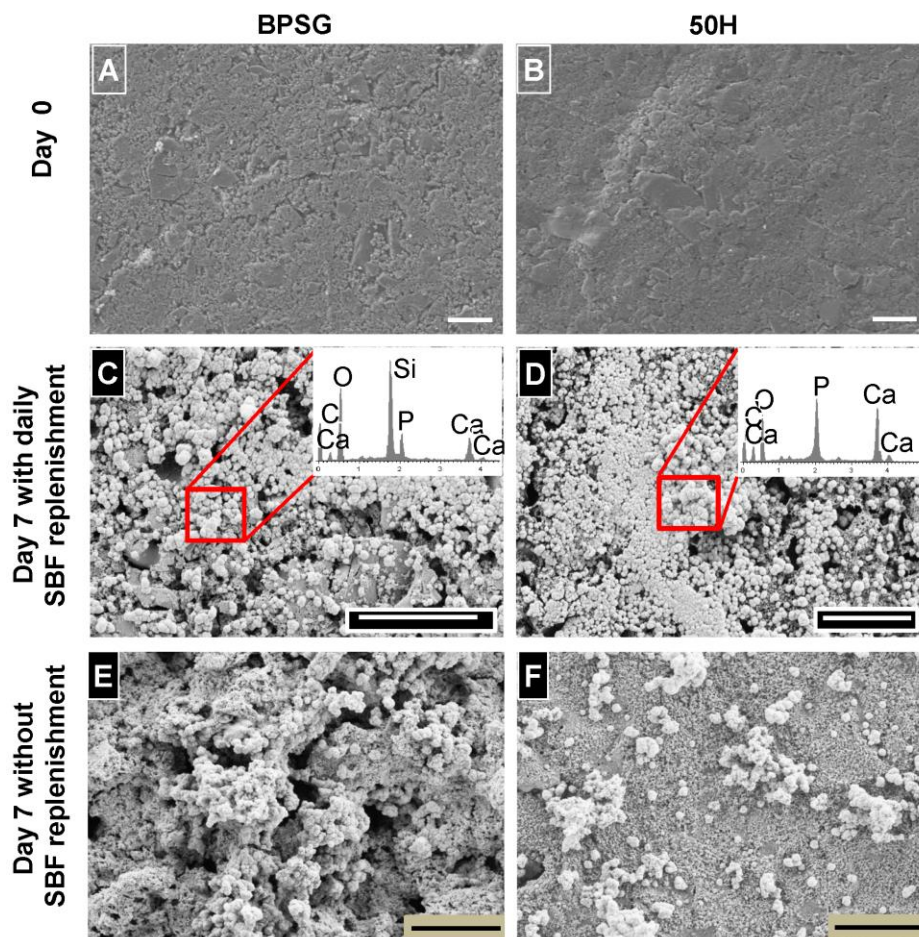


Figure 3. 9: SEM images of (A) pure glass BPSG and (B) 50H surfaces before incubated in SBF. (C) BPSG and (D) 50H surfaces after immersion in SBF for 7 days with refreshment of SBF. Inset of (C) and (D) represent the EDX spectra of rectangular area. (E) BPSG and (F) 50H surfaces after incubated in SBF for 10 days without refreshing the SBF solution. The scale bar is 20 μm . Insets in C and D are the EDX spectra apatite particles.

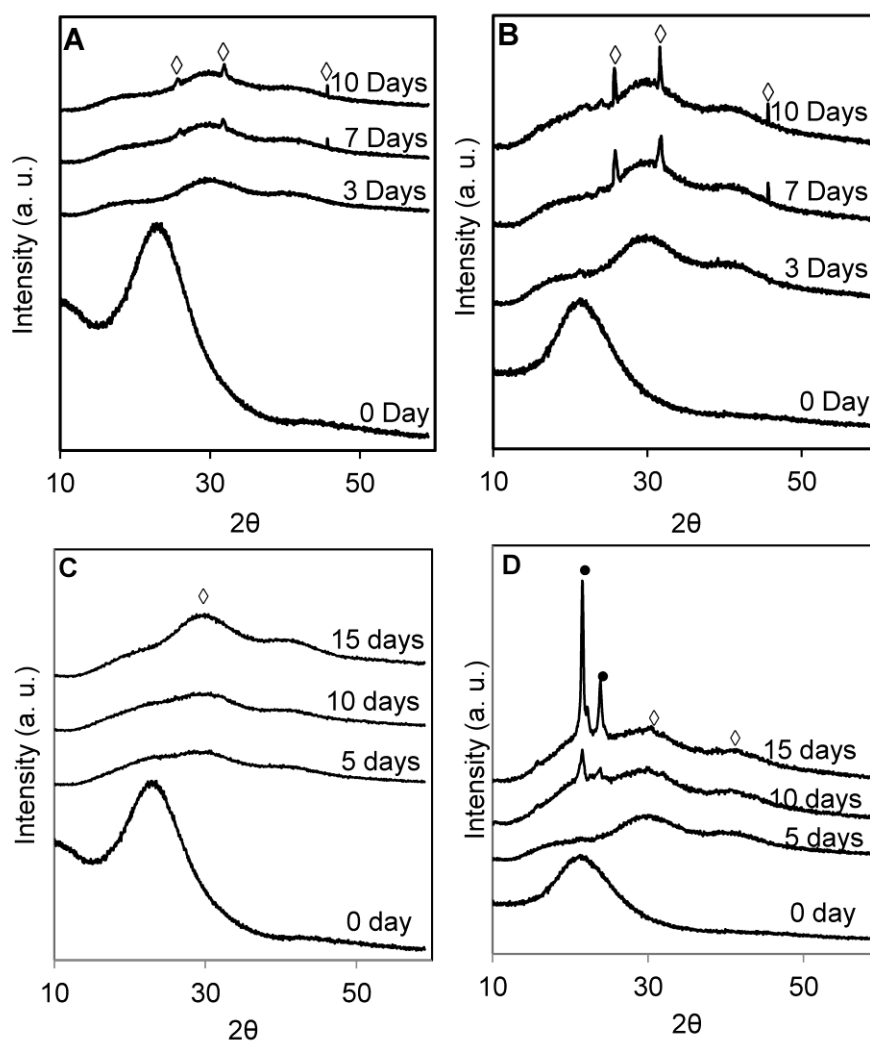


Figure 3. 10: XRD profiles of (A) BPSG and (B) 50H hybrid materials after incubated in SBF for 3, 7 and 10 days with daily refreshment of SBF. XRD profiles of (C) BPSG and (D) 50H hybrid materials after incubated in SBF for 5, 10 and 15 days without changing the SBF solution. (◊ hydroxyapatite peak and ● PCL peak).

3.4.6 Porous 3D scaffolds from class II PCL/BPSG hybrid biomaterials

Processability into 3D porous scaffolds is an important requirement for a hybrid organic-inorganic biomaterial for bone tissue engineering and regeneration applications. Electrospinning is by far the

most widely used technique to fabricate scaffolds from hybrid organic-inorganic biomaterials [15, 38]. However, the small pore sizes inherent to electrospun scaffolds limits cellular infiltration [39]. Another approach reported is foaming using surfactants but this approach often yields ill-defined pores with poor pore interconnectivity [40, 41]. The use of organic solvents or surfactants is also not desired since their post-fabrication complete removal is a challenge. In the current work, we have developed a solvent-free casting and particulate leaching method and fabricated well-defined and highly porous PCL/BPSG hybrid scaffolds (Figure 3.11). Contrary to the method of solid-state gas foaming which resulted in isolated pores [42, 43], our scaffolds were fully interconnected suggesting their utility as ideal scaffolds for bone tissue engineering.

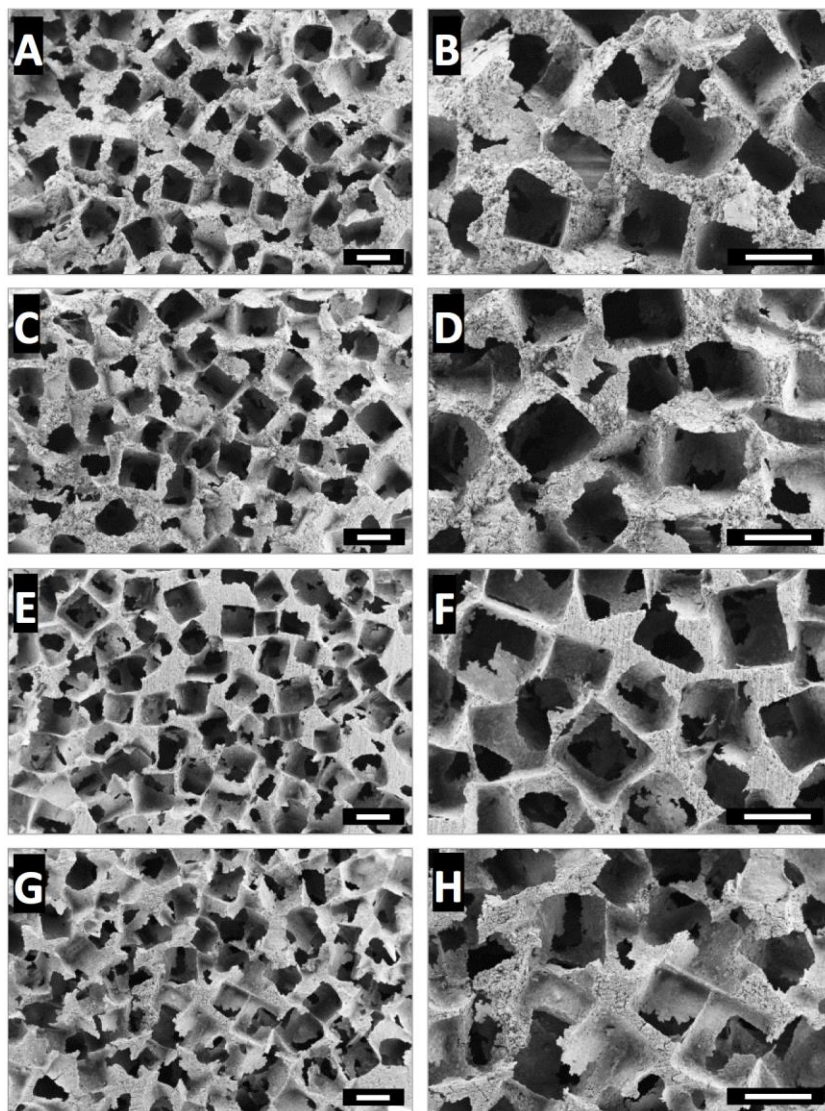


Figure 3. 11: SEM images of class II PCL/BPSG hybrid scaffolds fabricated by solvent-free casting and particulate leaching method with different NaCl particle loading. (A, B) 40 vol%; (C, D) 50 vol%; (E, F) 60 vol%; (G, H) 70 vol% NaCl particles. Scale bar is 200 μm .

3.5 Conclusions

PCL/BPSG class II hybrid biomaterials were successfully synthesized via a non-aqueous sol-gel process. The PCL chains were successfully end-capped by trimethoxysilane functional groups and

underwent carboxylation and condensation with glass precursors to form a single-phase organic-inorganic matrix. Solid-state ^{29}Si -NMR studies revealed that the hybrid materials possessed covalent bonding between PCL and BPSG phases. The SEM/EDX and XPS results revealed homogeneity of the hybrid system and the elemental analyses result indicated that all the elements were incorporated successfully. Hydroxyapatite deposition was observed on the hybrid materials and 3D porous scaffolds were successfully fabricated. Taken together, the synthesized hybrid materials could be potential candidates for bone tissue engineering applications.

3.6 References

- [1] Bose S, Roy M, Bandyopadhyay A. Recent advances in bone tissue engineering scaffolds. *Trends in Biotechnology* 2012;30:546-54.
- [2] Hutmacher DW. Scaffolds in tissue engineering bone and cartilage. *Biomaterials* 2000;21:2529-43.
- [3] O'Brien FJ. Biomaterials & scaffolds for tissue engineering. *Materials Today* 2011;14:88-95.
- [4] Jones JR. Review of bioactive glass: From Hench to hybrids. *Acta Biomaterialia* 2013;9:4457-86.
- [5] Niemelä T, Niiranen H, Kellomäki M, Törmälä P. Self-reinforced composites of bioabsorbable polymer and bioactive glass with different bioactive glass contents. Part I: Initial mechanical properties and bioactivity. *Acta Biomaterialia* 2005;1:235-42.
- [6] Rezwan K, Chen QZ, Blaker JJ, Boccaccini AR. Biodegradable and bioactive porous polymer/inorganic composite scaffolds for bone tissue engineering. *Biomaterials* 2006;27:3413-31.
- [7] Kickelbick G. Introduction to Hybrid Materials. *Hybrid Materials: Wiley-VCH Verlag GmbH & Co. KGaA*; 2006. p. 1-48.
- [8] Novak BM. Hybrid Nanocomposite Materials—between inorganic glasses and organic polymers. *Advanced Materials* 1993;5:422-33.
- [9] Wen J, Wilkes GL. Organic/Inorganic Hybrid Network Materials by the Sol–Gel Approach. *Chemistry of Materials* 1996;8:1667-81.

- [10] Shirotsaki Y, Tsuru K, Hayakawa S, Osaka A, Lopes MA, Santos JD, et al. Physical, chemical and in vitro biological profile of chitosan hybrid membrane as a function of organosiloxane concentration. *Acta Biomaterialia* 2009;5:346-55.
- [11] Ren L, Tsuru K, Hayakawa S, Osaka A. Sol-gel preparation and in vitro deposition of apatite on porous gelatin-siloxane hybrids. *Journal of Non-Crystalline Solids* 2001;285:116-22.
- [12] Pereira MM, Jones JR, Orefice RL, Hench LL. Preparation of bioactive glass-polyvinyl alcohol hybrid foams by the sol-gel method. *J Mater Sci: Mater Med* 2005;16:1045-50.
- [13] Viviane SG, Alessandra Z, Natalia MO, Alfredo MG, Rogéria S, Marivalda MP. In vitro and in vivo osteogenic potential of bioactive glass-PVA hybrid scaffolds colonized by mesenchymal stem cells. *Biomedical Materials* 2012;7:015004.
- [14] Valliant EM, Romer F, Wang D, McPhail DS, Smith ME, Hanna JV, et al. Bioactivity in silica/poly(γ -glutamic acid) sol-gel hybrids through calcium chelation. *Acta Biomaterialia* 2013;9:7662-71.
- [15] Allo BA, Rizkalla AS, Mequanint K. Synthesis and Electrospinning of ϵ -Polycaprolactone-Bioactive Glass Hybrid Biomaterials via a Sol-Gel Process. *Langmuir* 2010;26:18340-8.
- [16] Rhee S-H, Choi J-Y, Kim H-M. Preparation of a bioactive and degradable poly(ϵ -caprolactone)/silica hybrid through a sol-gel method. *Biomaterials* 2002;23:4915-21.
- [17] Bilecka I, Niederberger M. New developments in the nonaqueous and/or non-hydrolytic sol-gel synthesis of inorganic nanoparticles. *Electrochimica Acta* 2010;55:7717-25.
- [18] Hay JN, Raval HM. Synthesis of Organic-Inorganic Hybrids via the Non-hydrolytic Sol-Gel Process. *Chemistry of Materials* 2001;13:3396-403.
- [19] Vioux A. Nonhydrolytic Sol-Gel Routes to Oxides. *Chemistry of Materials* 1997;9:2292-9.
- [20] Kaur G, Pandey OP, Singh K, Homa D, Scott B, Pickrell G. A review of bioactive glasses: Their structure, properties, fabrication and apatite formation. *Journal of Biomedical Materials Research Part A* 2014;102:254-74.
- [21] Yao A, Wang D, Huang W, Fu Q, Rahaman MN, Day DE. In Vitro Bioactive Characteristics of Borate-Based Glasses with Controllable Degradation Behavior. *Journal of the American Ceramic Society* 2007;90:303-6.
- [22] Fu Q, Rahaman MN, Bal BS, Bonewald LF, Kuroki K, Brown RF. Silicate, borosilicate, and borate bioactive glass scaffolds with controllable degradation rate for bone tissue engineering applications. II. In vitro and in vivo biological evaluation. *Journal of Biomedical Materials Research Part A* 2010;95A:172-9.
- [23] Gu Y, Wang G, Zhang X, Zhang Y, Zhang C, Liu X, et al. Biodegradable borosilicate bioactive glass scaffolds with a trabecular microstructure for bone repair. *Materials Science and Engineering: C* 2014;36:294-300.
- [24] Ning J, Yao A, Wang D, Huang W, Fu H, Liu X, et al. Synthesis and in vitro bioactivity of a borate-based bioglass. *Materials Letters* 2007;61:5223-6.

- [25] Wu C, Miron R, Sculean A, Kaskel S, Doert T, Schulze R, et al. Proliferation, differentiation and gene expression of osteoblasts in boron-containing associated with dexamethasone deliver from mesoporous bioactive glass scaffolds. *Biomaterials* 2011;32:7068-78.
- [26] Rahaman MN, Day DE, Sonny Bal B, Fu Q, Jung SB, Bonewald LF, et al. Bioactive glass in tissue engineering. *Acta Biomaterialia* 2011;7:2355-73.
- [27] Xu S, Yang X, Chen X, Shao H, He Y, Zhang L, et al. Effect of borosilicate glass on the mechanical and biodegradation properties of 45S5-derived bioactive glass-ceramics. *Journal of Non-Crystalline Solids* 2014;405:91-9.
- [28] Kokubo T, Takadama H. How useful is SBF in predicting in vivo bone bioactivity? *Biomaterials* 2006;27:2907-15.
- [29] Shechter L, Wynstra J. Glycidyl Ether Reactions with Alcohols, Phenols, Carboxylic Acids, and Acid Anhydrides. *Industrial & Engineering Chemistry* 1956;48:86-93.
- [30] Debecker DP, Mutin PH. Non-hydrolytic sol-gel routes to heterogeneous catalysts. *Chemical Society Reviews* 2012;41:3624-50.
- [31] Niederberger M. Nonaqueous Sol-Gel Routes to Metal Oxide Nanoparticles. *Accounts of Chemical Research* 2007;40:793-800.
- [32] Viau L, Néouze M-A, Biolley C, Volland S, Brevet D, Gaveau P, et al. Ionic Liquid Mediated Sol-Gel Synthesis in the Presence of Water or Formic Acid: Which Synthesis for Which Material? *Chemistry of Materials* 2012;24:3128-34.
- [33] Karmakar B, De G, Kundu D, Ganguli D. Silica microspheres from the system tetraethyl orthosilicate-acetic acid-water. *Journal of Non-Crystalline Solids* 1991;135:29-36.
- [34] Sanchez C, Livage J, Henry M, Babonneau F. Glasses and Glass Ceramics from Gels Chemical modification of alkoxide precursors. *Journal of Non-Crystalline Solids* 1988;100:65-76.
- [35] Sharp K. A two-component, non-aqueous route to silica gel. *J Sol-Gel Sci Technol* 1994;2:35-41.
- [36] MacKenzie KJ, Smith ME. *Multinuclear Solid State NMR of Inorganic Materials*: Pergamon; 2002.
- [37] Bittiger H, Marchessault RH, Niegisch WD. Crystal structure of poly- ϵ -caprolactone. *Acta Crystallographica Section B* 1970;26:1923-7.
- [38] Kim HW, Kim HE, Knowles JC. Production and potential of bioactive glass nanofibers as a next-generation biomaterial. *Advanced Functional Materials* 2006;16:1529-35.
- [39] Nam J, Huang Y, Agarwal S, Lannutti J. Improved cellular infiltration in electrospun fiber via engineered porosity. *Tissue Engineering* 2007;13:2249-57.
- [40] Mahony O, Tsigkou O, Ionescu C, Minelli C, Ling L, Hanly R, et al. Silica-Gelatin Hybrids with Tailorable Degradation and Mechanical Properties for Tissue Regeneration. *Advanced Functional Materials* 2010;20:3835-45.

[41] Jones JR, Ehrenfried LM, Hench LL. Optimising bioactive glass scaffolds for bone tissue engineering. *Biomaterials* 2006;27:964-73.

[42] Zhou CC, Ma L, Li W, Yao DG. Fabrication of tissue engineering scaffolds through solid-state foaming of immiscible polymer blends. *Biofabrication* 2011;3.

[43] Ma L, Jiang W, Li W. Solvent-Free Fabrication of Tissue Engineering Scaffolds With Immiscible Polymer Blends. *International Journal of Polymeric Materials and Polymeric Biomaterials* 2014;63:510-7.

Chapter 4

Mechanically-competent and Cytocompatible Polycaprolactone-Borophosphosilicate Hybrid Biomaterials†

Overview: The mechanical properties, biodegradation and cell compatibility of class II hybrid biomaterials are elucidated in this chapter. In addition to class II hybrid biomaterials, a set of composites with similar compositions were prepared, and their properties were compared.

4.1 Summary

Organic-inorganic class II hybrid materials have domain sizes at the molecular level and chemical bonding between the organic and inorganic phases. We have previously reported the synthesis of class II hybrid biomaterials from alkoxy silane-functionalized polycaprolactone (PCL) and borophosphosilicate (B_2O_3 - P_2O_5 - SiO_2) glass (BPSG) through a non-aqueous sol-gel process. In the present study, the mechanical properties and degradability of these PCL/BPSG hybrid biomaterials were studied and compared to those of their conventional composite counterparts. The compressive strength, modulus and toughness of the hybrid biomaterials were significantly greater compared to the conventional composites, likely due to the covalent bonding between the organic and inorganic phases. A hybrid biomaterial (50wt% PCL and 50wt% BPSG) exhibited compressive strength, modulus and toughness values of 32.2 ± 3.5 MPa, 573 ± 85 MPa and 1.54 ± 0.03 MPa, respectively; whereas the values for composite of similar composition were 18.8 ± 1.6 MPa, 275 ± 28 MPa and 0.76 ± 0.03 MPa, respectively. Degradation in phosphate-buffered saline was slower for hybrid biomaterials compared to their composite counterparts. Thus, these hybrid materials possess superior mechanical properties and more controlled degradation characteristics compared to their corresponding conventional composites. To assess *in vitro*

†A version of this chapter has been published: D. Mondal, S.J. Dixon, K. Mequanint, A.S. Rizkalla, *J. Mech. Behav. Biomed. Mater.* **2017**, 75, 180-189

cytocompatibility, MC3T3-E1 pre-osteoblastic cells were seeded onto the surfaces of hybrid biomaterials and polycaprolactone (control). Compared to polycaprolactone, cells on the hybrid material displayed enhanced spreading, focal adhesion formation, and cell number, consistent with excellent cytocompatibility. Thus, based on their mechanical properties, degradability and cytocompatibility, these novel biomaterials have potential for use as scaffolds in bone tissue engineering and related applications.

4.2 Introduction

Scaffolds play a key role in bone tissue engineering, providing a 3-dimensional environment for cell seeding and proliferation as well as filling bone defects while providing mechanical competence during bone regeneration [1]. Ideally, scaffolds for bone tissue engineering are osteoinductive, osteoconductive, porous and biodegradable, properties that will support the attachment and proliferation of osteoblasts, and enhance bone formation and angiogenesis [2]. Conventional bioactive composites, made of organic and inorganic components, could be good candidates for this application. However, conventional composites consist of distinct phases, resulting in non-uniform physical, chemical, mechanical and biological properties, making them unsuitable as bone biomaterials [3, 4].

As the extracellular matrix of bone is primarily collagen and hydroxyapatite with molecular interactions between them, a logical strategy for bone tissue engineering is to develop hybrid biomaterials. These could be class I hybrids that are characterized by weak interactions, such as hydrogen bonds and/or van der Waal's forces, between components. Alternatively, these could be class II hybrids that are characterized by stronger interactions, such as covalent bonding, between

the organic and inorganic components [5, 6]. Class II hybrid biomaterials act as a single-phase material at the molecular level, yielding a material that can be uniformly tailored for specific applications.

SiO₂-P₂O₅-CaO-based bioactive glasses (BGs), biodegradable synthetic polymers and their composites have been widely studied as scaffold materials for bone tissue engineering. It has been reported that BGs have excellent biocompatibility, biodegradability and osteoconductivity, as well as the ability to induce the formation of bone-like mineral at the interface with living tissue [5, 7]. Recently, several studies revealed that BGs containing boron have higher bioactivity than SiO₂-P₂O₅-CaO bioactive glass [8-11]. Boron in the bioactive glass matrix inhibits formation of a silica-rich layer in contact with body fluid. Lack of the silica-rich layer results in relatively faster degradation of the glass matrix and the release of ions, which may promote cell attachment and apatite deposition on the biomaterial surface [8, 12-15].

Bioactive glasses prepared by sol-gel synthesis, can be combined with organic biopolymers such as poly(lactide-*co*-glycolide) (PLGA), poly(L-lactide) (PLA) or poly(D,L-lactide) (PDLLA) to improve strength, toughness and degradation behavior [5, 16-20]. However, when such conventional composites are made using BG particles or sol-gel derived BG networks, BG is generally covered by the polymer matrix. Therefore, the BG is not in direct contact with body fluid before polymer degradation, resulting in slow bonding to bone tissue *in vivo* [5, 19]. In addition, micron-size BG particles may result in inhomogeneity and inferior chemical and mechanical properties. Alternatively, organic-inorganic hybrids can be synthesized by introducing the polymer to the inorganic component and blending them on a molecular scale (yielding class I hybrids) or by chemical crosslinking *during* the hydrolysis stage (yielding class II hybrids). Class II hybrid

biomaterials have previously been synthesized using polymers such as poly(ϵ -caprolactone) (PCL) [21, 22], polyethylene glycol [23], gelatin [24], poly (tetramethylene oxide) [25], poly(dimethylsiloxane) [26, 27] as precursors. However, most of these studies used SiO_2 as the sole inorganic component, yielding hybrids which are not sufficiently bioactive to induce osteogenesis [5].

In our previous work, we successfully synthesized class II hybrid biomaterial from alkoxy silane-functionalized PCL and borophosphosilicate ($\text{B}_2\text{O}_3\text{-P}_2\text{O}_5\text{-SiO}_2$) glass (BPSG) through a non-aqueous sol-gel process [28]. However, it is essential to evaluate the mechanical, degradation and biological properties of this material to assess its potential for use in tissue engineering. In the present study, we also evaluated the effect of covalent crosslinking between PCL and BPSG on the mechanical and degradation properties of the resulting material. There is no systematic study currently published on the mechanical and degradation behavior of class II hybrid biomaterials comprising borophosphosilicate glass. In addition to class II hybrid biomaterials, a set of composites with similar compositions were prepared from non-functionalized PCL and BPSG, and their properties were compared. The suitability of these hybrids for bone tissue engineering applications was further assessed by studying the cell-material interactions using the pre-osteoblast MC3T3-E1 cell line. This study adds important information to our knowledge of the mechanical properties, degradability and cytocompatibility of class II hybrid biomaterials and their composite counterparts.

4.3 Materials and methods

4.3.1 Materials

Poly (ϵ -caprolactone) diol (PCL diol; MW 3000 g/mol) was obtained from Tri-Iso Inc. (Cardiff, CA). (3-Glycidoxypropyl) trimethoxysilane (GPTMS, 97%) and trimethyl borate (TMB, 99%) were purchased from Alfa Aesar (Ward Hill, MA). Tetraethyl orthosilicate (TEOS, 98%), triethyl phosphate (TEP, 99.8%), phosphate-buffered saline (PBS) and TritonTM X-100 were purchased from Sigma-Aldrich (Milwaukee, WI). Acetic acid glacial (AcOH) and toluene were purchased from Caledon Laboratory Chemicals (Georgetown, ON). Acetone, methanol and ethanol were purchased from BDH Chemicals (Toronto, ON). Minimal essential medium (α -MEM), fetal bovine serum (FBS), antibiotic-antimycotic solution (10,000 units/mL penicillin; 10,000 μ g/mL streptomycin; and 25 μ g/mL amphotericin B), paraformaldehyde (PFA) and trypsin were purchased from Gibco, ThermoFisher Scientific (USA). Bovine albumin (BSA) was purchased from MP Biomedicals LLC (USA).

4.3.2 Preparation of PCL/BPSG class II hybrids and composites

PCL/BPSG hybrid biomaterials were prepared via non-aqueous sol-gel process described previously [28]. BPSG composition was 91 mol % SiO₂, 5 mol % B₂O₃ and 4 mol % P₂O₅. Briefly, trimethoxysilane-functionalized PCL (PCL-Si) was synthesized by the reaction of PCL diol with GPTMS. TEOS was added to a solution of acetic acid in acetone (sol). After 6 h of mixing, TEP was added to the sol and stirred for 15 min. PCL-Si was separately dissolved in acetone (10% w/v) and added to the sol followed by addition of TMB. The contents were stirred gently for 12 h at

ambient temperature, then transferred into a Teflon mold and allowed to gel in a fume hood for 3 days covered by aluminum foil with few pinholes. Composites of PCL/BPSG were prepared using a similar process, except the PCL was not functionalized with alkoxy silane groups. After gelation of both the hybrid and composite sols, gels were dried for a further 2 days in a fume hood followed by vacuum drying (225 mm Hg) for one day at 50 °C. The resultant transparent class II PCL/BPSG hybrid biomaterials and opaque PCL/BPSG composites were transferred into sealed glass vials filled with deionized water and shaken for 1 day at 120 rpm to remove the unreacted AcOH and solvents. The chemical composition of the synthesized PCL/BPSG hybrid biomaterials and composites ranged between 10-50 wt% PCL and 90-50 wt% BPSG (Table 4.1).

Table 4. 1: Composition of PCL/BPSG hybrids and composites

PCL/BPSG (wt %)	Hybrid Nomenclature	Composite Nomenclature
0/100	BPSG	BPSG
10/90	10H	10C
30/70	30H	30C
40/60	40H	40C
50/50	50H	50C
100/0	PCL	PCL

4.3.3 Evaluation of mechanical properties

To prepare cylindrical specimens for mechanical testing, the as-prepared hybrid and composite monoliths were pulverized by a planetary ball mill (Laval Lab Inc., Germany) for 5 min; then 0.07 g of powder was weighed and heat pressed (Carver Inc., Wabash, IN) at 60 °C and 35 MPa for 15 min using a custom-made stainless steel mold. The cylindrical specimens had an aspect ratio 3:2

(9 mm in height and 6 mm in diameter). A uniaxial compression test was conducted using an Instron Universal Mechanical testing machine equipped with 5 kN load cell (Instron model 3345, Canton, MA) with crosshead speed of 1 mm/min at ambient temperature. The compressive strength and modulus were determined from ultimate stress values and the slope of the initial linear elastic portions of the stress–strain curves, respectively. Toughness values were obtained from the area under the stress-strain curves. The fracture surface of selected specimens was observed by scanning electron microscopy (SEM, see below).

4.3.4 Assessment of *in vitro* degradation

Degradation behavior was characterized by studying weight loss and ion release from PCL/BPSG hybrid and composite disk samples following incubation in PBS for various times. Hybrid and composite disks (15 of each) were composed of 50 wt% PCL and 50 wt% BPSG. Disk specimens (6 mm in diameter and 2 mm in thickness) were prepared using a similar procedure as that described in section 4.3.3 above and weighed (initial weight). Each specimen was then incubated in 10 mL PBS solution in polypropylene bottles covered with a tight lid. The bottles were placed in an orbital shaker (MaxQ4000, Barnstead Lab-line, IL) at 120 rpm and 37 °C and samples were incubated for 3, 6, 9, 12 or 15 days. After each time point, 3 hybrid and 3 composite specimens were removed, and the corresponding PBS was collected. For the remaining bottles, PBS was collected and bottles were replenished with fresh PBS. Once removed, disks were rinsed with deionized water, dried under vacuum at room temperature for 24 h, and weighed (final weight). The percentage weight loss for each specimen was calculated from its initial and final weight. Selected disks were examined by SEM (see below).

The release of silicon and boron ions was determined as follows. For each specimen, PBS samples were pooled and supplemented (where necessary) with fresh PBS to achieve a total volume of 50 mL. The concentrations of silicon and boron ions were determined using inductively coupled plasma optical-emission spectroscopy (ICP-OES; Vista-Pro Axial, Varian Inc., USA).

Equilibrium water uptake by hybrid and composite disk specimens (6 mm in diameter and 2 mm in thickness, prepared similarly as mentioned above) was measured in PBS at 37 °C for 10 min intervals until equilibrium was reached (1-2 h). Following each soaking period, the specimen was taken out, blotted with filter paper to remove excess surface liquid, and weighed. The percentage of equilibrium water uptake (EWU) was calculated for each sample using the following equation.

$$\% \text{ EWU} = \frac{w_s - w_0}{w_0} \times 100$$

Where, w_0 was the initial weight (mg) and w_s was the equilibrium weight (mg) following soaking.

4.3.5 Scanning Electron Microscopy (SEM)

Specimen surfaces were coated with osmium in Osmium Plasma Coater (OPC80T, Filgen Inc. Japan) prior to SEM imaging. Surface morphology was then visualized using a LEO 1530 SEM (Zeiss, Oberkochen, Germany) at 5 mm working distance and 3 kV electron beam voltage.

4.3.6 Cell culture and assessment of cellular morphology, spreading and focal adhesion formation

Pre-osteoblastic MC3T3-E1 cells (Subclone 4, American Type Culture Collection) were cultured in α -MEM supplemented with 10% FBS and 1% antibiotic-antimycotic solution. For the biological

studies, we used hybrid (50H) disks and, as control substrata, PCL disks and glass cover slips. Disks were 6 mm in diameter and 2 mm in thickness (prepared similarly as described in section 4.3.3) and coverslips were 12 mm in diameter and ~0.15 mm in thickness. Samples were disinfected by submerging twice in 70 vol% ethanol for 5 min and dried. Prior to seeding the cells, each specimen was incubated in 1 mL serum-free culture medium in 24-wells culture plates. After 24 h, the medium was aspirated and MC3T3-E1 cells were seeded at a density of 10,000 cells/cm² and incubated for 1, 3 and 6 h. After each time point, cells were fixed with 4% paraformaldehyde solution. After rinsing with PBS three times, cells were permeabilized for 5 min with 0.1% Triton X-100 in PBS and rinsed three times in PBS. Cells were then blocked with 1% BSA in PBS for 90 min at 4°C, followed by overnight incubation (at 4°C) with primary antibody (anti-vinculin antibody, MAB3574, clone VIIF9, EMD Milipore). After rinsing with PBS three times, substrata were blocked with 1% BSA in PBS for 90 min at 4 °C and rinsed three times in PBS. A mixture of secondary antibody (1:100 dilution, Cy5 Affinipure Goat anti-mouse IgG (H+L), Polyclonal, Jackson ImmunoResearch) and Alexa Fluor 488® phalloidin (1:200 dilution, ThermoFisher Scientific) was added and, after 35 min at room temperature, substrata were rinsed three times with PBS. Nuclei were labeled using Hoechst 33258 (ThermoFisher Scientific) for 5 min. Finally, substrata were rinsed three times with PBS.

Cells were imaged using a Carl Zeiss Imager M2m microscope with dipping objective (40 X) and Zen Pro 2012 software (Carl Zeiss, Jena, Germany). To enhance image sharpness, multiple images were merged using the extended depth of focus module. Images of Cy5 fluorescence (which labeled vinculin) were used to determine the number of focal adhesions per cell using ImageJ software. These images were first converted to 16 bit black and white. Focal adhesions were

identified as vinculin-containing structures with planar area between 0.1 and 0.5 μm^2 . The lower threshold of 0.1 μm^2 was selected to exclude vesicular staining in the perinuclear region, as described previously [29]. The upper threshold of 0.5 μm^2 was selected to exclude large accumulations of vinculin-labeled material with morphologies that were clearly inconsistent with those of focal adhesions. Images of Alexa Fluor 488® fluorescence (which labeled filamentous actin, F-actin) were used to determine the cell planar area using ImageJ software. Only single cells (10 per specimen) were measured for this analysis.

4.3.7 Assessment of cytocompatibility

Hybrid (50H) disks and, as control substrata, PCL disks and glass cover slips were prepared as described above. MC3T3-E1 cells were seeded at a density of 10,000 cells/cm² and incubated for 1 day, 3 days and 7 days. Medium was changed every 2 days. After each time point, cells were fixed with 4% PFA solution, rinsed with PBS three times, permeabilized with 0.1% Triton X-100/PBS for 5 min, and blocked with 1% BSA in PBS for 90 min at 4 °C. After rinsing with PBS three times, F-actin was labeled using Alexa Fluor 488® phalloidin (1:400) for 35 min at room temperature. Then substrata were rinsed with PBS three times and nuclei were labeled by staining with Hoechst 33258 for 5 min. Finally, substrata were rinsed with PBS three times and imaged as described above. Images of Hoechst fluorescence were used to determine the number of nuclei (cells) per unit area on the various substrata using ImageJ software. Nuclei were identified as Hoechst-stained structures with planar area between 50-500 μm^2 . Nuclei that straddled the edge of images were excluded during this analysis. In these experiments, cell density reflects the net effects

of cell attachment, cell proliferation and cell death, providing an excellent overall assessment of cytocompatibility.

4.3.8 Statistical analyses

Data are presented as means \pm standard deviations (SD) and were analysed using GraphPad Prism 6.0 (GraphPad Software Inc., CA, USA). Where indicated, curves were fit to second degree polynomials using nonlinear regression. Means were compared using one- or two-way analysis of variance (ANOVA) followed by a Tukey's multiple comparison test. Differences between means were considered statistically significant at $p < 0.05$.

4.4 Results

4.4.1 Mechanical competency of hybrid materials

Uniaxial mechanical testing was performed to determine the compressive strength, modulus, strain at fracture, and toughness of PCL/BPSG hybrid and composite biomaterials of different compositions. The stress-strain curves for 50 wt% PCL and 50 wt% BPSG (Table 4.1), revealed enhanced mechanical properties of the hybrid material (50H) compared to its composite counterpart (50C) (Figure 4.1A), consistent with covalent bonding between the organic and inorganic phases in the hybrid. Although the fabrication processes were similar, when the fracture surfaces were observed by SEM, composite materials appeared more granular and exhibited a higher density of micro-cracks than hybrid materials (Figure 4.1B).

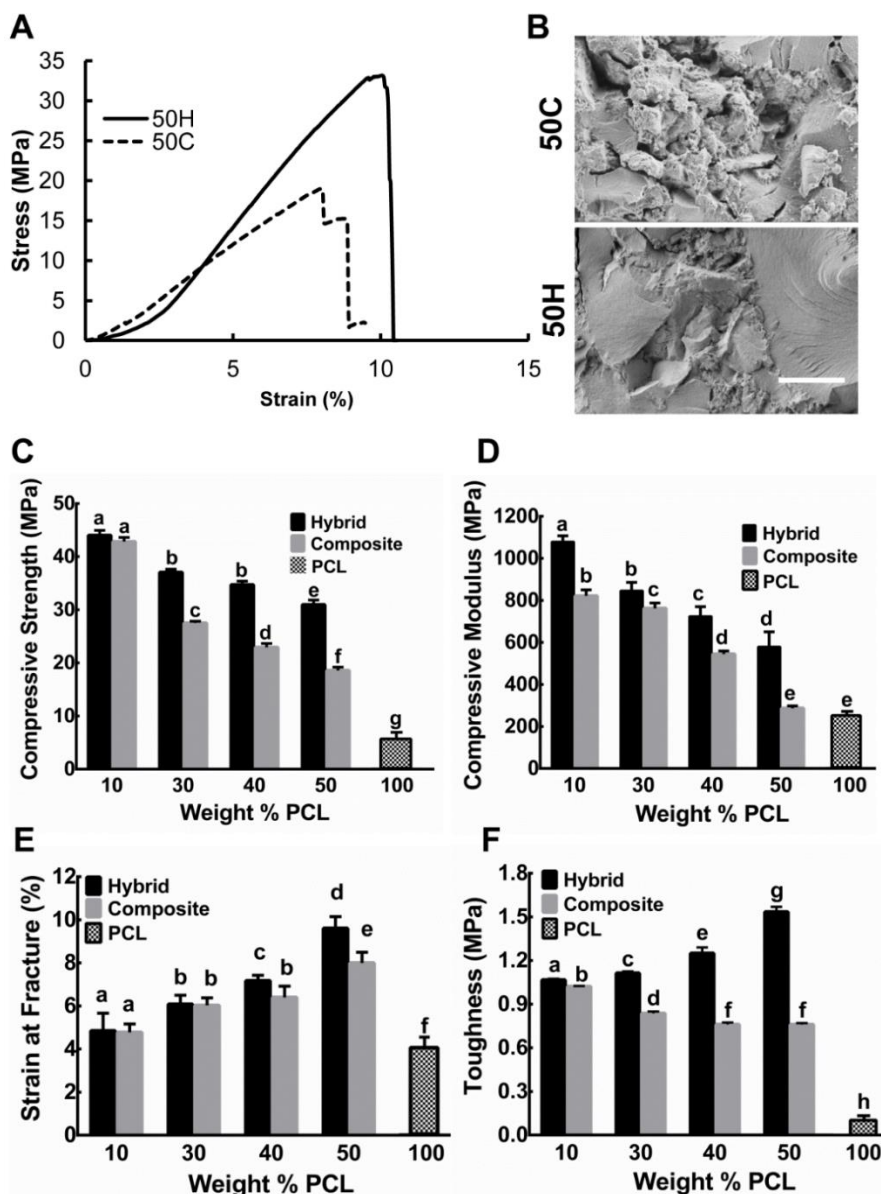


Figure 4. 1: Mechanical properties of class II hybrid and composite materials. **A)** Stress-strain curves of hybrid and composite specimens composed of 50 wt% PCL and 50 wt% BPSG (50H and 50C, respectively). Representative of 10 specimens each. **B)** SEM images of fractured surfaces of a 50C and 50H specimen. Scale bar is 20 μm . Images are representative at least 5 fields from 3 specimens each of 30C, 30H, 40C, 40H, 50C and 50H. **C, D, E)** Ultimate compressive strength, compressive modulus, and strain at fracture of hybrid and composite materials and PCL. **F)** Toughness values were calculated by integrating stress-strain curves up to the point of fracture. For panels **C** to **D**, data are means \pm SD ($n = 10$ specimens of each composition). Two-way ANOVA and Tukey's multiple comparison test were used for statistical analysis. Different lower case letters indicate significance at $p < 0.05$.

The ultimate compressive strength values decreased with increased PCL content for both of hybrid and composite materials (Figure 4.1C). There was no significant difference in compressive strength values between composite and hybrid at 10 wt% PCL. At PCL contents higher than 10%, the compressive strength values of the hybrids were significantly greater than those of their composite counterparts. At 50% PCL, the compressive strength of composite was 18.9 ± 1.6 MPa and of hybrid was 32.2 ± 3.5 MPa (71% greater). The compressive moduli of hybrids and composites (Figure 4.1D) behaved in a similar fashion as the compressive strength values. At 50% PCL, the compressive modulus of composite was 275 ± 28 MPa and of hybrid was 573 ± 85 MPa (108% greater). Unlike the strength and modulus values, the strain at fracture increased with increased PCL content for both of hybrid and composite materials (Figure 4.1E). There was no significant difference in strain at fracture between hybrids and composites at 10 and 30% PCL. At 40 and 50% PCL, the strain at fracture for composites was lower than that of the corresponding hybrids. It should be noted that both hybrids and composites showed significantly higher compressive strength and strain at fracture compared to pure PCL.

Interestingly, the toughness of hybrids increased with increased PCL content; whereas, the toughness of composites decreased with increased PCL content (Figure 4.1F). Moreover, in every case, the toughness of hybrids was significantly greater than that of their composite counterparts. At 50% PCL, the toughness of composite was 0.76 ± 0.02 MPa and of hybrid was 1.54 ± 0.03 MPa (102% greater). The ability of these hybrid biomaterials to absorb greater energy prior to fracture is consistent with covalent bonding between the organic and inorganic phases. The toughness of PCL was very low (0.11 ± 0.01 MPa), presumably due to its low molecular weight (3000 Da) and the brittle nature of the pure polymer.

4.4.2 *In vitro* degradation of hybrid materials

The degradation of 50H and 50C was evaluated in PBS over a period of 3-15 days. SEM of specimens revealed that micro-pits formed on the surface of 50H and these micro-pits increased in size with time (Figure 4.2A). In contrast, 50C exhibited severe surface micro-cracks after immersion after three days of immersion (Figure 4.3). Consistent with the formation of these micro-cracks, 50C exhibited considerable weight loss (10.57 ± 0.35 %) between 1 and 3 days of immersion, markedly greater than the corresponding hybrid (1.97 ± 0.35 %) (Figure 4.2B). After this initial rapid weight loss, 50C showed slower degradation. On the other hand, 50H showed a more linear rate of weight loss over 15 days. Importantly, 50H showed significantly less weight loss than its corresponding composite at all times. The weight loss data together with the SEM images are consistent with layer by layer surface erosion of hybrid materials.

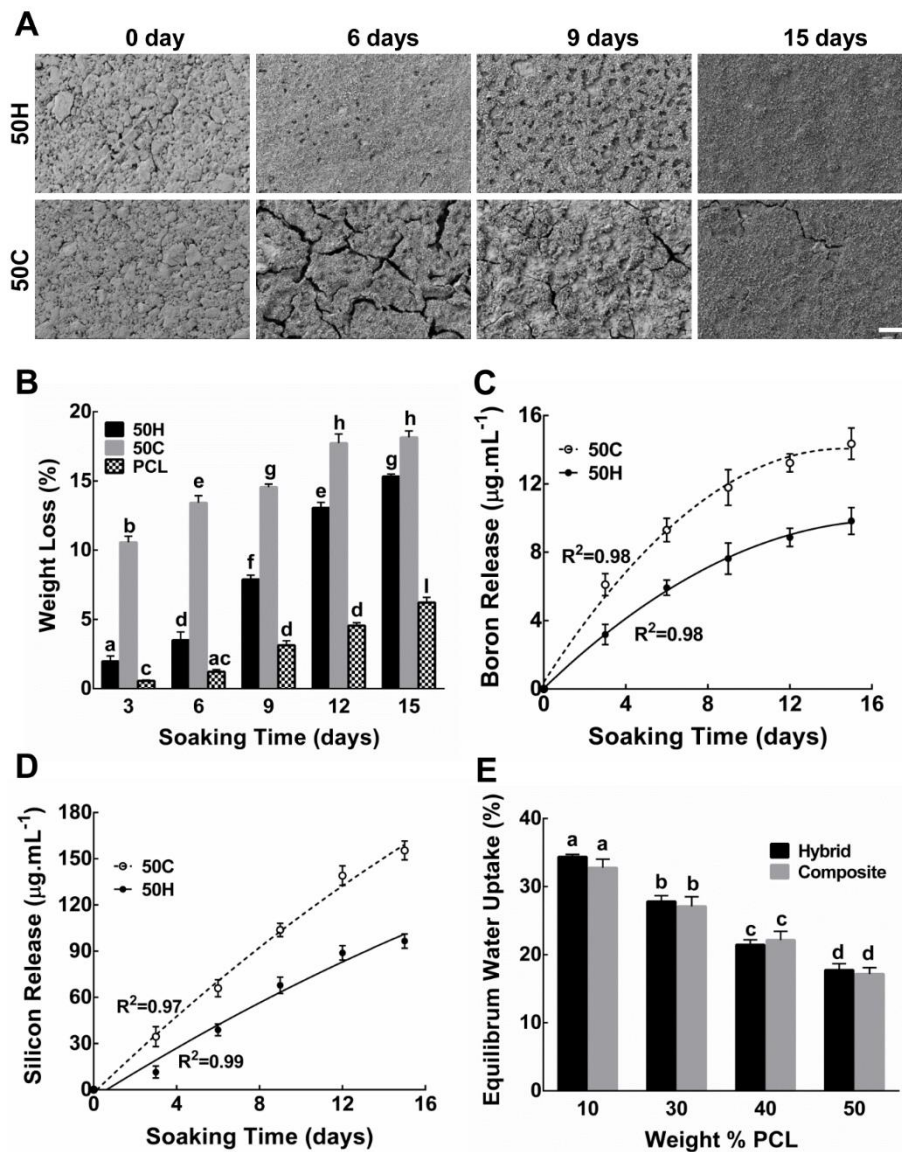


Figure 4. 2: Degradation behavior of hybrid 50H and composite 50C materials. For panels **A-D**, degradation was evaluated in PBS in a shaker incubator at 37°C over a period of 15 days. **A)** SEM images of surfaces before and after degradation in PBS. Scale bar is 50 μm . Images are representative at least 5 fields from 3 specimens each of 50C and 50H. **B)** Weight loss of hybrid 50H and composite 50C materials at the indicated times. **C and D)** Boron and silicon ion release was determined using ICP-OES. Data were fitted to second degree polynomial equations using nonlinear regression. **E)** Equilibrium water uptake of hybrids and composites was determined following incubation in PBS at 37°C with shaking for up to 2 hours. For panels **B-E**, data are means \pm SD ($n = 3$ specimens of each composition). Two-way ANOVA and Tukey's multiple comparison test were used for statistical analysis. In **B** and **E**, different lower case letters indicate significance at $p < 0.05$.

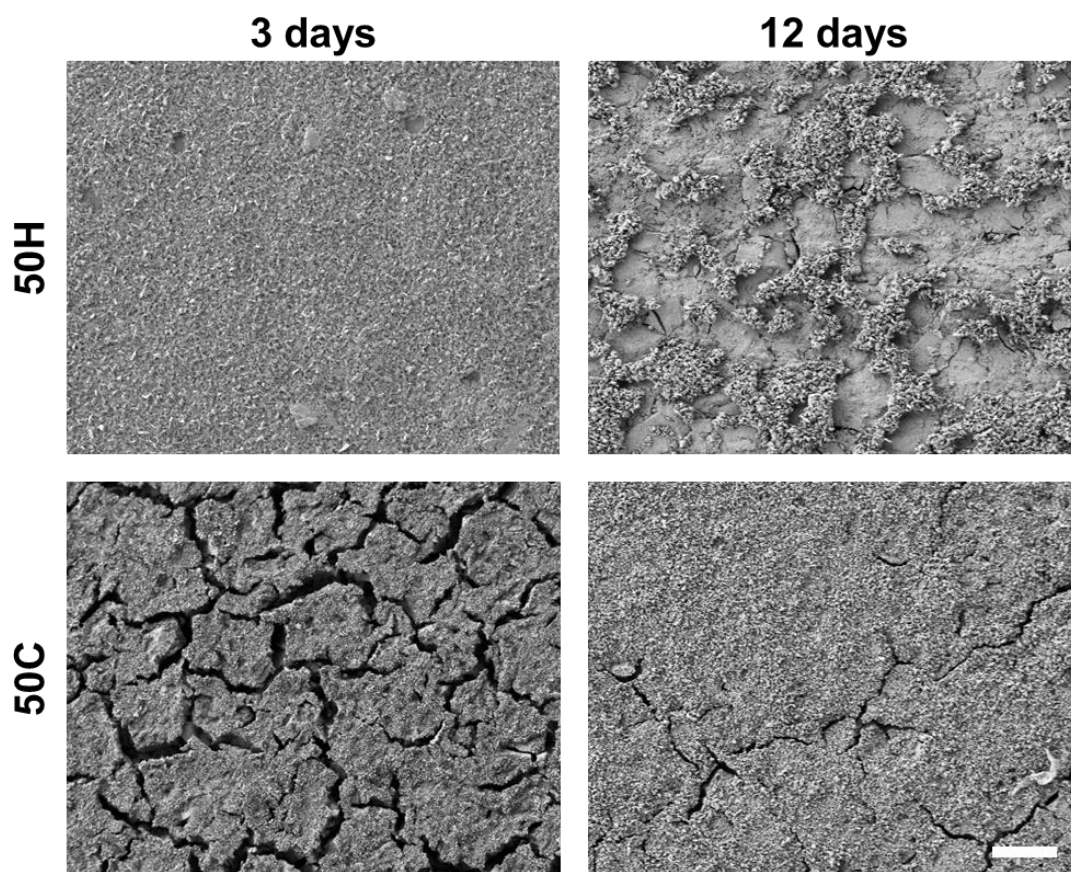


Figure 4. 3: SEM images of surfaces after degradation in PBS. Degradation behavior of hybrid 50H and composite 50C materials were evaluated in phosphate-buffered saline (PBS) in a shaker incubator at 37°C over a period of 15 days. Scale bar is 50 μm . Images are representative at least 5 fields from 3 specimens each of 50C and 50H.

Degradation behavior was further characterized by measuring the amount of ionized boron (Figure 4.2C) and silicon (Figure 4.2D) released over a period of 15 days. Consistent with the weight loss data, more B and Si ions were released from the composite compared to its corresponding hybrid. After 15 days of soaking, the release of B ions from the composite was $14.3 \pm 0.6 \mu\text{g/mL}$ and from

the hybrid was $9.8 \pm 0.7 \mu\text{g/mL}$. Similarly, after 15 days, the release of Si ions from the composite was $155.4 \pm 5.0 \mu\text{g/mL}$ and from the hybrid was $96.6 \pm 3.0 \mu\text{g/mL}$.

We next assessed equilibrium water uptake of hybrids and composites (PCL 10-50 wt%) following immersion in PBS for up to 2 hours. When PCL content increased, equilibrium water uptake for both hybrids and composites decreased significantly (Figure 4.2E), consistent with the hydrophobicity of PCL. On the other hand, water uptake by hybrids was not significantly different than uptake by their corresponding composites. Thus, it appears that covalent bonding between the organic and inorganic phases does not affect the water absorption properties of these materials.

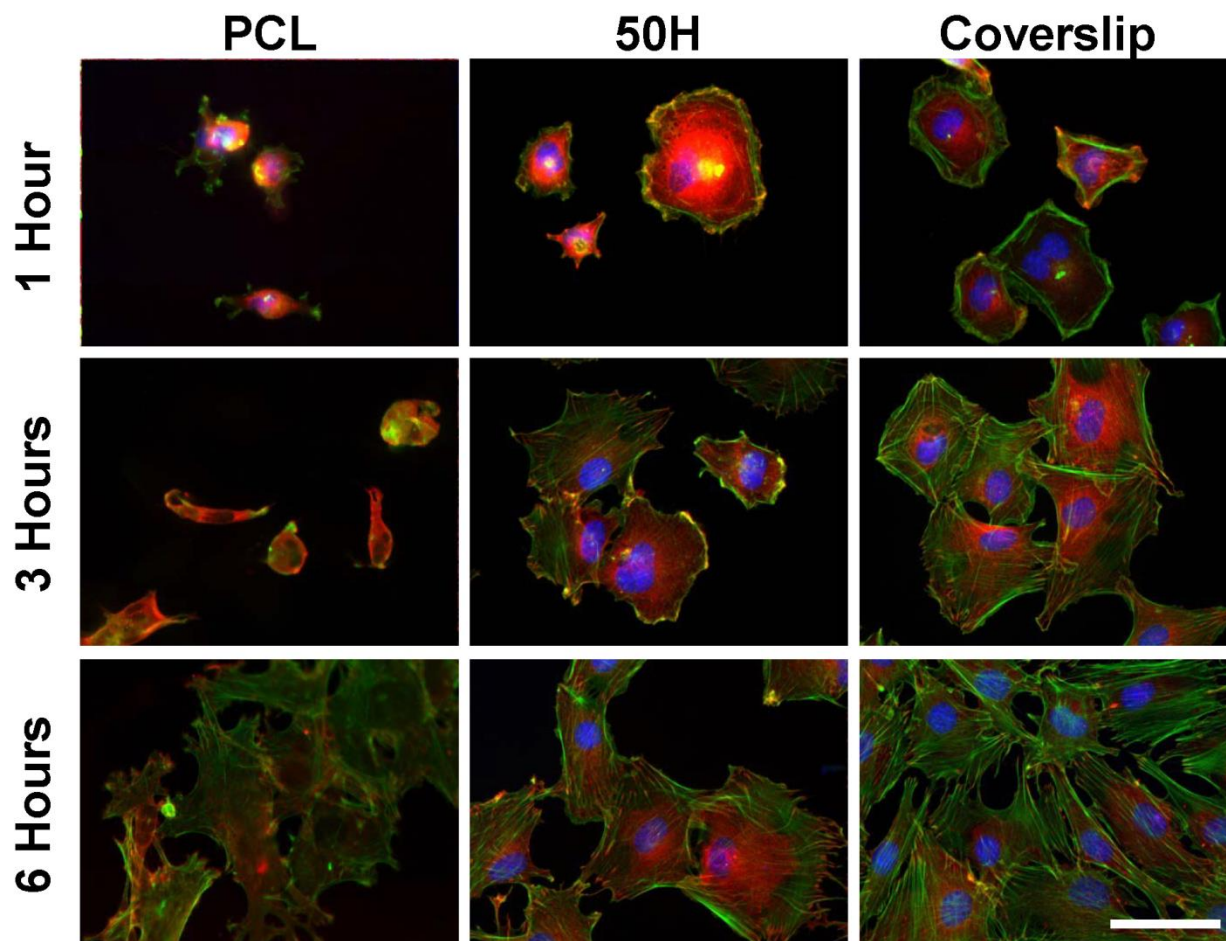


Figure 4. 4: Morphology and spreading of preosteoblastic MC3T3-E1 cells on hybrid biomaterial and control surfaces. Cells were fixed and labelled for F-actin (green), vinculin (red) and DNA (to label nuclei, blue). Scale bar is 50 μm for all panels. Images are representative of multiple fields on each specimen, from 3 independent experiments, each performed using triplicate specimens.

4.4.3 Cytocompatibility of hybrid material

We first assessed the morphology and spreading of preosteoblastic MC3T3-E1 cells on 50H, PCL and glass surfaces at 1, 3 and 6 hours following seeding. Composite disks were not evaluated because of the crack formation in aqueous media (Figure 4.5, explained at Section 4.4.2). Cells

were fixed and labelled for F-actin, vinculin and DNA (green, red and blue respectively in Figure 4.4) and planar cell area was quantified (Figure 4.6).

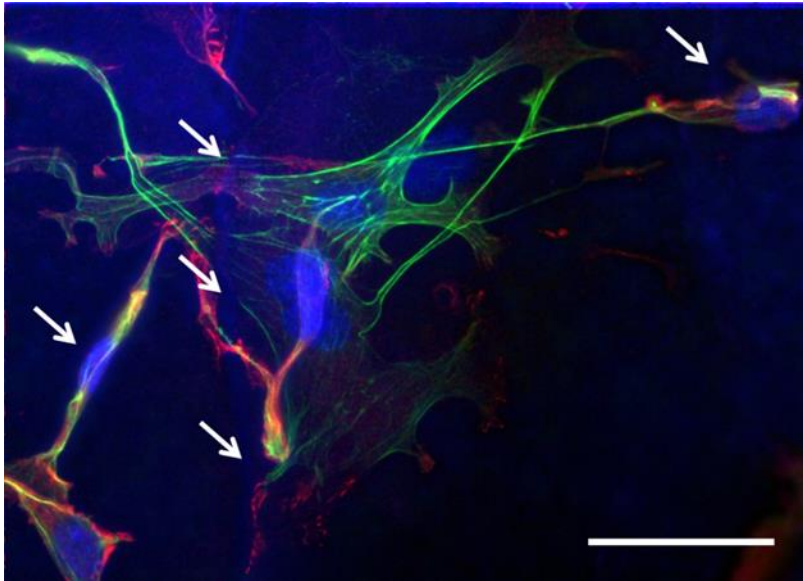


Figure 4. 5: Morphology and spreading of preosteoblastic MC3T3-E1 cells on composite 50C surface at 6 hours following seeding. Cells were fixed and labelled for F-actin (green), vinculin (red) and DNA (to label nuclei, blue). Scale bar is 50 μm . White arrows are indicating crack formation on composite surface. Image is representative of multiple fields on each specimen, from 1 experiment performed using triplicate specimens.

At 1 hour, cells on 50H had begun to spread, but the extent of spreading was not significantly greater than for cells on PCL. In contrast, at 1 hour, cells on glass coverslips were well spread and the actin cytoskeleton was already beginning to organize. At 3 hours, cells on 50H were more spread than those on PCL and actin microfilaments were clearly visible. At 3 hours, cells on glass coverslips exhibited numerous focal adhesions, in contrast to cells on hybrid or pure PCL. By 6 hours, cells on 50H were well spread with well-organized actin cytoskeleton and clearly visible focal adhesions, in contrast to cells on PCL in which the cytoskeleton was just forming and focal

adhesions were not apparent. At 6 hours, the area of cells seeded on 50H was $3141 \pm 284 \mu\text{m}^2$, significantly greater than cells seeded on PCL ($1280 \pm 309 \mu\text{m}^2$). The number of focal adhesions per cell was also quantified at 6 hours (Figure 4.7). The number of focal adhesions in cells on 50H was significantly greater than in cells on PCL, indicating excellent adhesion to the hybrid surface and consistent with the spreading data in Figure 4.6.

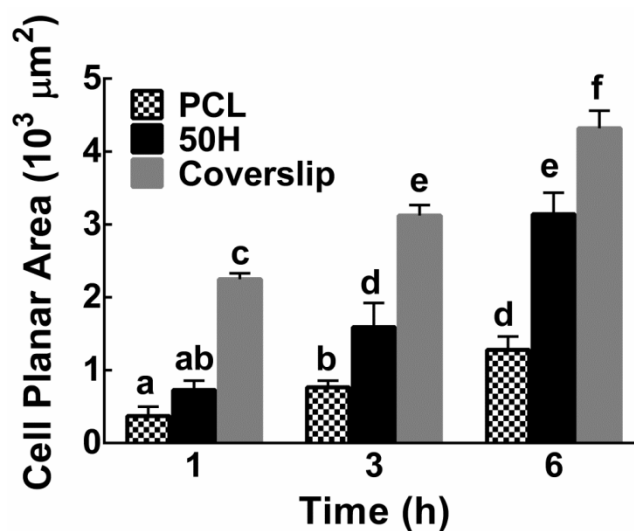


Figure 4. 6: Quantification of cell spreading on hybrid biomaterial and control surfaces. Cells were prepared as described in the legend to Figure 4.4. Planar cell area was determined for samples at 1, 3 and 6 hours following seeding. Data are means \pm SD of 10 cells each from 3 independent experiments ($n = 30$). Two-way ANOVA and Tukey's multiple comparison test were used for statistical analysis. Different lower case letters indicate significance at $p < 0.05$.

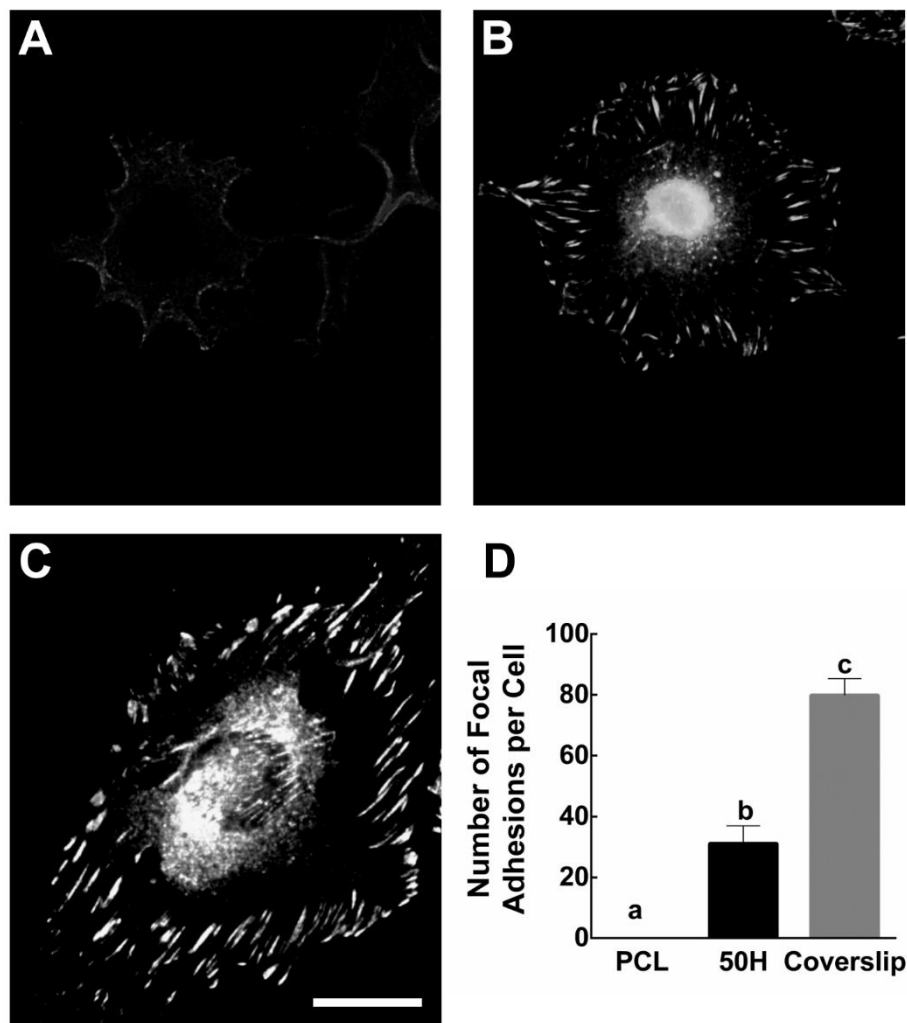


Figure 4. 7: Focal adhesion formation. **A-C)** Images are Cy5 fluorescence (which labeled vinculin) of cells 6 hours following seeding. Each image primarily shows one complete cell. Scale bar represents 20 μm . Images are representative of multiple fields on each specimen, from 3 independent experiments, each performed using triplicate specimens. **D)** The number of focal adhesions per cell was determined using ImageJ software. Focal adhesions were identified as vinculin-containing structures with planar area between 0.1 and 0.5 μm^2 . Data are means \pm SD of 10 cells each from 3 independent experiments ($n = 30$). One-way ANOVA and Tukey's multiple comparison test were used for statistical analysis. Different lower case letters indicate significance at $p < 0.05$.

Longer term cytocompatibility was assessed by seeding MC3T3-E1 cells on 50H, PCL and glass surfaces. At 1, 3 and 7 days following seeding, cells were fixed and labelled for F-actin and DNA

(green and blue respectively in Figure 4.8A) and cell density was quantified by counting the number of nuclei per unit area. At all times, cells on the hybrid material exhibited morphology and cytoskeletal organization similar to those of cells on coverslips. In contrast, cells on PCL were still less spread and exhibited a more poorly organized actin cytoskeleton. The number of cells on the hybrid was significantly greater than on PCL at all time points (Figure 4.8B). Although there were more cells on coverslips than on the hybrid at days 1 and 3, the rates of increase in cell number from day 1 to 3, which primarily reflect proliferation, were similar on these two substrates. In contrast, cells appeared to proliferate more slowly on PCL. By day 7, there was no significant difference between the cell density on the hybrid biomaterial and coverslips. Taken together, these data indicate excellent cytocompatibility of the hybrid biomaterial.

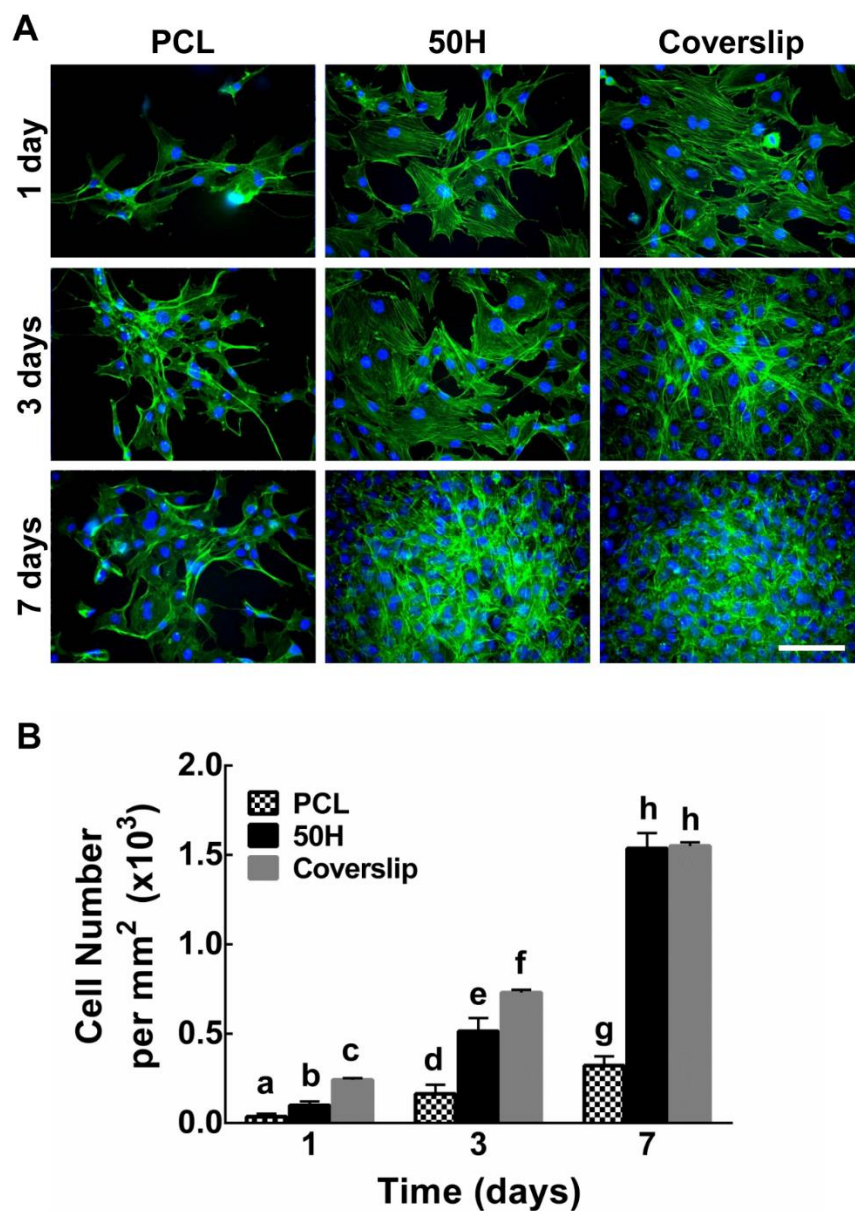


Figure 4. 8: Biocompatibility of the hybrid material. MC3T3-E1 cells were seeded on 50H, PCL and glass surfaces. At 1, 3 and 7 days following seeding, cells were fixed and labelled for F-actin (green) and DNA (to label nuclei, blue). **A)** Immunofluorescence images of cells on the substrate surfaces. Scale bar is 100 μm . Images are representative of multiple fields on each specimen, from 3 independent experiments, each performed using triplicate specimens. **B)** Cell density was quantified by counting the number of nuclei per unit area. Data are means \pm SD of 10 fields each from 3 independent experiments ($n = 30$). Two-way ANOVA and Tukey's multiple comparison test were used for statistical analysis. Different lower case letters indicate significance at $p < 0.05$.

4.5 Discussion

Organic biopolymers are flexible and tough, whereas bioceramics have excellent strength and stiffness. If these materials are chemically combined, new classes of high performance and functional hybrid biomaterials can be achieved [30, 31]. Previously, we reported the synthesis and characterization of novel organic–inorganic class II hybrids based on PCL and ternary BPSG for potential applications in bone tissue engineering [28]. However, the effects of composition on mechanical properties, degradability and cytocompatibility of these materials were not investigated. In the present study, we hypothesized that this class II hybrid biomaterial would exhibit superior mechanical properties, cytocompatibility and more controlled degradation compared to conventional composites. To test this hypothesis, a series of PCL/BPSG hybrids and composites containing 10-50 wt% of PCL were prepared. We restricted the maximum PCL content in the hybrid and composite systems to 50 wt %. This was due to the fact that, at 60 wt% PCL in the hybrid, phase separation occurred [28].

In this work, the hybrid monoliths showed greater compressive strength, modulus, toughness and strain at fracture, when compared to their composite counterparts and PCL. The significant increase in mechanical properties is likely due to the covalent bonding between organic and inorganic phases. On the other hand, in composites, the absence of chemical bonding resulted in lack of stress transfer between the organic and inorganic components; moreover, PCL acted as a weakening phase, which together resulted in poorer mechanical properties of the composite systems. It has been reported that low molecular weight PCL accelerates the biodegradability of PCL/SiO₂ hybrid biomaterials and affects their mechanical properties [21]. It has also been

reported that the use of a low molecular weight polymer in a class II hybrid material results in homogenous distribution of phases and improved properties [30]. When compared to a class I (hydrogen-bonded) hybrid biomaterial prepared using high molecular weight PCL [32], the current class II hybrid prepared using low molecular weight functionalized PCL exhibited improved compressive strength and modulus. In summary, the chemical bonding between PCL and the inorganic glass allowed the entire organic-inorganic network to function as a single phase, enhancing its mechanical properties.

The degradation profile of scaffolds for bone tissue engineering and regeneration is important. Ideally, scaffold materials should degrade at similar rate as new bone formation and should remain mechanically stable during the whole regeneration process [5]. This can be achieved if the biomaterial degrades through surface erosion rather than bulk breakdown. Although both hybrid and composite materials exhibited similar surface morphologies before degradation, considerable changes were observed during degradation. The degradation of 50H started with heterogeneous pit formation, which made the surface rougher, whereas severe micro-crack formation occurred on the surface of 50C and likely resulted in rapid weight loss. It is likely that the lack of covalent bonding between the hydrophobic PCL and hydrophilic BPSG in composites leads to the surface cracking observed. Differential hydration was not responsible, since there was no significant difference in water uptake by the hybrid and composites materials. However, the absorbed water may behave differently in the different phases within the composite, such that expansion of the structure during absorption might cause crack formation and propagation. The relatively faster degradation of the composite materials led to increased release of boron and silicon ions. Boron can promote bone growth, but its effect on bone cells and tissue formation depends on the initial

concentration in the bioactive glasses [33]. Higher concentrations of borate in bioactive glasses and rapid release of boron may inhibit cell proliferation [13]. In our study, the 5 mol% B₂O₃ in the inorganic component is lower than in several reported borate glasses, from which the released boron did not negatively affect cell proliferation and bone formation *in vitro* and *in vivo* [33-35].

Biomaterial surface topography influences the cell-material interactions, cell proliferation and new tissue formation. Osteoblast adhesion, spreading and proliferation are critical parameters that influence the osteoconductivity of a biomaterial. The primary subcellular structure that mediates cell attachment is the focal adhesion. Vinculin is one of the numerous structural proteins which act as scaffolding proteins that strengthen cell adhesion by anchoring the actin cytoskeleton to adhesion receptors [36]. Our investigations revealed that focal adhesions form more readily on hybrid biomaterials than on PCL. Numerous studies have suggested that bioactive glasses prepared by sol-gel process should go through thermal stabilization at high temperature (ca. 600 °C) to be nontoxic to cells, since the high temperature can burn off unreacted precursors and leachable toxic components [37-40]. However, most class II hybrid biomaterials including ours could not be thermally treated at high temperature, since it would degrade the organic phases. In view of this, it was critical to study the effect of any unreacted precursors or released boron on cell attachment and proliferation on the hybrid biomaterial. The attachment and proliferation results revealed that hybrid biomaterial was cytocompatible with no marked cytotoxicity.

4.6 Conclusions

This work revealed that hybrid biomaterials possess superior compressive strength, modulus and toughness compared to composites, likely due to covalent bonding between the organic and inorganic phases. After incubating in PBS, composites exhibit surface cracking and rapid weight loss, whereas hybrids show slow surface erosion with tailorable degradation properties. Moreover, cells attach and proliferate well on the hybrid, with excellent cell spreading and focal adhesion formation. Thus, these hybrid biomaterials are cytocompatible and have potential for use as scaffolds for bone tissue engineering and related applications.

4.7 References

- [1] Frohlich M, Grayson WL, Wan LQ, Marolt D, Drobic M, Vunjak-Novakovic G. Tissue engineered bone grafts: biological requirements, tissue culture and clinical relevance. *Current Stem Cell Research Therapy* 2008;3:254-64.
- [2] Zhang X, Chang W, Lee P, Wang Y, Yang M, Li J, et al. Polymer-ceramic spiral structured scaffolds for bone tissue engineering: effect of hydroxyapatite composition on human fetal osteoblasts. *PLoS One* 2014;9:e85871.
- [3] Hutmacher DW. Scaffolds in tissue engineering bone and cartilage. *Biomaterials* 2000;21:2529-43.
- [4] O'Brien FJ. Biomaterials & scaffolds for tissue engineering. *Materials Today* 2011;14:88-95.
- [5] Jones JR. Review of bioactive glass: From Hench to hybrids. *Acta Biomaterialia* 2013;9:4457-86.
- [6] Niemelä T, Niiranen H, Kellomäki M, Törmälä P. Self-reinforced composites of bioabsorbable polymer and bioactive glass with different bioactive glass contents. Part I: Initial mechanical properties and bioactivity. *Acta Biomaterialia* 2005;1:235-42.
- [7] Hench LL. Bioceramics: From Concept to Clinic. *Journal of the American Ceramic Society* 1991;74:1487-510.
- [8] Fu Q, Rahaman MN, Bal BS, Bonewald LF, Kuroki K, Brown RF. Silicate, borosilicate, and borate bioactive glass scaffolds with controllable degradation rate for bone tissue engineering

applications. II. In vitro and in vivo biological evaluation. *Journal of Biomedical Materials Research Part A* 2010;95A:172-9.

[9] Gu Y, Wang G, Zhang X, Zhang Y, Zhang C, Liu X, et al. Biodegradable borosilicate bioactive glass scaffolds with a trabecular microstructure for bone repair. *Materials Science and Engineering: C* 2014;36:294-300.

[10] Ning J, Yao A, Wang D, Huang W, Fu H, Liu X, et al. Synthesis and in vitro bioactivity of a borate-based bioglass. *Materials Letters* 2007;61:5223-6.

[11] Wu C, Miron R, Sculean A, Kaskel S, Doert T, Schulze R, et al. Proliferation, differentiation and gene expression of osteoblasts in boron-containing associated with dexamethasone deliver from mesoporous bioactive glass scaffolds. *Biomaterials* 2011;32:7068-78.

[12] Kaur G, Pandey OP, Singh K, Homa D, Scott B, Pickrell G. A review of bioactive glasses: Their structure, properties, fabrication and apatite formation. *Journal of Biomedical Materials Research Part A* 2014;102:254-74.

[13] Rahaman MN, Day DE, Sonny Bal B, Fu Q, Jung SB, Bonewald LF, et al. Bioactive glass in tissue engineering. *Acta Biomaterialia* 2011;7:2355-73.

[14] Xu S, Yang X, Chen X, Shao H, He Y, Zhang L, et al. Effect of borosilicate glass on the mechanical and biodegradation properties of 45S5-derived bioactive glass-ceramics. *Journal of Non-Crystalline Solids* 2014;405:91-9.

[15] Yao A, Wang D, Huang W, Fu Q, Rahaman MN, Day DE. In Vitro Bioactive Characteristics of Borate-Based Glasses with Controllable Degradation Behavior. *Journal of the American Ceramic Society* 2007;90:303-6.

[16] Boccaccini AR, Blaker JJ, Maquet V, Day RM, Jérôme R. Preparation and characterisation of poly(lactide-co-glycolide) (PLGA) and PLGA/Bioglass® composite tubular foam scaffolds for tissue engineering applications. *Materials Science and Engineering: C* 2005;25:23-31.

[17] Rezwani K, Chen QZ, Blaker JJ, Boccaccini AR. Biodegradable and bioactive porous polymer/inorganic composite scaffolds for bone tissue engineering. *Biomaterials* 2006;27:3413-31.

[18] Zhang K, Wang Y, Hillmyer MA, Francis LF. Processing and properties of porous poly(l-lactide)/bioactive glass composites. *Biomaterials* 2004;25:2489-500.

[19] Blaker JJ, Maquet V, Jérôme R, Boccaccini AR, Nazhat SN. Mechanical properties of highly porous PDLLA/Bioglass® composite foams as scaffolds for bone tissue engineering. *Acta Biomaterialia* 2005;1:643-52.

[20] Hong Z, Reis RL, Mano JF. Preparation and in vitro characterization of scaffolds of poly(l-lactic acid) containing bioactive glass ceramic nanoparticles. *Acta Biomaterialia* 2008;4:1297-306.

[21] Rhee S-H. Bone-like apatite-forming ability and mechanical properties of poly(ϵ -caprolactone)/silica hybrid as a function of poly(ϵ -caprolactone) content. *Biomaterials* 2004;25:1167-75.

- [22] Rhee S-H, Lee Y-K, Lim B-S, Yoo JJ, Kim HJ. Evaluation of a Novel Poly(ϵ -caprolactone)–Organosiloxane Hybrid Material for the Potential Application as a Bioactive and Degradable Bone Substitute. *Biomacromolecules* 2004;5:1575-9.
- [23] Granqvist B, Helminen A, Vehviläinen M, Ääritalo V, Seppälä J, Lindén M. Biodegradable and bioactive hybrid organic–inorganic PEG-siloxane fibers. Preparation and characterization. *Colloid and Polymer Science* 2004;282:495-501.
- [24] Mahony O, Tsigkou O, Ionescu C, Minelli C, Ling L, Hanly R, et al. Silica-Gelatin Hybrids with Tailorable Degradation and Mechanical Properties for Tissue Regeneration. *Advanced Functional Materials* 2010;20:3835-45.
- [25] Miyata N, Fuke K-i, Chen Q, Kawashita M, Kokubo T, Nakamura T. Apatite-forming ability and mechanical properties of PTMO-modified CaO–SiO₂–TiO₂ hybrids derived from sol–gel processing. *Biomaterials* 2004;25:1-7.
- [26] Chen Q, Miyata N, Kokubo T, Nakamura T. Bioactivity and mechanical properties of PDMS-modified CaO–SiO₂–TiO₂ hybrids prepared by sol-gel process. *Journal of Biomedical Materials Research* 2000;51:605-11.
- [27] Manzano M, Salinas AJ, Gil FJ, Vallet-Regí M. Mechanical properties of organically modified silicates for bone regeneration. *Journal of Materials Science: Materials in Medicine* 2009;20:1795-801.
- [28] Mondal D, Rizkalla AS, Mequanint K. Bioactive borophosphosilicate-polycaprolactone hybrid biomaterials via a non-aqueous sol gel process. *RSC Advances* 2016;6:92824-32.
- [29] Cora-Cruz JJ, Difffoot-Carlo N, Sundaram PA. Vinculin expression in MC3T3-E1 cells in response to mechanical stimulus. *Data in Brief* 2016;6:94-100.
- [30] Novak BM. Hybrid Nanocomposite Materials—between inorganic glasses and organic polymers. *Advanced Materials* 1993;5:422-33.
- [31] Sanchez C, Julian B, Belleville P, Popall M. Applications of hybrid organic-inorganic nanocomposites. *Journal of Materials Chemistry* 2005;15:3559-92.
- [32] Allo BA, Rizkalla AS, Mequanint K. Synthesis and Electrospinning of ϵ -Polycaprolactone-Bioactive Glass Hybrid Biomaterials via a Sol–Gel Process. *Langmuir* 2010;26:18340-8.
- [33] Pan HB, Zhao XL, Zhang X, Zhang KB, Li LC, Li ZY, et al. Strontium borate glass: potential biomaterial for bone regeneration. *Journal of The Royal Society Interface* 2010;7:1025.
- [34] Zhang X, Jia W, Gu Y, Xiao W, Liu X, Wang D, et al. Teicoplanin-loaded borate bioactive glass implants for treating chronic bone infection in a rabbit tibia osteomyelitis model. *Biomaterials* 2010;31:5865-74.
- [35] Brown RF, Rahaman MN, Dwilewicz AB, Huang W, Day DE, Li Y, et al. Effect of borate glass composition on its conversion to hydroxyapatite and on the proliferation of MC3T3-E1 cells. *Journal of Biomedical Materials Research Part A* 2009;88A:392-400.

- [36] Miyamoto S, Akiyama SK, Yamada KM. Synergistic roles for receptor occupancy and aggregation in integrin transmembrane function. *Science* 1995;267:883.
- [37] Meseguer-Olmo L, Ros-Nicolás MJ, Clavel-Sainz M, Vicente-Ortega V, Alcaraz-Baños M, Lax-Pérez A, et al. Biocompatibility and in vivo gentamicin release from bioactive sol-gel glass implants. *Journal of Biomedical Materials Research* 2002;61:458-65.
- [38] Valerio P, Guimarães MHR, Pereira MM, Leite MF, Goes AM. Primary osteoblast cell response to sol-gel derived bioactive glass foams. *Journal of Materials Science: Materials in Medicine* 2005;16:851-6.
- [39] Yun H-S, Park J-W, Kim S-H, Kim Y-J, Jang J-H. Effect of the pore structure of bioactive glass balls on biocompatibility in vitro and in vivo. *Acta Biomaterialia* 2011;7:2651-60.
- [40] Zhang K, Washburn NR, Simon Jr CG. Cytotoxicity of three-dimensionally ordered macroporous sol-gel bioactive glass (3DOM-BG). *Biomaterials* 2005;26:4532-9.

Chapter 5

Cell Infiltration and Differentiation on Polycaprolactone-Borophosphosilicate Glass Hybrid Scaffolds

Overview: This Chapter described the microstructure, pore morphologies, compressive mechanical properties and degradation of the hybrid scaffolds prepared by solvent-free casting and particulate leaching. Cell infiltration into the scaffolds, and osteogenic gene expression were also evaluated and discussed.

5.1 Summary

Scaffold materials and microstructures play significant role in cell infiltration and subsequent proliferation, differentiation and extracellular matrix production in bone tissue engineering. We have previously reported the synthesis of class II hybrid biomaterials from polycaprolactone and borophosphosilicate glass (PCL/BPSG), and their mechanical properties, biocompatibility and degradability for bone tissue engineering applications. In this study, we evaluated the porous morphology, cellular infiltration and the effect of class II hybrid biomaterial scaffolds on osteogenic gene expression. PCL/BPSG hybrid scaffolds were prepared by solvent-free casting and particulate leaching method to acquire consistent pore size distribution, controllable porosity, and pore interconnectivity. These hybrid scaffolds were mechanically-competent and their degradation behavior makes them ideal as bone tissue engineering scaffolds. In static cell culture experiments, significant number of cell infiltration and adhesion into the scaffolds interior were observed. Bone-associated gene expression by induced pluripotent stem cells (iPSCs) on these scaffolds revealed that hybrid scaffolds containing 5 mol% boron down-regulated bone gene expression, whereas, scaffolds containing 2 mol% boron had an upregulating effect on gene expressions for alkaline phosphatase (ALP), osteopontin (OPN) and osteocalcin (OCN). These

results suggest that PCL/BPSG hybrid scaffolds with optimum-level boron may enhance bone formation.

5.2 Introduction

Bone tissue engineering require three-dimensional (3D) porous biomaterial scaffolds for cell infiltration, differentiation and proliferation to guide the new tissue formation [1-5]. Cell-material interactions and cellular responses to physical and chemical micro-environments has been shown to play critical role in cell infiltration, differentiation, regulating cell fate, and extra-cellular matrix formation [6]. Ideal bone tissue engineering scaffolds should be osteoconductive and osteoinductive, and adequately porous so that osteo-progenitor cells can adhere, infiltrate, differentiate and proliferate [7]. In addition, the scaffold biomaterial must be biodegradable so that it can be replaced by newly formed bone and mechanically competent to facilitate the bone regeneration process. One of the major challenges to develop biomaterial scaffold for bone tissue engineering is to combine all these required properties into a single material system [8]. Several organic inorganic composite biomaterials have been proposed to fabricate scaffolds with tailorable physical, chemical and biological properties. However, conventional composites have distinct phases at the molecular scale which make them unsuitable for for bone tissue engineering applications [8].

Organic-inorganic hybrid materials are capable in providing consistent physical, chemical and biological properties due to their molecular level interactions between phases. These interactions

can be van der Waal's forces or hydrogen bonding which is referred as class I hybrid, or strong chemical bonding which is referred as class II hybrid material [9].

The size, shape and interconnectivity of the pores are crucial elements for scaffold fabrication to ensure vascularization and new bone formation throughout the scaffold [7]. Scaffold fabrication methods are highly dependent on biomaterial properties and the intended applications. There are several techniques developed to create interconnected porous 3D scaffolds, including electrospinning, fiber bonding, solvent casting/particulate leaching, 3D printing, melt molding, extrusion, gas foaming, freeze drying and phase separation [10]. Many of these techniques involved the use of organic solvents which may not be fully removed even after extended leaching process and may cause detrimental effects on cell adherence and proliferation [11]. To avoid the solvents during fabrication of tissue engineering scaffolds, several researchers reported solvent-free scaffold fabrication procedures [12-16]. In solvent-free casting and particulate leaching technique, it is possible to control the pore size distribution and porosity by choosing the appropriate porogen size and concentration.

Class II hybrid biomaterials prepared through sol-gel process are insoluble in common solvents. Therefore, solvent-free scaffold fabrication methods are more applicable for such biomaterials. Although electrospinning during the gelation stage of sol-gel process is a viable choice to fabricate scaffolds from hybrid biomaterial [17], the viscosity of hybrid material during gelation changes rapidly and provides a narrow window to electrospun into fibrous mats which lead to the difficulties of preparing large scaffolds.

Large pore sizes and interconnectivity assist the diffusion of nutrients and waste removal to mediate initial cell adhesion, proliferation and differentiation [18]. Scaffolds having interconnected porosity with mean pore diameter $\geq 100 \mu\text{m}$ are found favorable for successful diffusion of essential nutrients and oxygen for cell survivability [19]. In addition, mean pore diameter in the range of 200–350 μm are found to be optimum for bone tissue in-growth [20]. However, large pore diameters also compromises the mechanical properties and dimensional stability of the scaffolds [21].

Scaffolds should also affect stem cell fate to direct differentiation into bone-forming cells and mediate the bone-associated gene expression and subsequent extracellular matrix (ECM) formation. Bone ECM formation by differentiated osteoblasts is a series of integrated sequential process which can be evaluated by gene expressions associated with biosynthesis, organization, and mineralization of bone ECM [22].

Recently, several studies have reported that bioactive glass containing boron promotes faster degradation of the glass matrix, induced apatite deposition in simulated body fluid, and enhanced cell attachment compared with $\text{SiO}_2\text{-P}_2\text{O}_5\text{-CaO}$ based ternary bioactive glass [23-27]. In our previous studies, we successfully synthesized class II hybrid biomaterial scaffolds from alkoxy silane-functionalized PCL and $\text{B}_2\text{O}_3\text{-P}_2\text{O}_5\text{-SiO}_2$ glass (BPSG) through a non-aqueous sol-gel process [28]. We also evaluated the mechanical, degradation and biological properties of this material to assess its potential for bone tissue engineering applications [29]. In the present study, we evaluated porous microstructure, and mechanical properties of the PCL/BPSG hybrid scaffolds. We also studied change in mechanical properties with degradation in phosphate-buffered saline

(PBS). Cell infiltration within scaffolds were investigated using pre-osteoblastic MC3T3-E1 cell line and osteogenic differentiation of human induced pluripotent stem cells (iPSCs) derived mesenchymal stem cells (MSCs) by measuring gene expressions of ALP, OCN and OPN.

5.3 Materials and methods

5.3.1 Materials

Poly (ϵ -caprolactone) diol (PCL diol; MW 3000 g/mol) was obtained from Tri-Iso Inc. (Cardiff, CA). (3-Glycidoxypropyl) trimethoxysilane (GPTMS, 97%) and trimethyl borate (TMB, 99%) were procured from Alfa Aesar (Ward Hill, MA). Tetraethyl orthosilicate (TEOS, 98%), triethyl phosphate (TEP, 99.8%), PBS and TritonTM X-100 were purchased from Sigma-Aldrich (Milwaukee, WI). Acetic acid glacial (AcOH) and toluene were purchased from Caledon Laboratory Chemicals (Georgetown, ON). Acetone, methanol and ethanol were obtained from BDH Chemicals (Toronto, ON). Minimal essential medium (α -MEM), fetal bovine serum (FBS), antibiotic-antimycotic solution (10,000 units/mL penicillin; 10,000 μ g/mL streptomycin; and 25 μ g/mL amphotericin B), paraformaldehyde (PFA) and trypsin were purchased from Gibco, ThermoFisher Scientific (USA). Bovine albumin (BSA) was purchased from MP Biomedicals LLC (USA).

5.3.2 Fabrication of PCL/BPSG hybrid scaffolds

The synthesis of PCL/BPSG hybrid biomaterials via non-aqueous sol-gel process using acetone as the solvent described previously [28]. Briefly, PCL was first functionalized with trimethoxysilane (PCL-Si) by the reaction of PCL diol with GPTMS. The inorganic sol was prepared by adding

TEOS, TEP and TMB to a solution of acetic acid in acetone. PCL-Si solution in acetone was then added to the sol and stirred using a magnet stir bar gently for 12 h at ambient temperature. The organic-inorganic hybrid sol was then transferred into a Teflon mold and covered by aluminum foil with few pinholes and allowed to gel in a fume hood for 3 days. Hybrid gels were dried for a further 2 days in a fume hood followed by drying at reduced pressure (225 mm Hg) for one day at 50 °C. The resultant transparent class II PCL/BPSG hybrid biomaterials were transferred into sealed glass vials with deionized water and shaken for 1 day at 120 rpm to remove the unreacted AcOH and solvents followed by drying at reduced pressure at room temperature for further one day. The calculated chemical composition of the synthesized PCL/BPSG hybrid biomaterials ranged between 10-50 wt% PCL and 90-50 wt% BPSG. Sample nomenclature follows a number representing the % of PCL and the character H signifying the hybrid. As an example, 30H represents a hybrid having 30 wt% PCL-Si and 70 wt% BPSG.

Porous scaffolds of PCL/BPSG hybrid were fabricated by a medium heat (50 °C) compression moulding and salt leaching technique. Hybrid biomaterials were ground in a planetary ball mill to get fine powders. NaCl crystals were sieved to yield 150-250 µm size range. Mixtures of NaCl ranging from 40 to 70 vol% and hybrid particles were prepared by mechanical mixing. The mixtures were compression moulded for 1 h (at 1 MPa pressure and Porous scaffolds of PCL/BPSG hybrid were fabricated by a medium heat (50 °C) using stainless steel moulds to produce cylindrical hybrid-NaCl monoliths. NaCl particles were leached out with excess deionised water by shaking at 100 rpm for 2 days. Fresh water was replaced every 2 h for the first 10 h, then 2–3 times a day. The scaffolds were dried in vacuum at room temperature.

5.3.3 Micro-CT characterization of hybrid scaffolds

The scaffold morphology was imaged and studied by microcomputed tomography (microCT) (eXplore Locus SP, GE Healthcare, Canada). The samples (6 mm diameter, 3 mm height) were scanned at 20 μm voxel resolution, using an exposure time of 4500 ms, 10 frames per view, and a total of 900 views at an increment of 0.4°. Two-dimensional slice images were reassembled from the isotropic slice data, and compiled to generate a 3D image. 3D Images were analyzed and displayed using commercially available trabecular bone analysis software (MicroView version Viz+2.0, GE Healthcare). The threshold values differentiating the hybrid materials from air was carefully selected by using air and water as control objects. Detail analysis of these micro-CT images includes measurements of porosity, pore wall thickness and pore sizes, and surface area to volume ratio.

5.3.4 Evaluation of mechanical properties

A uniaxial compression test was conducted using an Instron Universal Mechanical testing machine equipped with 0.5 kN load cell (Instron model 3345, Canton, MA) with crosshead speed of 1 mm/min at ambient temperature. Scaffolds with 9 mm height and 6mm diameter were used to test their mechanical properties. To measure the mechanical properties at wet condition, scaffolds were soaked in PBS for 24 h prior to mechanical testing. The compressive strength and modulus were determined from the ultimate stress values and the slope of the linear elastic portions of the stress–strain curves, respectively. Toughness values were obtained from the area under the stress–strain curves.

5.3.5 Mechanical properties and mass loss of degraded hybrid scaffolds

Mechanical properties change due to degradation was characterized by studying compressive stress and modulus of hybrid scaffolds following incubation in PBS for various times. Scaffolds (25 of each) having porosity from 40-60 vol% were first weighed (initial weight). Each specimen was then incubated in 10 mL PBS solution in polypropylene bottles covered with a tight lid. The bottles were placed in an orbital shaker (MaxQ4000, Barnstead Lab-line, IL) at 120 rpm and 37 °C for 3, 6, 9, 12 or 15 days. After each time point, scaffolds were removed, rinsed with deionized water, dried under vacuum at room temperature for 24 h, and weighed (final weight). The percentage weight loss for each specimen was calculated for each sample using the following equation.

$$\frac{W_0 - W_f}{W_0} \times 100 \%$$

Where, W_0 was the initial weight (mg) and W_f was the final weight (mg) following soaking.

Change of mechanical properties of scaffolds with degradation were evaluated by compressive stress and modulus after each time point as described at section 2.4 above.

5.3.6 MC3T3-E1 preosteoblastic cell infiltration into the scaffolds

MC3T3-E1 (Subclone 4, American Type Culture Collection) were cultured in standard tissue culture flasks using α -MEM supplemented with 10% FBS and 1% antibiotic-antimycotic solution. Medium was changed every 2 days and cells were removed from flasks using trypsin-EDTA

solution. Cells were counted by using haemocytometer. To study the cell infiltration into hybrid scaffolds, cells were used from passages 4-7.

Scaffolds fabricated from hybrid 30H and 50H, with PCL as control using 50 vol% NaCl particles were used in this study. All scaffolds were 6 mm in diameter and 1.5 mm in thickness. Scaffolds were disinfected by submerging twice in 70 vol% ethanol for 5 min and dried. Prior to seeding the cells, each scaffold was incubated in 1 mL serum-free culture medium. After 24 h, the scaffolds were transferred to 48 well plates and MC3T3-E1 cells were seeded at a density of 10,000 cells/well and incubated for 1 and 2 weeks. Medium was changed every 2 days. After each time point, infiltrated and adhered cells were fixed with 4% paraformaldehyde solution for 24 hours at 4 °C.

Optimal cutting temperature (OCT) compound was used to embed the cell seeded scaffolds. After embedding, scaffolds were sectioned vertically from the middle (Leica CM350 Cryostat, Leica Biosystems, Canada). Two semi-cylindrical cross-sections were faced toward the blade and 75 µm thick parts from both sections were removed to avoid common imaging area. The OCT compound was then removed from scaffolds by submerging into PBS at room temperature for 1 hour and then rinsing with PBS for three times. After removal of OCT compound, cells were permeabilized for 5 min with 0.1% Triton X-100 in PBS and rinsed three times in PBS. Scaffolds were then treated with 1% BSA in PBS for 90 min at 4 °C to block cells. After rinsing with PBS three times, F-actin was labeled using Alexa Fluor 488[®] phalloidin (1:400) for 35 min at room temperature. Scaffolds were then rinsed with PBS three times and nuclei were labeled by staining with 4',6-diamidino-2-

phenylindole (DAPI, 300 nmol in PBS) for 5 min. Finally, scaffolds were rinsed with PBS three times.

Images were taken with a Zeiss LSM 510 Confocal Microscope (Zeiss, Canada) equipped with an argon/neon as well as a UV laser. To enhance image sharpness, multiple images were merged using the extended depth of focus module to cover $250 \pm 25 \mu\text{m}$ of Z-stack. Images of DAPI fluorescence were used to determine the number of nuclei (cells) per unit area on the various depths of the scaffolds using ImageJ software. Nuclei that straddled the edge of two sides of the frames were excluded during this analysis. In these experiments, cell densities at various depths of the scaffolds reflect the net effects of cell infiltration, attachment, proliferation and cell death.

5.3.7 Osteogenic differentiation of cells seeded on hybrid scaffolds

Human bone marrow-derived mesenchymal stem cells (hMSCs) (Lonza) were expanded without further characterization and passaged prior to confluency in growth medium according to vendor's protocol. Human induced pluripotent stem cells (iPSCs) were collected from healthy human donor. Harvesting and controlled differentiation of iPSCs were followed by procedures published recently [30]. Cells were used for differentiation study when they reached 70-90% confluency. Osteogenic gene expression was studied on 30H and 50H hybrid scaffolds, as well as in PCL scaffolds. The effect of boron in gene expression were studied using in various amount of boron-containing 50H hybrid biomaterial scaffolds. All scaffolds were 10 mm in diameter and 2 mm thickness, and prepared using 50 vol% NaCl particles as porogen. Prior to cell seeding, scaffolds were disinfected by 70% ethanol solution for 1 hour and incubated with osteogenic media for overnight. iPSC

derived MSCs were seeded onto scaffolds by 40,000 cell/scaffolds with osteogenic media for 7 and 14 days.

After pre-determined time, total RNA from differentiated cell was extracted by using Trizol reagent (ThermoFisher Scientific) following the manufacturer's instructions. Complementary DNA (cDNA) template was prepared by using 1 µg of total RNA primed with random primers according to Promega™ Random Hexamers protocol (ThermoFisher Scientific). q-PCR was carried out in 10 µL of reaction volumes, using a CFX96™ Real-Time System (C1000 Touch Thermal Cycler; Bio-Rad, Canada) and then measured with iQ™ SYBR® Green Supermix (Bio-Rad) according to the recommended protocol by the manufacturer. The sequences of primers were designed using Primer3Web and are as follows. hALPL primers: (forward) TGT GGA GTA TGA GAG TGA CGA; (reverse) GGA GTG CTT GTA TCT CGG TTT; hOCN primers: (forward) CTC ACA CTC CTC GCC CTA TT; (reverse) AAC TCG TCA CAG TCC GGA TT; hOPN primers: (forward) TCA CCT GTG CCA TAC CAG TT; (reverse) TGT GGT CAT GGC TTT CGT TG. The results were analyzed with the comparative threshold cycle method and normalized with GAPDH as an endogenous reference and reported as relative values ($\Delta\Delta$ CT) to those of control static cultures.

5.3.8 Statistical analyses

Data were analysed using GraphPad Prism 6.0 (GraphPad Software Inc., CA, USA) and presented as means \pm standard deviations (SD). Means were compared using one- or two-way analysis of variance (ANOVA) followed by a Tukey's multiple comparison test. Differences between means were considered statistically significant at $p < 0.05$.

5.4 Results

5.4.1 Microstructure, pore size and porosity of the PCL/BPSG class II hybrid scaffolds

Micro-CT imaging and subsequent analysis was performed to visualize the morphology as well as to evaluate the porosity, pore size distribution, and pore wall thickness of hybrid scaffolds consisting of 50 wt% PCL and 50 wt% BPSG (50H). The choice of this organic/inorganic ratio was based on our previous finding where this composition possessed the best mechanical competence having molecular level cross-linking within the organic and inorganic phases without phase separation [29]. Figure 5. 1 shows micro-CT isosurface images of porous hybrid scaffolds prepared through solvent-free casting and particulate leaching by using NaCl as the porogen. An isosurface is a binary image generated from a cylindrical sub-region of the scaffold's 3D image. Three different porous scaffolds were prepared from 50H by varying the porogen content from 40 to 60 vol%. Lower (<40 vol%) porogen content led to blocked pores and large non-interconnected regions. On the other hand, higher (>60 vol%) porogen had resulted mechanically weak scaffolds.

Different volume percentages of porogen resulted scaffolds with porous morphologies. The lighter gray regions in micro-CT images represent the organic-inorganic hybrid matrix while the air void is outlined by the darker regions. Cross-section of the isosurface images of these scaffolds revealed that the scaffolds fabricated from 50 and 60 vol% porogen were having uniformly distributed, open and interconnected pores whereas lower porogen contents (40 vol%) resulted in blocked pores and solid non-connective regions.

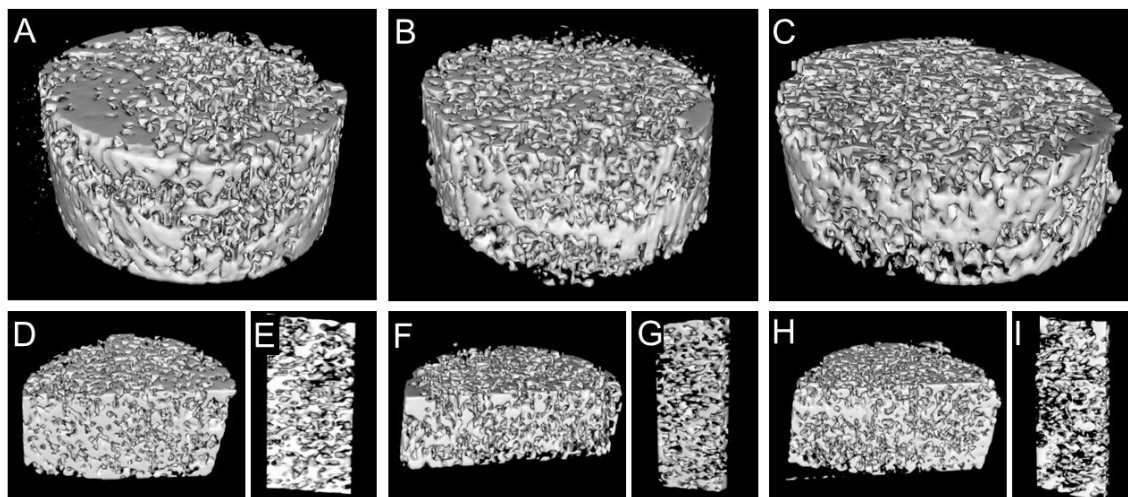


Figure 5. 1: Micro-CT images of PCL/BPSG hybrid scaffolds. Representative images of hybrids prepared from 50 wt% PCL and 50 wt% BPSG (50H). The scaffolds were prepared through particulate leaching using NaCl particles as porogens. **A, B, C)** scaffolds were prepared using 40, 50, and 60 vol% NaCl particles respectively with hybrid powders. **D, F, H)** are cross-sections of isosurface images of the scaffolds. **E, G, I)** represent 500 μm thick slices of randomly chosen 3D scaffolds.

The average porosity of the scaffolds were 43.9, 53.6 and 59.8% (by volume) as shown in Table 5.1. The volume fraction is a measure of the volume of the polymer material relative to the total volume of the region of interest. Pore wall thickness decreased with increasing the porosity. 40, 50 and 60 vol% porogen loading led to wall thickness values of 79.4 ± 1.7 , 66.9 ± 2.1 and 54.0 ± 1.4 μm respectively. The porogen particles had size distribution from 150-250 μm and all scaffolds had shown pore sizes in between this range. However, with increasing the porosity, pore size also increased maybe due to the interconnectivity and decrease of pore wall thickness. For 50 and 60 vol% porogen loading, mean pore size values were found 192.7 ± 11.4 and 201.4 ± 8.7 μm respectively, whereas 40 vol% porogen have resulted 169.0 ± 9.3 μm sized mean pore diameter. Surface area to volume ratio increased with increasing the average porosity. 40, 50 and 60 vol%

porogen loading led to the surface area to volume ratio values of 21.3 ± 0.8 , 26.4 ± 1.1 and 31.6 ± 0.7 , respectively. Higher surface area is desirable for bone tissue engineering because it enhances cell attachment and proliferation by allowing nutrient transport and oxygen availability.

Table 5. 1: Pore properties and porosity of PCL/BPSG hybrid scaffolds

Vol % of porogen	Porosity, volume fraction (%)	Pore wall thickness (μm)	Pore size (μm)	Surface area to volume ratio (mm^{-1})
40	43.9 ± 4.5	79.4 ± 1.7	169.0 ± 9.3	21.3 ± 0.8
50	53.6 ± 2.6	66.9 ± 2.1	192.7 ± 11.4	26.4 ± 1.1
60	59.8 ± 3.9	54.0 ± 1.4	201.4 ± 8.7	31.6 ± 0.7

5.4.2 Mechanical properties of hybrid scaffolds

In a previous study, we had reported composition-dependent mechanical properties of PCL/BPSG hybrids and their superiority over conventional composites as solid cylindrical monoliths [29]. As the mechanical properties of porous 3D scaffolds play critical role in tissue engineering, herein the compressive mechanical properties of class II hybrid scaffolds were investigated at dry and wet conditions. Data collectively presented in Figure 5.2 showed that compressive mechanical properties of scaffolds were significantly influenced by the porogen content, not by the test conditions (dry or wet). With increasing the porosity, the ultimate compressive stress (UCS), modulus and toughness values decreased. These mechanical properties values were consistent with the pore morphologies, mean pore wall thickness and pore size values. UCS values (Figure 5.2A) varied from 342.6 ± 23 kPa for 60% porogen loading to 177.45 ± 30 kPa for 60 vol% porogen at dry condition, and 376.1 ± 25 to 204.4 ± 49 kPa at wet condition. Scaffolds fabricated from different porogen contents had significantly higher compressive modulus values in wet condition

compared with values in dry condition (Figure 5.2B). However, in both test conditions, compressive modulus values significantly decreased with increasing the porosity. Compressive modulus values were varied from $20.6 \text{ MPa} \pm 1.8 \text{ MPa}$ for 40 to $9.3 \text{ MPa} \pm 2.0 \text{ MPa}$ for 60 vol% porogen content at dry condition, and $26.1 \text{ MPa} \pm 0.9 \text{ MPa}$ to $16.5 \text{ MPa} \pm 2.1 \text{ MPa}$ at wet condition. There was no significant difference in toughness values for 40 and 50 vol% porogen loading in dry and wet test conditions (Figure 5.2C). However, scaffolds fabricated using 60 vol% porogen had shown significant decrease in toughness. In contrast to the above-mentioned mechanical properties data, strain at fracture values of the scaffolds significantly increased when the porogen contents increased (Figure 5.2D).

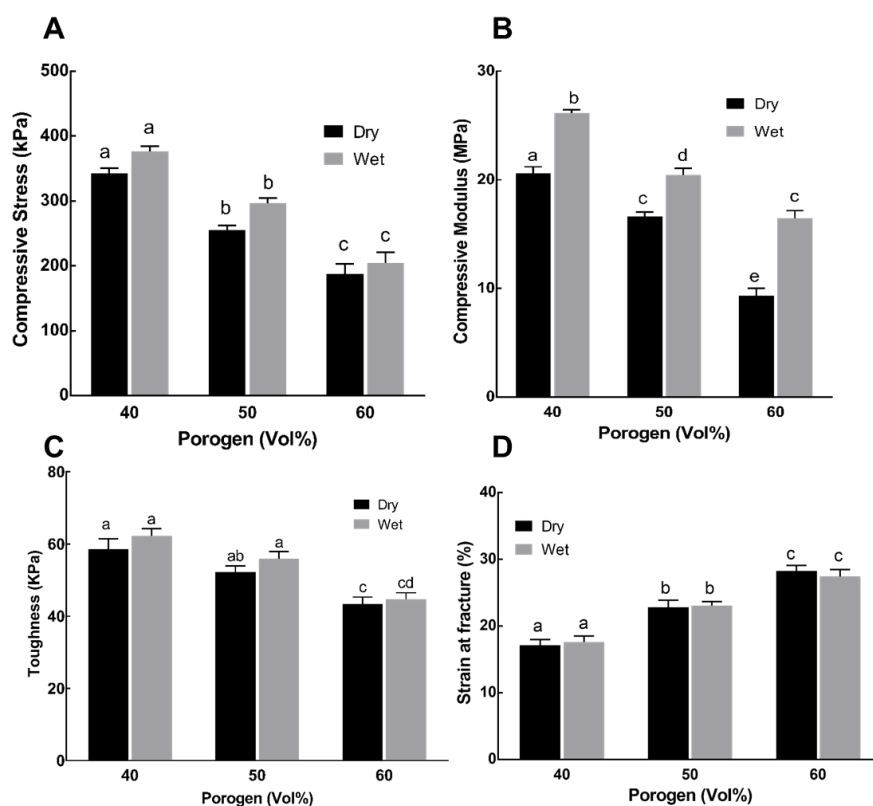


Figure 5. 2: Mechanical properties of 50H PCL/BPSG hybrid scaffolds tested in uniaxial compression at dry and wet conditions. **A)** ultimate compressive stress, **B)** compressive modulus, **C)** toughness, and **D)** strain at fracture. Toughness values were calculated by integrating stress-strain curve up to the point of fracture. Data are mean \pm SD (n=10 scaffold specimens at each conditions). Two-way ANOVA and Tukey's multiple comparison test were used for statistical analysis. Different lower-case letters indicate significant difference at $p < 0.05$.

5.4.3 Changes in mechanical properties of the hybrid scaffolds with degradation

Weight loss and the compressive mechanical properties changes of 30H and 50H scaffolds (fabricated using 50 vol% porogen content) degraded in PBS solution was evaluated over a period of 15 days and data are shown in Figure 5.3. Both hybrid compositions showed weight loss over time (Figure 5.3A) for the first 9 days of degradation, weight loss of 30H and 50H was not

significantly different. However, scaffolds fabricated from 30H have shown higher values of mass loss due to the higher inorganic content after 9 days. After 15 days of incubation in PBS, 30H and 50H scaffolds lost 21.0 ± 1.6 and 15.9 ± 1.0 % of their initial mass respectively. Consistent with the weight loss data, mechanical properties decreased linearly for both hybrid scaffolds degraded in PBS (Figure 5.3B-C). UCS values for 30H scaffolds had decreased from 521.2 ± 21.0 to 357.9 ± 14.2 kPa, and for 50H scaffolds from 255.2 ± 29.8 to 87.5 ± 15.7 kPa after 15 days of incubation. Compressive modulus values for 30H scaffolds decreased from 31.8 ± 2.0 to 14.3 ± 1.6 MPa, and for 50H scaffolds from 16.3 ± 1.9 to 6.6 ± 1.0 MPa after 15 days of PBS incubation.

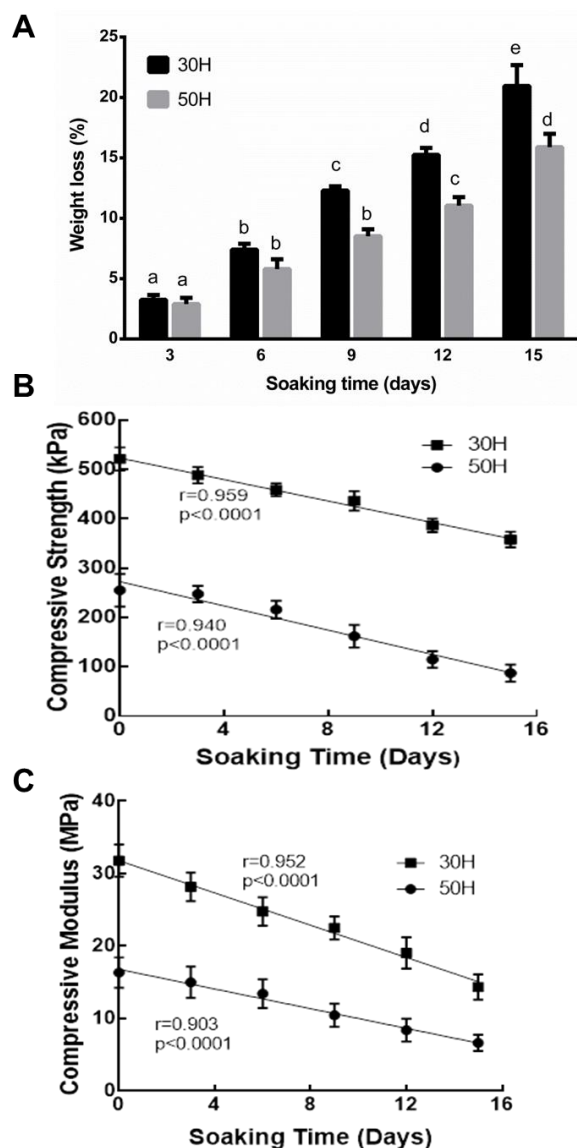


Figure 5. 3: Degradation and change of mechanical properties with degradation of PCL/BPSG hybrid scaffolds. All scaffolds were prepared using 50 vol% porogen. **A)** weight loss of 30H and 50H scaffolds, **B)** ultimate compressive stress, and **C)** compressive modulus values. For panels **B** and **C**, data were fit using linear regression. Data are mean \pm SD ($n=10$ scaffold specimens at each conditions). Two-way ANOVA and Tukey's multiple comparison test were used for statistical analysis. Different lower-case letters indicate significant difference at $p < 0.05$.

5.4.4 Preosteoblastic MC3T3-E1 infiltration studies

MC3T3-E1 preosteoblastic cells were seeded on top of the 30H, 50H and PCL scaffolds, and cultured for 7 and 14 days to investigate cell infiltration to the scaffolds. Representative confocal images after 7 days of culture are shown in Figure 5.4. Dense layer of cells was observed on the top surface of the scaffolds. The pores of the scaffolds are shown as dark circular regions. Deeper into the scaffold (up to 0.5 mm), the second row of images in Figure 5.4 are the representative images of vertical cross-sections of scaffolds. Cells were observed at this distance albeit at smaller numbers. However, below 500 μm the number of cells decreased considerably for all scaffolds. Figure 5.5 represents the number of cells infiltrated in various depths of the scaffolds for 7 days and 4 days of culture. For both cultures times (7 and 14 days of culture), the number of infiltrated cells within the first 500 μm in 50H were significantly higher than 30H and PCL scaffolds. The number of infiltrated cells in 30H were significantly higher than PCL scaffolds after 7 days of culture. We attributed this to the favourable cell adhesion properties of class II hybrid than PCL [29]. Interestingly, number of infiltrated cells in PCL scaffolds at this region were higher than the 30H scaffolds at 14 days. Between 500 to 1000 μm , the number of infiltrated cells in 50H scaffolds were still significantly higher than those of 30H and PCL scaffolds after 7 days of culture. But PCL scaffolds were having higher number of infiltrated cells than 30H scaffolds at both 7 and 14 days of culture. While some cells were encountered at the bottom region, the numbers at day 14 were negligible compared to day 7.

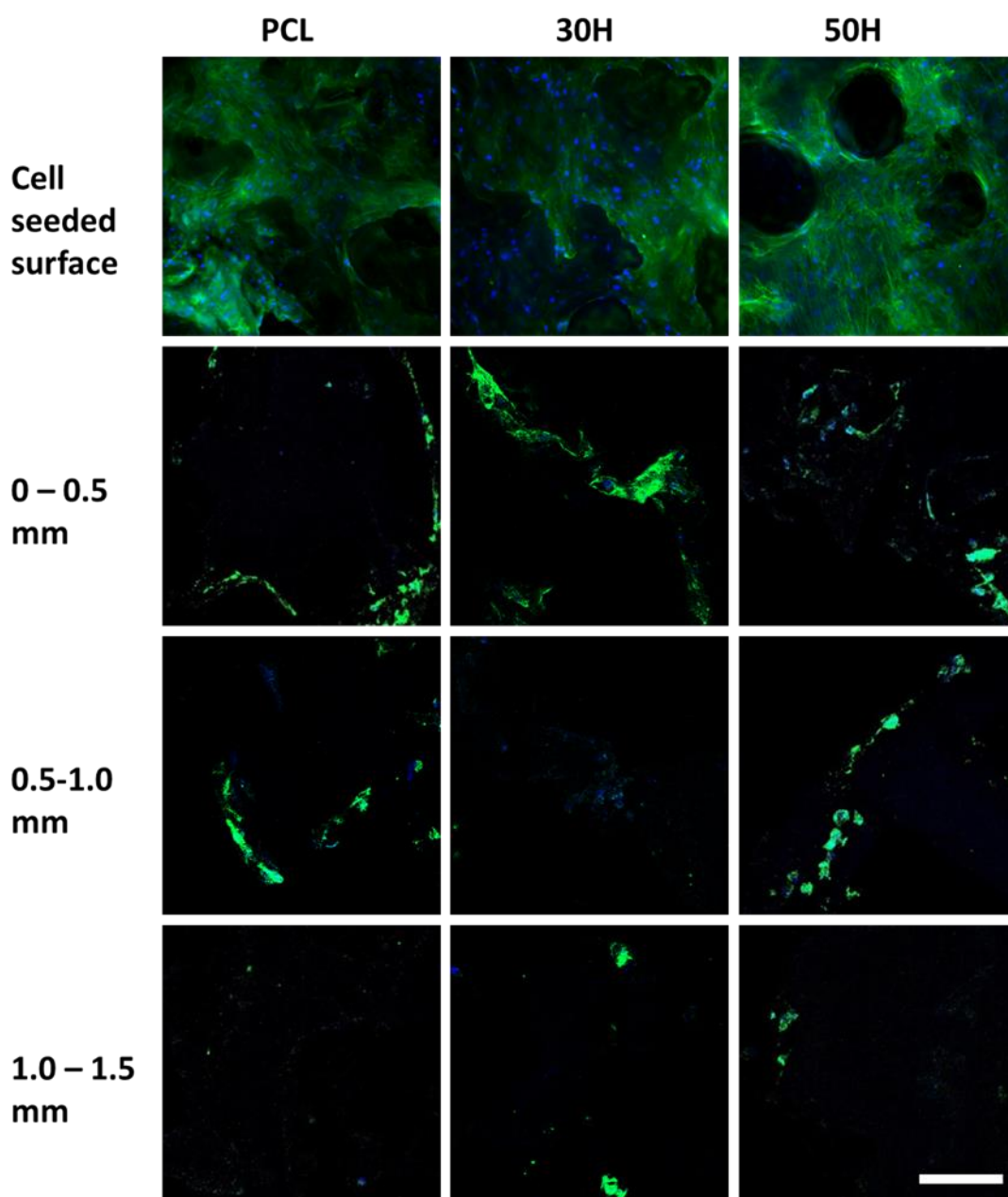


Figure 5. 4: Confocal images of infiltrated preosteoblast MC3T3-E1 cells on 30H, 50H, and PCL scaffolds. Cells were seeded on top of the scaffolds. 7 days following seeding, cells were fixed, and scaffolds were embedded using OCT compound and sectioned using cryostat. Cells were labelled for F-actin (green) and nuclei (blue). are representative of multiple fields on each specimens and different depth of cell-seeded top surfaces from 3 independent experiments, each performed using triplicate specimens. Scale bar for all is 200 μm .

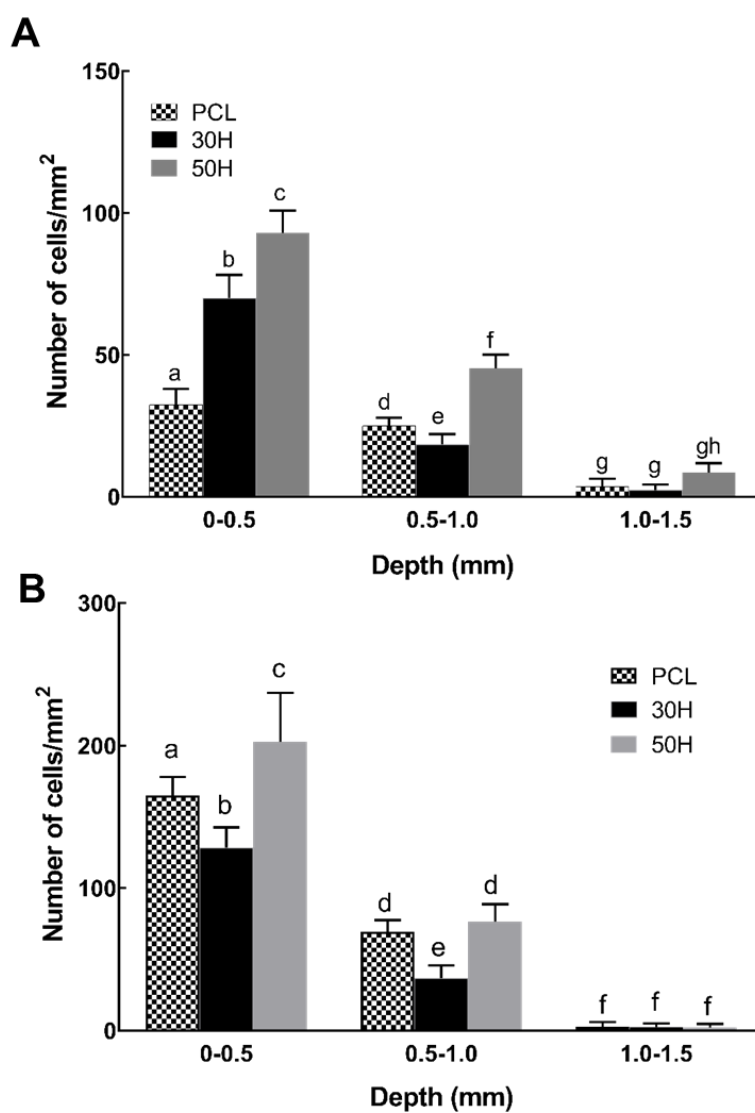


Figure 5. 5: Quantification of cell infiltration in hybrid and PCL scaffolds. Cells were prepared as described in the legend of Figure 5.4. Data are means \pm SD of 10 different regions in each depth regions from 3 independent experiments ($n = 30$), each performed using triplicate specimens. Two-way ANOVA and Tukey's multiple comparison test were used for statistical analysis. Different lower-case letters indicate significant difference at $p < 0.05$. **A)** 7 days culture, **B)** 14 days culture.

5.3.5 Differentiation of stem cells in hybrid scaffolds

Human mesenchymal stem cells are able to differentiate into osteoblasts and express the marker gene for early bone formation. To evaluate the effect of hybrid biomaterials on stem cell fate, human bone marrow derived mesenchymal stem cells (MSC) have been cultured on 30H, 50H and control PCL scaffolds. After 14 days of culture, early and mid-stage bone markers ALP, OPN and OCN were evaluated by qPCR (Figure 5.6 A, C, E). For all markers, hybrid biomaterial scaffolds down-regulated the gene expressions compared to MSC cultured in PCL scaffolds. As down-regulation was not anticipated, the possible role of boron on stem cell differentiation and osteogenic gene expression was studied by culturing induced pluripotent stem cells (iPSCs) on 0, 2 and 5 mol% boron (0B, 2B and 5B respectively). By reducing the boron content from 5 to 2 mol%, ALP, OPN and OCN gene expression increased (Figure 5.6 B, D, F). ALP gene expression was 55-fold upregulated in cells seeded on 2 mol% boron content scaffolds (Figure 5.6B) compared with those seeded on scaffolds on 5 mol% boron. OCN gene expression (Figure 5.7D) were upregulated 80-fold in cells seeded on 2 mol% boron containing scaffolds. Cells seeded on hybrid scaffolds without boron had shown the highest OPN gene expression. However, OPN gene expression (Figure 5.6F) from cells seeded on sample 2B hybrid scaffolds were significantly higher than cells seeded on 5B scaffolds. For all cases, cells in 2B scaffolds had significantly higher gene expression than PCL control scaffolds.

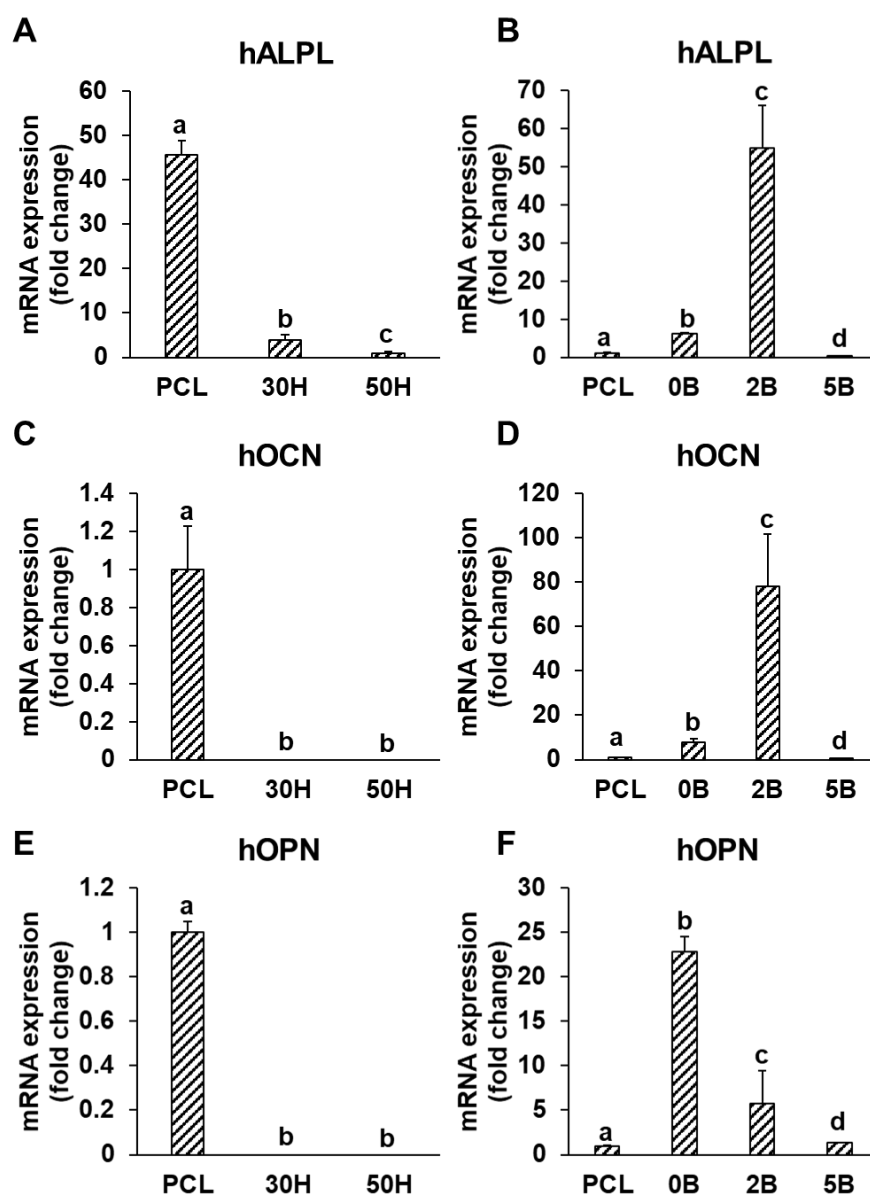


Figure 5. 6: ALP, OCN and OPN mRNA expression of bone marrow derived MSCs (**Panel A, C, E**) grown on 30H, 50H and PCL scaffolds; iPSC derived MSCs (**Panel B, D, F**) grown on scaffolds of PCL, and 50H hybrid prepared with 0 mol% boron (0B), 2 mol% boron (2B), 5 mol% boron (5B); measured by qPCR. All scaffolds were prepared using 50 vol% porogen. MSCs and iPSCs were seeded on scaffolds and cultured for 1 day. Stem cell culture medium were then replaced with osteogenic medium and cultured for additional 14 days (MSCs) and 7 days (iPSCs). Data are means \pm SEM. Two-way ANOVA and Tukey's multiple comparison test were used for statistical analysis. Different lower-case letters indicate significant difference at $p < 0.05$.

5.5 Discussion

Scaffold morphology, pore size distribution, interconnected porous networks are important for bone tissue engineering. Adequate porosity and interconnectivity are necessary for cell infiltration and nutrient diffusion to seeded cells [20, 31, 32]. We previously reported the synthesis of class II hybrid biomaterial from PCL and borophosphosilicate glass and fabrication of 3D porous scaffolds [28]. We also showed that these chemically crosslinked organic inorganic hybrid PCL/BPSG biomaterials provide controllable mechanical properties, biodegradability and bioactivity [29]. However, the detail characterization of the pore morphology and osteogenic differentiation of stem cells on these hybrid scaffolds were not investigated. In this Chapter, the effect of PCL/BPSG class II hybrid biomaterial scaffolds on cell infiltration and osteogenic differentiation was evaluated. In addition, the mechanical properties with and without degradation was investigated.

The strategy to engineer bone involves the fabrication of a biomaterial scaffold which will support initial cell attachment and provide guidance for new bone formation while having mechanical stability [33]. An optimum range of pore size is required to allow cell infiltration and tissue growth through the scaffold [31]. Several techniques are available in literature to fabricate porous scaffold for bone tissue engineering such as electrospinning, solvent casting/particulate leaching, 3D printing, gas foaming, freeze drying, etc. Among them, solvent casting and particulate leaching is widely popular due to the controllability over pore size and porosity, easy processing and less time-consuming process. Pore size and porosity can be control by choosing porogen sizes and optimizing the volume percentage of porogen. In this study, solvent-free casting and particulate leaching was used due to the insolubility of hybrid biomaterials after chemical crosslinking. NaCl

was used as particulate due to its availability, safety, and high solubility in water during the leaching process. Other water-soluble salt particles (as example NH_4Cl) can also be used to fabricate porous scaffolds.

The pores for bone tissue engineering scaffolds must be interconnected for successful cell infiltration and nutrient exchange [20]. Studies have suggested that a minimum pore size that can enhance bone formation is 75-100 μm [31]. Pores greater than 300 μm lead to direct osteogenesis and pores smaller than 300 μm can enhance osteochondral ossification. However, large pore size may compromise the mechanical properties of the scaffolds [21]. PCL/BPSG hybrid scaffolds prepared in this study have shown pore size around 200 μm , which is suitable for cell infiltration and nutrient transfer.

The mechanical properties of PCL/BPSG hybrid scaffolds decreased with increasing the porogen contents. Higher porosity and surface area to volume ratio with lower strut thickness reduced the mechanical properties (Figure 5.2). With higher porogen contents, the interconnectivity between pores increased which resulted the lower values of ultimate compressive stress and modulus. We characterized the mechanical properties of hybrid scaffolds in both dry and wet conditions. Interestingly mechanical properties increased during testing in wet condition suggesting that water entrapped in the pores might have an influence. Previous studies on degradation of non-porous PCL/BPSG hybrid disks revealed that these hybrid biomaterials went through surface erosion in PBS solution without forming cracks or bulk erosion [29]. In this study, the weight loss data of PCL/BPSG hybrid scaffolds have shown similar trend. Change of mechanical properties with degradation also remained consistent with the weight loss data. Slow surface erosion and layer by

layer degradation increased pore size while decreasing pore wall thickness affecting mechanical properties.

It is desired that after seeding the cells in 3D bone tissue engineering scaffolds, they will infiltrate into the scaffolds and lay down their ECM to remodel the constructs into new bone. Our study demonstrated that preosteoblastic MC3T3-E1 cell infiltration within the PCL/BPSG class II hybrid scaffolds after 7 and 14 days of culture. We seeded cells on one side of the scaffolds in static culture condition and investigated their migration and integration inside the scaffolds over time. The number of cells at different depths showed that PCL/BPSG hybrid scaffolds promote cell infiltration into the scaffolds. However, only the top one-third layer the surface was well populated compared to the deeper layers. Hybrid scaffolds with high organic content (50H) had significantly higher number of cells infiltrated compare to 30H and PCL scaffolds up to 1 mm depth.

Osteogenic differentiation and subsequent bone formation is characterised by gene expression during proliferation, ECM production and maturation, and ECM mineralization [34, 35]. Expression of ALP is characteristic marker of osteoblast during bone mineralization and post proliferative stage of ECM maturation [36, 37], whereas OCN and OPN are expressed during the period of bone mineralization [38, 39]. In the present study, both 30H and 50H scaffolds consisted with 5 mol% boron downregulated ALP, OCN and OPN gene expression after 14 days of stem cell culture in osteogenic medium (Figure 5.6) when compared with PCL scaffolds. Although boron can promote bone growth, its effect on bone cells depends on its initial concentration and release behavior in bioactive glass [40]. High borate content in bioactive glasses and rapid release in cell media may inhibit cell proliferation [25, 40]. Our previously reported study showed the

release of boron during degradation of PCL/BPSG hybrid biomaterials were not cytotoxic and did not negatively affect cell adhesion and proliferation on non-porous 2D disks [29]. The 3D porous microstructure and static cell culture might cause localized high concentration of boron which downregulated the osteogenic differentiation. Based on this hypothesis, we prepared PCL/BPSG hybrid with 2 mol% boron (2B) and PCL/SiO₂/P₂O₅ hybrid (0B), and seeded with iPSC derived MSCs to study the effect of boron on osteogenic differentiation. These experiments revealed that significant upregulation of ALP and OCN in cells seeded on 2B hybrid scaffolds compared to 0B and 5B. High ALP and OCN expression suggest differentiation into osteoblast and matrix mineralization on PCL/BPSG hybrid with <2 mol% boron. Taken together, the current study demonstrated the PCL/BPSG hybrid scaffolds were mechanically stable during degradation, promoted cell infiltration and osteogenic gene expression.

5.6 Conclusion

In this Chapter, porous 3D class II PCL/BPSG hybrid biomaterial scaffolds were successfully prepared through solvent-free casting and particulate leaching method. Weight loss of these hybrid scaffolds in PBS solution was organic/inorganic composition dependent and mechanical properties linearly decreased with degradation. Significant number of infiltrated cells indicated that PCL/BPSG hybrid scaffolds promote cell infiltration. When MSCs were seeded in hybrid scaffolds containing 2 mol% boron and cultured in osteogenic media, significant expression of ALP, OCN and OPN were observed. These findings demonstrated that PCL/BPSG scaffolds with ≤ 2 mol% boron may serve as scaffolds for promoting bone formation.

5.7 References

- [1] Frohlich M, Grayson WL, Wan LQ, Marolt D, Drobnic M, Vunjak- Novakovic G. Tissue Engineered Bone Grafts: Biological Requirements, Tissue Culture and Clinical Relevance. *Current Stem Cell Research & Therapy* 2008;3:254-64.
- [2] Li X, Wang L, Fan Y, Feng Q, Cui F-Z, Watari F. Nanostructured scaffolds for bone tissue engineering. *Journal of Biomedical Materials Research Part A* 2013;101A:2424-35.
- [3] Liu Y, Lim J, Teoh S-H. Review: Development of clinically relevant scaffolds for vascularised bone tissue engineering. *Biotechnology Advances* 2013;31:688-705.
- [4] Rezwan K, Chen QZ, Blaker JJ, Boccaccini AR. Biodegradable and bioactive porous polymer/inorganic composite scaffolds for bone tissue engineering. *Biomaterials* 2006;27:3413-31.
- [5] Wu S, Liu X, Yeung KWK, Liu C, Yang X. Biomimetic porous scaffolds for bone tissue engineering. *Materials Science and Engineering: R: Reports* 2014;80:1-36.
- [6] Schultz KM, Kyburz KA, Anseth KS. Measuring dynamic cell-material interactions and remodeling during 3D human mesenchymal stem cell migration in hydrogels. *Proceedings of the National Academy of Sciences* 2015;112:E3757-E64.
- [7] Bose S, Roy M, Bandyopadhyay A. Recent advances in bone tissue engineering scaffolds. *Trends in Biotechnology* 2012;30:546-54.
- [8] Jones JR. Review of bioactive glass: From Hench to hybrids. *Acta Biomaterialia* 2013;9:4457-86.
- [9] KICKELBICK G. Introduction to Hybrid Materials. *Hybrid Materials: Wiley-VCH Verlag GmbH & Co. KGaA*; 2006. p. 1-48.
- [10] Sultana N. Fabrication Techniques and Properties of Scaffolds. In: Sultana N, editor. *Biodegradable Polymer-Based Scaffolds for Bone Tissue Engineering*. Berlin, Heidelberg: Springer Berlin Heidelberg; 2013. p. 19-42.
- [11] Ma L, Jiang W, Li W. Solvent-free Fabrication of Tissue Engineering Scaffolds with Immiscible Polymer Blends. *International journal of polymeric materials* 2014;63:510-7.
- [12] Wang X, Li W, Kumar V. A method for solvent-free fabrication of porous polymer using solid-state foaming and ultrasound for tissue engineering applications. *Biomaterials* 2006;27:1924-9.
- [13] An J, Chua CK, Leong KF, Chen C-H, Chen J-P. Solvent-free fabrication of three dimensionally aligned polycaprolactone microfibers for engineering of anisotropic tissues. *Biomedical Microdevices* 2012;14:863-72.
- [14] Liu S-J, Hsueh C-L, Wen-Neng Ueng S, Lin S-S, Chen J-K. Manufacture of solvent-free polylactic-glycolic acid (PLGA) scaffolds for tissue engineering. *Asia-Pacific Journal of Chemical Engineering* 2009;4:154-60.

- [15] Spaans CJ, Belgraver VW, Rienstra O, de Groot JH, Veth RPH, Pennings AJ. Solvent-free fabrication of micro-porous polyurethane amide and polyurethane-urea scaffolds for repair and replacement of the knee-joint meniscus. *Biomaterials* 2000;21:2453-60.
- [16] Scaffaro R, Re GL, Rigogliuso S, Ghersi G. 3D polylactide-based scaffolds for studying human hepatocarcinoma processes in vitro. *Science and Technology of Advanced Materials* 2012;13:045003.
- [17] Allo BA, Rizkalla AS, Mequanint K. Synthesis and Electrospinning of ϵ -Polycaprolactone-Bioactive Glass Hybrid Biomaterials via a Sol-Gel Process. *Langmuir* 2010;26:18340-8.
- [18] Anselme K. Osteoblast adhesion on biomaterials. *Biomaterials* 2000;21:667-81.
- [19] Rouwkema J, Rivron NC, van Blitterswijk CA. Vascularization in tissue engineering. *Trends in Biotechnology* 2008;26:434-41.
- [20] Murphy CM, Haugh MG, O'Brien FJ. The effect of mean pore size on cell attachment, proliferation and migration in collagen-glycosaminoglycan scaffolds for bone tissue engineering. *Biomaterials* 2010;31:461-6.
- [21] Karageorgiou V, Kaplan D. Porosity of 3D biomaterial scaffolds and osteogenesis. *Biomaterials* 2005;26:5474-91.
- [22] Stein GS, Lian JB, Stein JL, Van Wijnen AJ, Montecino M. Transcriptional control of osteoblast growth and differentiation. *Physiological Reviews* 1996;76:593-629.
- [23] Fu Q, Rahaman MN, Bal BS, Bonewald LF, Kuroki K, Brown RF. Silicate, borosilicate, and borate bioactive glass scaffolds with controllable degradation rate for bone tissue engineering applications. II. In vitro and in vivo biological evaluation. *Journal of Biomedical Materials Research Part A* 2010;95A:172-9.
- [24] Kaur G, Pandey OP, Singh K, Homa D, Scott B, Pickrell G. A review of bioactive glasses: Their structure, properties, fabrication and apatite formation. *Journal of Biomedical Materials Research Part A* 2014;102:254-74.
- [25] Rahaman MN, Day DE, Sonny Bal B, Fu Q, Jung SB, Bonewald LF, et al. Bioactive glass in tissue engineering. *Acta Biomaterialia* 2011;7:2355-73.
- [26] Xu S, Yang X, Chen X, Shao H, He Y, Zhang L, et al. Effect of borosilicate glass on the mechanical and biodegradation properties of 45S5-derived bioactive glass-ceramics. *Journal of Non-Crystalline Solids* 2014;405:91-9.
- [27] Yao A, Wang D, Huang W, Fu Q, Rahaman MN, Day DE. In Vitro Bioactive Characteristics of Borate-Based Glasses with Controllable Degradation Behavior. *Journal of the American Ceramic Society* 2007;90:303-6.
- [28] Mondal D, Rizkalla AS, Mequanint K. Bioactive borophosphosilicate-polycaprolactone hybrid biomaterials via a non-aqueous sol gel process. *RSC Advances* 2016;6:92824-32.

- [29] Mondal D, Dixon SJ, Mequanint K, Rizkalla AS. Mechanically-competent and cytocompatible polycaprolactone-borophosphosilicate hybrid biomaterials. *Journal of the Mechanical Behavior of Biomedical Materials* 2017;75:180-9.
- [30] Esseltine JL, Shao Q, Brooks C, Sampson J, Betts DH, Séguin CA, et al. Connexin43 Mutant Patient-Derived Induced Pluripotent Stem Cells Exhibit Altered Differentiation Potential. *Journal of Bone and Mineral Research* 2017;32:1368-85.
- [31] Bružauskaitė I, Bironaitė D, Bagdonas E, Bernotienė E. Scaffolds and cells for tissue regeneration: different scaffold pore sizes—different cell effects. *Cytotechnology* 2016;68:355-69.
- [32] Loh QL, Choong C. Three-Dimensional Scaffolds for Tissue Engineering Applications: Role of Porosity and Pore Size. *Tissue Engineering Part B, Reviews* 2013;19:485-502.
- [33] Hutmacher DW. Scaffolds in tissue engineering bone and cartilage. *Biomaterials* 2000;21:2529-43.
- [34] Allo BA, Lin S, Mequanint K, Rizkalla AS. Role of Bioactive 3D Hybrid Fibrous Scaffolds on Mechanical Behavior and Spatiotemporal Osteoblast Gene Expression. *ACS Applied Materials & Interfaces* 2013;5:7574-83.
- [35] Siggelkow H, Rebenstorff K, Kurre W, Niedhart C, Engel I, Schulz H, et al. Development of the osteoblast phenotype in primary human osteoblasts in culture: Comparison with rat calvarial cells in osteoblast differentiation. *Journal of Cellular Biochemistry* 1999;75:22-35.
- [36] Balmayor ER, Flicker M, Käser T, Saalmüller A, Erben RG. Human Placental Alkaline Phosphatase as a Tracking Marker for Bone Marrow Mesenchymal Stem Cells. *BioResearch Open Access* 2013;2:346-55.
- [37] Golub EE, Boesze-Battaglia K. The role of alkaline phosphatase in mineralization. *Current Opinion in Orthopaedics* 2007;18:444-8.
- [38] Aubin JE. Bone stem cells. *Journal of Cellular Biochemistry* 1998;72:73-82.
- [39] Bellows CG, Reimers SM, Heersche JNM. Expression of mRNAs for type-I collagen, bone sialoprotein, osteocalcin, and osteopontin at different stages of osteoblastic differentiation and their regulation by 1,25 dihydroxyvitamin D₃. *Cell and Tissue Research* 1999;297:249-59.
- [40] Pan HB, Zhao XL, Zhang X, Zhang KB, Li LC, Li ZY, et al. Strontium borate glass: potential biomaterial for bone regeneration. *Journal of the Royal Society Interface* 2010;7:1025-31.

Chapter 6

Effect of Copolymer Functionality and Composition on Bioactivity, Degradation and Mechanical Properties of Poly(vinyl pyrrolidone-co- triethoxy vinyl silane)/Bioactive Glass Hybrids

Overview: This Chapter discusses the synthesis of class II hybrid biomaterials from polyvinyl pyrrolidone (PVP) and bioactive glass (BG) through sol gel process. First, copolymers of VP and triethoxyvinylsilane (TEVS) were prepared to increase the degree of crosslinking between organic and inorganic phases. Copolymers of various TEVS content were used to evaluate the effect of functionality on properties of hybrid biomaterial. Finally, scaffolds of these hybrids with well defined pore size and interconnectivity, were prepared through indirect 3D printing.

6.1 Summary

Presence of trialkoxysilane functional groups as side chains in polymer backbone increases the degree of covalent crosslinking between organic polymers and inorganic bioactive glass (BG) during the synthesis of class II organic/inorganic (O/I) hybrid biomaterials by sol gel process. The microstructure, bioactivity, degradation and mechanical properties of these hybrids can be tailored by varying the amount of functional groups in the polymer chains. In view of this, we synthesised a series of class II hybrid biomaterials from BG and triethoxysilane functionalized polyvinyl pyrrolidone (PVP). Prior to that, vinyl pyrrolidone (VP) and triethoxyvinylsilane (TEVS) monomers were copolymerized at various molar ratios, to obtain different amounts of functional groups in polymer chains. When these functional copolymers were added to sol gel mixture with inorganic BG precursors, such as tetraethyl orthosilicate and triethyl phosphate, they went through hydrolysis and polycondensation and formed Si-O-Si and Si-O-P bridging networks between organic and inorganic phases. This study, for the first time revealed that the functionality of polymers greatly affects the nature of O/I matrix formation and degradation behavior of class II

hybrid biomaterials. Higher amount of functional groups in the copolymer increased the copolymer-BG covalent bonding, and hence decreased the rate of degradation and release of BG dissolution products. Biomimetic apatite deposition on hybrid biomaterial surfaces, when incubated in simulated body fluid (SBF) was primarily dependent on O/I weight ratios. Higher BG content improved the apatite deposition and biocompatibility. Porous and interconnective three-dimensional (3D) scaffolds of these hybrid biomaterials were fabricated by indirect 3D printing using polycaprolactone as sacrificial template scaffold. These hybrid scaffolds have shown excellent compressive properties. Introducing functional groups into polymeric chains prior to synthesizing O/I hybrids, exposed the possibilities for tailoring physical, biochemical and mechanical properties of scaffold materials for tissue regeneration and related applications.

6.2 Introduction

Bone regeneration by tissue engineering is a well-orchestrated process which initiates with recruitment of bone forming cells into porous scaffold and their proliferation through interconnective pores and subsequent bone extracellular matrix (ECM) formation. The success of bone regeneration vastly relies on porous bioactive scaffolds, which need to be osteoinductive and osteoconductive to promote migration and recruitment of osteoprogenitor cells into the pores. The scaffold should have appropriate porosity and pore size to allow cell infiltration, angiogenesis and metabolic waste removal. The cells proliferate, differentiate, and form bone ECM and replace the scaffold with newly formed bone [1, 2]. The scaffold material need to be biodegradable and the rate of degradation should be compatible with the rate of bone formation, so that newly formed

bone can replace the scaffold. The degradation behavior also needs to be controlled so that the scaffold remains mechanically competent to support the bone regeneration process [3-5].

One of the major challenges is to combine all these properties into a single scaffold biomaterial [6]. Composites of various materials with those above-mentioned properties can be an alternative. However, conventional composites consisting of macro-scale distinct phases are not suitable for bone tissue engineering scaffolds, where molecular-scale homogeneity among phases and uniform physical, chemical, mechanical, biological properties are desired [6-8].

O/I hybrid biomaterials can be a better alternative compared to the conventional composites. These hybrids act as a single-phase material due to the molecular level interactions among various organic and inorganic components and provide synergistic combination of properties from all constituents [9-11]. Class I hybrids can be obtained through hydrogen bonding between the organic and inorganic constituents and Class II hybrids can result due to the chemical cross linking between the organic and inorganic phases [11, 12].

Sol gel derived $\text{SiO}_2\text{-P}_2\text{O}_5\text{-CaO}$ based bioactive glasses (BGs) have been widely used for bone regeneration due to their biocompatibility, osteoconductivity, biodegradability and ability to form bone-like mineral phases at the interface when in contact with living tissue [6, 13, 14]. Despite their excellent *in vitro* and *in vivo* performances, their brittle and stiff nature impose challenge to process into porous complex scaffolds, as well as their rapid degradation causes insufficient bone regeneration [13, 15-17].

These challenges can be easily overcome by preparing class II hybrid biomaterials using BGs as the inorganic components and degradable biopolymers as the organic moieties. It is possible to tailor the mechanical properties, degradation behavior and cell-material interactions of such class II hybrid scaffolds by varying the O/I ratios and degree of covalent crosslinking. Three different strategies are generally applied to synthesize class II hybrid biomaterials: 1) the use of a coupling agent that can bond with both the organic and inorganic phases, 2) the use of an organic polymer which is already containing silane functional group(s), and 3) in-situ polymerization of organic and inorganic phases from their precursor monomers [6, 11]. Coupling agents such as (3-aminopropyl)triethoxysilane etc. glycidoxypropyl)trimethoxysilane, (3-isocyanatopropyl)triethoxysilane, (3- have been used to functionalize polymers, such as chitosan [18-20], polycaprolactone [21, 22], gelatin [23], polyglutamic acid [24], etc. prior to synthesis O/I hybrid biomaterials. Functionalization of polymers with coupling agents delivers only a limited amount of functional group related to the polymer backbone. This can cause phase separation over a certain amount of organic moiety [25].

Polydimethoxysilane (PDMS) is an example of polymer containing functional silane groups in its backbone. PDMS was used to prepare class II hybrid by hydrolyzing it with tetraethylorthosilicate [26]. However, PDMS is not a degradable polymer, so it is not suitable to be used for bone regeneration. Another way to incorporate silane functional groups in polymer chains is to copolymerize the monomer with an alkoxy silane monomer. Copolymer of polystyrene [27], poly(2-hydroxyethylmethacrylate) [28], acrylonitrile butadiene styrene [29], poly(methyl methacrylate) [30, 31] have been prepared with several trialkoxysilyl ($-\text{Si}(\text{OR})_3$) monomers and associated hybrids have been prepared by hydrolyzing them with silica precursors. However, these

polymers were neither biodegradable nor water-soluble which restricted their application for bone regeneration. Moreover, class II hybrids consisted of SiO₂ as the sole inorganic component, yielding materials which were not sufficiently bioactive to induce osteogenesis [6].

In this study, we first prepared copolymers of VP and TEVS with various monomer ratios. These copolymers were then co-hydrolyzed and co-condensed with tetraethyl orthosilicate (TEOS) and triethyl phosphate (TEP) in aqueous sol gel process using ethanol as the solvent to achieve homogenous O/I network formation. PVP is widely used as drug carrier and FDA approved material [32, 33]. We evaluated the effect of copolymer functionality and O/I weight ratios on apatite deposition, degradation and cell-material interactions of these hybrid biomaterials.

3D porous scaffolds of these class II hybrid biomaterials were prepared through indirect rapid prototyping technique. This method helps design the pore morphology within the hybrid scaffolds upfront and independent of the material's physical properties [34]. In our study, we used polycaprolactone (PCL) templates as the 3D printed mold to fabricate poly(VP-co-TEVS)/BG hybrid scaffolds. PCL was chosen as template material because it is insoluble in water and ethanol which are the reactants and byproducts of sol gel process. It also has excellent solubility in common organic solvents, thus easy to leach out. We successfully fabricated poly(VP-co-TEVS)/BG hybrid scaffolds with well defined and interconnected porous microstructures. Pore morphology and porosity were analysed using micro-computed tomography (Micro-CT). Furthermore, we evaluated the compressive properties of these scaffolds. This study adds important information to our knowledge about how the functionality of organic polymers affects physical, chemical, mechanical and biological properties class II hybrid biomaterials.

6.3 Materials and methods

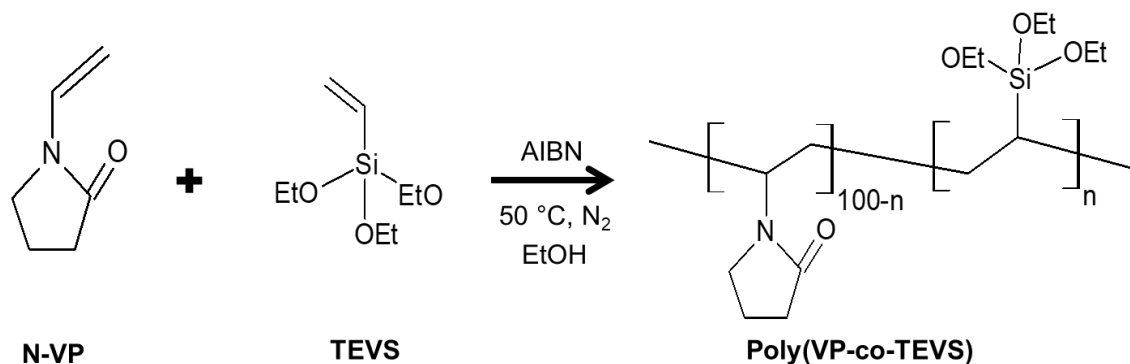
6.3.1 Materials

1-vinyl-2-pyrrolidone (NVP, 99%, contains NaOH as inhibitor), triethoxyvinylsilane (TEVS, 97%) and 2,2'-azobis(2-methylpropionitrile) (AIBN, 98%), tetraethyl orthosilicate (TEOS, 98%), triethyl phosphate (TEP, 99.8%), calcium chloride dihydrate ($\text{CaCl}_2 \cdot 2\text{H}_2\text{O}$, 99%), phosphate-buffered saline (PBS), TritonTM X-100, and all chemicals for preparing simulated body fluid (SBF) were purchased from Sigma Aldrich (Milwaukee, WI). Anhydrous ethanol was purchased from Commercial Alcohol (GreenField Specialty Alcohols Inc., Canada). Petroleum ether, Dichloromethane (DCM) was purchased from Caledon Labs (Brampton, ON, Canada). Minimal essential medium (α -MEM), fetal bovine serum (FBS), antibiotic-antimycotic solution (10,000 units/mL penicillin; 10,000 $\mu\text{g}/\text{mL}$ streptomycin; and 25 $\mu\text{g}/\text{mL}$ amphotericin B), paraformaldehyde (PFA) and trypsin were purchased from Gibco, ThermoFisher Scientific (USA). Bovine albumin (BSA) was purchased from MP Biomedicals LLC (USA).

6.3.2 Synthesis of poly(VP-co-TEVS)

NVP was first purified by passing through activated alumina (58 Å, Sigma Aldrich, Milwaukee, WI) filled glass column. Purified NVP was then transferred to a three-necked flask with TEVS at stoichiometric ratio and a magnetic stirrer bar. The copolymer was synthesized at 50 °C in N_2 atmosphere using anhydrous ethanol as solvent and AIBN as initiator (0.4 mol% of total NVP and TEVS) (Scheme 6.1). The flask was connected to a condenser to reflux the ethanol. Reaction time for copolymers with varying monomer ratios were optimised based on maintaining a consistent

range of weight average molecular weights (M_w) (35-45 kDa). Purification of the copolymers were carried out by repeated precipitation in excess (≥ 10 times than the copolymer solution) cold petroleum ether. The precipitated copolymer was dissolved in ethanol and re-precipitated again in petroleum ether for three times. Finally, the precipitated copolymer was dissolved in ethanol followed by transferring into a Teflon beaker and placed into a vacuum dryer to dry at room temperature for 24 hours. Copolymerization was confirmed with Fourier-transform infrared spectroscopy (FTIR), ^1H and ^{13}C Nuclear magnetic resonance (NMR) spectroscopy. The molecular weight and polydispersity index (PDI) of copolymers were measured by using gel permeation chromatography (GPC). TEVS content in monomer mixture were varied from 0 to 50 mol% (0, 6, 16, 24 and 36 mol%) to obtain different silane contents in copolymer chains.

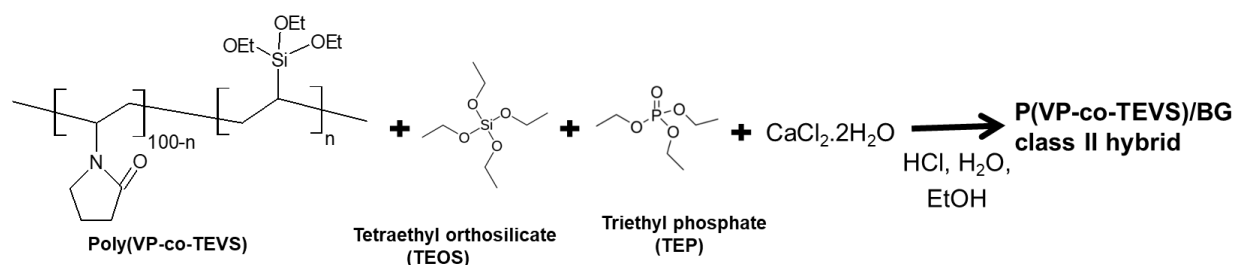


Scheme 6. 1: Copolymerization of N-Vinylpyrrolidone (NVP) and Vinyl triethoxysilane (TEVS). n= 6, 16, 24 and 36 mol% TEVS.

6.3.3 Synthesis of poly(VP-co-TEVS)/BG class II hybrid

Poly(VP-co-TEVS)/BG class II hybrid materials were synthesized through *in situ* copolymerization of organic poly(VP-co-TEVS) and inorganic bioactive glass (BG) via sol gel

process (Scheme 6.2). BG composition for all hybrid materials in this study was kept constant as 70 mol % SiO₂, 26 mol % CaCl₂ and 4 mol % P₂O₅. First pre-determined amount of copolymer and CaCl₂·2H₂O were dissolved in ethanol (10% w/v). Then TEOS was added to the solution. 70 mol % SiO₂ in BG was calculated by adding mole percentage of Si presence in the copolymer and TEOS. TEP was added after 1 h of mixing of the copolymer and TEOS solution, followed by addition of water to the sol and stirred for 2 h. Molar ratio of (TEOS + TEP + CaCl₂·2H₂O) to water was maintained at 1:4. The contents were then transferred into a Teflon mold and kept in a fume hood for 3 days covered by aluminum foil with few pinholes. Following gelation of the sol, the gel was first kept for 2 days in a fume hood, then dried under reduced pressure (225 mm Hg) for one day at room temperature. The resultant transparent class II hybrid materials were used for further characterization. An example of clarifying the nomenclature used in this study to identify the composition of hybrid biomaterials is presented as follows: 30P represents 30 wt% organic copolymer and 70 wt% BG.



Scheme 6. 2: Synthesis of class II poly(VP-co-TEVS)/BG hybrid materials.

Solid-state cross-polarization magic-angle spinning (CPMAS) ²⁹Si NMR spectra of Poly(VP-co-TEVS)/BG hybrids were acquired using a Varian Infinity Plus 400 NMR spectrometer ($\nu(^1\text{H}) =$

399.5 MHz, $\nu(^{29}\text{Si}) = 79.4$ MHz) equipped with a Varian HXY triple-resonance 7.5 mm magic-angle spinning NMR probe. The samples were packed tightly into 7.5 mm outer diameter ZrO_2 rotors and rotated at 5.5 kHz. A total of 4000 scans were summed using a $6.75 \mu\text{s}$ ^1H 90-degree pulse, 2 ms contact time, 10.24 ms acquisition time, 7 s recycle delay, 50 kHz spectral width and continuous-wave ^1H decoupling during acquisition. For processing, two zero-fills and 30 Hz line broadening were applied to the FID before Fourier transformation. The NMR spectra were referenced with respect to tetramethylsilane ($\delta(^{29}\text{Si}) = 0.0$ ppm) by setting the high-frequency peak of tetrakis(trimethylsilyl)silane to -9.8 ppm.

6.3.4 *In vitro* bioactivity evaluation of poly(VP-co-TEVS)/BG hybrid in SBF

The *in vitro* bioactivity tests were carried out by studying the deposition of hydroxyapatite (HA) on the surface of hybrid disk samples (6 mm in diameter and 2 mm in thickness) following incubation in simulated body fluid (SBF). The SBF solution has a composition and concentration similar to those of the inorganic part of human blood plasma and was prepared as described in the literature [35].

Each specimen was incubated with 10 mL of SBF contained in polypropylene bottles covered with a tight lid. The bottles were placed in an orbital shaker (MaxQ4000, Barnstead Lab-line, IL) at 120 rpm and 37°C at different time interval ranging from 6 hours to 7 days. SBF solution was refreshed daily. After each incubation period, the disks were rinsed with DI water and dried under vacuum at room temperature for 24 h prior to scanning electron microscopy (SEM) imaging and x-ray diffraction (XRD). SEM were performed using LEO 1540XB SEM (Hitachi, Japan). Energy dispersive spectroscopy (EDX) were measured by using the detector attached to the LEO 1540XB

SEM. The specimen surfaces were coated with 5 nm Osmium in Osmium Plasma Coater (OPC80T, Filgen Inc. Japan) prior to SEM and EDX. XRD was performed using an X-ray diffractometer AXS D2 PHASER (Bruker Corporation, USA) operating on CuK α radiation with $\lambda=1.5418\text{\AA}$. analysis. For XRD, dried specimens were grinded in mortar and pestle to get fine powder.

6.3.5 Degradation of poly(VP-co-TEVS)/BG hybrid biomaterials in PBS

Degradation behavior was characterized by studying the weight loss and ion release from poly(VP-co-TEVS)/BG hybrid disk samples following incubation in PBS for various times. Disk specimens (6 mm in diameter and 2 mm in thickness) were weighed (initial weight) and then incubated in 10 mL PBS solution in polypropylene bottles covered with a tight lid. The bottles were placed in an orbital shaker at 120 rpm and 37 °C and incubated for 3, 6, 9, 12 or 15 days. After each time point, 3 hybrid specimens for each composition were removed, and the corresponding PBS was collected. For the remaining bottles, PBS was collected and bottles were replenished with fresh PBS. Once removed, disks were rinsed with deionized water, dried under vacuum at room temperature for 24 h, and weighed (final weight). The percentage weight loss for each specimen was calculated from its initial and final weight.

The release of calcium and silicon ions was determined as follows. For each specimen, PBS samples were pooled and supplemented (where necessary) with fresh PBS to achieve a total volume of 50 mL. The concentrations of calcium and silicon ions were determined using inductively coupled plasma optical-emission spectroscopy (ICP-OES; Vista-Pro Axial, Varian Inc., USA).

6.3.6 Cell culture and assessment of cellular morphology on hybrid

Pre-osteoblastic MC3T3-E1 cells (Subclone 4, American Type Culture Collection) were cultured in α -MEM supplemented with 10% FBS and 1% antibiotic-antimycotic solution. Cell-material interaction were tested on 30P, 50P disks (6 mm in diameter and 2 mm in thickness) and glass cover slips (as control, 12 mm in diameter and ~0.15 mm in thickness). Specimens were disinfected by submerging twice in 70 vol% ethanol for 5 min and dried. Each specimen was incubated in 1 mL serum-free culture medium in 24-wells culture plates before seeding cells. After 24 h, the medium was aspirated and MC3T3-E1 cells were seeded at a density of 10,000 cells/cm² and incubated for 3 and 24 h. After each time point, cells were fixed with 4% PFA solution, rinsed with PBS three times, permeabilized with 0.1% Triton X-100/PBS for 5 min, and blocked with 1% BSA in PBS for 90 min at 4 °C. F-actin was labeled using Alexa Fluor 488® phalloidin (1:400 dilution, ThermoFisher Scientific) for 35 min at room temperature. Then substrata were rinsed with PBS three times and nuclei were labeled by staining with DAPI (ThermoFisher Scientific) for 5 min. Finally, substrata were rinsed three times with PBS.

Cells were imaged using a Carl Zeiss Imager M2m microscope with dipping objective (40 X) and Zen Pro 2012 software (Carl Zeiss, Jena, Germany). To enhance image sharpness, multiple images were merged using the extended depth of focus module. Images of DAPI fluorescence were used to determine the number of nuclei (cells) per unit area on the various substrata using ImageJ software. Nuclei that straddled the two edges of images were excluded during this analysis. In these experiments, cell density reflects the net effects of cell attachment, cell proliferation and cell death, providing an excellent overall assessment of cytocompatibility.

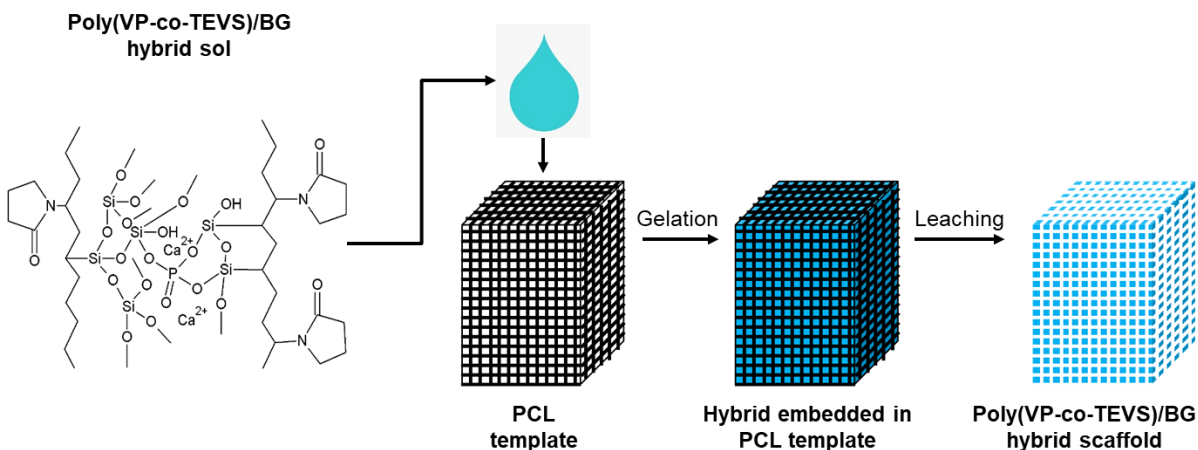
6.3.7 Poly(VP-co-TEVS)/BG class II hybrid scaffold fabrication

Porous hybrid scaffolds were prepared through embedding the hybrids into 3D printed sacrificial polycaprolactone (PCL) porous templates and leaching out. The PCL templates were designed using SOLIDWORKS and produced using a 3D printer (DeltaMaker desktop 3D printer, DeltaMaker LLC., Orlando, FL). PCL filament (eMate, 1.75mm, Shenzhen Esun Co., Toronto, Canada) was melted at 95 °C and extruded through a nozzle with an inner diameter of 0.4 mm to produce a large rectangular-shaped layered grid structure. The line spacing in x-y levels was set to 0.5 mm and the level spacing in z was set to 0.2 mm. The printing speed was optimized at 5 mm/s.

The 3D printed PCL templates were then immersed into poly(VP-co-TEVS)/BG hybrid sol in a teflon mold and kept at a reduced pressure to remove entrapped air so that the hybrid sol could fully infiltrate into the porous PCL structures (Scheme 6.3). The molds were kept at reduced pressure until the hybrids transformed from sol to gel and then gel to solid. All samples were then removed from the teflon mold and placed into a glass breaker with excess amount of DCM with gentle stirring for 2 days. Fresh DCM was replaced every 2 h for the first 10 h, then 2–3 times a day. The resultant hybrid scaffolds were then dried under vacuum at room temperature.

Hybrid scaffolds were imaged by SEM and micro-CT (eXplore Locus SP, GE Healthcare, Canada). For micro-CT, scanning was conducted at 20 μm voxel resolution, using an exposure time of 4500 ms, 10 frames per view, and a total of 900 views at an increment of 0.4°. Two-dimensional slice images were reassembled from the isotropic slice data, and compiled to generate a 3D image. 3D Images were analyzed and displayed using commercially available trabecular bone analysis software (MicroView version Viz+2.0, GE Healthcare). The threshold values

differentiating the hybrid materials from air was carefully selected by using air and water as control objects. Detail analysis of these micro-CT images includes measurements of porosity, pore wall thickness and pore sizes, and surface area to volume ratio.



Scheme 6. 3: Fabrication of hybrid scaffolds. First, PCL templates were designed and produced by 3D printing. Hybrid sol was embedded in that PCL templates at reduced pressure, and maintained until it gelled and dried. After that, PCL was leached out by using DCM, leaving the porous hybrid scaffolds.

6.3.8 Compressive properties of poly(VP-co-TEVS)/BG hybrid scaffolds

Uniaxial compressive testing of porous scaffold specimens (4 mm x 4 mm cross-section and 6 mm height) was conducted using an Instron Universal Mechanical testing machine equipped with 5 kN load cell (Instron model 3345, Canton, MA) and crosshead speed of 1 mm/min at ambient temperature. The compressive strength and modulus were determined from ultimate stress values and the slope of the initial linear elastic portions of the stress–strain curves, respectively. Toughness values were calculated from the area under the stress-strain curves.

6.3.9 Statistical analyses

Data are presented as means \pm standard deviations (SD) and were analysed using GraphPad Prism 6.0 (GraphPad Software Inc., CA, USA). Where indicated, curves were fit to second degree polynomial using nonlinear regression, $p < 0.001$. Means were compared using one- or two-way analysis of variance (ANOVA) followed by a Tukey's multiple comparison test. Differences between means were considered statistically significant at $p < 0.05$.

6.4 Results

6.4.1 Synthesis of poly(VP-co-TEVS)/BG class II hybrid biomaterials

Tri-ethoxysilane functionalized copolymer Poly(VP-co-TEVS) was prepared through free radical polymerization of N-vinylpyrrolidone and triethoxyvinylsilane, by using AIBN as initiator (Scheme 6.1). Preparing copolymer of VP and TEVS through similar methods have been reported earlier [36]. The effectiveness of VP and TEVS copolymerization were characterized by FTIR, ^1H and ^{13}C NMR (Figure 6.1-6.3). Characteristic FTIR bands for copolymer were observed at 1070 cm^{-1} (Si-O-C stretch.) and 770 cm^{-1} (Si-C stretch.); ^1H -NMR shifts for 16 mol% TEVS containing copolymer (C16) were at 0.40 (CHSi chain), 3.68 (CH_2OSi) and 3.8 ppm (CH-N chain); and ^{13}C -NMR shift at 58 ppm (CH_2OSi). Absence of peaks associated with C=C vinyl bonds indicated successful copolymerization. Copolymer nomenclatures, VP and TEVS compositions, molecular weights (M_w) and polydispersity indices are shown in Table 6.1.

Table 6. 1: Composition, yeild and molecular weight distribution for poly(VP-co-TEVS)

Copolymer nomenclature	N-Vinyl Pyrrolidone (NVP) (mol%)	Tri-ethoxy Vinylsilane (TEVS) (mol%)	Reaction time (hours)	M _w (kDa)	M _n (kDa)	PDI	Yield
PVP	100	0	1	43.3 ± 3.3	37.2 ± 5.1	1.17	73 ± 1
C6	94	6	4	39.6 ± 1.9	21.2 ± 4.2	1.87	61 ± 3
C16	84	16	6	40.9 ± 3.8	23.1 ± 3.7	1.78	49 ± 5
C24	76	24	10	38.6 ± 2.2	17.9 ± 5.9	2.15	36 ± 4
C36	64	36	24	-	-	-	13 ± 7

TEVS content in monomer mixture were varied from 0 to 36 mol% (0, 6, 16, 24 and 36 mol%) to obtain different contents of triethoxy-silane functional groups (i.e. functionality) in copolymer chains. In our study, it required longer reaction time to synthesis copolymers with higher TEVS contents. Reaction times were optimised to keep the M_w of copolymers ranging from 35 to 45 kD. Copolymers containing 6 to 24 mol% TEVS were possible to prepare within the desired M_w range. However, copolymers with 36 mol% TEVS (C36) required 24 hours to reach the desired M_w range and might have started to form some silane-silane crosslinking which made this C36 copolymer insoluble in common solvents. Thus, it was not possible to use C36 copolymer for *in situ* sol-gel synthesis to obtain class II hybrid biomaterials. Polydispersity indices of synthesised copolymers varied from 1.87 to 2.15 (Table 6.1).

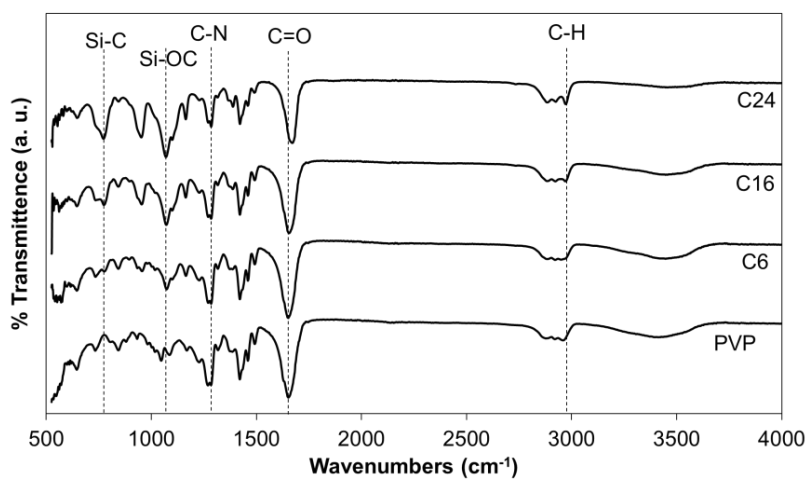


Figure 6. 1: FTIR spectra of PVP and poly(VP-co-TEVS) with 6, 16 and 24 mol% TEVS

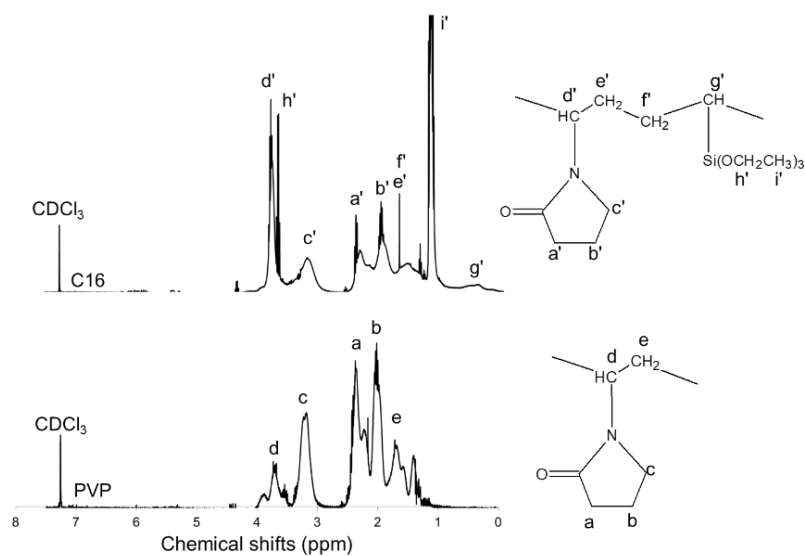


Figure 6. 2: ^1H -NMR spectra of PVP and poly(VP-co-TEVS) with 16 mol% TEVS

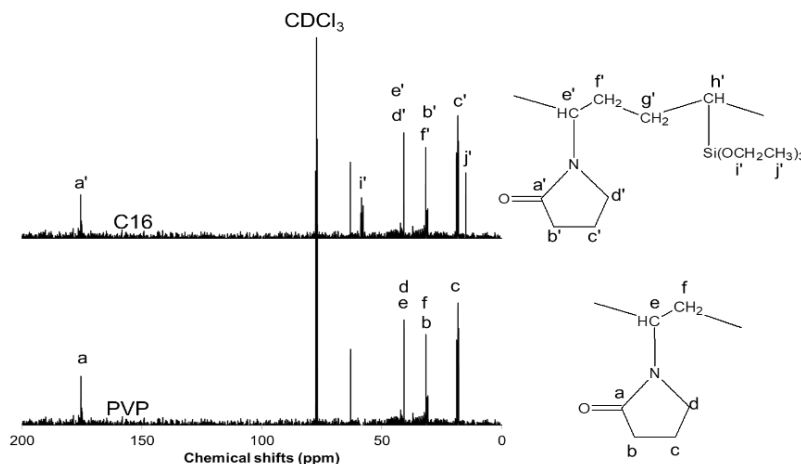


Figure 6. 3: ^{13}C -NMR spectra of PVP and poly(VP-co-TEVS) with 16 mol% TEVS

The copolymer and BG precursors were hydrolyzed *in situ* and co-condensed through sol gel process to form O/I hybrid networks (Scheme 6.2). Bridging and network formation in Poly(VP-co-TEVS)/BG class II hybrids were studied by FTIR and solid state ^{29}Si -NMR (Figure 6.4). The FTIR spectra (Figure 6.4A) for hybrids (made of 30, 50 and 70 wt% of C16 copolymer) exhibited characteristic peaks at 1072 cm^{-1} attributed to Si-O-Si stretching for all hybrid compositions. Whereas visible peak at 2840 cm^{-1} in C16 copolymer spectrum is due to the stretching vibrations of Si-O bonds from pendant Si-(OC₂H₅)₃ functional groups. The peak at 1295 cm^{-1} is associated with P=O bond from the inorganic glass network. The peaks observed at 1495 cm^{-1} are due to the Si-C bond from pendant TEVS functional groups in copolymers. ^{29}Si -NMR spectra (Figure 6.4B-C) of hybrids exhibited Tⁿ and Qⁿ species in all compositions. Tⁿ and Qⁿ correspond to the structures of -CSi(OSi-)_n(OH)_{3-n} and Si-O-Si(OSi-)_n(OH)_{4-n} respectively, where OH is referred to as non-bridging oxygen. The inorganic glass network would show only Qⁿ species whereas Tⁿ

peaks must be visible in class II hybrids due to the O/I covalent bonded crosslinking. Chemical shifts at ~ -93 , -100 and -110 ppm are associated with Q^2 , Q^3 and Q^4 species respectively, and at ~ -58 and -63 ppm are assigned to T^2 and T^3 species respectively. ^{29}Si -NMR spectra of 30P, 50P and 70P hybrids prepared from C24 copolymer (Figure 6.4B) have shown that higher organic content resulted in increasing T species compared to Q. This finding suggests that having more triethoxysilane functional groups in polymer chains increased the O/I covalent crosslinking. However, spectra of 70P hybrids prepared from C6, C16 and C24 copolymers (Figure 6.4C) revealed that, higher functionality of copolymers increased the O/I covalent crosslinking. In the case of 70P prepared with C6, most part of the silica came from the hydrolysis and polycondensation of TEOS, which increased the Q network formation. Dominant Q^3 and T^2 species were observed in all cases indicated the presence of abundant non-condensed Si-OH at least at one end of Si-O- bridging networks.

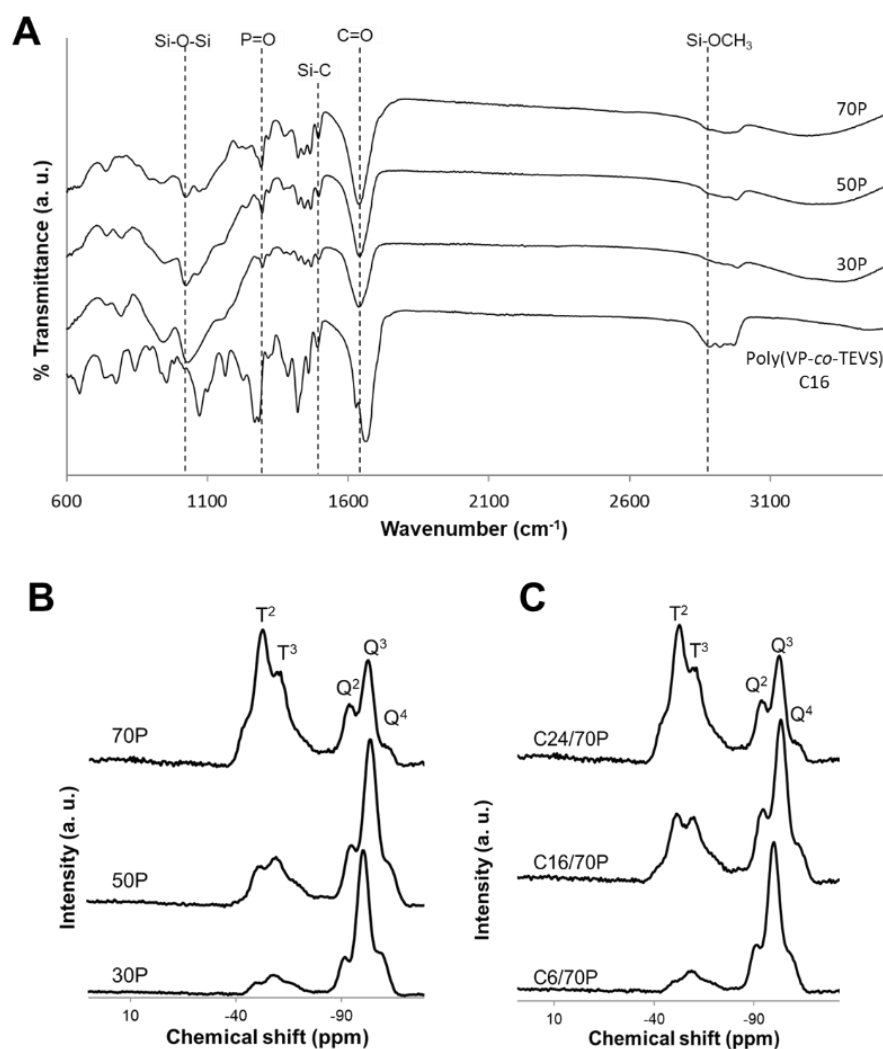


Figure 6. 4: (A) FTIR and (B-C) solid state ²⁹Si-CP MAS NMR spectra of poly(VP-co-TEVS)/BG hybrid biomaterials.

6.4.2 Apatite deposition on poly(VP-co-TEVS)/BG class II hybrid biomaterial surfaces

In vitro bioactivity of hybrid biomaterials was evaluated by studying the biomimetic apatite deposition on hybrid surfaces after incubating in SBF for different time intervals (Figure 6.5). Representative SEM images (Figure 6.5A) of the hybrid surfaces after incubating in SBF for 6h

and 72h have shown apatite particulates formation on hybrid surfaces at 6h of incubation. After 72 h, the hybrid surfaces were covered with apatite layers. The Ca/P ratio was calculated from EDX analysis (Figure 6.5A inset) of deposited apatite layer was 1.68 ± 0.05 at 72 h of incubation. This result suggests that the synthesized hybrids can induce biomimetic hydroxyapatite (HAp) layer formation on their surfaces during incubation in SBF. The XRD patterns of the synthesized hybrids following incubation in SBF (Figure 6.5B-C) have shown visible crystalline peaks for HAp at 1 day. These results are consistent with the EDX analysis. Sharp peaks for crystalline HAp ($2\theta = 31.77$ and 45.4) were observed at 7 days.

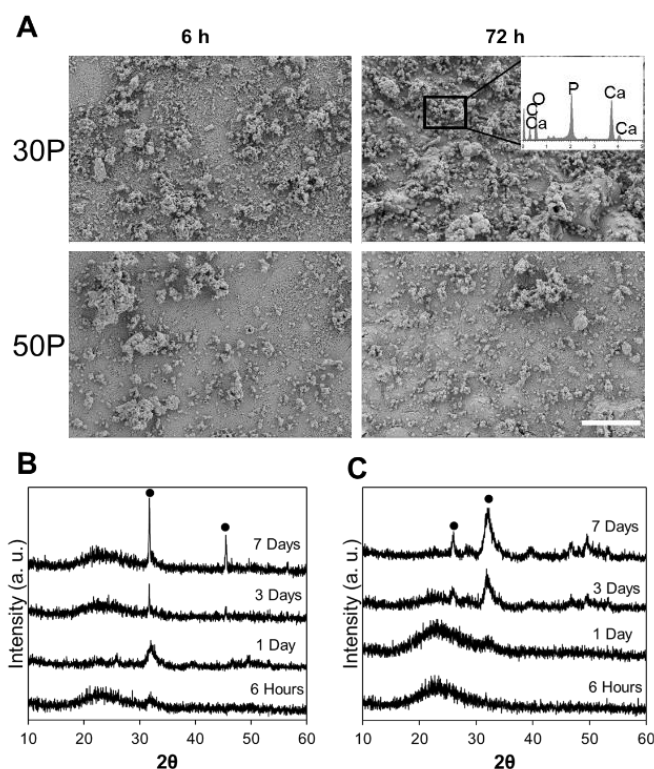


Figure 6. 5: Apatite deposition on 30P and 50P hybrids (prepared with C16 copolymers) biomaterial surfaces. **A)** Representative SEM images at 6 and 72 h post-incubation in SBF. Scale bar is 50 μm . Inset are showing EDX spectra of rectangular area. XRD patterns of **B)** 30P and **C)** 50P hybrid biomaterials after incubated in SBF. (●) indicates HAp peaks.

Low O/I ratio (30P) induces higher amount of apatite deposition due to the bioactive nature of the inorganic BG parts. The thickness of deposited HAp layers with various time courses of incubation are displayed in Figure 6.6. Layer thicknesses were not significantly different for the various O/I ratios at 24 h. However, significantly thicker HAp layers were deposited at 30P surfaces after 7 days of incubation, suggesting that hybrids of lower O/I ratios exhibit better bioactivity than the hybrids with higher ratios.

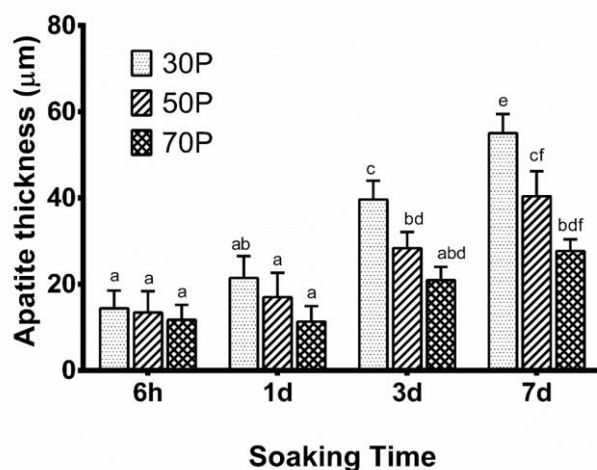


Figure 6. 6: Thickness of deposited hydroxyapatite (HAp) layers on poly(VP-co-TEVS)/BG hybrid surfaces incubated in SBF for 6 h and 1, 3 and 7 d. Data are means \pm SD of thickness measured from 10 images of 3 specimens from 3 independent experiments. Two-way ANOVA and Tukey's multiple comparison test were used for statistical analysis. Different lower-case letters indicate significance at $p < 0.05$.

6.4.3 Degradation of poly(VP-co-TEVS)/BG hybrid in PBS

The degradation of poly(VP-co-TEVS)/BG hybrid monoliths were studied by evaluating the weight loss and ion release in PBS over a period of 3-15 d (Figure 6.7). The synthesized hybrids prepared with C16 and C24 were used for the degradation study. The results are shown in Figure

6.7A-B. At the same O/I ratio, hybrids made of C16 copolymer exhibited higher weight loss compared to those made from C24. In addition, hybrids with higher O/I ratios (e.g. 70P) exhibited less weight loss when compared to 30P, regardless of the copolymer functionality. After 15 days of immersion in PBS, poly(VP-co-TEVS)/BG hybrids prepared using C16 exhibited weight loss values of 45.0 ± 2.7 , 38.2 ± 2.5 and 17.3 ± 1.5 % for 30P, 50P and 70P respectively. Similarly, the hybrids prepared using C24 copolymer had weight loss values of 25.8 ± 2.2 , 16.3 ± 1.2 and 6.9 ± 1.3 % for 30P, 50P and 70P respectively.

Degradation behavior was further characterized by measuring the amount of calcium (Figure 6.7C) and silicon (Figure 6.7D) ions released in PBS over a period of 15 days. Consistent with the weight loss results, more Ca and Si ions were released from hybrids with low O/I ratio (30P), and those with lower copolymer functionality (C16). At 15 days of post-incubation, the cumulative Ca ions released were 195.2 ± 13.7 and 107.4 ± 2.6 ppm from C16 based hybrids 30P and 50P respectively. In case of C24 based hybrids, the cumulative Ca ions released were 129.7 ± 7.0 and 55.4 ± 4.6 ppm. Similarly, at 15 days of post-incubation, the release of Si ions from C16 based hybrids 30P and 50P were 339.8 ± 10.1 and 210.0 ± 9.2 ppm respectively, and from C24 based hybrids 30P and 50P were 150.2 ± 10.0 and 54.3 ± 1.5 ppm respectively.

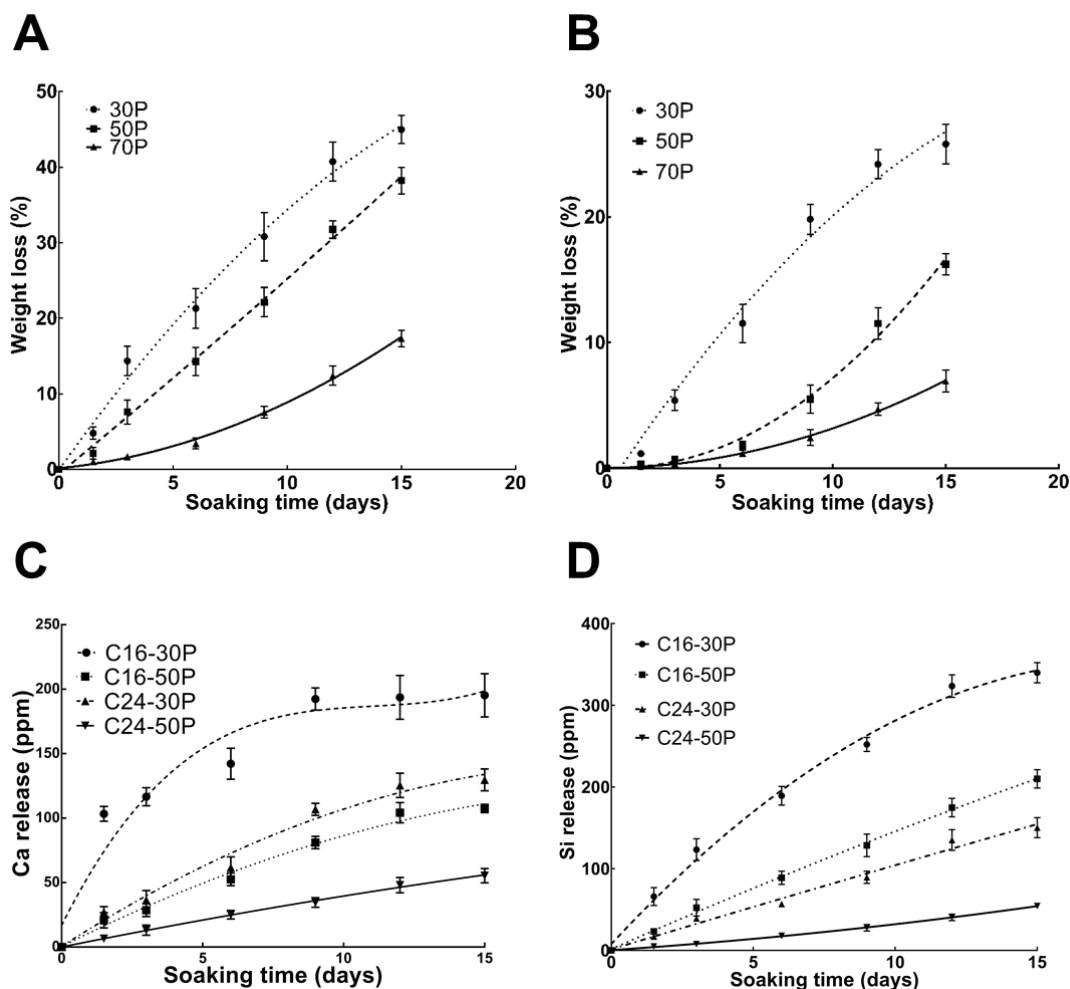


Figure 6. 7: Degradation behavior of poly(VP-co-TEVS)/BG hybrid biomaterials. Degradation was evaluated in PBS at 37 °C in a shaker incubator. Weight loss of hybrids prepared with **A)** C16 copolymer and **B)** C24 copolymer at the indicated times. **C)** and **D)** are calcium and silicon ion release measured by ICP-OES. Data are mean \pm SD (n=5 specimens of each compositions). Data were fit using nonlinear regression analysis, $P < 0.001$.

6.4.4 Hybrid biomaterials are cytocompatible and support cell spreading

Bone biocompatibility of the synthesized poly(VP-co-TEVS)/BG hybrids were assessed by the morphology and spreading of preosteoblastic MC3T3-E1 cells on 30P, 50P and glass coverslip

(control) surfaces at 3 and 24 h following seeding. Cells were fixed and labelled for F-actin and DNA (green and blue respectively in Figure 6.8A), and cell number and planar cell area were quantified. At 3 h, cells on 30P and 50P surfaces had begun to spread. However, cells on 50P were more spread than those on 30P and actin microfilaments were slightly visible. In contrast, cells on glass coverslips were well spread at 3 h and the actin cytoskeleton was already beginning to organize. By 24 h, cells on both hybrid surfaces were well spread with well-organized actin cytoskeleton. At 3 h, the area of cells seeded on 50P was $2690 \pm 319 \mu\text{m}^2$, which were significantly larger than cells seeded on 30P ($1265 \pm 86 \mu\text{m}^2$), but were not significantly different than glass coverslips ($3122 \pm 543 \mu\text{m}^2$). At 24 h, cell planar areas were not significantly different for cells seeded on hybrids and glass coverslips. Cell density was also quantified by counting the number of nuclei per unit area (Figure 6.8B). Although there were significantly more cells on coverslips than on the 30P and 50P hybrids, the rates of increase in cell numbers from 3 h to 24 h, which primarily reflect proliferation, were similar on hybrids and coverslips. These abundant number of cells attached to the both hybrid surfaces indicate excellent cytocompatibility of poly(VP-co-TEVS)/BG hybrid biomaterials.

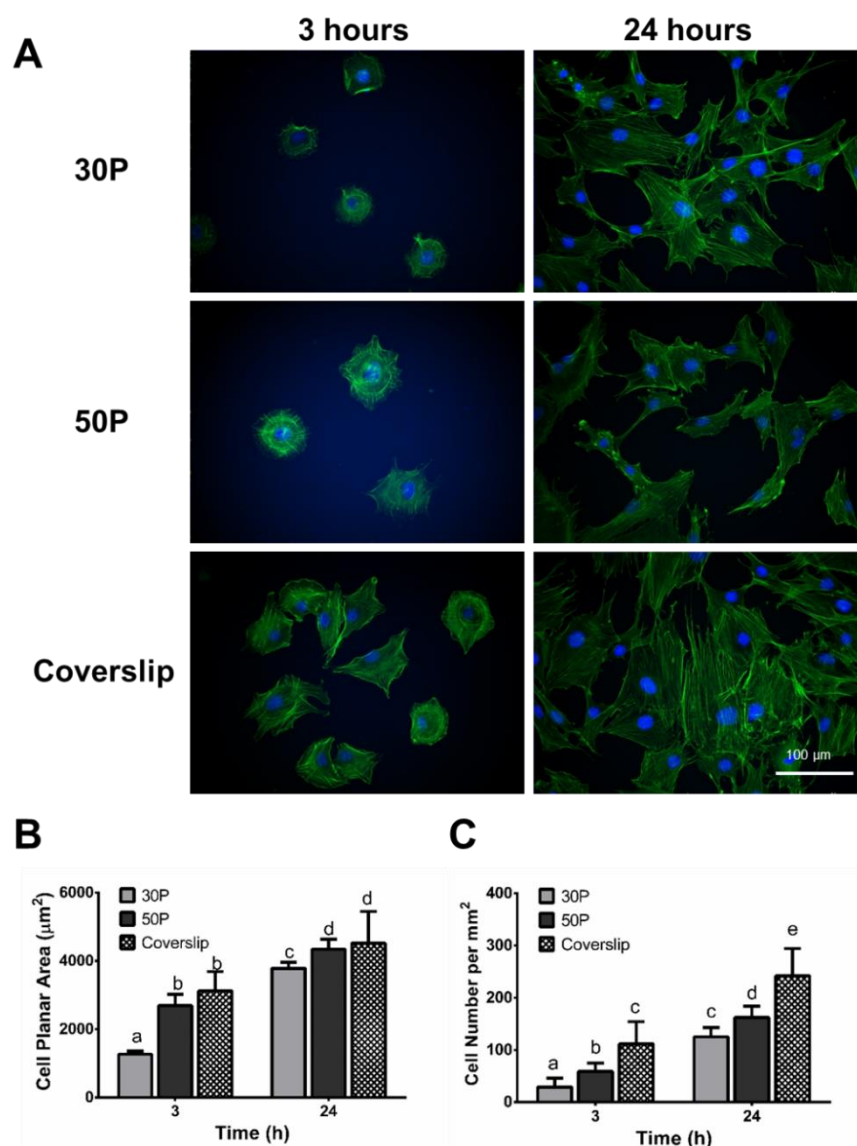


Figure 6. 8: Morphology and spreading of preosteoblastic MC3T3-E1 cells on hybrid biomaterial surfaces. Cells were seeded on 30P, 50P and glass surfaces. At 3 and 24 h following seeding, cells were fixed and labelled for F-actin (green) and DNA (to label nuclei, blue). **A**) Immunofluorescence images of cells on the substrate surfaces. Scale bar is 100 μm for all panels. Images are representative of multiple fields on each specimen, from 3 independent experiments, each performed using triplicate specimens. **B**) Quantification of cell spreading on hybrid biomaterial and control surfaces. Data are means \pm SD of 10 cells each from 3 independent experiments ($n = 30$). **C**) Cell density was quantified by counting the number of nuclei per unit area. Data are means \pm SD of 10 fields each from 3 independent experiments ($n = 30$). Two-way ANOVA and Tukey's multiple comparison test were used for statistical analysis. Different lower-case letters indicate significance at $p < 0.05$.

6.4.5 Microstructures and pore morphology of hybrid scaffolds

The SEM and micro-CT isosurface images of 3D printed PCL template and as-fabricated poly(VP-co-TEVS)/BG hybrid scaffolds are shown in Figure 6.9. PCL templates were 4 x 4 mm in cross-section and 8 mm in height. SEM images of the PCL templates displayed smooth surfaces and interconnected pores, Figure 6.9A-B. Poly(VP-co-TEVS)/BG hybrid sol was forced to infiltrate these templates by keeping it at reduced pressure, and after gelation and drying, PCL was leached out without damaging the microstructure of the scaffolds. Fabricated hybrid scaffolds displayed crack-free microstructures with uniform, interconnected pores (Figure 6.9C-D). Due to the shrinkage of poly(VP-co-TEVS)/BG hybrid during drying stage, their resultant pores were larger than the ones in PCL templates.

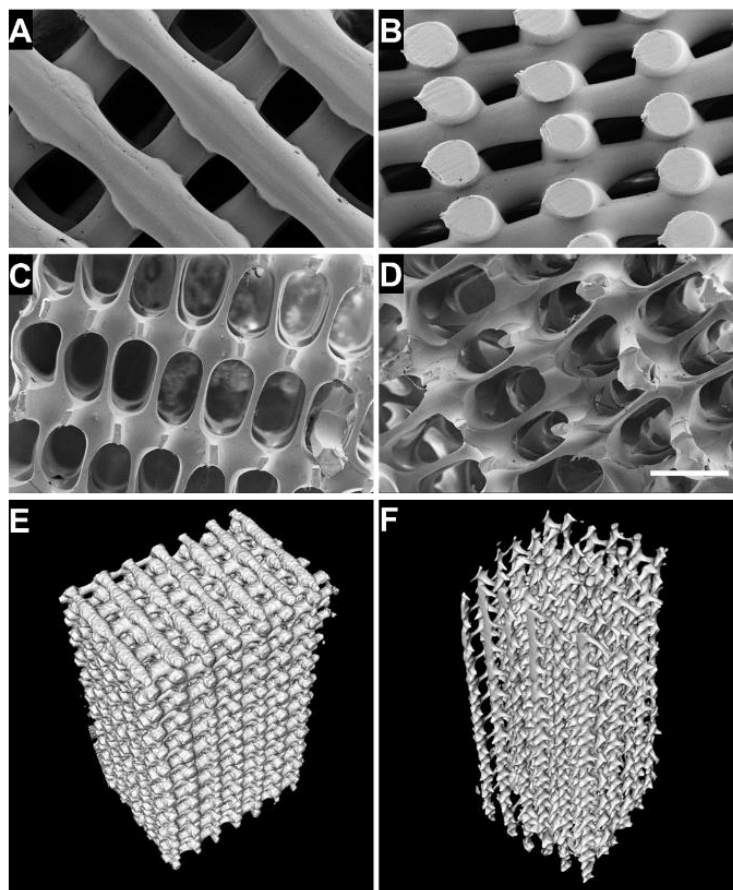


Figure 6. 9: Morphology of PCL template and hybrid scaffolds. SEM images of **A-B)** 3D printed PCL template, **C-D)** Poly(VP-co-TEVS)/BG hybrid scaffolds. Scale bar is 500 μm for panels A-D. Micro-CT images of **E)** PCL template and **F)** hybrid scaffold.

Micro-CT images of PCL template (Figure 6.9E) and poly(VP-co-TEVS)/BG hybrid scaffold (Figure 6.9F) reveals uniform microstructure, consistent with that in the SEM images. The lighter gray regions in the micro-CT images represent the O/I hybrid matrix, while the air void is outlined by the darker regions.

The percentage porosity, pore wall thickness, pore size and surface area to volume ratio of PCL templates and hybrid scaffolds determined from the Micro-CT analysis are summarized in Table

6.2. PCL scaffolds had 49.4 ± 4.5 vol% porosity, whereas due to the shrinkage of hybrids, 30P and 50P, the vol% porosity values were 85.5 ± 2.6 and 88.2 ± 3.9 of respectively. As the PCL scaffolds were negative templates of the hybrid scaffolds, the pores of PCL scaffolds should be the pore wall for hybrid scaffolds. Although the pore size of PCL scaffolds is measured 171.2 ± 15.6 μm , shrinkage led the pore wall thickness of hybrid scaffolds are 92.0 ± 5.6 μm and 94.6 ± 11.4 μm for 30P and 40P respectively. In similar manner, pore size values of 30P (547.0 ± 33.4 μm) and 50P (694.5 ± 83.5 μm) were increased 3 to 4 folds compared to the pore wall thickness of PCL templates (162 ± 14.8 μm). Higher O/I ratios in hybrids caused higher shrinkage, thus 50P scaffolds had larger pore size than 30P scaffolds. Surface area to volume ratios of 30P and 50P were found to be 21.8 ± 1.4 and 21.5 ± 2.8 mm^{-1} respectively. Higher surface area is desirable for bone tissue engineering because it enhances cell attachment and proliferation by allowing more nutrient transportation and oxygen availability.

Table 6. 2: Porosity, pore wall thickness, pore size, and surface area to volume ratio of poly(VP-co-TEVS)/BG hybrid scaffolds

Scaffold	Porosity, volume fraction (%)	Pore wall thickness (μm)	Pore size (μm)	Surface area to volume ratio (mm^{-1})
PCL	49.4 ± 4.5	162.0 ± 14.8	171.2 ± 15.6	12.4 ± 1.1
30P	85.5 ± 2.6	92.0 ± 5.6	547.0 ± 33.4	21.8 ± 1.4
50P	88.2 ± 3.9	94.6 ± 11.4	694.5 ± 83.5	21.5 ± 2.8

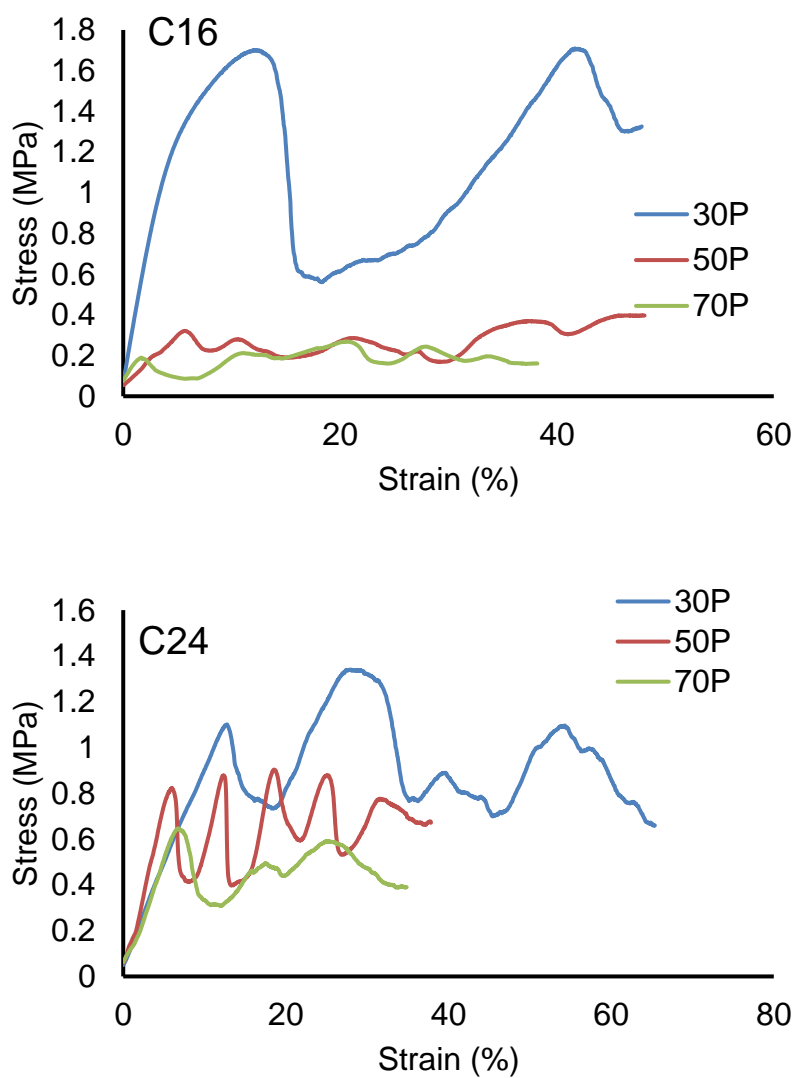


Figure 6. 10: Representative stress-strain curves of poly(VP-co-TEVS)/BG hybrid scaffolds

6.4.6 Compressive mechanical properties of hybrid scaffolds

Mechanical properties of porous 3D scaffolds play a critical role in tissue engineering. Uniaxial mechanical testing was performed to determine the compressive stress, modulus, strain at fracture, and toughness of poly(VP-co-TEVS)/BG hybrid scaffolds of different compositions. All data are collectively presented in Table 6.3. Representative stress-strain curves (Figure 6.10) have shown that both functionality of copolymer and O/I ratio affect the compressive properties of hybrid scaffolds. Higher functionality of copolymer allowed more crosslinking with the inorganic phases and resulted excellent consistency in layer by layer fracture during compressive loading. Increasing the O/I ratio, the values resulted in a decrease in the mechanical properties, possibly due to the increase of pore size and percentage porosity.

Table 6. 3: Compressive mechanical properties of poly(VP-co-TEVS)/BG hybrid scaffolds

Functionality of copolymer	O/I ratio	Ultimate compressive stress (MPa)	Compressive modulus (MPa)	Toughness (MPa)	Strain at fracture (%)
C16	30P	1.57 ± 0.26	22.31 ± 3.84	0.36 ± 0.09	45.59 ± 16.76
	50P	1.2 ± 0.28	17.36 ± 3.77	0.23 ± 0.05	38.33 ± 9.33
	70P	0.38 ± 0.11	5.59 ± 1.69	0.08 ± 0.03	32.16 ± 10.26
C24	30P	1.27 ± 0.16	15.46 ± 2.48	0.46 ± 0.08	51.45 ± 11.19
	50P	1.01 ± 0.13	12.34 ± 2.43	0.21 ± 0.06	32.2 ± 7.68
	70P	0.61 ± 0.19	10.54 ± 2.74	0.11 ± 0.05	36.31 ± 16.33

6.5 Discussion

Class II hybrid biomaterials, in which the organic and inorganic phases are chemically bonded, act as a single-phase material on molecular scale, and provide synergistic combinations of properties from all constituents [11, 12, 37]. Biomaterials should be biocompatible, mechanically competent and biodegradable in a suitable rate, and tailorable into 3D porous scaffold to apply for bone regeneration. Covalent crosslinking between biopolymers and bioactive glasses exhibited superior physical, mechanical and biological properties as well as predictable degradation behavior when compared to their conventional composite counterparts [38]. To synthesize class II hybrid material, organic polymer must have functional group(s) so that inorganic building blocks can react with the polymers [6, 25]. One strategy for class II hybrid preparation involves functionalization of polymer chains with alkoxy silicon, so that they can be hydrolyzed and polycondensed with the inorganic BG matrix through Si-O-Si linkages. Several class II hybrid biomaterials have been synthesised by adding alkoxy silicon functional groups at the end of biopolymer chains (end-capping) prior to incorporate with inorganic networks [21, 23, 39, 40]. However, adding functional groups at the end only delivers limited functionality which may result in phase separations above certain amount of organic or inorganic phases. Contrary to end group modifications, biopolymers with pendant trialkoxy silicon functional groups provide much higher reactive sites to inorganic BGs. In this work, we successfully added pendant triethoxy silicon functional groups in polymer chain so that these triethoxy silicon can go through hydrolysis and subsequent poly-condensation with inorganic glass building blocks (here TEOS and TEP) and resulted in highly crosslinked hybrids with molecular level distribution of O/I phases. We hypothesised that covalent bonding

between the polymer chains and BGs through pendant triethoxysilicon functional groups would exhibit excellent bioactivity, degradation behavior, cell-material interaction, and processability into porous 3D scaffolds for bone tissue engineering applications. Copolymers with 6, 16 and 24 mol% triethoxysilicon functional groups were used to prepare poly(VP-co-TEVS)/BG class II hybrid biomaterials with 30-70 wt% O/I ratios.

Higher molecular weight (MW) of organic phase may increase the mechanical properties of hybrid biomaterials but it also may affect the dissolution. Low MW polymers are ideal for use in implanted medical devices because a polymer whose MW larger than 50 kDa might not be released into the body as it has limited ability to pass into and out of the vascular system [41]. In this study, we used copolymers having MW values ranging between 35-45 kDa to synthesize class II hybrid biomaterials. The effect of the MW of the copolymers on the properties of hybrid biomaterials demands detailed analysis which is beyond the scope of current study.

O/I weight ratio in final class II hybrid biomaterials, as well as the molar percentage of functional groups present in the polymer chains greatly affected the polycondensation and -Si-O- bridging network formation. Higher O/I ratio presumably would increase the T network formation due to the increased overall polymer content. Similarly, low functionality in polymer decreased the number of -C-Si-O network formation. Solid state ^{29}Si -CP MAS NMR results are consistent with these assumption (Figure 6.4). Dominant Q^3 and T^2 in this study indicated the presence of non-condensed -Si-OH in -Si-O- networks due to the absence of heat treatment as the hybrid were synthesized at room temperature. Presence of these -Si-OH sites would enhance the bioactivity by

inducing biomimetic apatite deposition while incubated with SBF [35, 42, 43] due to the reactivity of Si-OH towards Ca^{2+} , hence increase the rate of degradation.

Apatite formation was directly related to inorganic content in the synthesized hybrids. BGs induced carbonated hydroxyapatite layer formation on their surfaces when incubated in SBF or bone-BG interfaces when implanted in animal [6]. In this study, the HAp layer thickness was not significantly higher than that for 30P after 1 day of incubation compared to 50P and 70P, but crystalline HAp particles were visible on the surface. The deposited layer thickness significantly increased after 3 days of incubation. As the BGs were covalently bonded to the organic network, the bioactivity can be tailored by controlling the amount of O/I ratios in hybrid matrices.

Bioactive materials applied for bone regeneration should exhibit controlled degradation behavior, so that the dissolution products can be fully utilized by newly formed ECM or excreted, and also the mechanical properties can be sustained until the materials are fully replaced by the newly formed tissue [44]. Conventional O/I composites of BGs are susceptible to bulk degradation and inconsistent rapid weight loss when compared with class II hybrids [38]. Our study revealed that the degradation behavior of class II hybrid biomaterials is affected by both O/I ratio and functionality of organic polymer. However, hybrids prepared with lower percentage of functional groups in the copolymers exhibited higher amount of weight losses for all O/I ratios. Higher functionality induced higher degree of crosslinking between the O/I network and therefore increased the T^n network formation over the Q^n . The percentage weight loss decreased with the increase of T^n species in class II hybrids. Sol gel derived amorphous BGs are resorbable both *in vitro* and *in vivo* [6] thus, it was desirable to use lower O/I ratio in order to achieve higher rate of

weight loss. All synthesized hybrids exhibited consistent rates of weight loss over the time course without having any rapid increase which indicated that by optimizing functionality of organic moiety and O/I ratio, the degradation behavior of class II hybrid biomaterials can be tailorable.

The release profiles of calcium and silicon ions in PBS were consistent with the weight loss data. It is obvious that having higher degree of crosslinking between the organic and inorganic phases, assisted in better entrapment of calcium in the O/I hybrid matrices. Thus, hybrid prepared from copolymer with lower functionality (i.e. C16) showed rapid release of calcium ions. On the contrary, the release profiles of silicon ions followed a linear trend, as it was the crosslinker between the organic and inorganic phases.

Adhesion, spreading and proliferation of bone cells on biomaterial surfaces are critical parameters that influence the osteoconductivity of the biomaterial. Preosteoblastic cells seeded on the surfaces of poly(VP-co-TEVS)/BG hybrids revealed excellent morphology with developed cyto-skeleton. Cell planar area and number of cells attached to these hybrid surfaces indicated excellent cytocompatibility and no marked cytotoxicity.

The size, shape and interconnectivity of the pores for tissue engineering scaffolds are crucial design parameters to ensure vascularization and new bone formation throughout the scaffolds. Scaffolds having interconnected porosity with mean pore diameter $\geq 100 \mu\text{m}$ are found favorable for successful diffusion of essential nutrients and oxygen for cell survivability [45]. In addition, the mean pore diameter in the range of 200–350 μm were found to be optimum for bone tissue in-growth [46]. However, while large pore diameters enhance tissue formation, it also compromises the mechanical properties and stability of the scaffolds [47]. In this study, we prepared poly(VP-

co-TEVS)/BG class II hybrid scaffolds by indirect rapid prototyping technique. Scaffolds with crack-free surface and well-defined geometry were possible to produce successfully. However, the pore size and strut thickness were different than the estimated values from 3D printed templates due to the shrinkage of the hybrids during the drying step. Shrinkage is a consequence of the evaporation of ethanol and water, released during the hydrolysis and polycondensation of Si-O-Si and Si-O-P bridging network formation. In our study, the pore diameters increased about 3 to 4 folds, whereas pore wall thickness decreased almost 50%. Although pore morphologies and porosity were not optimized in this study, some insights into the correlation between shrinkage and pore morphologies were established.

Hybrid scaffolds have shown excellent mechanical properties under uniaxial compression loading. Functionality of copolymer did not have significant effect on the mechanical properties of prepared scaffolds. On the other hand, O/I ratio greatly affected the compressive mechanical properties. It is revealed that lower O/I ratio exhibited better values of compressive stress, modulus, toughness and strain at fracture values.

6.6 Conclusion

This work revealed that functional groups present in organic polymer as side groups, increase the degree of covalent crosslinking between the organic and inorganic phases during the synthesis of O/I class II hybrid biomaterials through sol gel process. By carefully designing the polymer functionality and O/I ratio, it is possible to tailor the bioactivity, degradation behavior as well as the mechanical properties of these hybrids. 3D printed porous scaffolds to be utilized as sacrificial

templates in order to fabricate poly(VP-co-TEVS)/BG hybrid scaffolds, allows precise control of the pore size, porosity and interconnectivity of the resultant scaffolds as well as their mechanical properties. Taken together, these hybrid biomaterials are excellent candidates for bone tissue engineering and related applications.

6.7 References

- [1] Bose S, Roy M, Bandyopadhyay A. Recent advances in bone tissue engineering scaffolds. *Trends in Biotechnology* 2012;30:546-54.
- [2] Khan Y, Yaszemski MJ, Mikos AG, Laurencin CT. Tissue Engineering of Bone: Material and Matrix Considerations. *JBJS* 2008;90:36-42.
- [3] Rezwani K, Chen QZ, Blaker JJ, Boccaccini AR. Biodegradable and bioactive porous polymer/inorganic composite scaffolds for bone tissue engineering. *Biomaterials* 2006;27:3413-31.
- [4] Jones AC, Arns CH, Sheppard AP, Hutmacher DW, Milthorpe BK, Knackstedt MA. Assessment of bone ingrowth into porous biomaterials using MICRO-CT. *Biomaterials* 2007;28:2491-504.
- [5] Fröhlich M, Grayson WL, Wan LQ, Marolt D, Drobic M, Vunjak-Novakovic G. Tissue Engineered Bone Grafts: Biological Requirements, Tissue Culture and Clinical Relevance. *Current stem cell research & therapy* 2008;3:254-64.
- [6] Jones JR. Review of bioactive glass: From Hench to hybrids. *Acta Biomaterialia* 2013;9:4457-86.
- [7] Hutmacher DW. Scaffolds in tissue engineering bone and cartilage. *Biomaterials* 2000;21:2529-43.
- [8] O'Brien FJ. Biomaterials & scaffolds for tissue engineering. *Materials Today* 2011;14:88-95.
- [9] Sanchez C, Julian B, Belleville P, Popall M. Applications of hybrid organic-inorganic nanocomposites. *Journal of Materials Chemistry* 2005;15:3559-92.
- [10] Vallet-Regi M, Colilla M, Gonzalez B. Medical applications of organic-inorganic hybrid materials within the field of silica-based bioceramics. *Chemical Society Reviews* 2011;40:596-607.
- [11] Novak BM. Hybrid Nanocomposite Materials—between inorganic glasses and organic polymers. *Advanced Materials* 1993;5:422-33.
- [12] Kickelbick G. Introduction to Hybrid Materials. *Hybrid Materials: Wiley-VCH Verlag GmbH & Co. KGaA*; 2006. p. 1-48.

- [13] Wheeler DL, Eschbach EJ, Hoellrich RG, Montfort MJ, Chamberland DL. Assessment of resorbable bioactive material for grafting of critical-size cancellous defects. *Journal of Orthopaedic Research* 2000;18:140-8.
- [14] Hench LL, Polak JM. Third-Generation Biomedical Materials. *Science* 2002;295:1014-7.
- [15] Jones JR, Ehrenfried LM, Hench LL. Optimising bioactive glass scaffolds for bone tissue engineering. *Biomaterials* 2006;27:964-73.
- [16] Fu Q, Saiz E, Tomsia AP. Bioinspired Strong and Highly Porous Glass Scaffolds. *Advanced Functional Materials* 2011;21:1058-63.
- [17] Owens GJ, Singh RK, Foroutan F, Alqaysi M, Han C-M, Mahapatra C, et al. Sol-gel based materials for biomedical applications. *Progress in Materials Science* 2016;77:1-79.
- [18] Liu Y-L, Su Y-H, Lai J-Y. In situ crosslinking of chitosan and formation of chitosan-silica hybrid membranes with using γ -glycidoxypropyltrimethoxysilane as a crosslinking agent. *Polymer* 2004;45:6831-7.
- [19] Connell LS, Romer F, Suarez M, Valliant EM, Zhang Z, Lee PD, et al. Chemical characterisation and fabrication of chitosan-silica hybrid scaffolds with 3-glycidoxypropyl trimethoxysilane. *Journal of Materials Chemistry B* 2014;2:668-80.
- [20] Shirosaki Y, Tsuru K, Hayakawa S, Osaka A, Lopes MA, Santos JD, et al. Physical, chemical and in vitro biological profile of chitosan hybrid membrane as a function of organosiloxane concentration. *Acta Biomaterialia* 2009;5:346-55.
- [21] Mondal D, Rizkalla AS, Mequanint K. Bioactive borophosphosilicate-polycaprolactone hybrid biomaterials via a non-aqueous sol gel process. *RSC Advances* 2016;6:92824-32.
- [22] Tian D, Dubois P, Grandfils C, Jérôme R, Viville P, Lazzaroni R, et al. A Novel Biodegradable and Biocompatible Ceramer Prepared by the Sol-Gel Process. *Chemistry of Materials* 1997;9:871-4.
- [23] Mahony O, Tsigkou O, Ionescu C, Minelli C, Ling L, Hanly R, et al. Silica-Gelatin Hybrids with Tailorable Degradation and Mechanical Properties for Tissue Regeneration. *Advanced Functional Materials* 2010;20:3835-45.
- [24] Poologasundarampillai G, Yu B, Tsigkou O, Valliant E, Yue S, Lee PD, et al. Bioactive silica-poly(γ -glutamic acid) hybrids for bone regeneration: effect of covalent coupling on dissolution and mechanical properties and fabrication of porous scaffolds. *Soft Matter* 2012;8:4822-32.
- [25] Kickelbick G. The search of a homogeneously dispersed material—the art of handling the organic polymer/metal oxide interface. *Journal of Sol-Gel Science and Technology* 2008;46:281-90.
- [26] Yabuta T, Bescher EP, Mackenzie JD, Tsuru K, Hayakawa S, Osaka A. Synthesis of PDMS-Based Porous Materials for Biomedical Applications. *Journal of Sol-Gel Science and Technology* 2003;26:1219-22.

- [27] Wei Y, Yang D, Tang L, Hutchins MK. Synthesis, characterization, and properties of new polystyrene-SiO₂ hybrid sol-gel materials. *Journal of Materials Research* 2011;8:1143-52.
- [28] Costa ROR, Vasconcelos WL. Structural modification of poly(2-hydroxyethyl methacrylate)-silica hybrids utilizing 3-methacryloxypropyltrimethoxysilane. *Journal of Non-Crystalline Solids* 2002;304:84-91.
- [29] Hsu YG, Lin FJ. Organic-inorganic composite materials from acrylonitrile-butadiene-styrene copolymers (ABS) and silica through an *in situ* sol-gel process. *Journal of Applied Polymer Science* 2000;75:275-83.
- [30] Chung JJ, Li S, Stevens MM, Georgiou TK, Jones JR. Tailoring Mechanical Properties of Sol-Gel Hybrids for Bone Regeneration through Polymer Structure. *Chemistry of Materials* 2016;28:6127-35.
- [31] Wei Y, Jin D, Brennan DJ, Rivera DN, Zhuang Q, DiNardo NJ, et al. Atomic Force Microscopy Study of Organic-Inorganic Hybrid Materials. *Chemistry of Materials* 1998;10:769-72.
- [32] General notes on synthesis. In: Bühler V, editor. *Polyvinylpyrrolidone Excipients for Pharmaceuticals: Povidone, Crospovidone and Copovidone*. Berlin, Heidelberg: Springer Berlin Heidelberg; 2005. p. 1-4.
- [33] Teodorescu M, Bercea M. Poly(vinylpyrrolidone) – A Versatile Polymer for Biomedical and Beyond Medical Applications. *Polymer-Plastics Technology and Engineering* 2015;54:923-43.
- [34] Hendrikx S, Kascholke C, Flath T, Schumann D, Gressenbuch M, Schulze FP, et al. Indirect rapid prototyping of sol-gel hybrid glass scaffolds for bone regeneration – Effects of organic crosslinker valence, content and molecular weight on mechanical properties. *Acta Biomaterialia* 2016;35:318-29.
- [35] Kokubo T, Takadama H. How useful is SBF in predicting *in vivo* bone bioactivity? *Biomaterials* 2006;27:2907-15.
- [36] Gatica N, Díaz FR, Gargallo L, Radić D. Vinyltrimethylsilane-co-N-vinyl-2-pyrrolidone and vinyltrimethoxysilane-co-N-vinyl-2-pyrrolidone copolymers Synthesis and reactivity ratios. *Polymer Bulletin* 1998;40:707-13.
- [37] Grosso D, Ribot F, Boissiere C, Sanchez C. Molecular and supramolecular dynamics of hybrid organic-inorganic interfaces for the rational construction of advanced hybrid nanomaterials. *Chemical Society Reviews* 2011;40:829-48.
- [38] Mondal D, Dixon SJ, Mequanint K, Rizkalla AS. Mechanically-competent and cytocompatible polycaprolactone-borophosphosilicate hybrid biomaterials. *Journal of the Mechanical Behavior of Biomedical Materials* 2017;75:180-9.
- [39] Rhee S-H, Choi J-Y, Kim H-M. Preparation of a bioactive and degradable poly(ϵ -caprolactone)/silica hybrid through a sol-gel method. *Biomaterials* 2002;23:4915-21.
- [40] Valliant EM, Jones JR. Softening bioactive glass for bone regeneration: sol-gel hybrid materials. *Soft Matter* 2011;7:5083-95.

- [41] Yamaoka T, Tabata Y, Ikada Y. Body distribution of intravenously administered gelatin with different molecular weights. *Journal of Controlled Release* 1994;31:1-8.
- [42] Henstock JR, Canham LT, Anderson SI. Silicon: The evolution of its use in biomaterials. *Acta Biomaterialia* 2015;11:17-26.
- [43] Tsuru K, Ohtsuki C, Osaka A, Iwamoto T, Mackenzie JD. Bioactivity of sol–gel derived organically modified silicates: Part I: In vitro examination. *Journal of Materials Science: Materials in Medicine* 1997;8:157-61.
- [44] Griffith LG, Naughton G. Tissue Engineering--Current Challenges and Expanding Opportunities. *Science* 2002;295:1009-14.
- [45] Rouwkema J, Rivron NC, van Blitterswijk CA. Vascularization in tissue engineering. *Trends in Biotechnology* 2008;26:434-41.
- [46] Murphy CM, Haugh MG, O'Brien FJ. The effect of mean pore size on cell attachment, proliferation and migration in collagen–glycosaminoglycan scaffolds for bone tissue engineering. *Biomaterials* 2010;31:461-6.
- [47] Karageorgiou V, Kaplan D. Porosity of 3D biomaterial scaffolds and osteogenesis. *Biomaterials* 2005;26:5474-91.

Chapter 7

General Discussion

Overview: *This chapter provides a general summary of the overall work, and briefly outlines how the specific objectives mentioned in chapter 2 are met. Contributions to the current knowledge, and limitations of the thesis are discussed. Finally, some future directions related to this research topic are recommended.*

7.1 Summary and conclusions

The main objective of this study was to develop degradable and bioactive class II (covalently-bonded) O/I hybrid biomaterial scaffolds with tailorable physical, chemical, mechanical and biological properties. In this thesis, polycaprolactone/borophosphosilicate glass (PCL/BPSG) and poly(vinylpyrrolidone-co-triethoxyvinylsilane)/bioactive glass (P(VP-co-TEVS)/BG) were prepared *via* sol gel process. The inorganic materials selected for this study were borophosphosilicate glass (91-95 mole% SiO₂, 0-5 mole % of B₂O₃, and 4 mole % P₂O₅) and conventional bioactive glass (70 mole% SiO₂, 26 mole % CaCl₂, and 4 mole % P₂O₅). The organic materials were 3-glycidoxypropyl trimethoxysilane (GPTMS) functionalized polycaprolactone, and poly(vinylpyrrolidone-co-triethoxyvinylsilane). BGs are well known for their bone-bioactivity through HCA layer formation *in vitro* and strong bond formation with native bone *in vivo*, as well as having excellent osteoconductivity [1, 2]. Recent studies have shown that BGs containing boron improved the bone-bioactivity *in vitro* and *in vivo* [3-6]. However, BGs and BPSG are brittle, have low toughness and undergo rapid bulk degradation *in vitro*. These issues limited their applications for bone tissue engineering. Therefore, bioactive, biocompatible and biodegradable polymers need to be incorporated in order to improve the mechanical properties and degradation behavior of BG based scaffolds prior to applying them for bone regeneration applications. Synthesis of class II O/I

hybrid biomaterials is the most promising method to achieve tailorable physical, chemical, mechanical and biological properties. Both PCL and PVP are FDA-approved biocompatible and biodegradable/bioresorbable polymers, with many biomedical applications [7, 8].

To prepare class II O/I hybrid biomaterials, various issues needed to be addressed such as improving polymer reactivity towards inorganic phase, solubility of polymer in the sol during sol gel synthesis, incorporation of all inorganic components into the organic-inorganic matrices, on a molecular-scale and homogenous distribution of all phases, etc. The organic polymer chain needed to be functionalized, so that could chemically bond with the inorganic phase. These issues were resolved in this research to successfully synthesise PCL/BPSG and P(VP-co-TEVS)/BG class II O/I hybrid biomaterials.

PCL diol was functionalized (end-capped) with GPTMS to introduce trimethoxysilane ($-\text{Si}(\text{OCH}_3)_3$) functional groups so that it can bond with the inorganic BPSG network through $-\text{Si}-\text{O}-\text{Si}$ bridging. Conventional sol gel process involves water as a reactant for the hydrolysis of inorganic precursors and subsequent condensation to form $\text{Si}-\text{O}-\text{Si}$ network. As PCL is hydrophobic and tends to phase separate in the presence of water, non-aqueous sol gel process was introduced to synthesize PCL/BPSG class II hybrid. Instead of hydrolysis, $\text{Si}-\text{O}-\text{Si}$ network can be formed in non-aqueous sol gel process *via* carboxylation. Acetic acid and acetone were used as reactant and solvent, respectively to carry out the sol gel process and carboxylation of trimethoxysilane (functionalized with PCL), TEOS, TEP and TMB. To the best of the author's knowledge, Chapter 3 is the first work that describes the synthesis of PCL/BPSG class II O/I hybrid biomaterials *via* non-aqueous sol gel process [9]. Compositions ranging from 10 to 50 wt%

PCL were successfully bonded with the inorganic BPSG through covalent -C-Si-O-Si- bridging network formation. All PCL/BPSG hybrid compositions displayed transparent monoliths, amorphous microstructure and homogeneous dispersion of silicon, boron and phosphorus atoms in O/I hybrid matrix. 2D surfaces of these hybrids exhibited bone-like hydroxyapatite deposition *in vitro* when incubated in SBF, indicating bioactivity.

To understand the synergistic effects of covalent bonding between the organic and inorganic phases, mechanical properties and degradability of these PCL/BPSG class II hybrids were studied and compared to those of their conventional composite counterparts (Chapter 4) [10]. PCL/BPSG composites were prepared *via* non-aqueous sol gel process similar as hybrids except using non-functionalized PCL diol. The ultimate compressive stress, compressive modulus and toughness values for PCL/BPSG hybrids were significantly higher when compared with PCL/BPSG composites. The stress and modulus values decreased with increasing PCL content in both hybrids and composites due to the lower stiffness of PCL. Interestingly, toughness values of hybrids increased with increasing PCL content, likely due to the covalent bonding between O/I phases. Degradation behavior was studied by incubating the hybrid and composite materials in PBS at different time interval ranging from 0-15 days. Composites exhibited severe surface microcracks and rapid dissolution for first 6 days. Hybrids on the other hand, displayed consistent and more controlled trend of dissolution. Preosteoblastic cells attached and proliferated well on the PCL/BPSG hybrid surfaces, with excellent cell spreading and focal adhesion. This study demonstrated for the first time, how covalent bonding between the O/I phases in class II hybrids affected their mechanical properties and degradation behavior, and how to tailor them into desired properties.

Despite their excellent mechanical properties, degradation behavior and cell-material interactions (Chapter 4), the application of PCL/BPSG class II hybrids for bone tissue engineering required well-defined and interconnected porous scaffold to mimic bone ECM. Porous scaffolds of PCL/BPSG hybrids were prepared through solvent-free casting and particulate leaching method. Chapter 5 described the evaluation of pore size and porosity, and mechanical properties of PCL/BPSG hybrid scaffolds. These hybrid scaffolds have shown linear weight loss when incubated in PBS. Although, their compressive properties decreased with soaking time in PBS, no abrupt change was observed, indicating PCL/BPSG hybrid scaffolds were mechanically stable during degradation. Cell infiltration in the porous scaffolds is critical to remodel the scaffolds into new bone. Our study demonstrated that preosteoblastic MC3T3-E1 cell infiltrated into the PCL/BPSG hybrid scaffolds in static culture conditions. In addition, these materials promoted osteogenic gene expression when cultured with hMSCs.

In summary, results from Chapter 3 to Chapter 5 demonstrated that PCL/BPSG class II hybrid scaffolds demonstrated excellent and tailorable physical, mechanical and biological properties. However, end-functionalization of polymers with coupling agents delivered only a limited number of functional groups to the polymer backbone and may have caused phase separation over higher content of organic moiety during synthesis of these materials [11]. We hypothesised that, functional groups present as side groups in polymer chains increase the degree of covalent crosslinking between organic and inorganic phases. In Chapter 6, we synthesised a copolymer poly(VP-co-TEVS) having triethoxysilane functional groups as pendant side chains prior to preparing class II O/I hybrid biomaterials through sol gel process. The study described in chapter 6 revealed that having functional groups as side chains increased the degree of covalent

crosslinking between O/I phases, which made the synthesis of these hybrids containing higher organic moieties possible without phase separation. Consistent release of calcium ions from these hybrids indicated excellent potential for bone regeneration. By carefully designing the polymer functionality and O/I ratio, it is possible to tailor the bioactivity, degradation behavior as well as the mechanical properties of these hybrids. Scaffolds were prepared from these hybrids using a combination of rapid prototyping/template leaching method, using 3D printed PCL scaffolds as the sacrificial template. Predictable and well-designed pore size, porosity and interconnectivity of these resultant hybrid scaffolds exhibiting excellent compressive mechanical properties made them prominent candidates for bone tissue engineering applications.

7.2 Contributions to the current knowledge

In this thesis work, two system of novel class II O/I hybrid biomaterial scaffolds were prepared from degradable polymers and bioactive glasses. These hybrids demonstrated improved bioactivity, mechanical properties, and degradation behavior for bone tissue engineering applications. Previous studies by other groups confirmed that composites of degradable polymers and bioactive inorganic fillers can potentially mimic structural and functional properties of bone ECM [12, 13]. However, without having molecular-level chemical interactions between the O/I phases, uniform physical, chemical and mechanical properties could not be achieved through these composites. Designing class II O/I hybrid biomaterials, in which the organic and inorganic phases are chemically bonded can resolve these issues [2]. However, most of the class II hybrid biomaterials reported in the literature, involved water-soluble polymers due to their preparation

through conventional aqueous sol gel process, and incorporated single inorganic component (i.e. SiO₂), which were not adequate for bone regeneration.

This work has successfully demonstrated the synthesis O/I class II hybrid biomaterials for the first time through non-aqueous sol gel process using water-insoluble yet biocompatible and degradable polymer. This non-aqueous sol gel process will allow synthesising hybrid biomaterials incorporating several biocompatible polymers through strong covalent crosslinking. In this study, multicomponent inorganic glasses were utilized to form inorganic network which will enhance the osteogenic properties of class II hybrids.

Addition of reactive sites as pendant side groups in polymer chains significantly improved the degree of covalent crosslinking with inorganic phases as described in Chapter 6. Preparing copolymer of alkoxy silane functional groups is a unique way to add reactive sites in polymer chain prior to synthesizing O/I class II hybrids through the sol gel process. This study revealed that changing functionality of polymers allowed us to tailor the mechanical properties and degradation behavior of these materials.

Calcium plays vital role in osteogenesis during *in vitro* and *in vivo* bone regeneration. Thus, one of the objectives of this work was to obtain a homogenous distribution of calcium ion and control its release during degradation of the hybrids. As described in Chapter 6, by optimising the degree of covalent crosslinking, it is possible to control the dissolution of hybrids and release of calcium ions in the medium. Hence, the ability to tailor the properties of the hybrid biomaterials by adjusting the functionality of polymer and O/I weight ratios for the desired application provides unique approach to develop scaffolds with multifunctional characteristics.

Fabricating well-defined and interconnected porous scaffolds of class II hybrid biomaterials was a major challenge. By combining 3D printing and template leaching, it was possible to fabricate predefined porous scaffolds with desired pore morphologies. Depending on the different parameters such as organic and inorganic moieties, functionality of polymers and template characteristics, the mechanical and degradation behavior of the class II hybrids scaffolds could be optimised to desired properties. The other significant contributions of this work were the extensive characterization of class II O/I hybrid biomaterial scaffolds based on bioactivity, mechanical properties, degradation behavior, ion release due to the hybrid degradation, cell-biomaterial interactions, and osteogenesis *in vitro*. This study can be used as a foundation for further improvement of class II O/I hybrid biomaterial scaffolds and their performance for bone tissue engineering.

7.3 Limitations

Although PCL/BPSG class II hybrid biomaterials have shown superior mechanical properties, cell-material interactions and controllable degradation behavior, preliminary boron concentration in these hybrids (5 mole% B_2O_3) did not up-regulate the osteogenic gene expression of hMSCs. However, 2 mole% B_2O_3 based class II hybrids (inorganic BPSG composition: 93 mole% SiO_2 , 5 mole% P_2O_5 and 2 mole% B_2O_3) exhibited significant up-regulation compared to the PCL/ SiO_2 - P_2O_5 class II hybrids. Hence, the mechanical properties and degradation behavior of this composition was not evaluated due to time constraint.

Calcium ion in these class II hybrids was not incorporated as network modifier. Inorganic BGs prepared through sol gel process using CaCl_2 as calcium precursor (or any calcium salt) required to be heated above $400\text{ }^\circ\text{C}$ to incorporate the calcium as network modifier [14]. Class II hybrids could not be heated to that high temperature in order not to decompose the polymer component. Other available sources of calcium (e.g. calcium methoxyethoxide) are strongly reactive and caused rapid precipitation during sol gel synthesis. A new calcium precursor is required to incorporate calcium as network modifier in class II hybrids which is still unknown [2]. This current study successfully entrapped the calcium in O/I hybrid matrix and its release during degradation process was predictable. However, it is a limitation worth to mention that calcium was not chemically bonded with class II network.

In addition, the cell-biomaterial interactions studied in this work were conducted in static culture conditions. A dynamic culture condition is required for bone tissue engineering which was not performed in this study due to the time constraint.

7.4 Future directions

The current thesis work established the foundation for developing O/I class II hybrid biomaterial scaffolds with tailorable properties. It is beneficial to investigate future endeavours to broaden the horizon of class II hybrid biomaterials for bone tissue engineering applications.

1. Incorporating other inorganic components: Boron was successfully incorporated in class II hybrid matrix to improve the degradation behavior and osteogenesis. It is useful to explore

possibility to incorporate several other elements such as Strontium, Silver, Magnesium, etc. and evaluate their effects.

2. Drug delivery: In this thesis work, class II hybrid biomaterials with controllable degradation behavior were prepared through both non-aqueous and aqueous sol gel process. Polymers were functionalized in two different methods to improve the degree of covalent crosslinking between organic and inorganic phases. Consistent release profiles were exhibited during degradation whether the component is chemically bonded (boron in PCL/BPSG hybrid) or physically entrapped (calcium in poly(VP-co-TEVS)/BG hybrid). The hybrids can be loaded with drugs or growth factors in similar fashion, which may further enhance bone formation.

3. Dynamic cell culture studies: The ability of bone formation *in vitro* of the O/I hybrid scaffolds developed in this study, can be further investigated in dynamic culture conditions in a bioreactor. This requires extensive research to optimise the process parameters for the development bone grafts under this dynamic condition. Bone grafts developed in a bioreactor could mimic the autologous bone grafts and may resolve the clinical need for bone replacement and regeneration.

7.5 References

[1] Hench LL, Thompson I. Twenty-first century challenges for biomaterials. *Journal of The Royal Society Interface* 2010;7:S379-91.

[2] Jones JR. Review of bioactive glass: From Hench to hybrids. *Acta Biomaterialia* 2013;9:4457-86.

[3] Fu Q, Rahaman MN, Bal BS, Bonewald LF, Kuroki K, Brown RF. Silicate, borosilicate, and borate bioactive glass scaffolds with controllable degradation rate for bone tissue engineering applications. II. *In vitro* and *in vivo* biological evaluation. *Journal of Biomedical Materials Research Part A* 2010;95A:172-9.

- [4] Gu Y, Wang G, Zhang X, Zhang Y, Zhang C, Liu X, et al. Biodegradable borosilicate bioactive glass scaffolds with a trabecular microstructure for bone repair. *Materials Science and Engineering: C* 2014;36:294-300.
- [5] Kaur G, Pandey OP, Singh K, Homa D, Scott B, Pickrell G. A review of bioactive glasses: Their structure, properties, fabrication and apatite formation. *Journal of Biomedical Materials Research Part A* 2014;102:254-74.
- [6] Wu C, Miron R, Sculean A, Kaskel S, Doert T, Schulze R, et al. Proliferation, differentiation and gene expression of osteoblasts in boron-containing associated with dexamethasone deliver from mesoporous bioactive glass scaffolds. *Biomaterials* 2011;32:7068-78.
- [7] Porter JR, Henson A, Papat KC. Biodegradable poly(epsilon-caprolactone) nanowires for bone tissue engineering applications. *Biomaterials* 2009;30:780-8.
- [8] Teodorescu M, Bercea M. Poly(vinylpyrrolidone) – A Versatile Polymer for Biomedical and Beyond Medical Applications. *Polymer-Plastics Technology and Engineering* 2015;54:923-43.
- [9] Mondal D, Rizkalla AS, Mequanint K. Bioactive borophosphosilicate-polycaprolactone hybrid biomaterials via a non-aqueous sol gel process. *RSC Advances* 2016;6:92824-32.
- [10] Mondal D, Dixon SJ, Mequanint K, Rizkalla AS. Mechanically-competent and cytocompatible polycaprolactone-borophosphosilicate hybrid biomaterials. *Journal of the Mechanical Behavior of Biomedical Materials* 2017;75:180-9.
- [11] Kickelbick G. The search of a homogeneously dispersed material—the art of handling the organic polymer/metal oxide interface. *Journal of Sol-Gel Science and Technology* 2008;46:281-90.
- [12] Hong Z, Reis RL, Mano JF. Preparation and in vitro characterization of scaffolds of poly(l-lactic acid) containing bioactive glass ceramic nanoparticles. *Acta Biomaterialia* 2008;4:1297-306.
- [13] Webster TJ, Ergun C, Doremus RH, Siegel RW, Bizios R. Specific proteins mediate enhanced osteoblast adhesion on nanophase ceramics. *Journal of Biomedical Materials Research* 2000;51:475-83.
- [14] Lin S, Ionescu C, Pike KJ, Smith ME, Jones JR. Nanostructure evolution and calcium distribution in sol-gel derived bioactive glass. *Journal of Materials Chemistry* 2009;19:1276-82.

Appendix

Letters of copyright permission for peer-reviewed articles

1. Mondal D, Rizkalla AS, Mequanint K. Bioactive borophosphosilicate-polycaprolactone hybrid biomaterials via a non-aqueous sol gel process. RSC Advances 2016;6:92824-32.

RE: Requesting for copyright permission

RSC1 (shared)

Mon 2018-01-15 4:39 AM

To: Dibakar Mondal

Dear Dibakar Mondal

Permission is granted to reproduce your article in your thesis as long as it is fully acknowledged and includes a link back to the article on our website. Please ensure that all authors are aware that it is being included.

If you have any further questions, please let me know.

Best wishes

Publishing Assistant, Customer Services
Royal Society of Chemistry

-----Original Message-----

From:

Sent: 12 January 2018 18:36

To: RSC1 (shared)

Subject: Requesting for copyright permission

Name: Dibakar Mondal

Message: Dear Publisher,

I am Doctoral Candidate at The University of Western Ontario, Canada. Part of my thesis was published in RSC Advances, titled "Bioactive borophosphosilicate-polycaprolactone hybrid biomaterials via a non-aqueous sol gel process", 2016, 6, 92824-92832 (DOI: 10.1039/C6RA08339K). I am writing my thesis for defense and I would like to have a copyright permission allowing the article to be included in my PhD thesis as a chapter.

Thank you in advance.

Sincerely,

Dibakar Mondal

2. Mondal D, Dixon SJ, Mequanint K, Rizkalla AS. Mechanically-competent and cytocompatible polycaprolactone-borophosphosilicate hybrid biomaterials. *Journal of the Mechanical Behavior of Biomedical Materials* 2017;75:180-9.

RE: Requesting for copyright permission

Permissions Helpdesk

Fri 2018-01-12 1:46 PM

To: Dibakar Mondal

Dear Dibakar,

As an Elsevier journal author, you retain the right to include the article in a thesis or dissertation (provided that this is not to be published commercially) whether in full or in part, subject to proper acknowledgment; see <https://www.elsevier.com/about/our-business/policies/copyright/personal-use> for more information. As this is a retained right, no written permission from Elsevier is necessary.

If I may be of further assistance, please let me know.

Best of luck with your thesis and best regards,

Permissions Helpdesk Associate
ELSEVIER | Global E-Operations Books

Curriculum vitae

DIBAKAR MONDAL

EDUCATION

The University of Western Ontario, London, Canada PhD in Chemical and Biochemical Engineering	2018
SoonChunHyang University, Asan, South Korea MSc in Medical Science	2012
Bangladesh University of Engineering & Technology Dhaka, Bangladesh BSc in Chemical Engineering	2009

WORK EXPERIENCE

Graduate Research Assistant The University of Western Ontario, Department of Chemical and Biochemical Engineering	2013-2018
Graduate Teaching Assistant The University of Western Ontario, Department of Chemical and Biochemical Engineering CBE 3315A: Reaction Engineering CBE 2224B: Chemical Engineering Thermodynamics CBE 2290A: Biochemical and Environmental Engineering CBE 4421A: Introduction to Biomaterials Engineering CBE 9250B: Advanced Biomaterials Engineering	2013-2016
Research Assistant The University of Western Ontario, Canada	2013-2018
Research Assistant Research Center for Biomedical Materials, SoonChunHyang University, South Korea	2010-2012
Process Engineer Crescent Chemicals Limited, Bangladesh	2009-2010

PUBLICATIONS

- 1) Mondal, D.; Dixon, S. J.; Mequanint, K; Rizkalla, A. S., Effect of Copolymer Functionality and Composition on Bioactivity, Degradation and Mechanical Properties of Poly(vinyl pyrrolidone-co- triethoxy vinyl silane)/Bioactive Glass Hybrids. *To be Submitted*
- 2) Mondal, D.; Lin, S; Dixon, S. J.; Rizkalla, A. S.; Mequanint, K., Cell Infiltration and Osteogenic Differentiation on Polycaprolactone- Borophosphosilicate Glass Hybrid Scaffolds. *To be Submitted*
- 3) Mondal, D.; Zaharia, A.; Mequanint, K; Rizkalla, A. S., Sol-gel derived SiO₂-CaO-P₂O₅ bioactive glass nanorods via alkaline hydrothermal process. *To be Submitted*
- 4) Mondal, D.; Dixon, S. J.; Mequanint, K; Rizkalla, A. S., Mechanically-competent and Cytocompatible Polycaprolactone-Borophosphosilicate Hybrid Biomaterials. *Journal of the Mechanical Behavior of Biomedical Material* **2017**, 75, 180-189
- 5) Mondal, D.; Rizkalla, A. S.; Mequanint, K., Bioactive Borophosphosilicate-polycaprolactone Hybrid Biomaterials via a Non-aqueous Sol Gel Process. *RSC Advances* **2016**, 6 (95), 92824-92832
- 6) Linh, T. B.; Mondal, D.; Lee, B.-T., In Vitro Study of CaTiO₃ Hydroxyapatite Composites for Bone Tissue Engineering. *ASAIO Journal* **2014**, 60 (6), 722-729
- 7) Mondal, D.; Nguyen, L.; Oh, I.-H.; Lee, B.-T., Microstructure and biocompatibility of composite biomaterials fabricated from titanium and tricalcium phosphate by spark plasma sintering. *Journal of Biomedical Materials Research Part A* **2013**, 101A (5), 1489-1501
- 8) Mondal, D.; So-Ra, S.; Lee, B.-T., Fabrication and characterization of ZrO₂-CaO-P₂O₅-Na₂O-SiO₂ bioactive glass ceramics. *Journal of Materials Science* **2012**, 48 (5), 1863-1872
- 9) Mondal, D. et al, Fabrication of multilayer ZrO₂-biphasic calcium phosphate-polycaprolactone unidirectional channeled scaffold for bone tissue formation. *Journal of Biomaterials Applications* **2012**, 28 (3), 462-472
- 10) Mondal, D.; Sarkar, S. K.; Oh, I.-H.; Lee, B.-T., Comparative Study of Microstructures and Material Properties in the Vacuum and Spark Plasma Sintered Ti-Calcium Phosphate Composites. *Materials Transactions* **2011**, 52 (7), 1436-1442
- 11) Mondal, D. et al, Fabrication and characterization of the Ti-Ca-P composites by vacuum sintering. *Journal of Biomedical Science and Engineering* **2011**, 4, 583-590

SCHOLARSHIPS & AWARDS

Scholarships:

- Vanier Canada Graduate Scholarship, NSERC, Canada (May 2014 to April 2017, CAD 150,000)
- Doctoral Excellence Research Award, University of Western Ontario, Canada (2016-2017, CAD 10,000)

- VP Research Support Grant, University of Western Ontario, Canada (2014-2017, CAD 10,000)
- SoonChunHyang University scholarship, South Korea (March 2010 to December 2011, \$20,000)
- Research grant from SoonChunHyang University, South Korea (March 2010 to December 2011, \$15,000)
- Bangladesh Education Board Merit scholarship, Bangladesh (2004 to 2009, \$200)

Awards:

- Travel Award, 33rd Annual Meeting of Canadian Biomaterials Society, May 2017, Winnipeg, Canada
- Best Poster Presentation, 7th International Conference on Porous Metals and Metallic Foams, September 2011, Korea.
- Best Poster Presentation, Fall Conference 2010, Material Research Society of Korea, November 2010. Korea.

CONFERENCE PRESENTATIONS

1. 33rd Annual Meeting of Canadian Biomaterials Society, May 2017, Winnipeg, Canada (Oral)
2. Annual Dentistry Research Day, University of Western Ontario, October 2016, London, Canada (Poster)
3. 10th World Biomaterial Congress, May 2016, Montreal, Canada (Poster)
4. Canadian Bone and Joint Conference, April 2016, London, Canada (Poster)
5. Annual Dentistry Research Day, University of Western Ontario, October 2015, London, Canada (Poster)
6. 32nd Annual Meeting of Canadian Biomaterials Society, May 2015, Toronto, Canada (Poster)
7. 14th Annual Meeting of Korean Tissue Engineering and Regenerative Medicine Society, May 2012, South Korea (Poster)
8. 7th International Conference on Porous Metals and Metallic Foams, September 2011, Korea (Poster)
9. Spring Conference 2011, Material Research Society of Korea, May 2011, South Korea (Oral)
10. Fall Conference 2011, Material Research Society of Korea, October 2011, South Korea (Poster)
11. Fall Conference 2011, Korean Ceramic Society, October 2011, South Korea (Poster)
12. Spring Conference 2011, Korean Ceramic Society, April 2011, South Korea (Poster)
13. 27th International Korea-Japan Seminar on Ceramics, November 2010, South Korea (Poster)
14. Fall Conference 2010, Material Research Society of Korea, November 2010, South Korea (Poster)
15. Spring Conference 2010, Material Research Society of Korea, May 2010, South Korea (Poster)